WESTINGHOUSE NON-PROPRIETARY CLASS 3

WCAP-14363

# ANALYSIS OF CAPSULE Y FROM THE PACIFIC GAS AND ELECTRIC COMPANY DIABLO CANYON UNIT 2 REACTOR VESSEL RADIATION SURVEILLANCE PROGRAM


P. A. Peter
S. L. Anderson
J. F. Williams


August 1995

Work Performed Under Shop Order LUKP-106

Prepared by Westinghouse Electric Corporation
for the Pacific Gas and Electric Company

Approved by: R. D. Rishel
R. D. Rishel, Manager
Metallurgical & NDE Analysis


WESTINGHOUSE ELECTRIC CORPORATION
Nuclear Technology Division
P.O. Box 355
Pittsburgh, Pennsylvania 15230-0355

# PREFACE

This report has been technically reviewed and verified.

| | Reviewer: |
|---|---|
| Sections 1 through 5, 7, 8 and Appendix A | E. Terek _____ |
| Section 6 | A. H. Fero _____ |

TABLE OF CONTENTS

LIST OF TABLES

LIST OF TABLES (CONTINUED)

LIST OF TABLES (CONTINUED)

LIST OF TABLES (CONTINUED)

LIST OF ILLUSTRATIONS

LIST OF ILLUSTRATIONS (CONTINUED)

LIST OF ILLUSTRATIONS (CONTINUED)

LIST OF ILLUSTRATIONS (CONTINUED)

LIST OF ILLUSTRATIONS (CONTINUED)

LIST OF ILLUSTRATIONS (CONTINUED)

## SECTION 1.0
## SUMMARY OF RESULTS

The analysis of the reactor vessel materials contained in surveillance capsule Y, the third capsule to be removed from the Pacific Gas and Electric Company Diablo Canyon Unit 2 reactor pressure vessel, led to the following conclusions:

- The capsule received an average fast neutron fluence (E > 1.0 MeV) of $1.32 \times 10^{19}$ n/cm$^2$ after 7.0 Effective Full Power Years (EFPY) of plant operation.

- Irradiation of the reactor vessel intermediate shell plate B5454-1 Charpy specimens, oriented with the longitudinal axis of the specimen parallel to the major rolling direction (longitudinal orientation), to $1.32 \times 10^{19}$ n/cm$^2$ (E > 1.0 MeV) resulted in a 30 ft-lb transition temperature increase of 113.0°F and a 50 ft-lb transition temperature increase of 119.8°F. This results in an irradiated 30 ft-lb transition temperature of 117.6°F and an irradiated 50 ft-lb transition temperature of 153.1°F for the longitudinally-oriented specimens.

- Irradiation of the reactor vessel intermediate shell plate B5454-1 Charpy specimens, oriented with the longitudinal axis of the specimen perpendicular to the major rolling direction (transverse orientation), to $1.32 \times 10^{19}$ n/cm$^2$ (E > 1.0 MeV) resulted in a 30 ft-lb transition temperature increase of 110.7°F and a 50 ft-lb transition temperature increase of 111.1°F. This results in an irradiated 30 ft-lb transition temperature of 137.3°F and an irradiated 50 ft-lb transition temperature of 185.7°F for the transversely-oriented specimens.

- Irradiation of the weld metal Charpy specimens to $1.32 \times 10^{19}$ n/cm$^2$ (E > 1.0 MeV) resulted in a 30 ft-lb transition temperature increase of 212.5 and a 50 ft-lb transition temperature increase of 246.0°F. This results in an irradiated 30 ft-lb transition temperature of 198.9°F and an irradiated 50 ft-lb transition temperature of 260.9°F.

- Irradiation of the weld Heat-Affected-Zone (HAZ) metal Charpy specimens to $1.32 \times 10^{19}$ n/cm$^2$ (E > 1.0 MeV) resulted in a 30 ft-lb transition temperature increase of 255.3°F and a 50 ft-lb transition temperature increase of 258.1°F. This results in an irradiated 30 ft-lb transition temperature of 27.9°F and an irradiated 50 ft-lb transition temperature of 105.8°F.

- The average upper shelf energy of intermediate shell plate B5454-1 (longitudinal orientation) resulted in an energy decrease of 26.6 ft-lb after irradiation to $1.32 \times 10^{19}$ n/cm$^2$ (E > 1.0 MeV). This results in an irradiated average upper shelf energy of 118.1 ft-lb for the longitudinally-oriented specimens.

- The average upper shelf energy of intermediate shell plate B5454-1 (transverse orientation) resulted in an energy decrease of 6.3 ft-lb after irradiation to $1.32 \times 10^{19}$ n/cm$^2$ (E > 1.0 MeV). This results in an irradiated average upper shelf energy of 88.6 ft-lb for the transversely-oriented specimens.

- The average upper shelf energy of the weld metal Charpy specimens resulted in an energy decrease of 43.6 ft-lb after irradiation to $1.32 \times 10^{19}$ n/cm$^2$ (E > 1.0 MeV). This results in an irradiated upper shelf energy of 77.3 ft-lb for the weld metal specimens.

- The average upper shelf energy of the weld HAZ metal decreased 55.2 ft-lb after irradiation to $1.32 \times 10^{19}$ n/cm$^2$ (E > 1.0 MeV). This results in an irradiated upper shelf energy of 92.3 ft-lb for the weld HAZ metal.

- The surveillance capsule Y test results indicate that intermediate shell plate B5454-1 surveillance material 30 ft-lb transition temperature shifts are in good agreement with the Regulatory Guide 1.99, Revision 2[1] predictions, and the average upper shelf energy decreases are less than the Regulatory Guide 1.99, Revision 2, predictions.

- The surveillance capsule Y test results indicate that the surveillance weld metal 30 ft-lb transition temperature shift and average upper shelf energy decrease is less than the Regulatory Guide 1.99, Revision 2, predictions.

- The Diablo Canyon Unit 2 surveillance capsule Y data has been determined to be credible per the criteria presented in Regulatory Guide 1.99, Revision 2.

- The surveillance capsule materials exhibit a more than adequate upper shelf energy level for continued safe plant operation and are expected to maintain an upper shelf energy of no less than 50 ft-lb throughout the life (32 EFPY) of the vessel as required by 10 CFR Part 50, Appendix G[2].

- The calculated end-of-life (32 EFPY) maximum neutron fluence (E > 1.0 MeV) for the Diablo Canyon Unit 2 reactor vessel is as follows:

| | |
|---|---|
| Vessel inner radius* | $= 1.41 \times 10^{19}$ n/cm$^2$ |
| Vessel 1/4 thickness | $= 7.80 \times 10^{18}$ n/cm$^2$ |
| Vessel 3/4 thickness | $= 1.73 \times 10^{18}$ n/cm$^2$ |

* Clad/base metal interface

# SECTION 2.0
# INTRODUCTION

This report presents the results of the examination of Capsule Y, the third capsule to be removed from the reactor in the continuing surveillance program which monitors the effects of neutron irradiation on the Pacific Gas and Electric Company Diablo Canyon Unit 2 reactor pressure vessel materials under actual operating conditions.

The surveillance program for the Pacific Gas and Electric Company Diablo Canyon Unit 2 reactor pressure vessel materials was designed and recommended by the Westinghouse Electric Corporation. A description of the surveillance program and the pre-irradiation mechanical properties of the reactor vessel materials is presented in WCAP-8783 entitled "Pacific Gas and Electric Company Diablo Canyon Unit No. 2 Reactor Vessel Radiation Surveillance Program"[3]. The surveillance program was planned to cover the 40-year design life of the reactor pressure vessel and was based on ASTM E185-73, "Standard Recommended Practice for Surveillance Tests for Nuclear Reactor Vessels". Westinghouse personnel were contracted to aid in the preparation of procedures for removing Capsule Y from the reactor and its shipment to the Westinghouse Science and Technology Center Hot Cell Facility, where, the post-irradiation mechanical testing of the Charpy V-notch impact and tensile surveillance specimens was performed.

This report summarizes the testing of and the post-irradiation data obtained from surveillance Capsule Y removed from the Pacific Gas and Electric Company Diablo Canyon Unit 2 reactor vessel and discusses the analysis of the data.

## SECTION 3.0
## BACKGROUND

The ability of the large steel pressure vessel containing the reactor core and its primary coolant to resist fracture constitutes an important factor in ensuring safety in the nuclear industry. The beltline region of the reactor pressure vessel is the most critical region of the vessel because it is subjected to significant fast neutron bombardment. The overall effects of fast neutron irradiation on the mechanical properties of low alloy, ferritic pressure vessel steels such as SA533 Grade B Class 1 (base material of the Diablo Canyon Unit 2 reactor pressure vessel) are well documented in the literature. Generally, low alloy ferritic materials show an increase in hardness and tensile properties and a decrease in ductility and toughness under certain conditions of irradiation.

A method for performing analyses to guard against fast fracture in reactor pressure vessels has been presented in "Protection Against Nonductile Failure," Appendix G to Section III of the ASME Boiler and Pressure Vessel Code[4]. The method uses fracture mechanics concepts and is based on the reference nil-ductility temperature ($RT_{NDT}$).

$RT_{NDT}$ is defined as the greater of either the drop weight nil-ductility transition temperature (NDTT per ASTM E208[5]) or the temperature 60°F less than the 50 ft-lb (and 35-mil lateral expansion) temperature as determined from Charpy specimens oriented normal (transverse) to the major working direction of the plate. The $RT_{NDT}$ of a given material is used to index that material to a reference stress intensity factor curve ($K_{IR}$ curve) which appears in Appendix G to the ASME Code. The $K_{IR}$ curve is a lower bound of dynamic, crack arrest, and static fracture toughness results obtained from several heats of pressure vessel steel. When a given material is indexed to the $K_{IR}$ curve, allowable stress intensity factors can be obtained for this material as a function of temperature. Allowable operating limits can then be determined using these allowable stress intensity factors.

$RT_{NDT}$ and, in turn, the operating limits of nuclear power plants can be adjusted to account for the effects of radiation on the reactor vessel material properties. The radiation embrittlement changes in mechanical properties of a given reactor pressure vessel steel can be monitored by a reactor surveillance program, such as the Diablo Canyon Unit 2 Reactor Vessel Radiation Surveillance Program[3], in which a surveillance capsule is periodically removed from the operating nuclear reactor and the encapsulated specimens tested. The increase in the average Charpy V-notch 30 ft-lb temperature ($\Delta RT_{NDT}$) due to irradiation is added to the initial $RT_{NDT}$ to adjust the $RT_{NDT}$ for radiation embrittlement. This adjusted reference temperature ($ART = IRT_{NDT} + \Delta RT_{NDT} + M$) is used to index

the material to the $K_{IR}$ curve and, in turn, to set operating limits for the nuclear power plant which take into account the effects of irradiation on the reactor vessel materials.

# SECTION 4.0
# DESCRIPTION OF PROGRAM

Six surveillance capsules for monitoring the effects of neutron exposure on the Diablo Canyon Unit 2 reactor pressure vessel core region materials were inserted in the reactor vessel prior to initial plant start-up. The six capsules were positioned in the reactor vessel between the neutron shielding pads and the vessel wall as shown in Figure 4-1. The vertical center of the capsules is opposite the vertical center of the core.

Capsule Y was removed after 7.0 Effective Full Power Years (EFPY) of plant operation. The capsule contained specimens made from intermediate shell plate B5454-1, weld metal made from sections of plate B5454-1 and adjoining intermediate shell plate B5454-2 using weld wire (Heat 21935/12008) representative of that used in the original fabrication, and heat-affected-zone specimens obtained from the weld-heat-affected zone of plate B5454-1. Additionally, tensile, bend bar, and 1/2T compact tension test specimens were included in the capsule (Figure 4-2).

Test material obtained from the intermediate shell plate (after thermal heat treatment and forming of the plate) was taken at least one plate thickness (9 5/8 inches) from the quenched edges of the plate. All test specimens were machined from the 1/4 thickness location of the plate after performing a simulated postweld stress-relieving treatment. Specimens were machined from weld metal and the heat-affected-zone (HAZ) metal of a stress-relieved weldment joining sections of two intermediate shell plates. All heat-affected-zone specimens were obtained from the weld heat-affected-zone of plate B5454-1.

Charpy V-notch impact specimens from intermediate shell plate B5454-1 were machined in both the longitudinal orientation (longitudinal axis of specimen parallel to major working direction) and transverse orientation (longitudinal axis of specimen perpendicular to major working direction). The core region weld Charpy impact specimens were machined from the weldment such that the long dimension of the Charpy was normal to the weld direction; the notch was machined such that the direction of crack propagation in the specimen was in the weld direction.

Capsule Y also contained one bend bar specimen from intermediate shell plate B5454-1, machined such that the simulated crack in the specimen would propagate in the rolling direction of the plate. All specimens were fatigue pre-cracked according to ASTM E399.

The compact tension test specimens from plate B5454-1 were machined in the transverse and longitudinal orientation, to obtain fracture toughness data both normal and parallel to the rolling direction of the plate. Compact tension test specimens from the weld metal were machined normal to the weld direction, with the notch oriented in the direction of the weld. All specimens were fatigue pre-cracked according to ASTM E399.

The chemical composition and heat treatment of the surveillance material is presented in Tables 4-1 through 4-4. The chemical analysis reported in Table 4-1 was obtained from unirradiated material used in the surveillance program[3]. In addition, a chemical analysis using Inductively Coupled Plasma Spectrometry (ICPS) was performed on four irradiated Charpy specimens, one plate metal and three weld metal, and is presented in Table 4-3. The chemistry results from the NBS certified reference standards are reported in Table 4-4.

Capsule Y contained dosimeter wires of pure copper, nickel, and aluminum-0.15 weight percent cobalt wire (cadmium-shielded and unshielded). In addition, cadmium shielded dosimeters of neptunium ($Np^{237}$) and uranium ($U^{238}$) were placed in the capsule to measure the integrated flux at specific neutron energy levels.

Thermal monitors made from the two low-melting eutectic alloys and sealed in Pyrex tubes were included in the capsule. These thermal monitors were used to define the maximum temperature attained by the test specimens during irradiation. The composition of the two alloys and their melting points are as follows:

| | |
|---|---|
| 2.5% Ag, 97.5% Pb | Melting Point: 579°F (304°C) |
| 1.75% Ag, 0.75% Sn, 97.5% Pb | Melting Point: 590°F (310°C) |

The arrangement of the various mechanical specimens, dosimeters and thermal monitors contained in Capsule Y is shown in Figure 4-2.

| TABLE 4-1 | | |
|---|---|---|
| Chemical Composition (wt%) of the Unirradiated Diablo Canyon Unit 2 Reactor Vessel Surveillance Materials[3] | | |
| Element | Plate B5454-1 (W Analysis) | Weld Metal[a] (W Analysis) |
| C | 0.23 | 0.13 |
| S | 0.010 | 0.010 |
| $N_2$ | 0.008 | 0.008 |
| Co | 0.002 | 0.012 |
| Cu | 0.15 | 0.22 |
| Si | 0.22 | 0.22 |
| Mo | 0.43 | 0.47 |
| Ni | 0.67 | 0.83 |
| Mn | 1.28 | 1.32 |
| Cr | 0.071 | 0.031 |
| V | 0.001 | 0.001 |
| P | 0.012 | 0.017 |
| Sn | 0.010 | 0.010 |
| Al | 0.031 | 0.009 |

NOTE:

a) Surveillance weldment made from sections of plate B5454-1 and adjoining intermediate shell plate B5454-2 using weld wire representative of that used in the original fabrication.

| TABLE 4-2 | | | |
|---|---|---|---|
| Heat Treatment of the Diablo Canyon Unit 2 Reactor Vessel Surveillance Materials[3] | | | |
| Material | Temperature (°F) | Time (hr) | Coolant |
| Intermediate Shell Plate B5454-1 | 1550 - 1650 | 4 | Water quench |
| | 1225 ± 25 | 4 | Air cool |
| | 1150 ± 25 | 40 | Furnace cool |
| Weld | 1150 ± 25 | 40 | Furnace cool |

| TABLE 4-3 | | | | |
|---|---|---|---|---|
| Chemical Composition of Four Diablo Canyon Unit 2 Charpy Specimens Removed from Surveillance Capsule Y | | | | |
| | Weld Metal | | | Plate B5454-1 |
| Element | PW-61 | PW-62 | PW-65 | PT-74 |
| Al | <0.02 | <0.02 | <0.02 | 0.03 |
| As | <0.02 | 0.02 | <0.02 | <0.02 |
| B | 0.008 | 0.010 | 0.009 | 0.008 |
| Co | 0.014 | 0.018 | 0.018 | 0.011 |
| Cr | 0.041 | 0.049 | 0.049 | 0.078 |
| Cu | 0.196 | 0.240 | 0.230 | 0.137 |
| Fe | matrix-- | -- | -- | -- |
| Mn | 1.24 | 1.53 | 1.48 | 1.27 |
| Mo | 0.45 | 0.56 | 0.54 | 0.47 |
| Ni | 0.763 | 0.958 | 0.910 | 0.668 |
| P | 0.015 | 0.019 | 0.018 | 0.009 |
| Si | 0.198 | 0.167 | 0.176 | 0.201 |
| Sn | <0.01 | <0.01 | <0.01 | <0.01 |
| Ti | <0.002 | <0.002 | <0.002 | <0.002 |
| V | <0.004 | <0.004 | <0.004 | <0.004 |
| W | <0.05 | <0.05 | <0.05 | <0.05 |
| Zr | <0.01 | <0.01 | <0.01 | <0.01 |
| C | 0.128 | 0.124 | 0.121 | 0.237 |
| S | 0.007 | 0.008 | 0.008 | 0.015 |

METHOD OF ANALYSIS:
Metals - Inductively Coupled Plasma Spectrometry
Carbon - LECO Analyzer
Sulfur - Combustion/titration
Silicon - Gravimetric

| TABLE 4-4 | | | | |
|---|---|---|---|---|
| Chemistry Results from the Low Alloy Steel NBS Certified Reference Standards | | | | |
| | Concentration in Weight Percent | | | |
| | NBS 361 | | NBS 362 | |
| Metals | Certified | Measured | Certified | Measured |
| Al | 0.021 | 0.021 | 0.095 | 0.076 |
| As | 0.017 | 0.02 | 0.092 | 0.089 |
| B | 0.0004 | <0.002 | 0.0025 | 0.003 |
| Co | 0.032 | 0.030 | 0.30 | 0.295 |
| Cr | 0.694 | 0.073 | 0.30 | 0.288 |
| Cu | 0.042 | 0.041 | 0.50 | 0.481 |
| Fe | matrix-- | -- | -- | -- |
| Mn | 0.66 | 0.632 | 1.04 | 0.968 |
| Mo | 0.19 | 0.19 | 0.068 | 0.060 |
| Ni | 2.00 | 1.97 | 0.59 | 0.56 |
| P | 0.014 | 0.014 | 0.041 | 0.034 |
| Si | -- | -- | 0.390 | 0.383 |
| Sn | 0.010 | <0.01 | 0.016 | 0.015 |
| Ti | 0.020 | 0.014 | 0.08 | 0.021 |
| V | 0.011 | 0.010 | 0.04 | 0.035 |
| W | 0.017 | <0.05 | 0.20 | 0.205 |
| Zr | 0.009 | 0.009 | 0.19 | 0.12 |
| C | 0.383 | 0.384 | 0.160 | 0.158 |
| S | -- | -- | 0.036 | 0.036 |

NOTES:

NBS 363: Certified Si % = 0.74
Measured Si % = 0.711

NBS 364: Certified S % = 0.025
Measured S % = 0.026

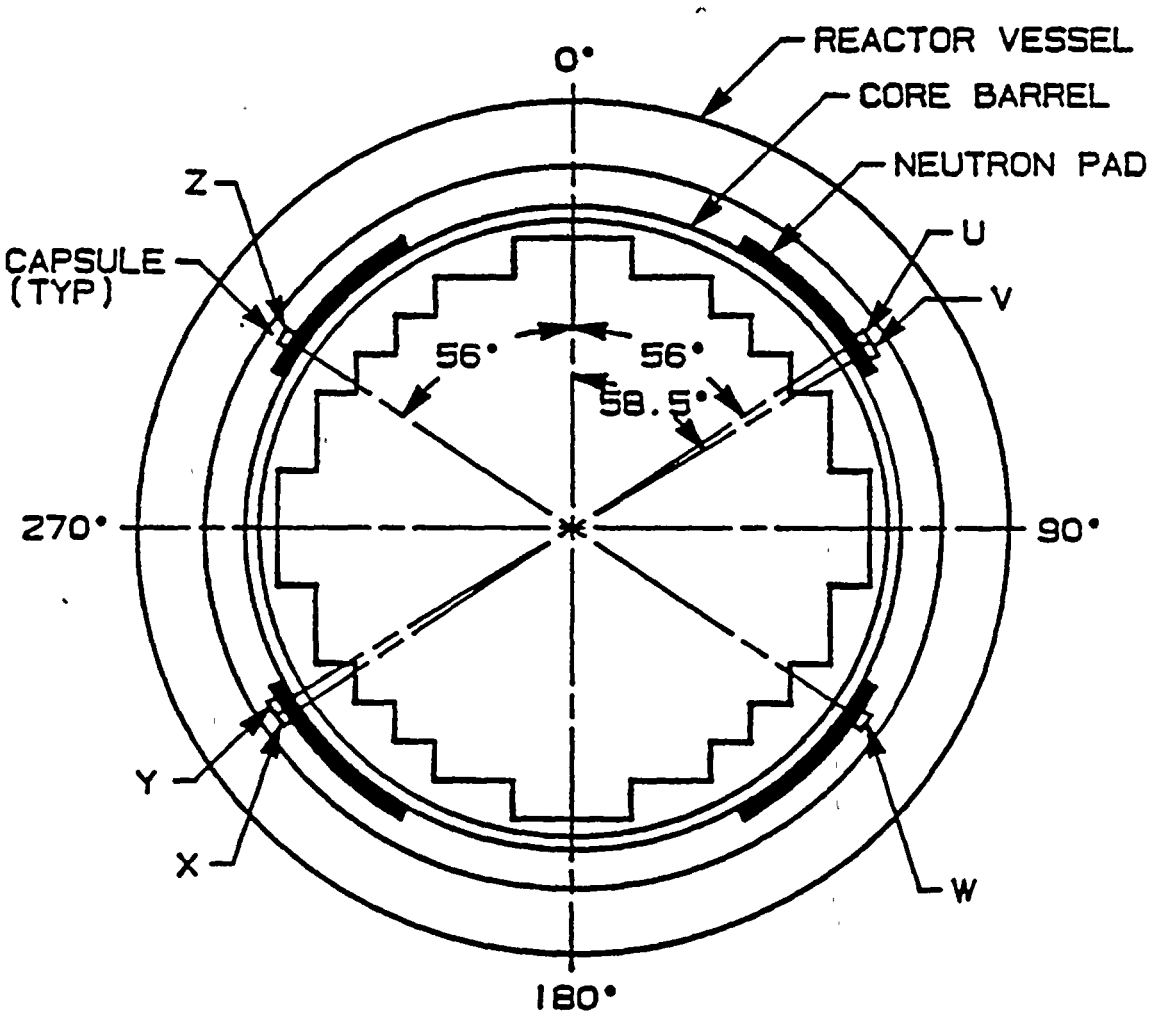


Figure 4-1 Arrangement of Surveillance Capsules in the Diablo Canyon Unit 2 Reactor Vessel

LEGEND:

PL - PLATE B5454-1 (LONGITUDINAL)

PT - PLATE B5454-1 (TRANSVERSE)

PW - WELD METAL

PH - HEAT-AFFECTED-ZONE MATERIAL

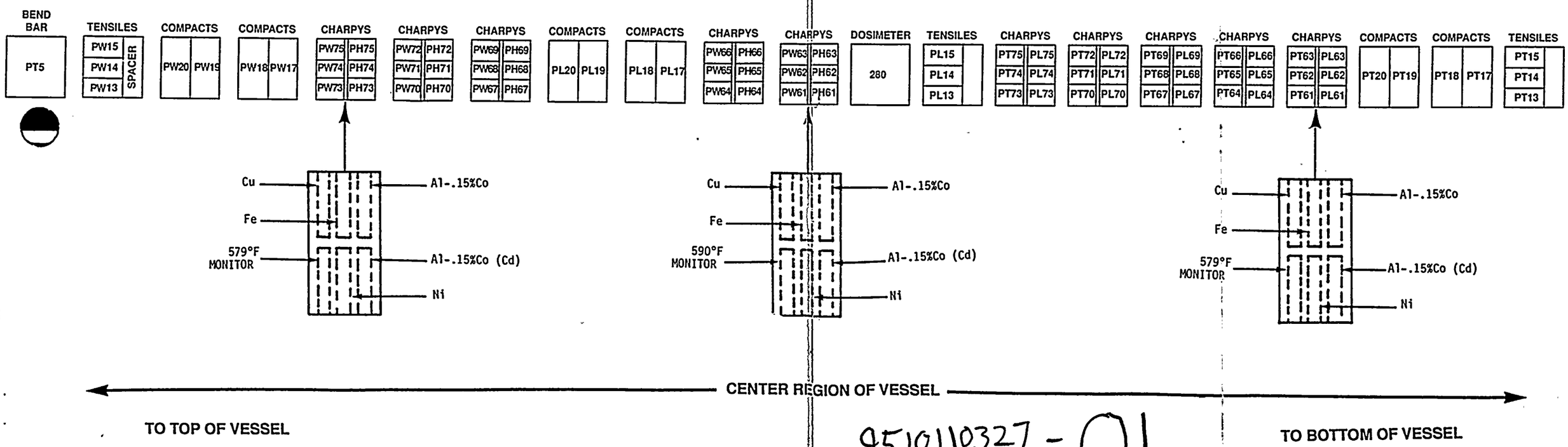


9510110327 - 01

Figure 4-2 Capsule Y Diagram Showing the Location of Specimens, Thermal Monitors and Dosimeter

## SECTION 5.0
## TESTING OF SPECIMENS FROM CAPSULE Y

### 5.1 Overview

The post-irradiation mechanical testing of the Charpy V-notch and tensile specimens was performed at the Remote Metallographic Facility at the Westinghouse Science and Technology Center (STC). Testing was performed in accordance with 10 CFR Part 50, Appendix H[6], ASTM Specification E185-82[7], and Westinghouse Procedure MHL 8402, Revision 2, as modified by Westinghouse RMF Procedures 8102, Revision 1 and 8103, Revision 1.

Upon receipt of the capsule at the hot cell laboratory, the specimens and spacer blocks were carefully removed, inspected for identification number, and checked against the master list in WCAP-8783[3].

Thermal monitors were not found in the capsule. After examination of the capsule contents, it was concluded that the thermal monitors were never placed inside the thermal monitor blocks. A scanning electron microscope (SEM) was used in combination with energy dispersive spectroscopy (EDS) on the capsule flux monitors to check the wire chemistries to ensure that the thermal monitors were not placed in the wrong location. Examination of the flux monitors with EDS indicated that lead was not present in any of these wires. This examination verified that the thermal monitors were not present.

The Charpy impact tests were performed per ASTM Specification E23-93a[8] and RMF Procedure 8103, Revision 1, on a Tinius-Olsen Model 74, 358J machine. The tup (striker) of the Charpy machine is instrumented with a GRC 830-I instrumentation system, feeding into an IBM compatible 486 computer. With this system, load-time and energy-time signals can be recorded in addition to the standard measurement of Charpy energy ($E_D$). From the load-time curve (Appendix A), the load of general yielding ($P_{GY}$), time to general yielding ($t_{GY}$), maximum load ($P_M$), and time to maximum load ($t_M$) can be determined. Under some test conditions, a sharp drop in load indicative of fast fracture was observed. The load at which fast fracture was initiated is identified as the fast fracture load ($P_F$), and the load at which fast fracture terminated is identified as the arrest load ($P_A$).

The energy at maximum load ($E_M$) was determined by comparing the energy-time record and the load-time record. The energy at maximum load is approximately equivalent to the energy required to initiate a crack in the specimen. Therefore, the propagation energy for the crack ($E_p$) is the difference between the total energy to fracture ($E_D$) and the energy at maximum load ($E_M$).

The yield stress ($\sigma_Y$) was calculated from the three-point bend formula having the following expression:

$$\sigma_Y = P_{GY} * \{ L / [ B * ( W - a )^2 * C ]\} \quad (1)$$

where L is the distance between the specimen supports in the impact testing machine; B is the width of the specimen measured parallel to the notch; W is the height of the specimen, measured perpendicularly to the notch; and a is the notch depth. The constant C is dependent on the notch flank angle ($\phi$), notch root radius ($\rho$), and the type of loading (i.e., pure bending or three-point bending).

In three-point bending a Charpy specimen in which $\phi = 45°$ and $\rho = 0.010$ inches, Equation 1 is valid with C = 1.21. Therefore (for L = 4W),

$$\sigma_Y = P_{GY} * \{ L / [ B * ( W - a )^2 * 1.21 ] \} = [ 3.31 P_{GY} W ] / [ B ( W - a )^2 ] \quad (2)$$

For the Charpy specimens, B is 0.394 in., W is 0.394 in., and a is 0.079 in. Equation 2 then reduces to:

$$\sigma_Y = 33.3 * P_{GY} \quad (3)$$

where $\sigma_Y$ is in units of psi and $P_{GY}$ is in units of lb. The flow stress was calculated from the average of the yield and maximum loads, also using the three-point bend formula.

Symbol A is columns 4, 5, and 6 of Tables 5-5 through 5-8 is the cross-sectional area under the notch of the Charpy specimens:

$$A = B * (W - a) = 0.1241 \text{ square inches} \quad (4)$$

Percent shear was determined from post-fracture photographs using the ratio-of-areas methods in compliance with ASTM Specification A370-92[9]. The lateral expansion was measured using a dial gage rig similar to that shown in the same specification.

Tension tests were performed on a 20,000-pound Instron Model 1115, split-console test machine, per ASTM Specification E8-93[10] and E21-92[11], and RMF Procedure 8102, Revision 1. The upper pull rod of the test machine was connected through a universal joint to improve axiality of loading. The tests were conducted at a constant crosshead speed of 0.05 inches per minute throughout the test.

Extension measurements were made with a linear variable displacement transducer (LVDT) extensometer. The extensometer knife edges were spring-loaded to the specimen and operated through specimen failure. The extensometer gage length is 1.00 inch. The extensometer is rated as Class B-2 per ASTM E83-93[12].

Elevated test temperatures were obtained with a three-zone electric resistance split-tube furnace with a nine-inch hot zone. All tests were conducted in air.

Because of the difficulty in remotely attaching a thermocouple directly to the specimen, the following procedure was used to monitor specimen temperature. Chromel-alumel thermocouples were inserted in shallow holes in the center of each end of the gage section of a dummy specimen and in each grip. In the test configuration, with a slight load on the specimen, a plot of specimen temperature versus upper and lower grip and controller temperatures was developed over the range of room temperature to 550°F (288°C). The upper grip was used to control the furnace temperature. During the actual testing, the grip temperatures were used to obtain desired specimen temperatures. Experiments indicate that this method is accurate to ±2°F.

The yield load, ultimate load, fracture load, total elongation, and uniform elongation were determined directly from the load-extension curve. The yield strength, ultimate strength, and fracture strength were calculated using the original cross-sectional area. The final diameter and final gage length were determined from post-fracture photographs. The fracture area used to calculate the fracture stress (true stress at fracture) and percent reduction in area was computed using the final diameter measurement.

## 5.2 Charpy V-Notch Impact Test Results

The results of the Charpy V-notch impact tests performed on the various materials contained in Capsule Y, which was irradiated to $1.32 \times 10^{19}$ n/cm$^2$ (E > 1.0 MeV), are presented in Tables 5-1 through 5-8 and are compared with unirradiated results as shown in Figures 5-13 through 5-24. The transition temperature increases and upper shelf energy decreases for the Capsule Y materials are summarized in Table 5-9.

Irradiation of the reactor vessel intermediate shell plate B5454-1 Charpy specimens oriented with the longitudinal axis of the specimen parallel to the major rolling direction of the plate (longitudinal orientation) to $1.32 \times 10^{19}$ n/cm$^2$ (E > 1.0 MeV) (Figure 5-13) resulted in a 30 ft-lb transition temperature increase of 113.0°F and a 50 ft-lb transition temperature increase of 119.8°F. This

resulted in an irradiated 30 ft-lb transition temperature of 117.6°F and an irradiated 50 ft-lb transition temperature of 153.1°F (longitudinal orientation).

The average upper shelf energy (USE) of the intermediate shell plate B5454-1 Charpy specimens (longitudinal orientation) resulted in a energy decrease of 26.6 ft-lb after irradiation to $1.32 \times 10^{19}$ n/cm$^2$ (E > 1.0 MeV). This results in an irradiated average USE of 118.1 ft-lb (Figure 5-13).

Irradiation of the reactor vessel intermediate shell plate B5454-1 Charpy specimens oriented with the longitudinal axis of the specimen perpendicular to the major rolling direction of the plate (transverse orientation) to $1.32 \times 10^{19}$ n/cm$^2$ (E > 1.0 MeV) (Figure 5-16) resulted in a 30 ft-lb transition temperature increase of 110.7°F and a 50 ft-lb transition temperature increase of 111.1°F. This resulted in an irradiated 30 ft-lb transition temperature of 137.3°F and an irradiated 50 ft-lb transition temperature of 185.7°F (transverse orientation).

The average upper shelf energy (USE) of the intermediate shell plate B5454-1 Charpy specimens (transverse orientation) resulted in a energy decrease of 6.3 ft-lb after irradiation to $1.32 \times 10^{19}$ n/cm$^2$ (E > 1.0 MeV). This results in an irradiated average USE of 88.6 ft-lb (Figure 5-16).

Irradiation of the surveillance weld metal Charpy specimens to $1.32 \times 10^{19}$ n/cm$^2$ (E > 1.0 MeV) (Figure 5-19) resulted in a 30 ft-lb transition temperature shift of 212.5°F and a 50 ft-lb transition temperature increase of 246.0°F. This results in an irradiated 30 ft-lb transition temperature of 198.9°F and an irradiated 50 ft-lb transition temperature of 260.9°F.

The average upper shelf energy (USE) of the surveillance weld metal resulted in an energy decrease of 43.6 ft-lb after irradiation to $1.32 \times 10^{19}$ n/cm$^2$ (E > 1.0 MeV). This resulted in an irradiated average USE of 77.3 ft-lb (Figure 5-19).

Irradiation of the reactor vessel weld HAZ metal Charpy specimens to $1.32 \times 10^{19}$ n/cm$^2$ (E > 1.0 MeV) (Figure 5-22) resulted in a 30 ft-lb transition temperature increase of 255.3°F and a 50 ft-lb transition temperature increase of 258.1°F. This resulted in an irradiated 30 ft-lb transition temperature of 27.9°F and an irradiated 50 ft-lb transition temperature of 105.8°F.

The average upper shelf energy (USE) of the weld HAZ metal resulted in an energy decrease of 55.2 ft-lb after irradiation to $1.32 \times 10^{19}$ n/cm$^2$ (E > 1.0 MeV). This resulted in an irradiated average USE of 92.3 ft-lb (Figure 5-22).

The fracture appearance of each irradiated Charpy specimen from the various materials is shown in Figures 5-25 through 5-28 and show an increasingly ductile or tougher appearance with increasing test temperature.

A comparison of the measured 30 ft-lb transition temperature increases and upper shelf energy decreases for the various Diablo Canyon Unit 2 surveillance materials with predicted values using the methods of NRC Regulatory Guide 1.99, Revision 2[1], is presented in Table 5-10 and led to the following conclusions:

- The 30 ft-lb transition temperature increases of intermediate shell plate B5454-1 are in good agreement with the Regulatory Guide 1.99, Revision 2, predictions and the USE decreases are less than the Regulatory Guide 1.99, Revision 2, predictions.

- The 30 ft-lb transition temperature increases and USE decreases of the weld metal are less than the Regulatory Guide 1.99, Revision 2, predictions.

The load-time records for the individual instrumented Charpy specimen tests are presented in Appendix A.

5.3 Tensile Test Results

The results of the tensile tests performed on the various materials contained in Capsule Y, irradiated to $1.32 \times 10^{19}$ n/cm$^2$ (E > 1.0 MeV), are presented in Table 5-11 and are compared with unirradiated results as shown in Figures 5-29 through 5-31.

The results of the tensile tests performed on the intermediate shell plate B5454-1 (longitudinal orientation) indicated that irradiation to $1.32 \times 10^{19}$ n/cm$^2$ (E > 1.0 MeV) caused a 15 to 20 ksi increase in the 0.2 percent offset yield strength and a 15 to 18 ksi increase in the ultimate tensile strength when compared to unirradiated data (Figure 5-29).

The results of the tensile tests performed on the intermediate shell plate B5454-1 (transverse orientation) indicated that irradiation to $1.32 \times 10^{19}$ n/cm$^2$ (E > 1.0 MeV) caused a 7 to 16 ksi increase in the 0.2 percent offset yield strength and a 13 to 15 ksi increase in the ultimate tensile strength when compared to unirradiated data (Figure 5-30).

The results of the tensile tests performed on the surveillance weld metal indicated that irradiation to $1.32 \times 10^{19}$ n/cm$^2$ (E > 1.0 MeV) caused a 23 to 26 ksi increase in the 0.2 percent offset yield strength and a 22 to 28 ksi increase in the ultimate tensile strength when compared to unirradiated data (Figure 5-31).

The fractured tensile specimens for the intermediate shell plate B5454-1 material are shown in Figures 5-32 and 5-33, while the fractured specimens for the surveillance weld metal are shown in Figure 5-34.

The engineering stress-strain curves for the tensile tests are shown in Figures 5-35 through 5-40. The true stress-strain curves for the tensile tests are shown in Figures 5-41 through 5-46.

## 5.4 Bend Bar and 1/2T Compact Tension Specimens

Per the surveillance capsule testing contract with the Pacific Gas and Electric Company, bend bar and 1/2T compact tension specimens will not be tested. The specimens will be stored at the Westinghouse Science and Technology Center Hot Cell.

TABLE 5-1

Charpy V-notch Data for the Diablo Canyon Unit 2 Intermediate Shell Plate B5454-1 Irradiated to a Fluence of $1.32 \times 10^{19}$ n/cm$^2$ (E > 1.0 MeV) (Longitudinal Orientation)

| Sample Number | Temperature | | Impact Energy | | Lateral Expansion | | Shear |
|---|---|---|---|---|---|---|---|
| | (°F) | (°C) | (ft-lb) | (J) | (mils) | (mm) | (%) |
| PL63 | 0 | -18 | 6 | 8 | 6 | 0.15 | 0 |
| PL64 | 25 | -4 | 6 | 8 | 4 | 0.10 | 5 |
| PL72 | 50 | 10 | 9 | 12 | 8 | 0.20 | 10 |
| PL68 | 72 | 22 | 15 | 20 | 13 | 0.33 | 10 |
| PL62 | 85 | 29 | 20 | 27 | 18 | 0.46 | 15 |
| PL73 | 100 | 38 | 34 | 46 | 27 | 0.69 | 20 |
| PL61 | 125 | 52 | 32 | 43 | 27 | 0.69 | 20 |
| PL75 | 150 | 66 | 48 | 65 | 38 | 0.97 | 25 |
| PL70 | 175 | 79 | 57 | 77 | 42 | 1.07 | 30 |
| PL66 | 185 | 85 | 59 | 80 | 43 | 1.09 | 30 |
| PL74 | 225 | 107 | 104 | 141 | 75 | 1.91 | 95 |
| PL69 | 250 | 121 | 104 | 141 | 77 | 1.96 | 100 |
| PL65 | 250 | 121 | 108 | 146 | 78 | 1.98 | 100 |
| PL71 | 300 | 149 | 117 | 159 | 86 | 2.18 | 100 |
| PL67 | 375 | 191 | 105 | 142 | 80 | 2.03 | 100 |

TABLE 5-2

Charpy V-notch Data for the Diablo Canyon Unit 2 Intermediate Shell Plate B5454-1 Irradiated to a Fluence of 1.32 x $10^{19}$ n/cm$^2$ (E > 1.0 MeV) (Transverse Orientation)

| Sample | Temperature | | Impact Energy | | Lateral Expansion | | Shear |
|---|---|---|---|---|---|---|---|
| Number | (°F) | (°C) | (ft-lb) | (J) | (mils) | (mm) | (%) |
| PT67 | 0 | -18 | 7 | 9 | 6 | 0.15 | 5 |
| PT75 | 25 | -4 | 9 | 12 | 8 | 0.20 | 5 |
| PT69 | 50 | 10 | 9 | 12 | 8 | 0.20 | 5 |
| PT70 | 73 | 23 | 20 | 27 | 16 | 0.41 | 10 |
| PT66 | 100 | 38 | 19 | 26 | 19 | 0.48 | 15 |
| PT62 | 125 | 52 | 24 | 33 | 22 | 0.56 | 20 |
| PT65 | 150 | 66 | 32 | 43 | 28 | 0.71 | 25 |
| PT61 | 175 | 79 | 40 | 54 | 36 | 0.91 | 30 |
| PT73 | 200 | 93 | 55 | 75 | 46 | 1.17 | 35 |
| PT68 | 225 | 107 | 69 | 94 | 55 | 1.40 | 65 |
| PT63 | 250 | 121 | 76 | 103 | 62 | 1.57 | 95 |
| PT72 | 300 | 149 | 89 | 121 | 70 | 1.78 | 100 |
| PT74 | 325 | 163 | 80 | 108 | 74 | 1.88 | 100 |
| PT64 | 400 | 204 | 80 | 108 | 65 | 1.65 | 100 |
| PT71 | 450 | 232 | 91 | 123 | 70 | 1.78 | 100 |

TABLE 5-3

Charpy V-notch Data for the Diablo Canyon Unit 2 Surveillance Weld Medal Irradiated to a Fluence of $1.32 \times 10^{19}$ n/cm$^2$ (E > 1.0 MeV)

| Sample Number | Temperature (°F) | Temperature (°C) | Impact Energy (ft-lb) | Impact Energy (J) | Lateral Expansion (mils) | Lateral Expansion (mm) | Shear (%) |
|---|---|---|---|---|---|---|---|
| PW63 | 50 | 10 | 6 | 8 | 4 | 0.10 | 5 |
| PW71 | 100 | 38 | 10 | 14 | 9 | 0.23 | 5 |
| PW72 | 150 | 66 | * | * | * | * | * |
| PW64 | 150 | 66 | 20 | 27 | 16 | 0.41 | 15 |
| PW67 | 185 | 85 | 22 | 30 | 22 | 0.56 | 20 |
| PW62 | 200 | 93 | 24 | 33 | 22 | 0.56 | 25 |
| PW75 | 210 | 99 | 37 | 50 | 31 | 0.79 | 55 |
| PW66 | 225 | 107 | 44 | 60 | 38 | 0.97 | 50 |
| PW68 | 250 | 121 | 50 | 68 | 32 | 0.81 | 60 |
| PW69 | 275 | 135 | 42 | 57 | 35 | 0.89 | 50 |
| PW65 | 300 | 149 | 68 | 92 | 55 | 1.40 | 100 |
| PW70 | 325 | 163 | 68 | 92 | 57 | 1.45 | 100 |
| PW73 | 375 | 191 | 69 | 94 | 59 | 1.50 | 100 |
| PW61 | 400 | 204 | 73 | 99 | 59 | 1.50 | 100 |
| PW74 | 450 | 232 | 77 | 104 | 60 | 1.52 | 100 |

NOTE:
* Specimen alignment was incorrect in impact machine; test is not valid.

TABLE 5-4

Charpy V-notch Data for the Diablo Canyon Unit 2 Heat-Affected-Zone (HAZ) Metal Irradiated to a Fluence of $1.32 \times 10^{19}$ n/cm$^2$ (E > 1.0 MeV)

| Sample | Temperature | | Impact Energy | | Lateral Expansion | | Shear |
|---|---|---|---|---|---|---|---|
| Number | (°F) | (°C) | (ft-lb) | (J) | (mils) | (mm) | (%) |
| PH65 | -50 | -46 | 3 | 4 | 7 | 0.18 | 5 |
| PH64 | 0 | -18 | 19 | 26 | 12 | 0.30 | 25 |
| PH72 | 50 | 10 | 28 | 38 | 26 | 0.66 | 25 |
| PH73 | 65 | 18 | 62 | 84 | 47 | 1.19 | 70 |
| PH69 | 72 | 22 | 50 | 68 | 38 | 0.97 | 60 |
| PH63 | 100 | 38 | 30 | 41 | 27 | 0.69 | 40 |
| PH68 | 125 | 52 | 73 | 99 | 54 | 1.37 | 60 |
| PH75 | 150 | 66 | 58 | 79 | 42 | 1.07 | 40 |
| PH71 | 175 | 79 | 72 | 98 | 56 | 1.42 | 90 |
| PH61 | 200 | 93 | 47 | 64 | 42 | 1.07 | 70 |
| PH67 | 250 | 121 | 94 | 127 | 74 | 1.88 | 100 |
| PH62 | 300 | 149 | 71 | 96 | 59 | 1.50 | 100 |
| PH70 | 325 | 163 | 97 | 132 | 73 | 1.85 | 100 |
| PH74 | 350 | 177 | 75 | 102 | 57 | 1.45 | 100 |
| PH66 | 400 | 204 | 104 | 141 | 73 | 1.85 | 100 |

TABLE 5-5

Instrumented Charpy Impact Test Results for the Diablo Canyon Unit 2 Intermediate Shell Plate B5454-1
Irradiated to a Fluence of 1.32 x $10^{19}$ n/cm$^2$ (E > 1.0 MeV)
(Longitudinal Orientation)

| Sample No. | Test Temp. (°F) | Charpy Energy $E_D$ (ft-lb) | Normalized Energies (ft-lb/in$^2$) | | | Yield Load $P_{GY}$ (lbs) | Time to Yield $t_{GY}$ (msec) | Max. Load $P_M$ (lbs) | Time to Max. $t_M$ (msec) | Fract. Load $P_F$ (lbs) | Arrest Load $P_A$ (lbs) | Yield Stress $\sigma_Y$ (ksi) | Flow Stress (ksi) |
|---|---|---|---|---|---|---|---|---|---|---|---|---|---|
| | | | Charpy Ed/A | Max. Em/A | Prop. Ep/A | | | | | | | | |
| PL63 | 0 | 6 | 48 | 24 | 25 | 3066 | 0.13 | 3066 | 0.13 | 3066 | 109 | 102 | 102 |
| PL64 | 25 | 6 | 48 | 24 | 24 | 3141 | 0.13 | 3141 | 0.13 | 3141 | 239 | 104 | 104 |
| PL72 | 50 | 9 | 72 | 31 | 41 | 3437 | 0.15 | 3437 | 0.15 | 3437 | 363 | 114 | 114 |
| PL68 | 72 | 15 | 121 | 76 | 44 | 3594 | 0.15 | 4032 | 0.23 | 4032 | 466 | 119 | 127 |
| PL62 | 85 | 20 | 161 | 109 | 52 | 3439 | 0.14 | 4115 | 0.30 | 4115 | 737 | 114 | 125 |
| PL73 | 100 | 34 | 274 | 233 | 41 | 3414 | 0.15 | 4582 | 0.52 | 4582 | 257 | 113 | 133 |
| PL61 | 125 | 32 | 258 | 186 | 71 | 3365 | 0.14 | 4412 | 0.44 | 4412 | 828 | 112 | 129 |
| PL75 | 150 | 48 | 387 | 294 | 93 | 3275 | 0.15 | 4495 | 0.64 | 4495 | 1330 | 109 | 129 |
| PL70 | 175 | 57 | 459 | 293 | 166 | 3254 | 0.14 | 4449 | 0.63 | 4343 | 1840 | 108 | 128 |
| PL66 | 185 | 59 | 475 | 307 | 168 | 3221 | 0.15 | 4484 | 0.67 | 4425 | 2047 | 107 | 128 |
| PL74 | 225 | 104 | 837 | 313 | 525 | 3043 | 0.14 | 4378 | 0.69 | 2985 | 2150 | 101 | 123 |
| PL69 | 250 | 104 | 837 | 299 | 538 | 2966 | 0.14 | 4258 | 0.68 | N/A | N/A | 99 | 120 |
| PL65 | 250 | 108 | 870 | 313 | 556 | 3040 | 0.14 | 4423 | 0.69 | N/A | N/A | 101 | 124 |
| PL71 | 300 | 117 | 942 | 306 | 636 | 3018 | 0.14 | 4286 | 0.69 | N/A | N/A | 100 | 121 |
| PL67 | 375 | 105 | 845 | 292 | 553 | 2917 | 0.14 | 4119 | 0.68 | N/A | N/A | 97 | 117 |

N/A - Fully ductile fracture. No arrest load.

TABLE 5-6

Instrumented Charpy Impact Test Results for the Diablo Canyon Unit 2 Intermediate Shell Plate B5454-1
Irradiated to a Fluence of 1.32 x $10^{19}$ n/cm$^2$ (E > 1.0 MeV)
(Transverse Orientation)

| Sample No. | Test Temp. (°F) | Charpy Energy $E_D$ (ft-lb) | Normalized Energies (ft-lb/in$^2$) | | | Yield Load $P_{GY}$ (lbs) | Time to Yield $t_{GY}$ (msec) | Max. Load $P_M$ (lbs) | Time to Max. $t_M$ (msec) | Fract. Load $P_F$ (lbs) | Arrest Load $P_A$ (lbs) | Yield Stress $\sigma_Y$ (ksi) | Flow Stress (ksi) |
|---|---|---|---|---|---|---|---|---|---|---|---|---|---|
| | | | Charpy Ed/A | Max. Em/A | Prop. Ep/A | | | | | | | | |
| PT67 | 0 | 7 | 56 | 30 | 26 | 3548 | 0.14 | 3548 | 0.14 | 3548 | 157 | 118 | 118 |
| PT75 | 25 | 9 | 72 | 36 | 36 | 3654 | 0.16 | 3654 | 0.16 | 3654 | 268 | 121 | 121 |
| PT69 | 50 | 9 | 72 | 35 | 37 | 3609 | 0.16 | 3609 | 0.16 | 3609 | 301 | 120 | 120 |
| PT70 | 73 | 20 | 161 | 107 | 54 | 3501 | 0.14 | 4165 | 0.29 | 4165 | 473 | 116 | 127 |
| PT66 | 100 | 19 | 153 | 81 | 72 | 3359 | 0.14 | 3862 | 0.25 | 3862 | 264 | 112 | 120 |
| PT62 | 125 | 24 | 193 | 127 | 66 | 3311 | 0.14 | 4112 | 0.34 | 4112 | 1016 | 110 | 123 |
| PT65 | 150 | 32 | 258 | 164 | 94 | 3387 | 0.17 | 4174 | 0.42 | 4174 | 1624 | 113 | 126 |
| PT61 | 175 | 40 | 322 | 185 | 137 | 3173 | 0.16 | 4202 | 0.46 | 4202 | 1833 | 105 | 122 |
| PT73 | 200 | 55 | 443 | 228 | 215 | 3118 | 0.14 | 4354 | 0.53 | 4330 | 1981 | 104 | 124 |
| PT68 | 225 | 69 | 556 | 221 | 335 | 3023 | 0.15 | 4186 | 0.54 | 3810 | 3382 | 100 | 120 |
| PT63 | 250 | 76 | 612 | 217 | 395 | 3021 | 0.14 | 4167 | 0.52 | 3616 | 2894 | 100 | 119 |
| PT72 | 300 | 89 | 717 | 280 | 437 | 2950 | 0.14 | 4180 | 0.64 | N/A | N/A | 98 | 118 |
| PT74 | 325 | 80 | 644 | 212 | 432 | 2883 | 0.14 | 4106 | 0.52 | N/A | N/A | 96 | 116 |
| PT64 | 400 | 80 | 644 | 201 | 443 | 2802 | 0.14 | 3947 | 0.52 | N/A | N/A | 93 | 112 |
| PT71 | 450 | 91 | 733 | 232 | 501 | 2686 | 0.18 | 3861 | 0.62 | N/A | N/A | 89 | 109 |

N/A - Fully ductile fracture. No arrest load.

TABLE 5-7

Instrumented Charpy Impact Test Results for the Diablo Canyon Unit 2 Surveillance Weld Metal Irradiated to a Fluence of $1.32 \times 10^{19}$ n/cm$^2$ (E > 1.0 MeV)

| Sample No. | Test Temp. (°F) | Charpy Energy $E_D$ (ft-lb) | Normalized Energies (ft-lb/in$^2$) | | | Yield Load $P_{GY}$ (lbs) | Time to Yield $t_{GY}$ (msec) | Max. Load $P_M$ (lbs) | Time to Max. $t_M$ (msec) | Fract. Load $P_F$ (lbs) | Arrest Load $P_A$ (lbs) | Yield Stress $\sigma_Y$ (ksi) | Flow Stress (ksi) |
|---|---|---|---|---|---|---|---|---|---|---|---|---|---|
| | | | Charpy Ed/A | Max. Em/A | Prop. Ep/A | | | | | | | | |
| PW63 | 50 | 6 | 48 | 22 | 26 | 3018 | 0.13 | 3018 | 0.13 | 3018 | 130 | 100 | 100 |
| PW71 | 100 | 10 | 81 | 45 | 35 | 3835 | 0.18 | 3835 | 0.18 | 3835 | 140 | 127 | 127 |
| PW72 | 150 | * | * | * | * | * | * | * | * | * | * | * | * |
| PW64 | 150 | 20 | 161 | 125 | 36 | 3455 | 0.14 | 4282 | 0.32 | 4282 | 325 | 115 | 128 |
| PW67 | 185 | 22 | 177 | 102 | 75 | 3474 | 0.15 | 4083 | 0.28 | 4083 | 1197 | 115 | 126 |
| PW62 | 200 | 24 | 193 | 110 | 83 | 3398 | 0.14 | 4115 | 0.30 | 4115 | 1530 | 113 | 125 |
| PW75 | 210 | 37 | 298 | 142 | 156 | 3376 | 0.16 | 4230 | 0.37 | 4230 | 2963 | 112 | 126 |
| PW66 | 225 | 44 | 354 | 169 | 185 | 3492 | 0.17 | 4329 | 0.42 | 4329 | 2917 | 116 | 130 |
| PW68 | 250 | 50 | 403 | 218 | 184 | 3308 | 0.15 | 4327 | 0.50 | 4327 | 2578 | 110 | 127 |
| PW69 | 275 | 42 | 338 | 204 | 135 | 3253 | 0.14 | 4389 | 0.47 | 4389 | 2935 | 108 | 127 |
| PW65 | 300 | 68 | 548 | 213 | 334 | 3052 | 0.14 | 4208 | 0.51 | N/A | N/A | 101 | 121 |
| PW70 | 325 | 68 | 548 | 216 | 331 | 3063 | 0.14 | 4208 | 0.51 | N/A | N/A | 102 | 121 |
| PW73 | 375 | 69 | 556 | 214 | 341 | 3191 | 0.17 | 4066 | 0.52 | N/A | N/A | 106 | 121 |
| PW61 | 400 | 73 | 588 | ** | ** | ** | ** | ** | ** | ** | ** | ** | ** |
| PW74 | 450 | 77 | 620 | 209 | 411 | 3205 | 0.17 | 4066 | 0.51 | N/A | N/A | 106 | 121 |

* Specimen alignment was incorrect in impact machine; test not valid.
** Computer error - instrumented data not available for this specimen.
N/A Fully ductile fracture. No arrest load.

TABLE 5-8

Instrumented Charpy Impact Test Results for the Diablo Canyon Unit 2 Heat-Affected-Zone (HAZ) Metal Irradiated to a Fluence of 1.32 x $10^{19}$ n/cm$^2$ (E > 1.0 MeV)

| Sample No. | Test Temp. (°F) | Charpy Energy $E_D$ (ft-lb) | Normalized Energies (ft-lb/in$^2$) | | | Yield Load $P_{GY}$ (lbs) | Time to Yield $t_{GY}$ (msec) | Max. Load $P_M$ (lbs) | Time to Max. $t_M$ (msec) | Fract. Load $P_F$ (lbs) | Arrest Load $P_A$ (lbs) | Yield Stress $\sigma_Y$ (ksi) | Flow Stress (ksi) |
|---|---|---|---|---|---|---|---|---|---|---|---|---|---|
| | | | Charpy Ed/A | Max. Em/A | Prop. Ep/A | | | | | | | | |
| PH65 | -50 | 3 | 24 | 10 | 14 | 1790 | 0.09 | 1790 | 0.09 | 1790 | 116 | 59 | 59 |
| PH64 | 0 | 19 | 153 | 84 | 69 | 4337 | 0.17 | 4337 | 0.24 | 4337 | 1045 | 144 | 144 |
| PH72 | 50 | 28 | 225 | 112 | 114 | 3734 | 0.14 | 4307 | 0.29 | 4157 | 1379 | 124 | 134 |
| PH73 | 65 | 62 | 499 | 251 | 248 | 3684 | 0.14 | 4838 | 0.52 | 4838 | 3786 | 122 | 142 |
| PH69 | 72 | 50 | 403 | 264 | 138 | 3717 | 0.16 | 4712 | 0.55 | 4699 | 1132 | 123 | 140 |
| PH63 | 100 | 30 | 242 | 122 | 120 | 3472 | 0.14 | 4230 | 0.32 | 4230 | 2676 | 115 | 128 |
| PH68 | 125 | 73 | 588 | 257 | 331 | 3450 | 0.14 | 4630 | 0.55 | 4062 | 2889 | 115 | 134 |
| PH75 | 150 | 58 | 467 | 334 | 133 | 3465 | 0.14 | 4678 | 0.69 | 4568 | 1989 | 115 | 135 |
| PH71 | 175 | 72 | 580 | 324 | 256 | 3404 | 0.15 | 4629 | 0.67 | 4273 | 3271 | 113 | 133 |
| PH61 | 200 | 47 | 378 | 189 | 189 | 3318 | 0.14 | 4330 | 0.45 | 4309 | 3089 | 110 | 127 |
| PH67 | 250 | 94 | 757 | 306 | 451 | 3261 | 0.14 | 4485 | 0.65 | N/A | N/A | 108 | 129 |
| PH62 | 300 | 71 | 572 | 212 | 360 | 3202 | 0.17 | 4234 | 0.51 | N/A | N/A | 106 | 123 |
| PH70 | 325 | 97 | 781 | 296 | 485 | 3022 | 0.14 | 4260 | 0.67 | N/A | N/A | 100 | 121 |
| PH74 | 350 | 75 | 604 | 218 | 386 | 3046 | 0.16 | 4165 | 0.53 | N/A | N/A | 101 | 120 |
| PH66 | 400 | 104 | 837 | 293 | 544 | 3071 | 0.14 | 4227 | 0.67 | N/A | N/A | 102 | 121 |

N/A - Fully ductile fracture. No arrest load.

TABLE 5-9

Effect of Irradiation to 1.32 x 10 n/cm (E > 1.0 MeV) on the Notch Toughness Properties of the Diablo Canyon Unit 2 Reactor Vessel Surveillance Materials

| Material | Average 30 (ft-lb) Transition Temperature (°F) | | | Average 35 mil Lateral Expansion Temperature (°F) | | | Average 50 ft-lb Transition Temperature (°F) | | | Average Energy Absorption at Full Shear (ft-lb) | | |
|---|---|---|---|---|---|---|---|---|---|---|---|---|
| | Unirrad. | Irrad. | ΔT | Unirrad. | Irrad. | ΔT | Unirrad. | Irrad. | ΔT | Unirrad. | Irrad. | Δ |
| Plate B5454-1 (Longitudinal) | 4.6 | 117.6 | 113.0 | 18.4 | 144.1 | 125.7 | 33.3 | 153.1 | 119.8 | 144.7 | 118.1 | -26.6 |
| Plate B5454-1 (Transverse) | 26.6 | 137.3 | 110.7 | 54.4 | 162.2 | 107.7 | 74.6 | 185.7 | 111.1 | 94.9 | 88.6 | -6.3 |
| Weld Metal | -13.6 | 198.9 | 212.5 | -0.7 | 239.7 | 240.4 | 14.9 | 260.9 | 246.0 | 120.9 | 77.3 | -43.6 |
| HAZ Metal | -227.4 | 27.9 | 255.3 | -190.1 | 82.2 | 272.3 | -152.3 | 105.8 | 258.1 | 147.5 | 92.3 | -55.2 |

NOTE:

(a) The Charpy data was fit by PG&E using the EPRI Hyperbolic Tangent Curve Fitting Routine, Revision 2.0. (See Figures 5-13, 5-16, 5-19, and 5-22).

| TABLE 5-10 | | | | | | |
|---|---|---|---|---|---|---|
| Comparison of the Diablo Canyon Unit 2 Surveillance Material 30 ft-lb Transition Temperature Shifts and Upper Shelf Energy Decreases with Regulatory Guide 1.99, Revision 2, Predictions | | | | | | |
| | | | 30 ft-lb Transition Temperature Shift | | Upper Shelf Energy Decrease | |
| Material | Capsule | Fluence (x 10 n/cm) (E > 1.0 MeV) | Predicted (°F) | Measured (°F) | Predicted (%) | Measured (%) |
| Plate B5454-1 (Longitudinal) | U | 0.357 | 74.0 | 65.9 | 18 | 14.4 |
| | X | 0.866 | 99.2 | 101.0 | 22 | 20.7 |
| | Y | 1.32 | 111.3 | 113.0 | 24 | 18.4 |
| Plate B5454-1 (Transverse) | U | 0.357 | 74.0 | 72.3 | 18 | 0.4 |
| | X | 0.866 | 99.2 | 98.9 | 22 | 10.3 |
| | Y | 1.32 | 111.3 | 110.7 | 24 | 6.6 |
| Surveillance Weld Metal | U | 0.357 | 150.9 | 173.8 | 28 | 29.7 |
| | X | 0.866 | 202.3 | 204.2 | 34 | 38.5 |
| | Y | 1.32 | 226.9 | 212.5 | 38 | 36.1 |
| Heat Affected Zone Metal | U | 0.357 | - - | 234.2 | - - | 40.3 |
| | X | 0.866 | - - | 253.5 | - - | 31.4 |
| | Y | 1.32 | - - | 255.3 | - - | 37.4 |

NOTES:
(a) Based on Regulatory Guide 1.99, Revision 2, methodology.
(b) The Charpy data was fit by PG&E using the EPRI Hyperbolic Tangent Curve Fitting Routine, Revision 2.0. (See Figures 5-13, 5-16, 5-19, and 5-22.)

TABLE 5-11

Tensile Properties of the Diablo Canyon Unit 2 Reactor Vessel Surveillance Materials Irradiated $1.32 \times 10^{19}$ n/cm$^2$ (E > 1.0 MeV)

| Material | Sample Number | Test Temp. (°F) | 0.2% Yield Strength (ksi) | Ultimate Strength (ksi) | Fracture Load (kip) | Fracture Stress (ksi) | Fracture Strength (ksi) | Uniform Elongation (%) | Total Elongation (%) | Reduction in Area (%) |
|---|---|---|---|---|---|---|---|---|---|---|
| Plate B5454-1 (Longitudinal) | PL13 | 125 | 80.5 | 100.6 | 3.45 | 186.0 | 70.3 | 12.0 | 24.5 | 62 |
| | PL14 | 200 | 75.4 | 95.3 | 3.30 | 157.3 | 67.2 | 12.0 | 24.3 | 57 |
| | PL15 | 550 | 70.3 | 95.7 | 3.45 | 155.1 | 70.3 | 10.2 | 20.7 | 55 |
| Plate B5454-1 (Transverse) | PT13 | 150 | 77.9 | 96.8 | 3.65 | 146.6 | 74.3 | 11.3 | 21.2 | 49 |
| | PT14 | 300 | 72.8 | 93.1 | 3.65 | 142.7 | 74.4 | 10.5 | 16.7 | 48 |
| | PT15 | 550 | 70.3 | 93.7 | 3.65 | 159.4 | 75.0 | 11.3 | 19.2 | 53 |
| Surveillance Weld Metal | PW13 | 210 | 87.6 | 102.9 | 3.85 | 207.6 | 78.4 | 12.0 | 22.8 | 62 |
| | PW14 | 300 | 84.5 | 99.8 | 3.65 | 184.9 | 74.4 | 11.3 | 22.1 | 60 |
| | PW15 | 550 | 81.0 | 99.2 | 3.80 | 175.9 | 77.4 | 9.8 | 19.0 | 56 |

Upper Shelf Energy: 118.1 Temp. at 30 ft-lbs: 117.6 Temp. at 50 ft-lbs: 153.1 Lower Shelf Energy: 2.2 Fixed

Material: PLATE B5454-1 Heat No.: C5161-1 Capsule: Y Orientation: L Total Fluence: 1.32E+19

Correlation Coefficient for this Data Set is 0.9774

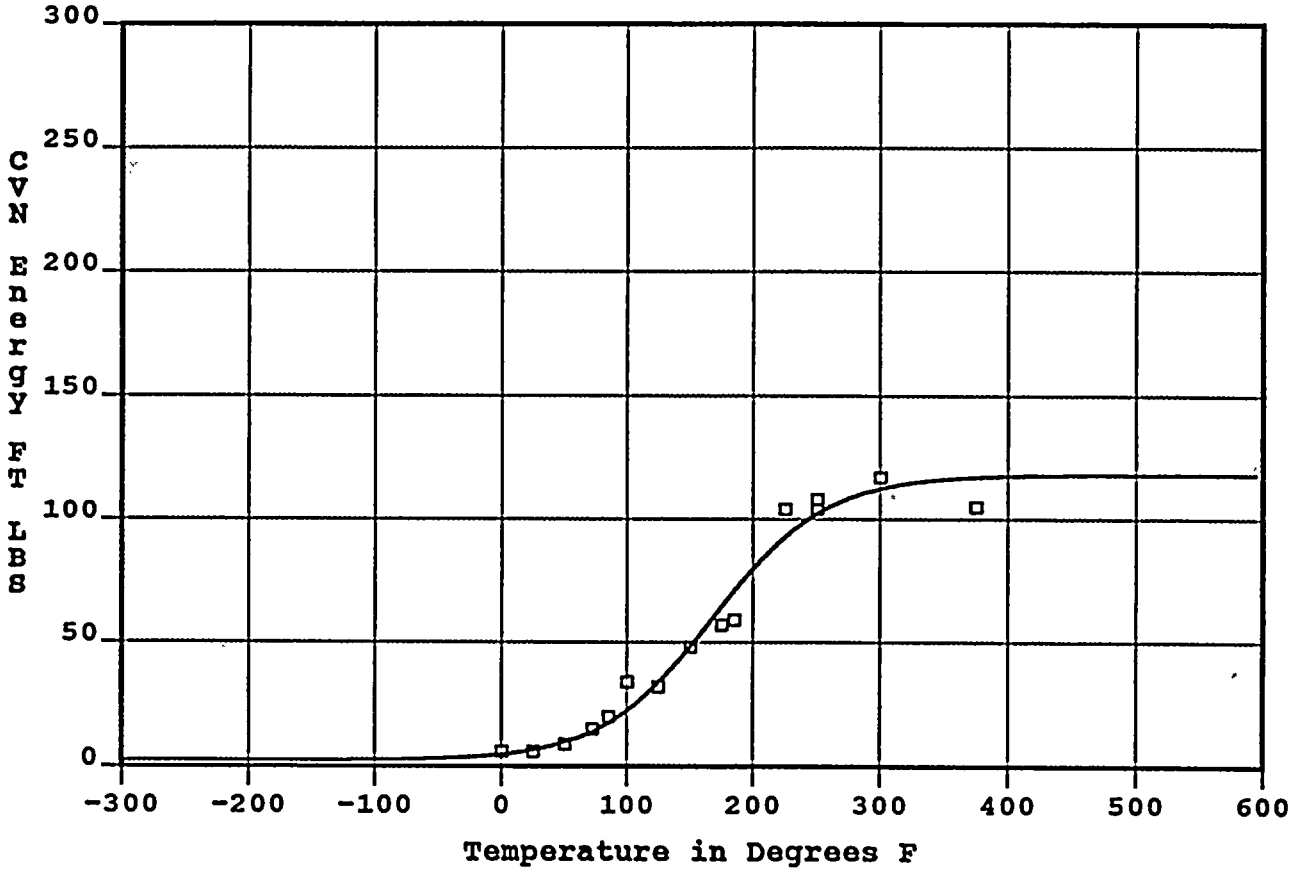


Charpy V-Notch Data

| Temperature | Input CVN Energy | Computed CVN Energy | Differential |
|---|---|---|---|
| 0.00 | 6.00 | 4.72 | 1.28 |
| 25.00 | 6.00 | 6.56 | -0.56 |
| 50.00 | 9.00 | 9.64 | -0.64 |
| 72.00 | 15.00 | 13.94 | 1.06 |
| 85.00 | 20.00 | 17.42 | 2.58 |
| 100.00 | 34.00 | 22.48 | 11.52 |
| 125.00 | 32.00 | 33.67 | -1.67 |
| 150.00 | 48.00 | 48.08 | -0.08 |
| 175.00 | 57.00 | 64.23 | -7.23 |
| 185.00 | 59.00 | 70.66 | -11.66 |
| 225.00 | 104.00 | 92.68 | 11.32 |
| 250.00 | 104.00 | 102.13 | 1.87 |
| 250.00 | 108.00 | 102.13 | 5.87 |
| 300.00 | 117.00 | 112.40 | 4.60 |
| 375.00 | 105.00 | 117.02 | -12.02 |
| | | SUM of RESIDUALS = | 6.24 |

Figure 5-1 Charpy V-Notch Impact Energy vs. Temperature for Diablo Canyon Unit 2 Reactor Vessel Capsule Y Intermediate Shell Plate B5454-1 (Longitudinal Orientation)

Upper Shelf L.E.: 88.8 Temperature at L.E. 35 is 144.1 Lower Shelf L.E.: 1.0 Fixed

Material: PLATE B5454-1 Heat No.: C5161-1 Capsule: Y Orientation: L Total Fluence: 1.32E+19

Correlation Coefficient for this Data Set is 0.9814

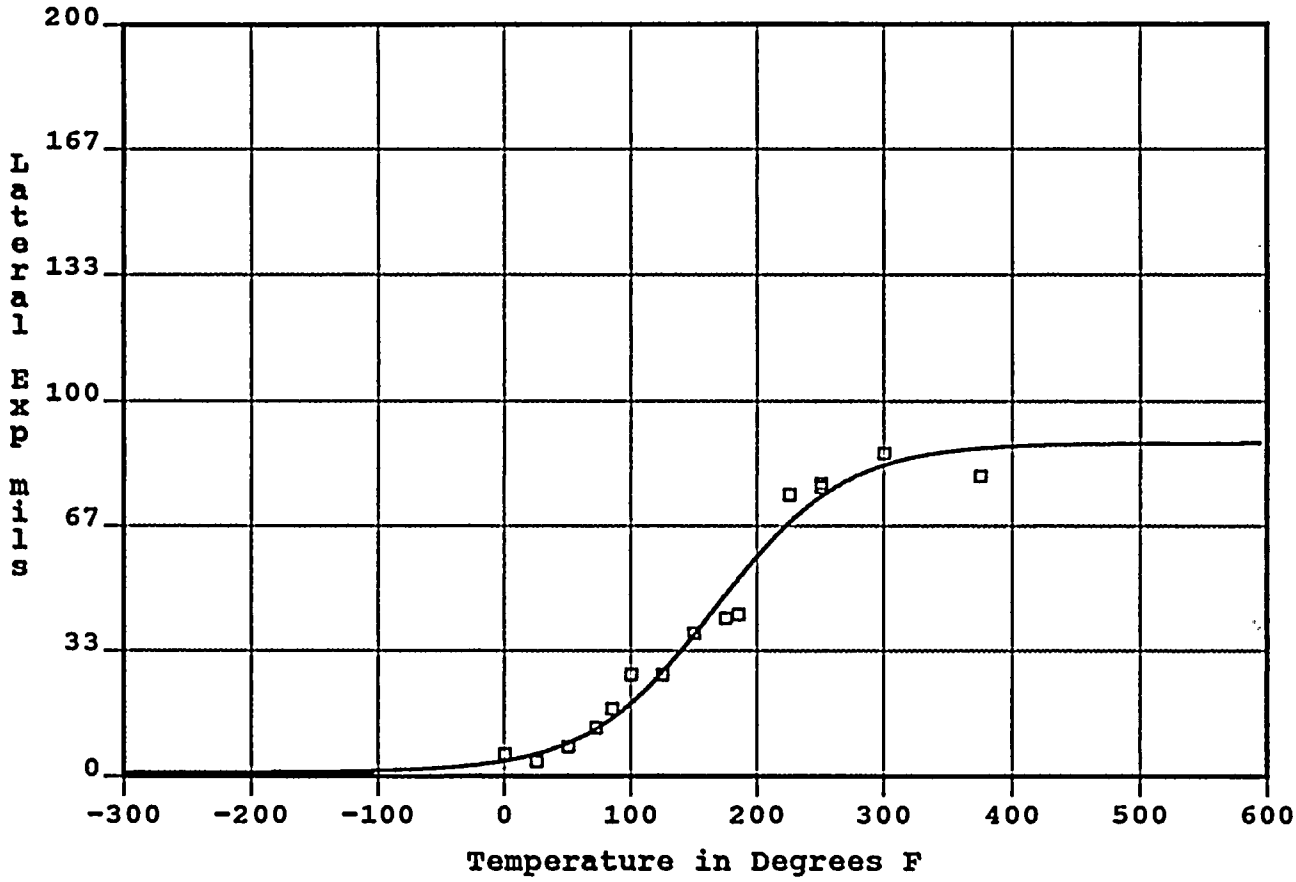


Charpy V-Notch Data

| Temperature | Input Lateral Expansion | Computed Lateral Expansion | Differential |
|---|---|---|---|
| 0.00 | 6.00 | 4.11 | 1.89 |
| 25.00 | 4.00 | 5.98 | -1.98 |
| 50.00 | 8.00 | 8.87 | -0.87 |
| 72.00 | 13.00 | 12.59 | 0.41 |
| 85.00 | 18.00 | 15.42 | 2.58 |
| 100.00 | 27.00 | 19.36 | 7.64 |
| 125.00 | 27.00 | 27.53 | -0.53 |
| 150.00 | 38.00 | 37.44 | 0.56 |
| 175.00 | 42.00 | 48.20 | -6.20 |
| 185.00 | 43.00 | 52.47 | -9.47 |
| 225.00 | 75.00 | 67.49 | 7.51 |
| 250.00 | 77.00 | 74.43 | 2.57 |
| 250.00 | 78.00 | 74.43 | 3.57 |
| 300.00 | 86.00 | 82.82 | 3.18 |
| 375.00 | 80.00 | 87.35 | -7.35 |
| | | SUM of RESIDUALS = | 3.52 |

Figure 5-2 Charpy V-Notch Lateral Expansion vs. Temperature for Diablo Canyon Unit 2 Reactor Vessel Capsule Y Intermediate Shell Plate B5454-1 (Longitudinal Orientation)

Temperature at 50% Shear is 188.4

Material: PLATE B5454-1 Heat No.: C5161-1 Capsule: Y Orientation: L Total Fluence: 1.32E+1

Correlation Coefficient for this Data Set is 0.9386

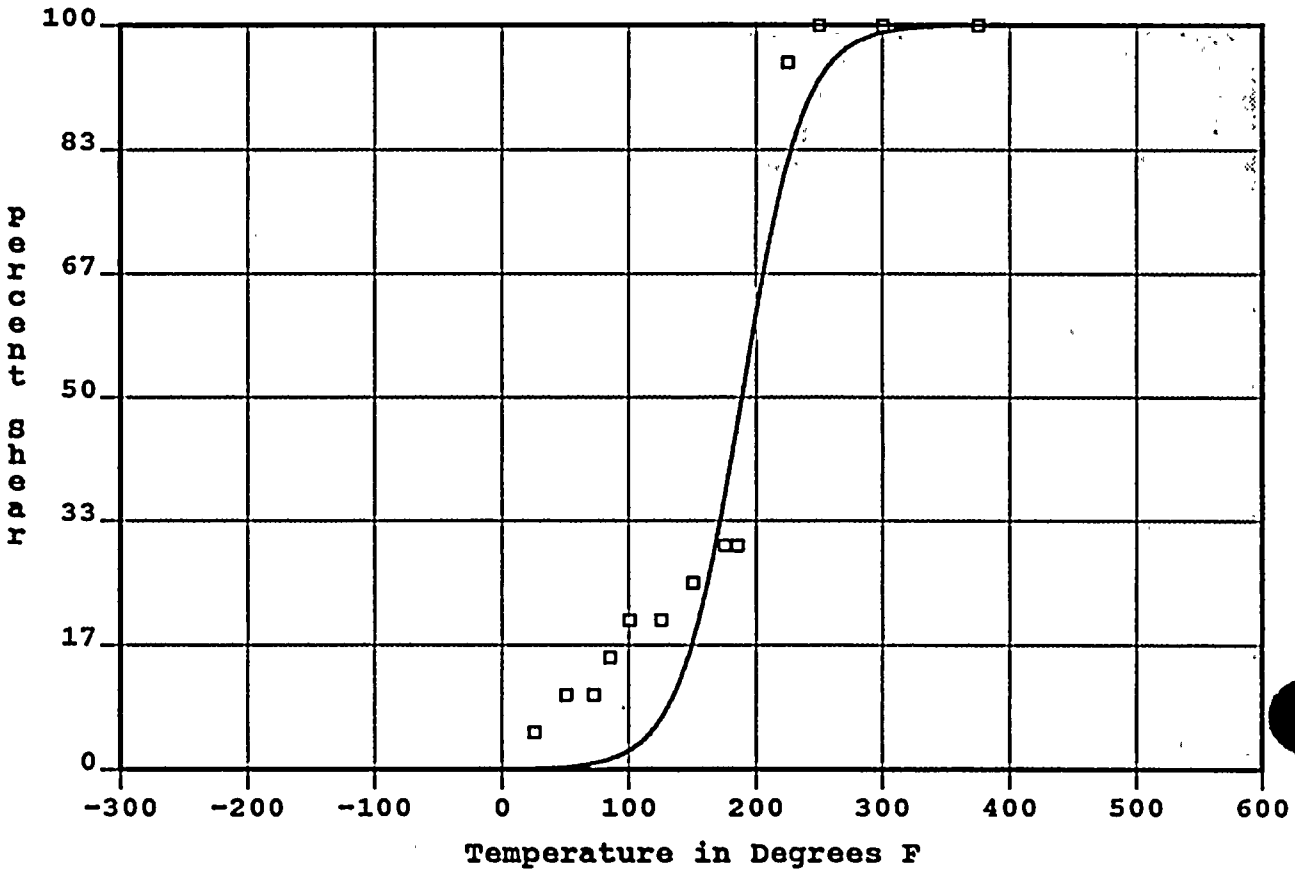


Charpy V-Notch Data

| Temperature | Input Shear Percent | Computed Shear Percent | Differential |
|---|---|---|---|
| 25.00 | 5.00 | 0.12 | 4.88 |
| 50.00 | 10.00 | 0.33 | 9.67 |
| 72.00 | 10.00 | 0.81 | 9.19 |
| 85.00 | 15.00 | 1.38 | 13.62 |
| 100.00 | 20.00 | 2.53 | 17.47 |
| 125.00 | 20.00 | 6.79 | 13.21 |
| 150.00 | 25.00 | 16.98 | 8.02 |
| 175.00 | 30.00 | 36.48 | -6.48 |
| 185.00 | 30.00 | 46.46 | -16.46 |
| 225.00 | 95.00 | 81.90 | 13.10 |
| 250.00 | 100.00 | 92.70 | 7.30 |
| 250.00 | 100.00 | 92.70 | 7.30 |
| 300.00 | 100.00 | 99.01 | 0.99 |
| 375.00 | 100.00 | 99.95 | 0.05 |
| | | SUM of RESIDUALS = | 81.86 |

Figure 5-3 Charpy V-Notch Percent Shear vs. Temperature for Diablo Canyon Unit 2 Reactor Vessel Capsule Y Intermediate Shell Plate B5454-1 (Longitudinal Orientation)

Upper Shelf Energy: 88.6 Temp. at 30 ft-lbs: 137.3 Temp. at 50 ft-lbs: 185.7 Lower Shelf Energy: 2.2 Fixed

Material: PLATE B5454-1 Heat No.: C5161-1 Capsule: Y Orientation: T Total Fluence: 1.32E+19

Correlation Coefficient for this Data Set is 0.9448

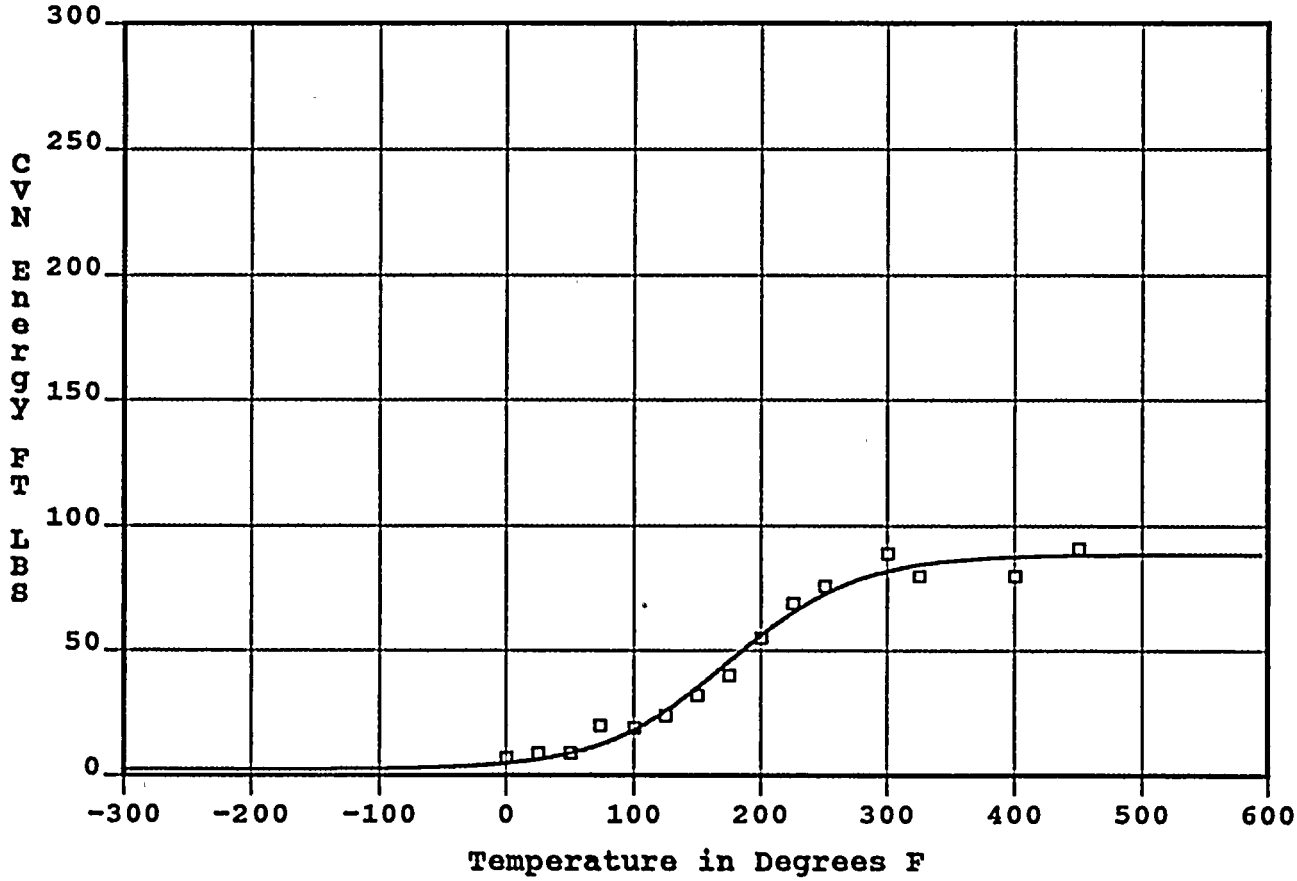


Charpy V-Notch Data

| Temperature | Input CVN Energy | Computed CVN Energy | Differential |
|---|---|---|---|
| 0.00 | 7.00 | 4.82 | 2.18 |
| 25.00 | 9.00 | 6.41 | 2.59 |
| 50.00 | 9.00 | 8.90 | 0.10 |
| 73.00 | 20.00 | 12.32 | 7.68 |
| 100.00 | 19.00 | 18.16 | 0.84 |
| 125.00 | 24.00 | 25.63 | -1.63 |
| 150.00 | 32.00 | 34.96 | -2.96 |
| 175.00 | 40.00 | 45.45 | -5.45 |
| 200.00 | 55.00 | 55.93 | -0.93 |
| 225.00 | 69.00 | 65.24 | 3.76 |
| 250.00 | 76.00 | 72.68 | 3.32 |
| 300.00 | 89.00 | 81.90 | 7.10 |
| 325.00 | 80.00 | 84.38 | -4.38 |
| 400.00 | 80.00 | 87.59 | -7.59 |
| 450.00 | 91.00 | 88.20 | 2.80 |
| | | SUM of RESIDUALS = | 7.40 |

Figure 5-4 Charpy V-Notch Impact Energy vs. Temperature for Diablo Canyon Unit 2 Reactor Vessel Capsule Y Intermediate Shell Plate B5454-1 (Transverse Orientation)

Upper Shelf L.E.: 72.2 Temperature at L.E. 35 is 162.2 Lower Shelf L.E.: 1.0 Fixed

Material: PLATE B5454-1 Heat No.: C5161-1 Capsule: Y Orientation: T Total Fluence: 1.32E

Correlation Coefficient for this Data Set is 0.9863

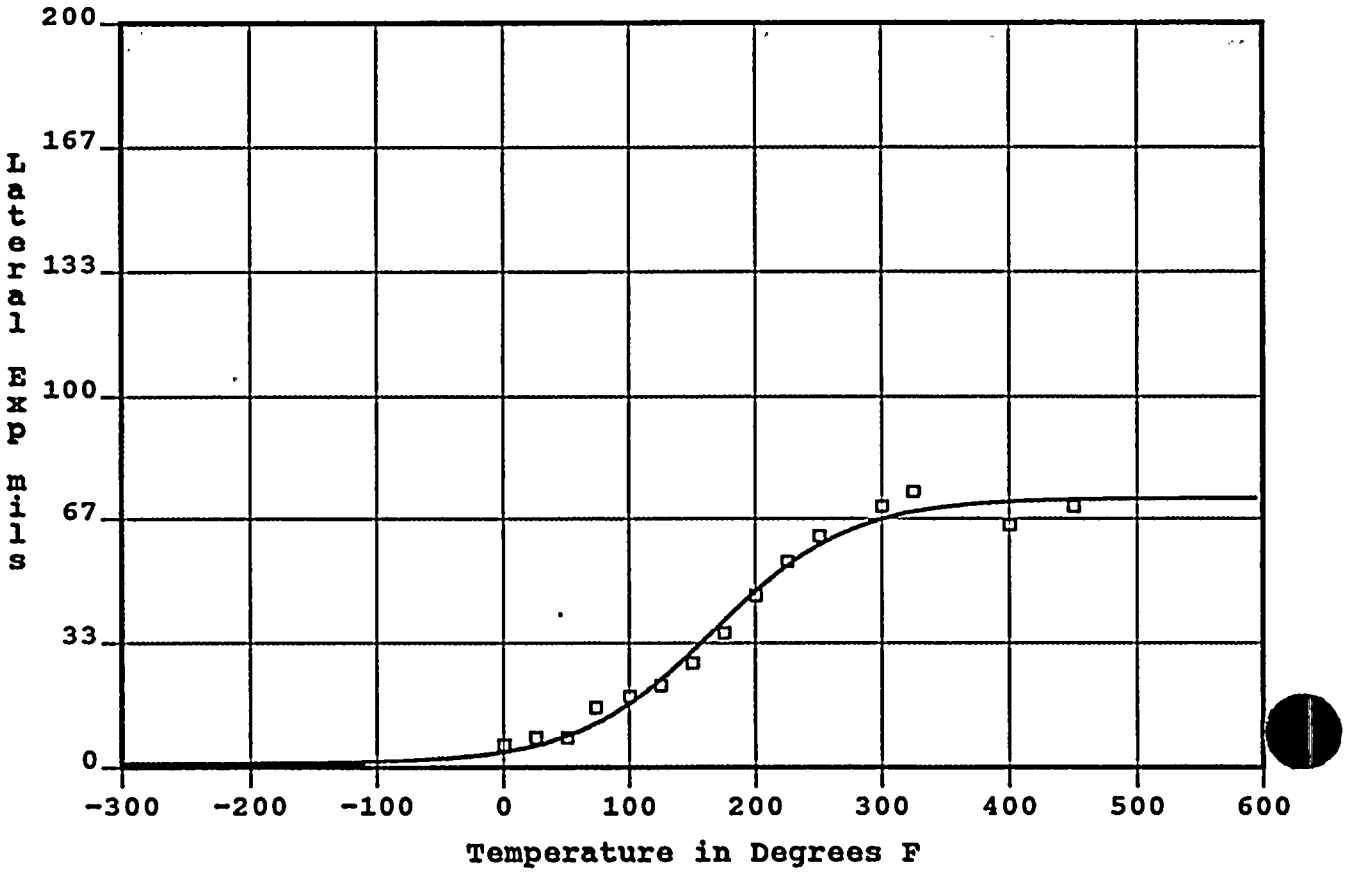


Charpy V-Notch Data

| Temperature | Input Lateral Expansion | Computed Lateral Expansion | Differential |
|---|---|---|---|
| 0.00 | 6.00 | 4.13 | 1.87 |
| 25.00 | 8.00 | 5.84 | 2.16 |
| 50.00 | 8.00 | 8.38 | -0.38 |
| 73.00 | 16.00 | 11.69 | 4.31 |
| 100.00 | 19.00 | 17.04 | 1.96 |
| 125.00 | 22.00 | 23.46 | -1.46 |
| 150.00 | 28.00 | 31.06 | -3.06 |
| 175.00 | 36.00 | 39.20 | -3.20 |
| 200.00 | 46.00 | 47.09 | -1.09 |
| 225.00 | 55.00 | 53.98 | 1.02 |
| 250.00 | 62.00 | 59.50 | 2.50 |
| 300.00 | 70.00 | 66.52 | 3.48 |
| 325.00 | 74.00 | 68.50 | 5.50 |
| 400.00 | 65.00 | 71.21 | -6.21 |
| 450.00 | 70.00 | 71.78 | -1.78 |
| | | SUM of RESIDUALS = | 5.62 |

Figure 5-5 Charpy V-Notch Lateral Expansion vs. Temperature for Diablo Canyon Unit 2 Reactor Vessel Capsule Y Intermediate Shell Plate B5454-1 (Transverse Orientation)

Temperature at 50% Shear is 199.2

Material: PLATE B5454-1 Heat No.: C5161-1 Capsule: Y Orientation: T Total Fluence: 1.32E+19

Correlation Coefficient for this Data Set is 0.9589

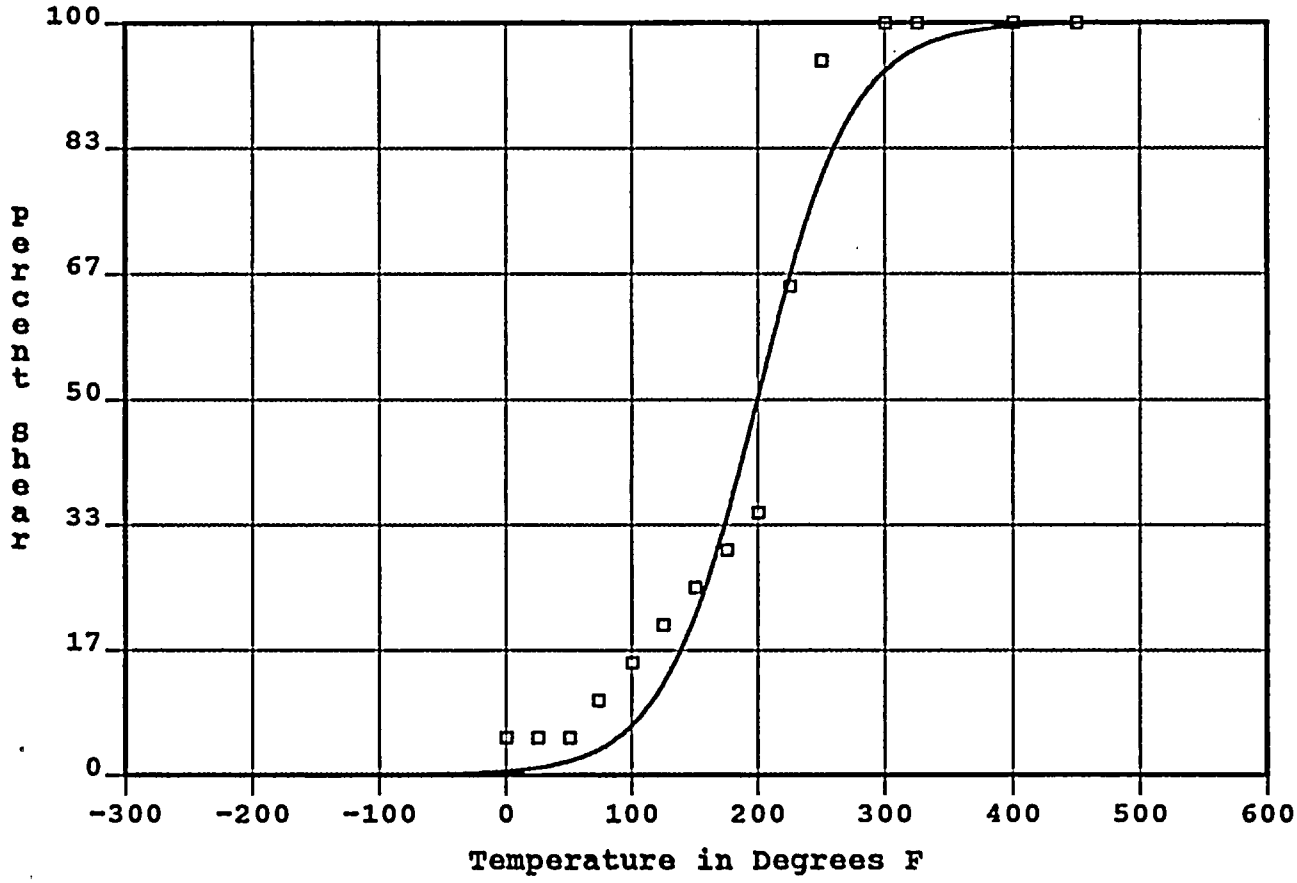


Charpy V-Notch Data

| Temperature | Input Shear Percent | Computed Shear Percent | Differential |
|---|---|---|---|
| 0.00 | 5.00 | 0.49 | 4.51 |
| 25.00 | 5.00 | 0.95 | 4.05 |
| 50.00 | 5.00 | 1.83 | 3.17 |
| 73.00 | 10.00 | 3.33 | 6.67 |
| 100.00 | 15.00 | 6.62 | 8.38 |
| 125.00 | 20.00 | 12.13 | 7.87 |
| 150.00 | 25.00 | 21.20 | 3.80 |
| 175.00 | 30.00 | 34.39 | -4.39 |
| 200.00 | 35.00 | 50.52 | -15.52 |
| 225.00 | 65.00 | 66.55 | -1.55 |
| 250.00 | 95.00 | 79.49 | 15.51 |
| 300.00 | 100.00 | 93.63 | 6.37 |
| 325.00 | 100.00 | 96.63 | 3.37 |
| 400.00 | 100.00 | 99.53 | 0.47 |
| 450.00 | 100.00 | 99.88 | 0.12 |
| | | SUM of RESIDUALS = | 42.83 |

Figure 5-6 Charpy V-Notch Percent Shear vs. Temperature for Diablo Canyon Unit 2 Reactor Vessel Capsule Y Intermediate Shell Plate B5454-1 (Transverse Orientation)

Upper Shelf Energy: 77.3 Temp. at 30 ft-lbs: 198.9 Temp. at 50 ft-lbs: 260.9 Lower Shelf Energy: 2.2 [redacted]

Material: WELD Heat No.: 21935/1208 Capsule: Y Orientation: Total Fluence: 1.32E+[redacted]

Correlation Coefficient for this Data Set is 0.9697

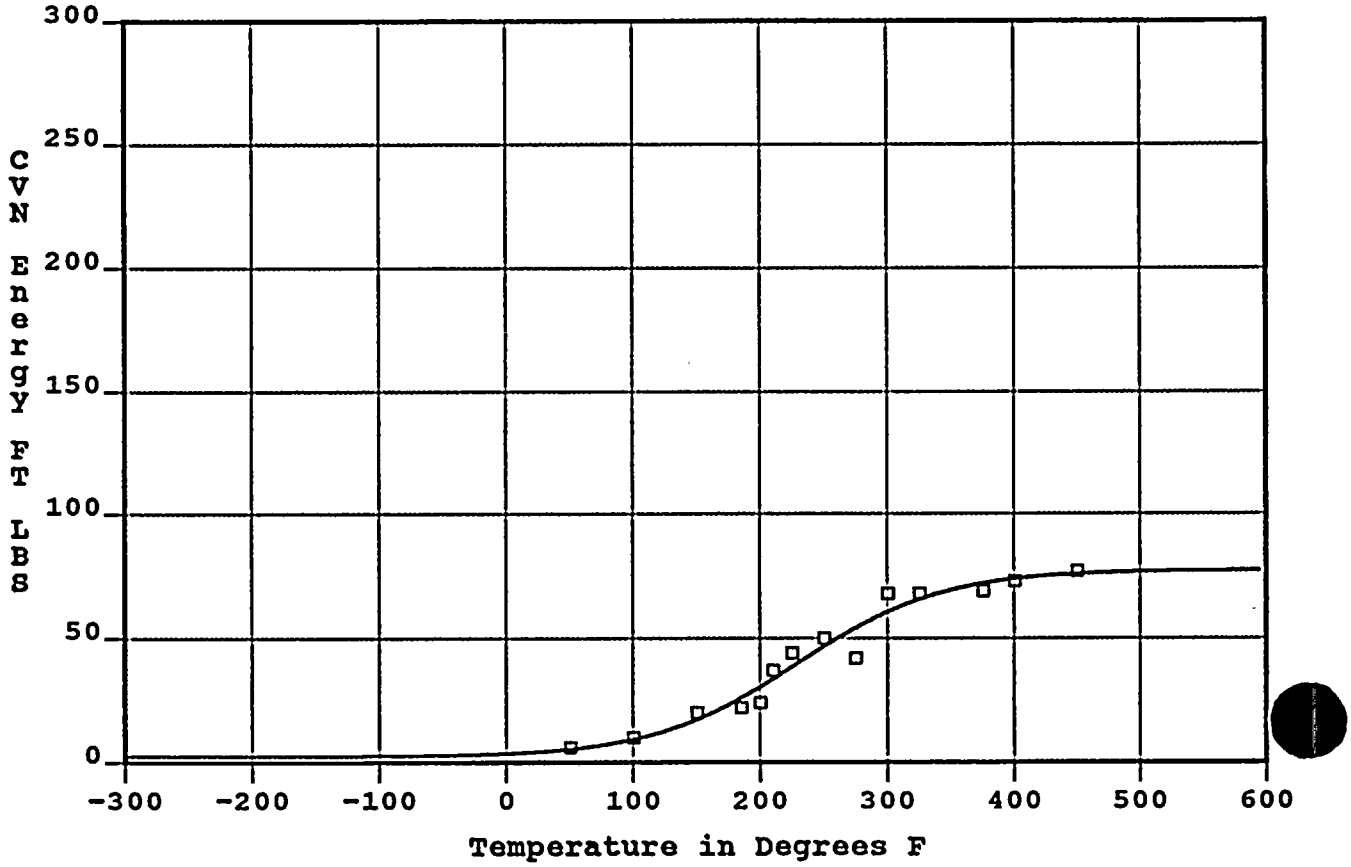


Charpy V-Notch Data

| Temperature | Input CVN Energy | Computed CVN Energy | Differential |
|---|---|---|---|
| 50.00 | 6.00 | 5.27 | 0.73 |
| 100.00 | 10.00 | 9.20 | 0.80 |
| 150.00 | 20.00 | 17.13 | 2.87 |
| 185.00 | 22.00 | 25.86 | -3.86 |
| 200.00 | 24.00 | 30.33 | -6.33 |
| 210.00 | 37.00 | 33.49 | 3.51 |
| 225.00 | 44.00 | 38.40 | 5.60 |
| 250.00 | 50.00 | 46.59 | 3.41 |
| 275.00 | 42.00 | 54.16 | -12.16 |
| 300.00 | 68.00 | 60.57 | 7.43 |
| 325.00 | 68.00 | 65.61 | 2.39 |
| 375.00 | 69.00 | 71.97 | -2.97 |
| 400.00 | 73.00 | 73.79 | -0.79 |
| 450.00 | 77.00 | 75.81 | 1.19 |
| | | SUM of RESIDUALS = | 1.80 |

Figure 5-7 Charpy V-Notch Impact Energy vs. Temperature for Diablo Canyon Unit 2 Reactor Vessel Capsule Y Weld Metal [redacted]

Upper Shelf L.E.: 61.8 Temperature at L.E. 35 is 239.7 Lower Shelf L.E.: 1.0 Fixed

Material: WELD Heat No.: 21935/1208 Capsule: Y Orientation: Total Fluence: 1.32E+19

Correlation Coefficient for this Data Set is 0.9426

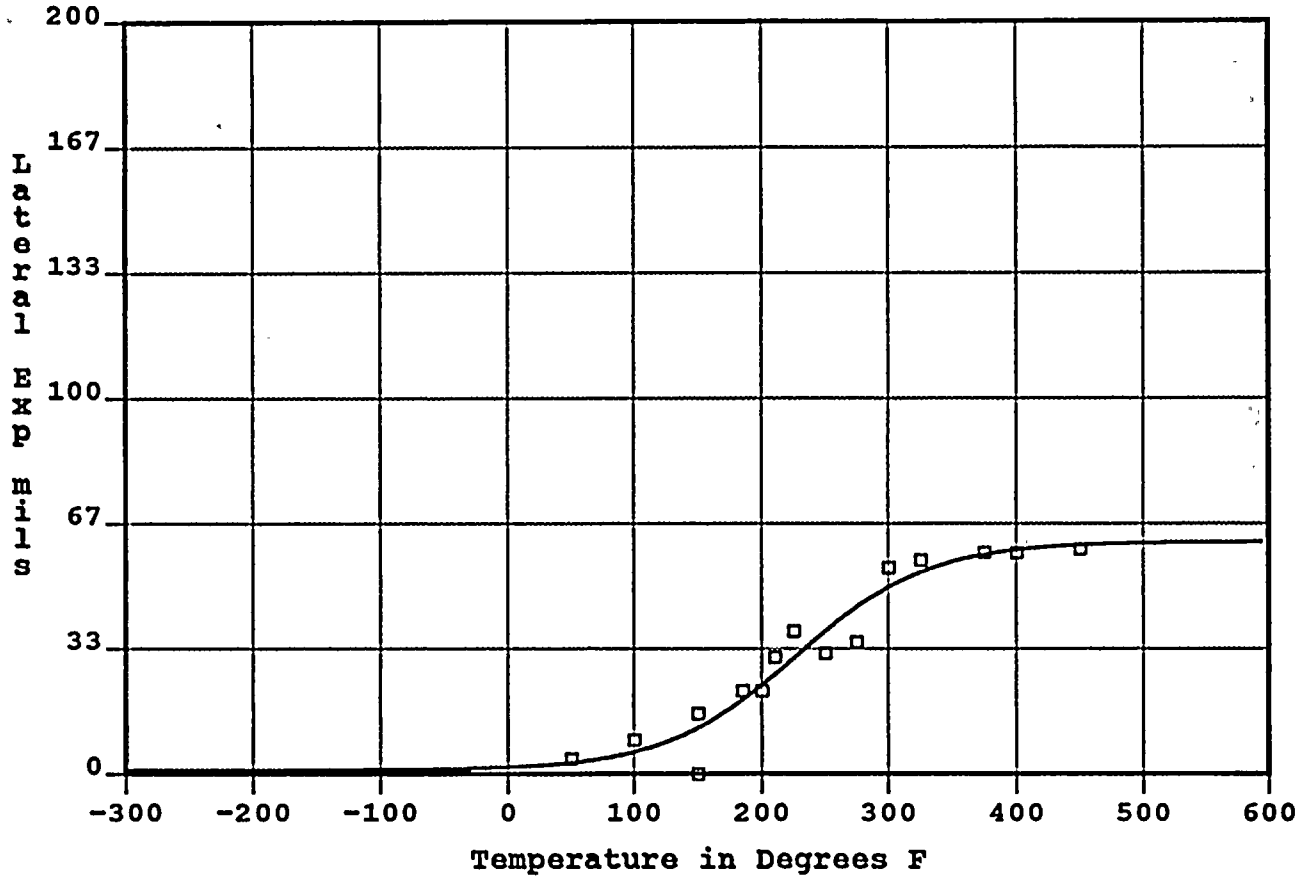


Charpy V-Notch Data

| Temperature | Input Lateral Expansion | Computed Lateral Expansion | Differential |
|---|---|---|---|
| 50.00 | 4.00 | 2.93 | 1.07 |
| 100.00 | 9.00 | 5.82 | 3.18 |
| 150.00 | 0.00 | 12.18 | -12.18 |
| 150.00 | 16.00 | 12.18 | 3.82 |
| 185.00 | 22.00 | 19.64 | 2.36 |
| 200.00 | 22.00 | 23.57 | -1.57 |
| 210.00 | 31.00 | 26.36 | 4.64 |
| 225.00 | 38.00 | 30.70 | 7.30 |
| 250.00 | 32.00 | 37.92 | -5.92 |
| 275.00 | 35.00 | 44.44 | -9.44 |
| 300.00 | 55.00 | 49.77 | 5.23 |
| 325.00 | 57.00 | 53.76 | 3.24 |
| 375.00 | 59.00 | 58.47 | 0.53 |
| 400.00 | 59.00 | 59.71 | -0.71 |
| 450.00 | 60.00 | 61.00 | -1.00 |
| | | SUM of RESIDUALS = | 0.55 |

Figure 5-8 Charpy V-Notch Lateral Expansion vs. Temperature for Diablo Canyon Unit 2 Reactor Vessel Capsule Y Weld Metal

Temperature at 50% Shear is 231.1

Material: WELD  Heat No.: 21935/1208 Capsule: Y  Orientation:  Total Fluence: 1.32E

Correlation Coefficient for this Data Set is 0.9346

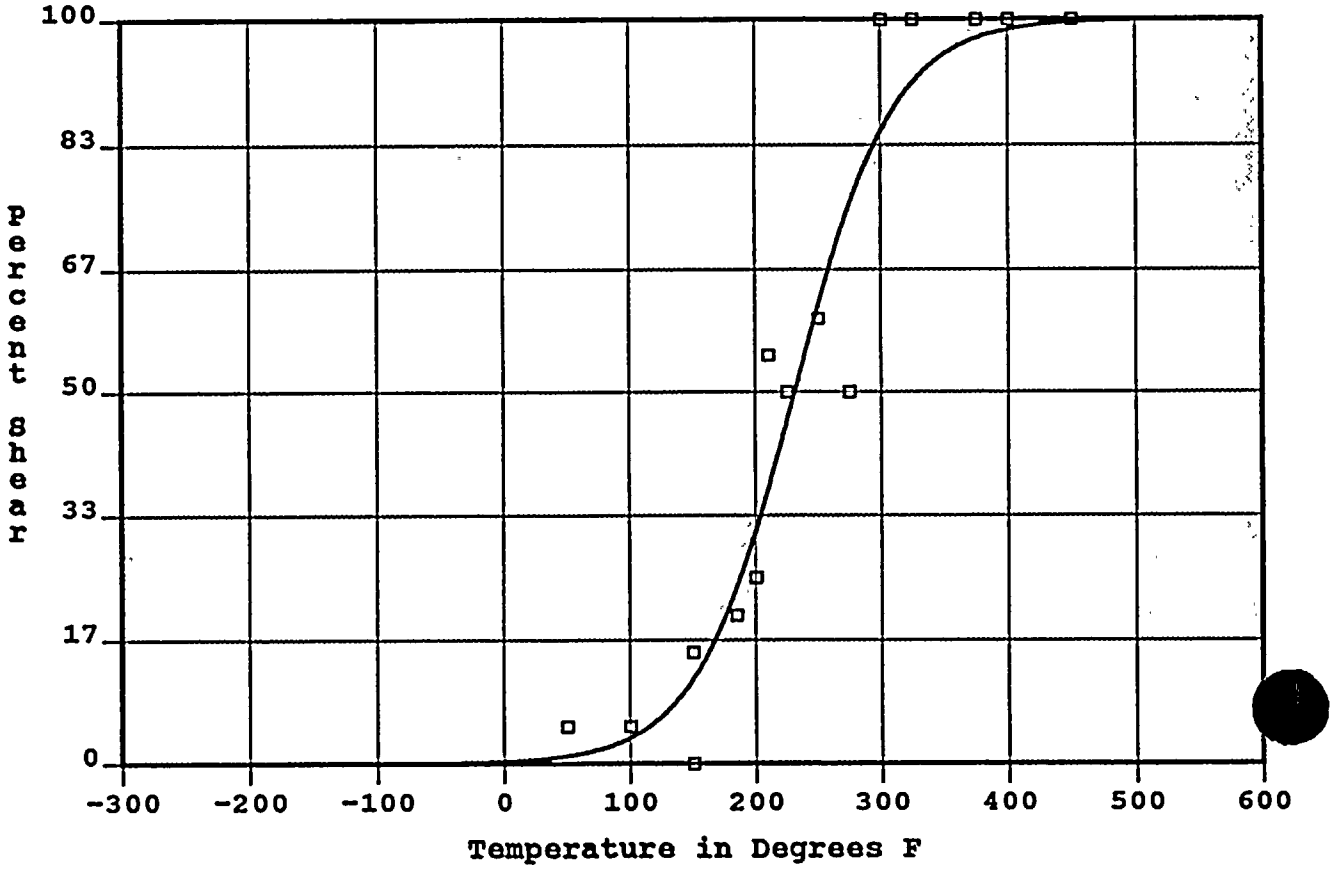


Charpy V-Notch Data

| Temperature | Input Shear Percent | Computed Shear Percent | Differential |
|---|---|---|---|
| 50.00 | 5.00 | 1.00 | 4.00 |
| 100.00 | 5.00 | 3.46 | 1.54 |
| 150.00 | 0.00 | 11.31 | -11.31 |
| 150.00 | 15.00 | 11.31 | 3.69 |
| 185.00 | 20.00 | 23.68 | -3.68 |
| 200.00 | 25.00 | 31.23 | -6.23 |
| 210.00 | 55.00 | 36.92 | 18.08 |
| 225.00 | 50.00 | 46.14 | 3.86 |
| 250.00 | 60.00 | 61.78 | -1.78 |
| 275.00 | 50.00 | 75.31 | -25.31 |
| 300.00 | 100.00 | 85.19 | 14.81 |
| 325.00 | 100.00 | 91.56 | 8.44 |
| 375.00 | 100.00 | 97.48 | 2.52 |
| 400.00 | 100.00 | 98.65 | 1.35 |
| 450.00 | 100.00 | 99.62 | 0.38 |
| | | SUM of RESIDUALS = | 10.38 |

Figure 5-9 Charpy V-Notch Percent Shear vs. Temperature for Diablo Canyon Unit 2 Reactor Vessel Capsule Y Weld Metal

Upper Shelf Energy: 92.3 Temp. at 30 ft-lbs: 27.9 Temp. at 50 ft-lbs: 105.8 Lower Shelf Energy: 2.2 Fixed

Material: HAZ B5454-1 Heat No.: C5161-1 Capsule: Y Orientation: Total Fluence: 1.32E+19

Correlation Coefficient for this Data Set is 0.8404

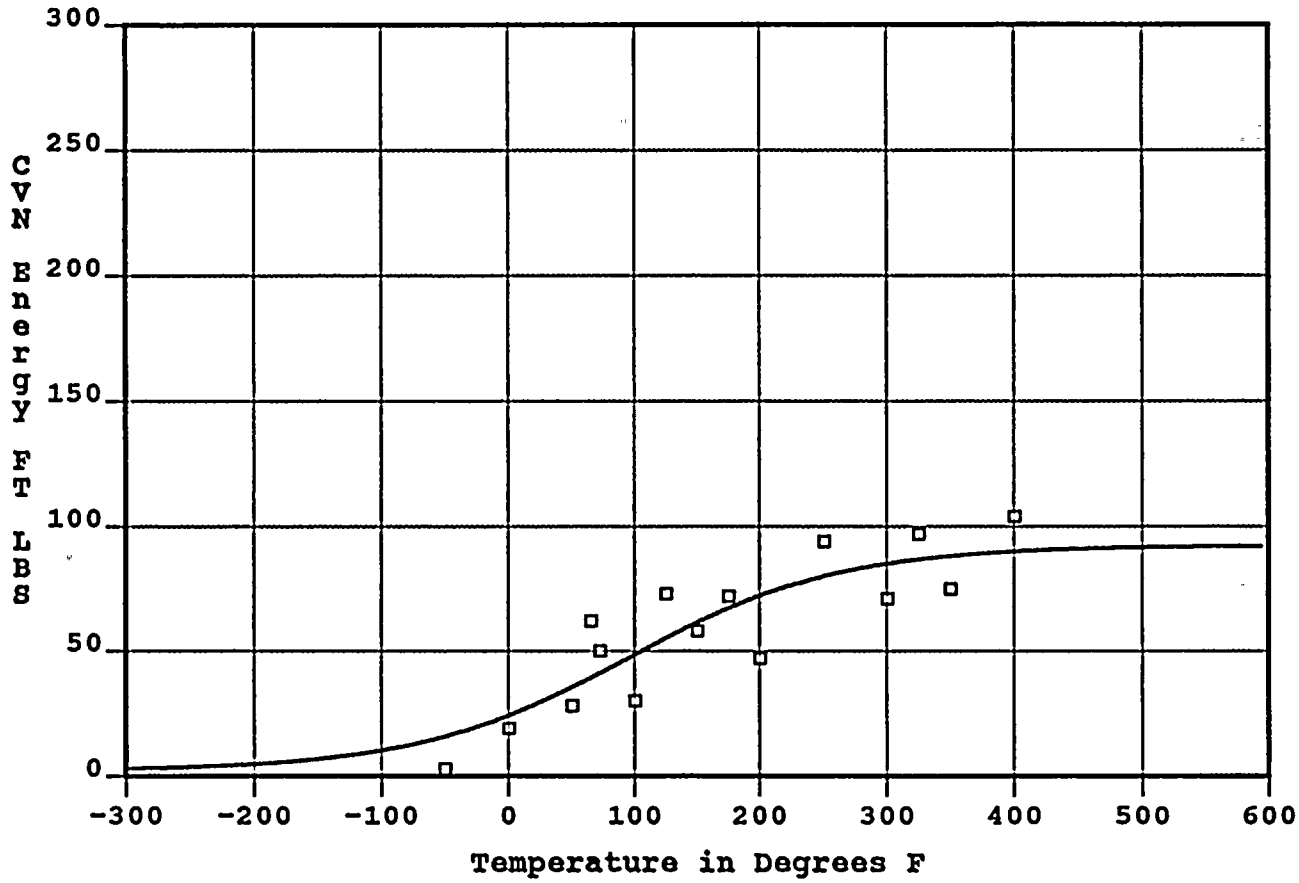


Charpy V-Notch Data

| Temperature | Input CVN Energy | Computed CVN Energy | Differential |
|---|---|---|---|
| -50.00 | 3.00 | 15.71 | -12.71 |
| 0.00 | 19.00 | 24.04 | -5.04 |
| 50.00 | 28.00 | 35.30 | -7.30 |
| 65.00 | 62.00 | 39.13 | 22.87 |
| 72.00 | 50.00 | 40.96 | 9.04 |
| 100.00 | 30.00 | 48.44 | -18.44 |
| 125.00 | 73.00 | 55.07 | 17.93 |
| 150.00 | 58.00 | 61.37 | -3.37 |
| 175.00 | 72.00 | 67.11 | 4.89 |
| 200.00 | 47.00 | 72.16 | -25.16 |
| 250.00 | 94.00 | 79.97 | 14.03 |
| 300.00 | 71.00 | 85.07 | -14.07 |
| 325.00 | 97.00 | 86.82 | 10.18 |
| 350.00 | 75.00 | 88.17 | -13.17 |
| 400.00 | 104.00 | 89.99 | 14.01 |
| | | SUM of RESIDUALS = | -6.31 |

Figure 5-10 Charpy V-Notch Impact Energy vs. Temperature for Diablo Canyon Unit 2 Reactor Vessel Capsule Y Heat-Affected-Zone (HAZ) Metal

Upper Shelf L.E.: 68.3 Temperature at L.E. 35 is 82.2 Lower Shelf L.E.: 1.0 Fixed

Material: HAZ B5454-1 Heat No.: C5161-1 Capsule: Y Orientation: Total Fluence: 1.32E

Correlation Coefficient for this Data Set is 0.8557

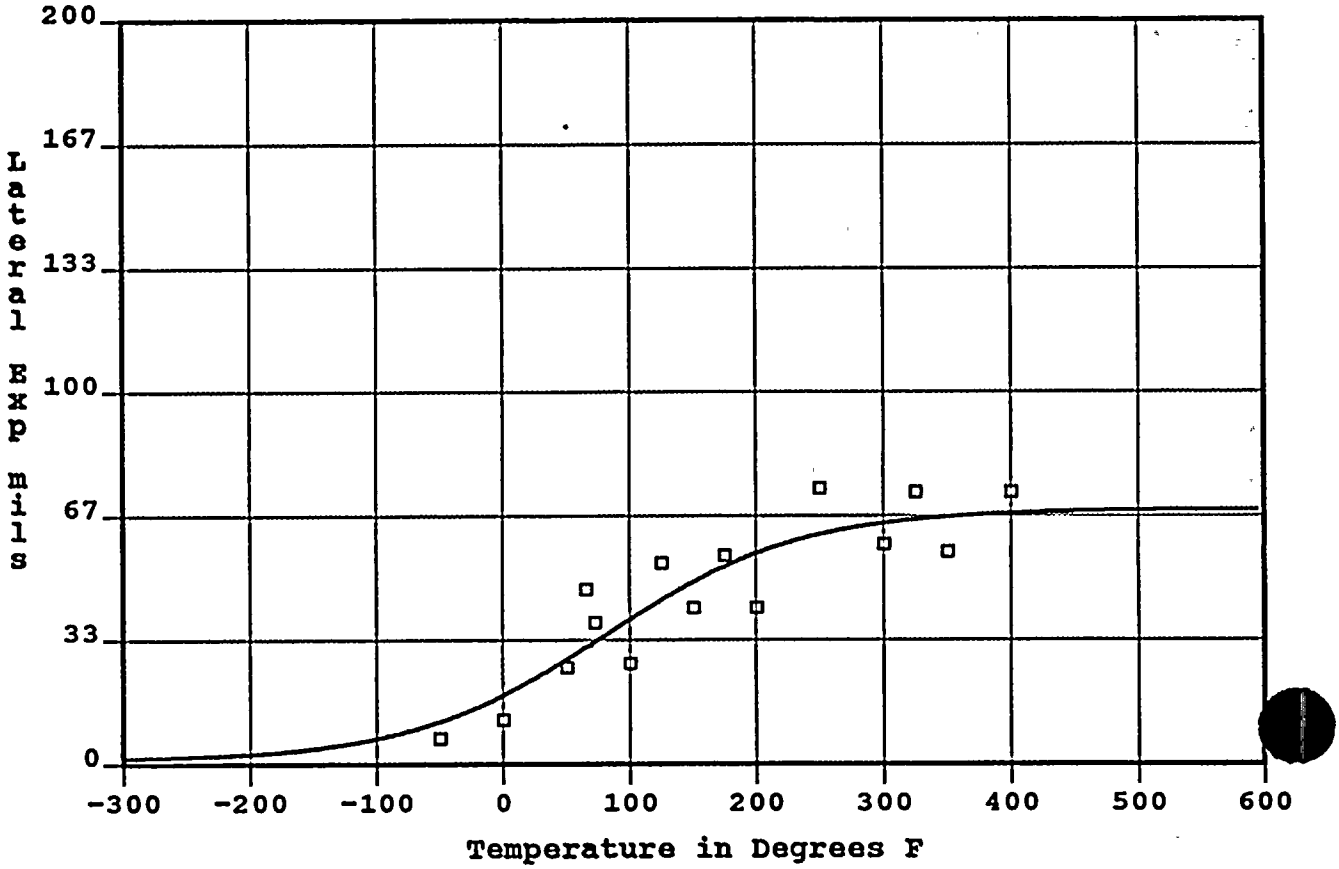


Charpy V-Notch Data

| Temperature | Input Lateral Expansion | Computed Lateral Expansion | Differential |
|---|---|---|---|
| -50.00 | 7.00 | 11.42 | -4.42 |
| 0.00 | 12.00 | 18.48 | -6.48 |
| 50.00 | 26.00 | 28.05 | -2.05 |
| 65.00 | 47.00 | 31.26 | 15.74 |
| 72.00 | 38.00 | 32.78 | 5.22 |
| 100.00 | 27.00 | 38.88 | -11.88 |
| 125.00 | 54.00 | 44.11 | 9.89 |
| 150.00 | 42.00 | 48.89 | -6.89 |
| 175.00 | 56.00 | 53.06 | 2.94 |
| 200.00 | 42.00 | 56.55 | -14.55 |
| 250.00 | 74.00 | 61.62 | 12.38 |
| 300.00 | 59.00 | 64.65 | -5.65 |
| 325.00 | 73.00 | 65.63 | 7.37 |
| 350.00 | 57.00 | 66.35 | -9.35 |
| 400.00 | 73.00 | 67.28 | 5.72 |
| | | SUM of RESIDUALS = | -1.99 |

Figure 5-11 Charpy V-Notch Lateral Expansion vs. Temperature for Diablo Canyon Unit 2 Reactor Vessel Capsule Y Heat-Affected-Zone (HAZ) Metal

Temperature at 50% Shear is 89.5

Material: HAZ B5454-1 Heat No.: C5161-1 Capsule: Y Orientation: Total Fluence: 1.32E+19

Correlation Coefficient for this Data Set is 0.8991

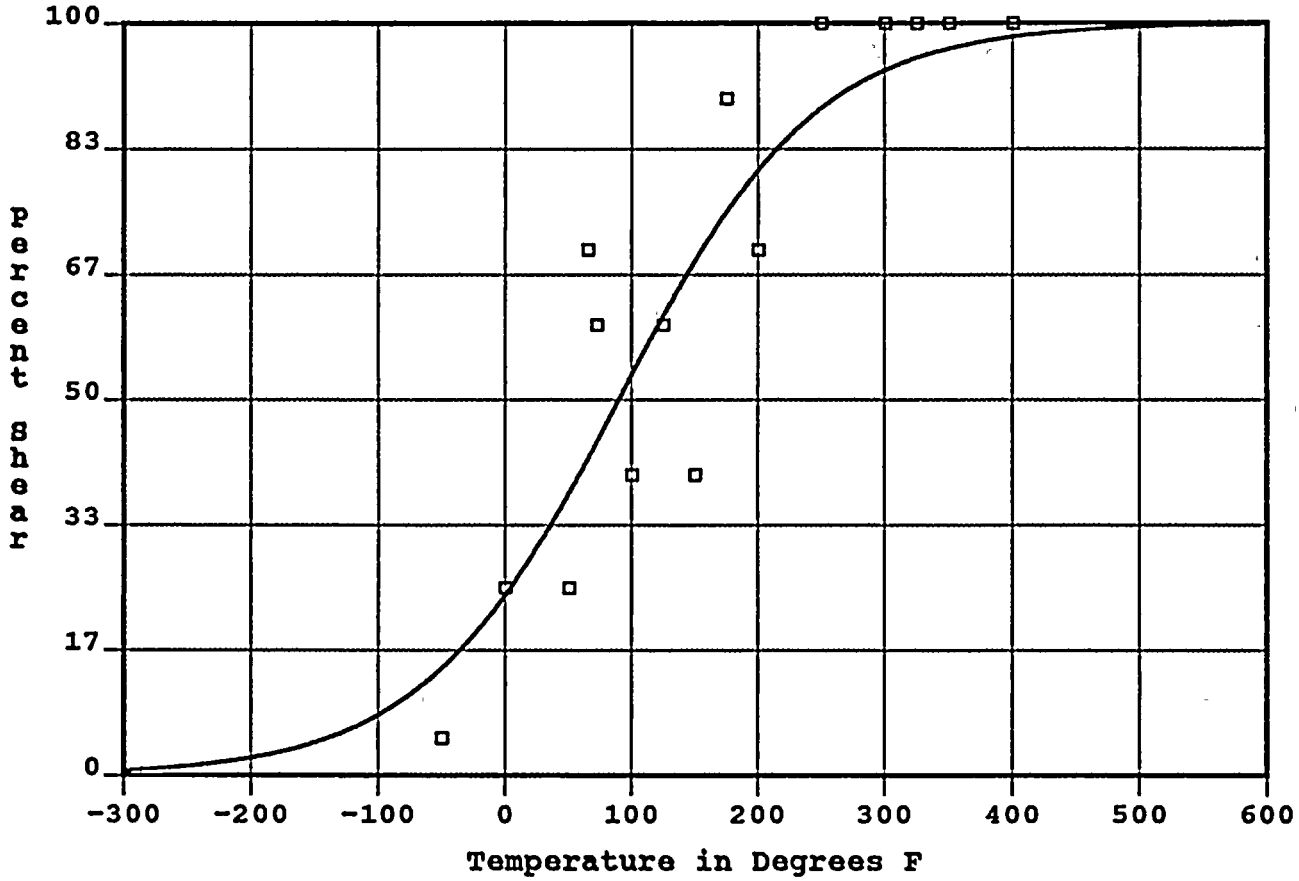


Charpy V-Notch Data

| Temperature | Input Shear Percent | Computed Shear Percent | Differential |
|---|---|---|---|
| -50.00 | 5.00 | 14.26 | -9.26 |
| 0.00 | 25.00 | 24.03 | 0.97 |
| 50.00 | 25.00 | 37.56 | -12.56 |
| 65.00 | 70.00 | 42.18 | 27.82 |
| 72.00 | 60.00 | 44.39 | 15.61 |
| 100.00 | 40.00 | 53.36 | -13.36 |
| 125.00 | 60.00 | 61.21 | -1.21 |
| 150.00 | 40.00 | 68.52 | -28.52 |
| 175.00 | 90.00 | 75.01 | 14.99 |
| 200.00 | 70.00 | 80.54 | -10.54 |
| 250.00 | 100.00 | 88.73 | 11.27 |
| 300.00 | 100.00 | 93.74 | 6.26 |
| 325.00 | 100.00 | 95.38 | 4.62 |
| 350.00 | 100.00 | 96.61 | 3.39 |
| 400.00 | 100.00 | 98.19 | 1.81 |
| | | SUM of RESIDUALS = | 11.31 |

Figure 5-12 Charpy V-Notch Percent Shear vs. Temperature for Diablo Canyon Unit 2 Reactor Vessel Capsule Y Heat-Affected-Zone (HAZ) Metal

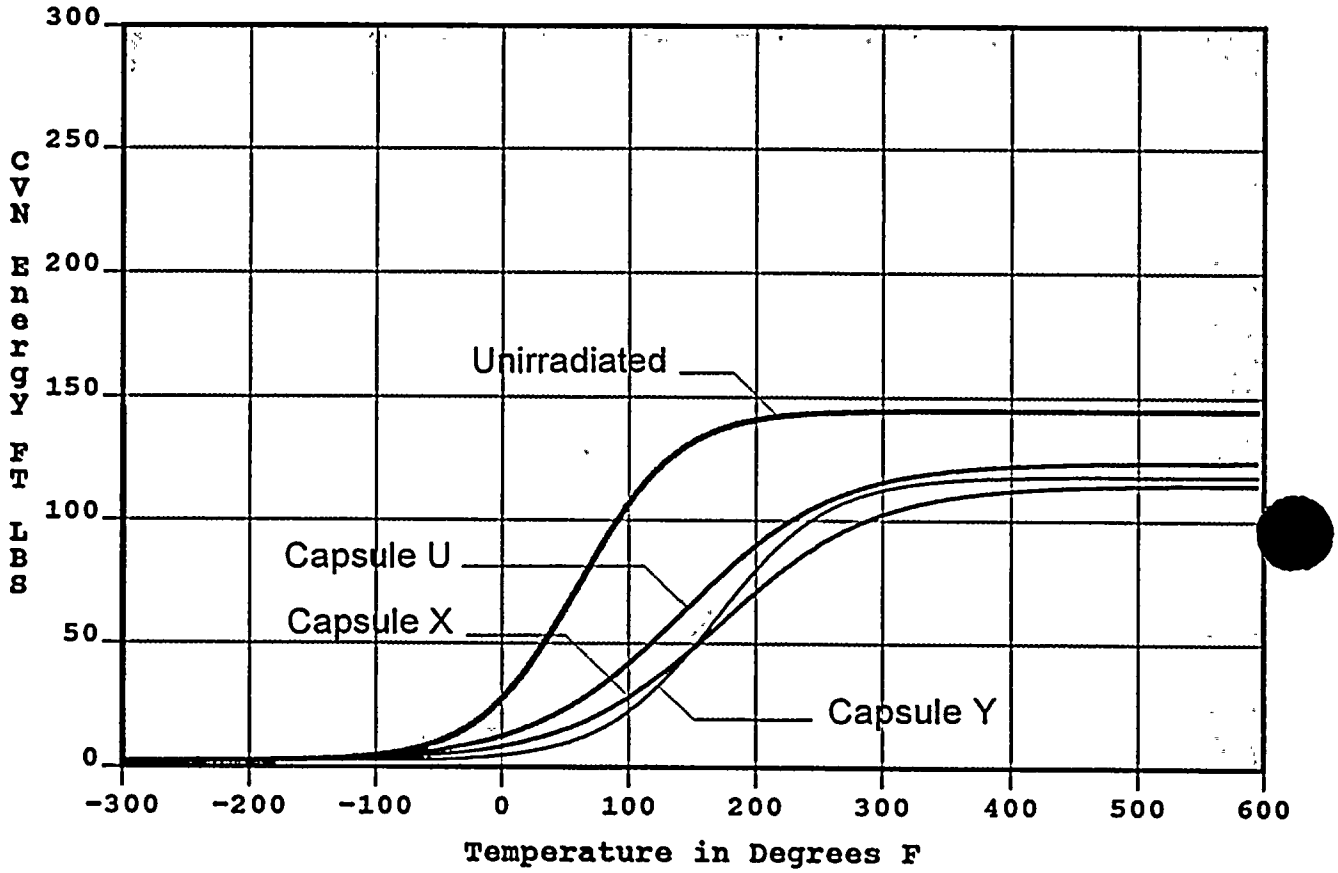


| Curve | Fluence | LSE | d-LSE | USE | d-USE | T @ 30 | d-T @ 30 | T @ 50 | d-T @ 50 |
|---|---|---|---|---|---|---|---|---|---|
| 1 | 0.00E+00 | 2.2 | 0.0 | 144.7 | 0.0 | 4.6 | 0.0 | 33.3 | 0.0 |
| 2 | 3.57E+18 | 2.2 | 0.0 | 123.8 | -20.9 | 70.5 | 65.9 | 117.4 | 84.1 |
| 3 | 8.66E+18 | 2.2 | 0.0 | 114.7 | -30.0 | 105.5 | 101.0 | 154.7 | 121.4 |
| 4 | 1.32E+19 | 2.2 | 0.0 | 118.1 | -26.6 | 117.6 | 113.0 | 153.1 | 119.8 |

Figure 5-13 Charpy V-Notch Impact Energy vs. Temperature for Diablo Canyon Unit 2 Reactor Vessel Intermediate Shell Plate B5454-1 (Longitudinal Orientation)

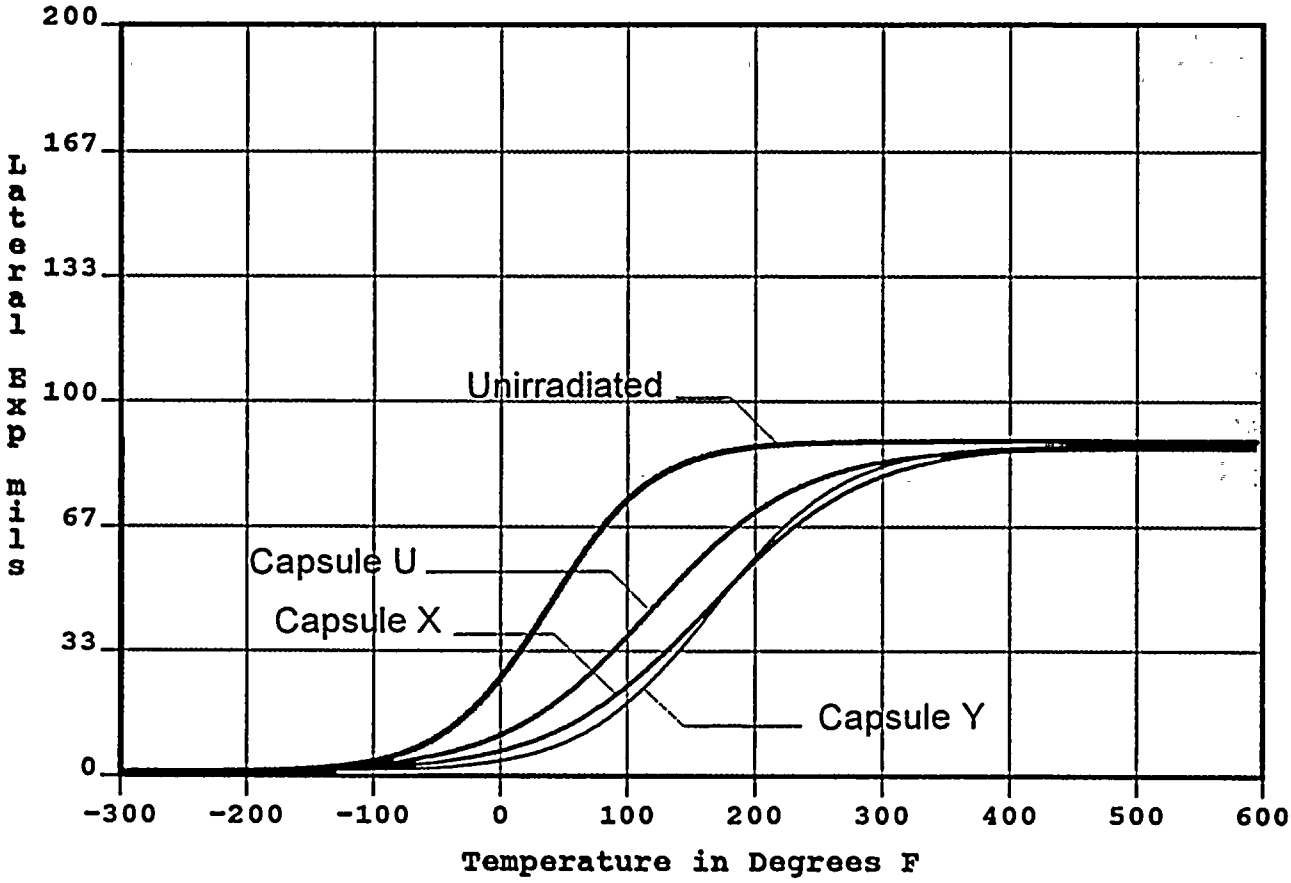


| Curve | Fluence | USLE | d-USLE | T @ LE35 | d-T @ LE35 |
|---|---|---|---|---|---|
| 1 | 0.00E+00 | 89.6 | 0.0 | 18.4 | 0.0 |
| 2 | 3.57E+18 | 87.7 | -1.9 | 93.3 | 74.9 |
| 3 | 8.66E+18 | 88.8 | -0.7 | 135.6 | 117.2 |
| 4 | 1.32E+19 | 88.8 | -0.8 | 144.1 | 125.7 |

Figure 5-14 Charpy V-Notch Lateral Expansion vs. Temperature for Diablo Canyon Unit 2 Reactor Vessel Intermediate Shell Plate B5454-1 (Longitudinal Orientation)

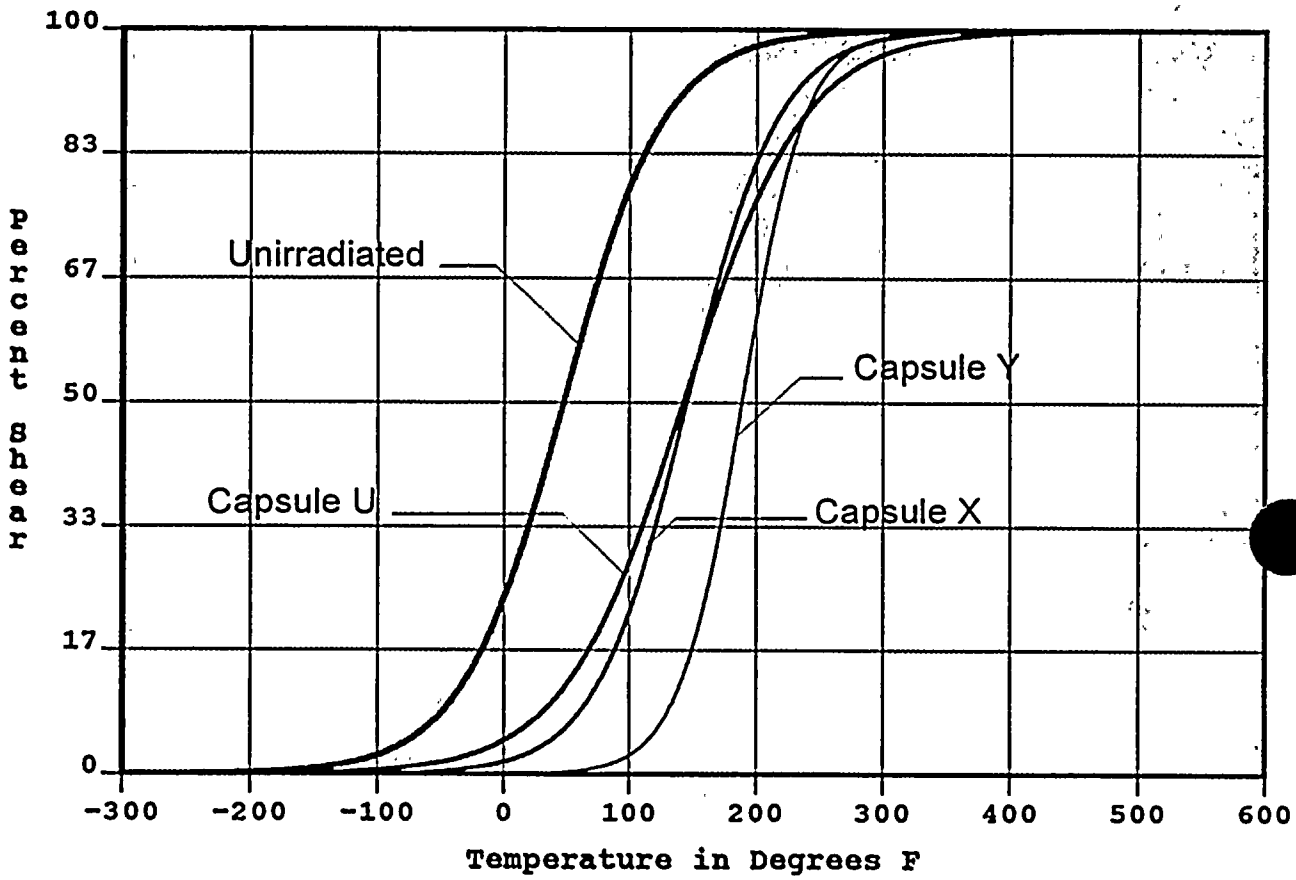


| Curve | Fluence | T @ 50% Shear | d-T @ 50% Shear |
|---|---|---|---|
| 1 | 0.00E+00 | 46.9 | 0.0 |
| 2 | 3.57E+18 | 142.7 | 95.8 |
| 3 | 8.66E+18 | 145.3 | 98.4 |
| 4 | 1.32E+19 | 188.4 | 141.6 |

Figure 5-15 Charpy V-Notch Percent Shear vs. Temperature for Diablo Canyon Unit 2 Reactor Vessel Intermediate Shell Plate B5454-1 (Longitudinal Orientation)

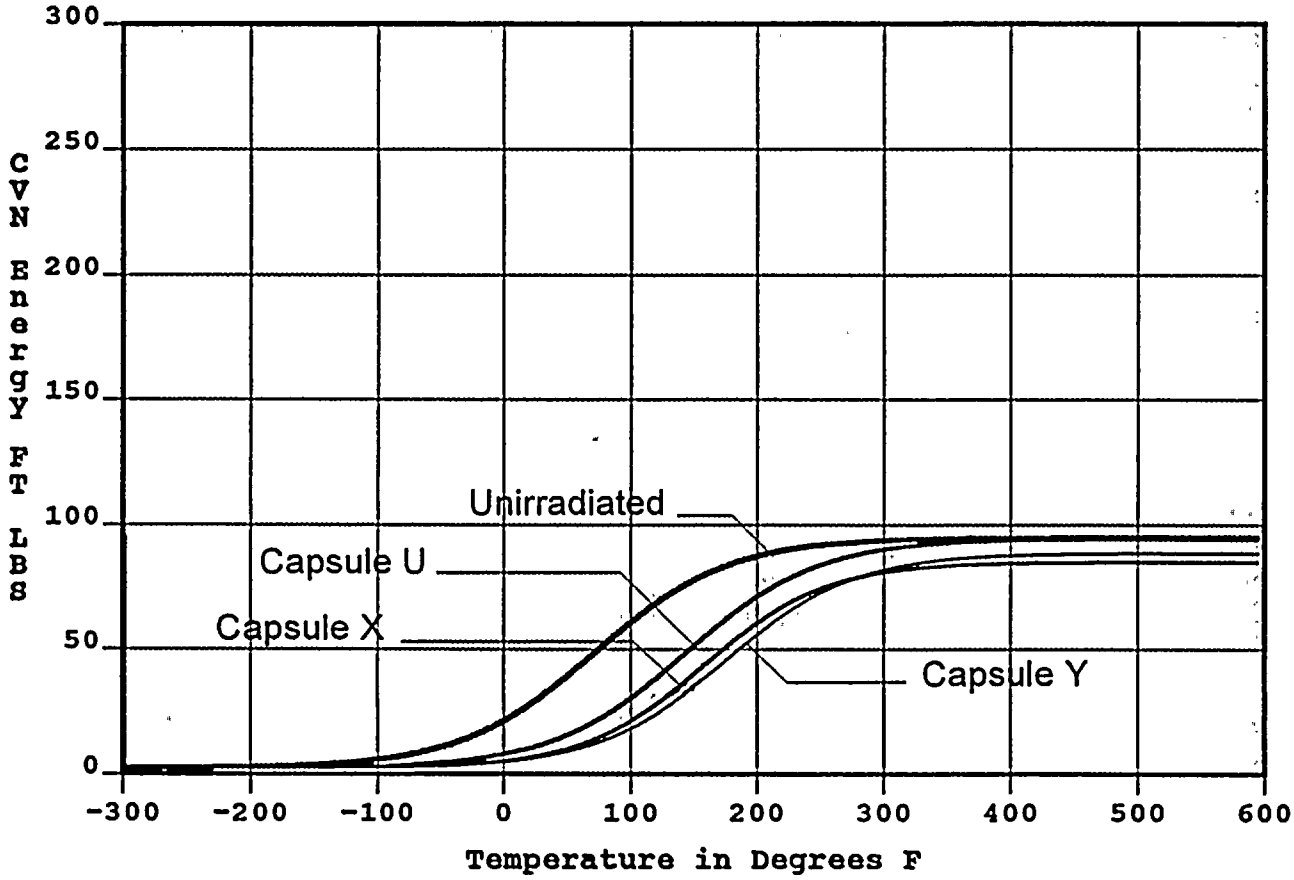


| Curve | Fluence | LSE | d-LSE | USE | d-USE | T @ 30 | d-T @ 30 | T @ 50 | d-T @ 50 |
|---|---|---|---|---|---|---|---|---|---|
| 1 | 0.00E+00 | 2.2 | 0.0 | 94.9 | 0.0 | 26.6 | 0.0 | 74.6 | 0.0 |
| 2 | 3.57E+18 | 2.2 | 0.0 | 94.5 | -0.4 | 98.9 | 72.3 | 146.8 | 72.1 |
| 3 | 8.66E+18 | 2.2 | 0.0 | 85.0 | -9.8 | 125.5 | 98.9 | 173.1 | 98.5 |
| 4 | 1.32E+19 | 2.2 | 0.0 | 88.6 | -6.3 | 137.3 | 110.7 | 185.7 | 111.1 |

Figure 5-16 Charpy V-Notch Impact Energy vs. Temperature for Diablo Canyon Unit 2 Reactor Vessel Intermediate Shell Plate B5454-1 (Transverse Orientation)

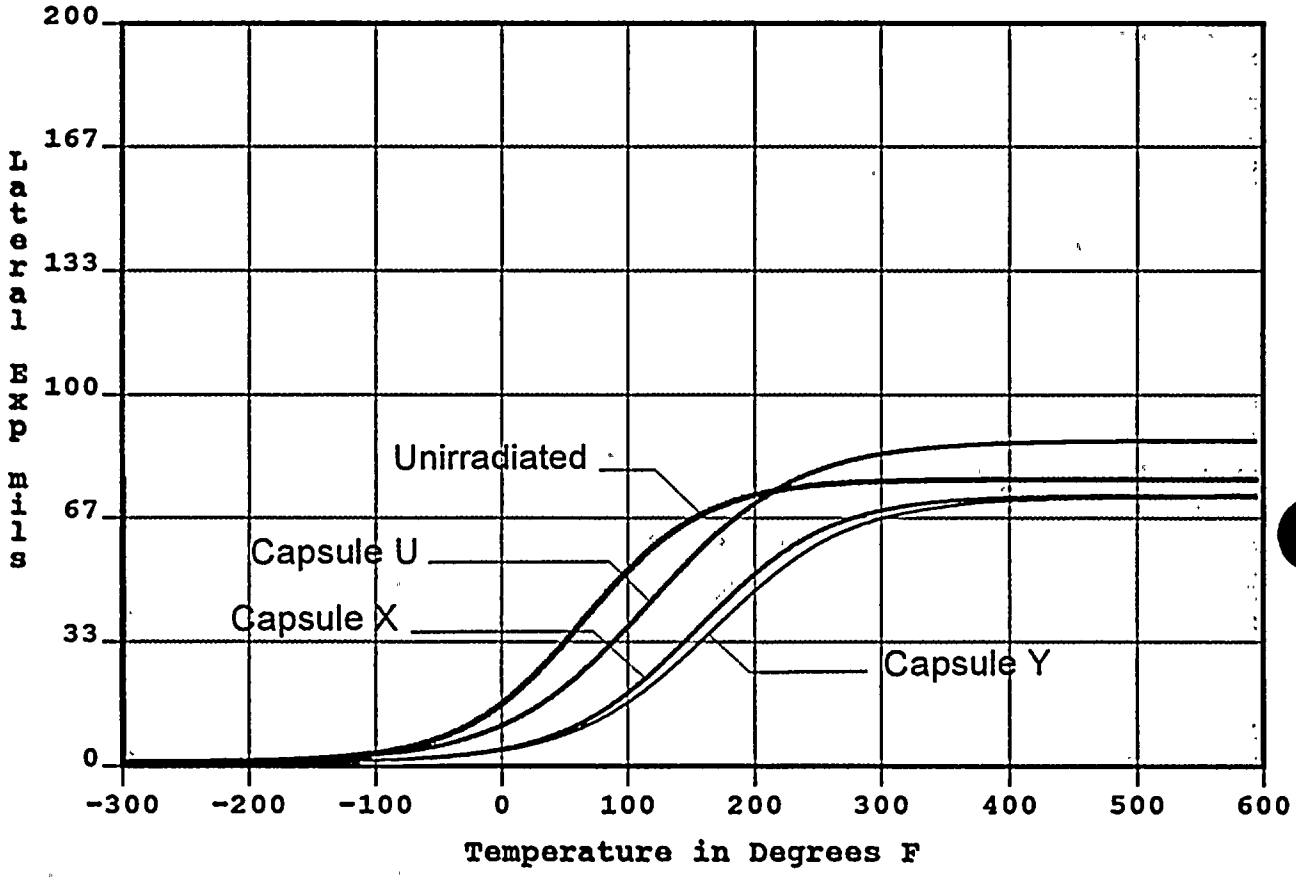


| Curve | Fluence | USLE | d-USLE | T @ LE35 | d-T @ LE35 |
|---|---|---|---|---|---|
| 1 | 0.00E+00 | 77.1 | 0.0 | 54.4 | 0.0 |
| 2 | 3.57E+18 | 87.7 | 10.5 | 93.3 | 38.9 |
| 3 | 8.66E+18 | 72.8 | -4.3 | 149.2 | 94.8 |
| 4 | 1.32E+19 | 72.2 | -4.9 | 162.2 | 107.7 |

Figure 5-17 Charpy V-Notch Lateral Expansion vs. Temperature for Diablo Canyon Unit 2 Reactor Vessel Intermediate Shell Plate B5454-1 (Transverse Orientation)

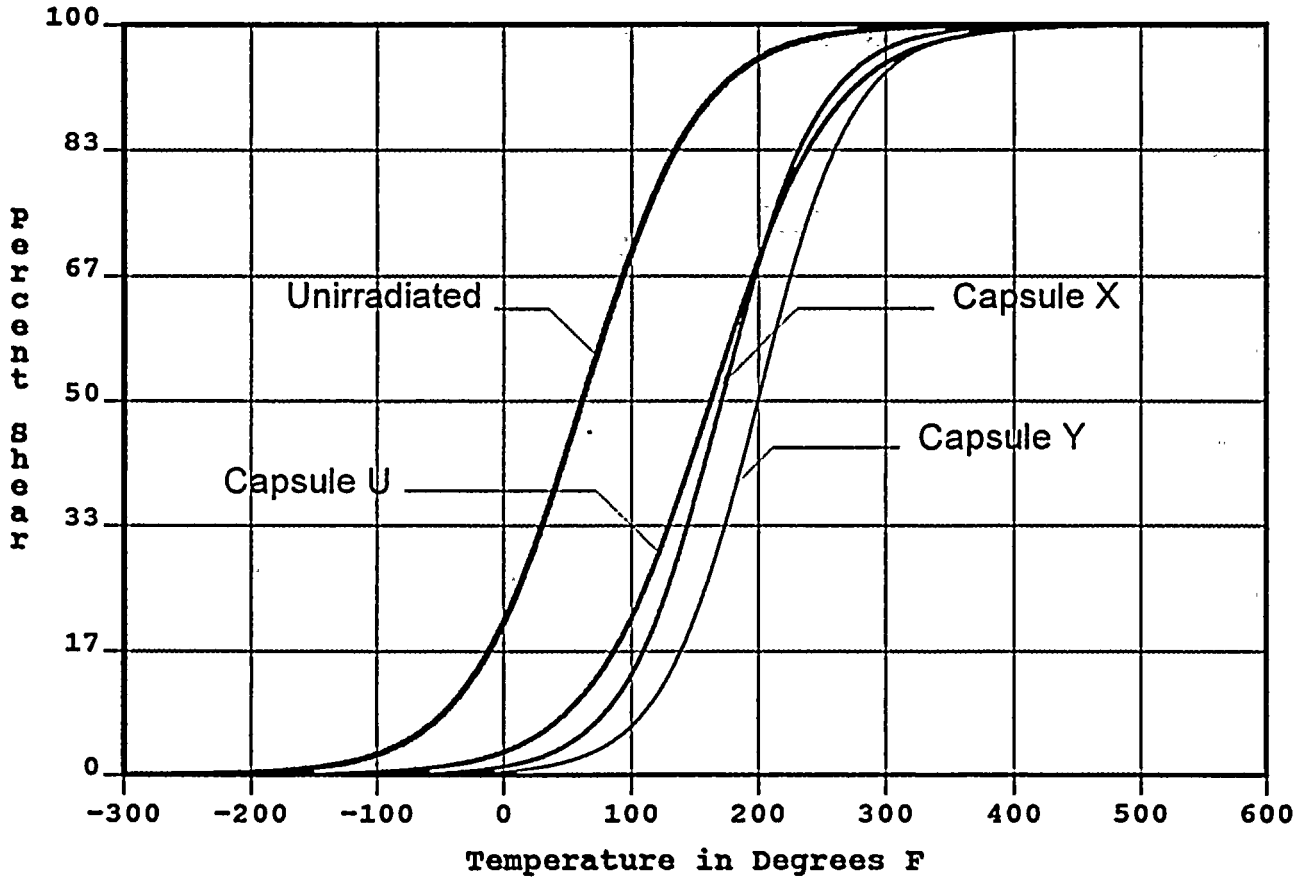


| Curve | Fluence | T @ 50% Shear | d-T @ 50% Shear |
|---|---|---|---|
| 1 | 0.00E+00 | 61.4 | 0.0 |
| 2 | 3.57E+18 | 162.2 | 100.8 |
| 3 | 8.66E+18 | 170.5 | 109.1 |
| 4 | 1.32E+19 | 199.2 | 137.8 |

Figure 5-18 Charpy V-Notch Percent Shear vs. Temperature for Diablo Canyon Unit 2 Reactor Vessel Intermediate Shell Plate B5454-1 (Transverse Orientation)

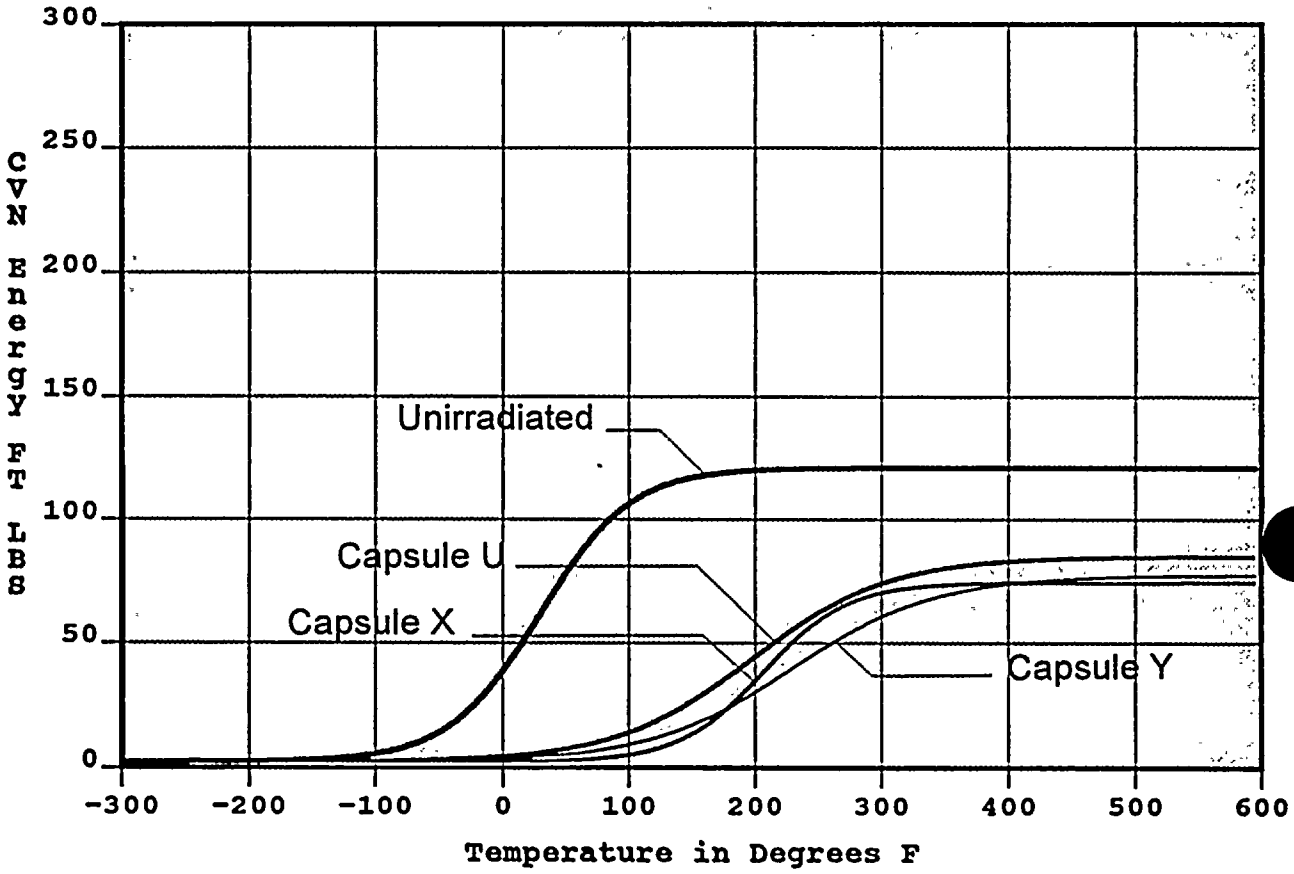


| Curve | Fluence | LSE | d-LSE | USE | d-USE | T @ 30 | d-T @ 30 | T @ 50 | d-T @ 50 |
|---|---|---|---|---|---|---|---|---|---|
| 1 | 0.00E+00 | 2.2 | 0.0 | 120.9 | 0.0 | -13.6 | 0.0 | 14.9 | 0.0 |
| 2 | 3.57E+18 | 2.2 | 0.0 | 85.0 | -35.9 | 160.2 | 173.8 | 214.5 | 199.7 |
| 3 | 8.66E+18 | 2.2 | 0.0 | 74.4 | -46.5 | 190.6 | 204.2 | 228.7 | 213.9 |
| 4 | 1.32E+19 | 2.2 | 0.0 | 77.3 | -43.6 | 198.9 | 212.5 | 260.9 | 246.0 |

Figure 5-19 Charpy V-Notch Impact Energy vs. Temperature for Diablo Canyon Unit 2 Reactor Vessel Weld Metal

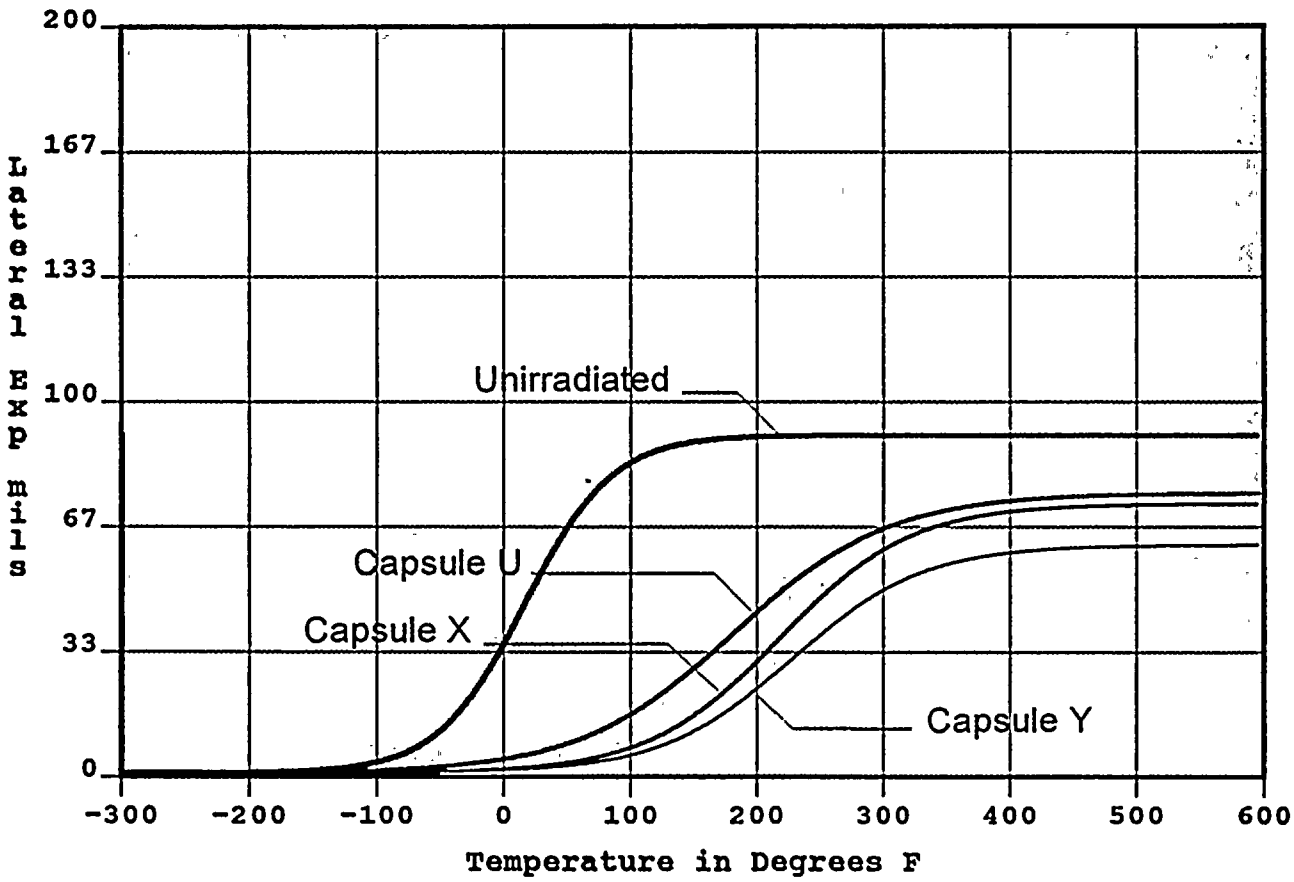


| Curve | Fluence | USLE | d-USLE | T @ LE35 | d-T @ LE35 |
|---|---|---|---|---|---|
| 1 | 0.00E+00 | 91.1 | 0.0 | -0.7 | 0.0 |
| 2 | 3.57E+18 | 75.8 | -15.3 | 170.7 | 171.4 |
| 3 | 8.66E+18 | 72.9 | -18.2 | 212.3 | 213.0 |
| 4 | 1.32E+19 | 61.8 | -29.3 | 239.7 | 240.4 |

Figure 5-20 Charpy V-Notch Lateral Expansion vs. Temperature for Diablo Canyon Unit 2 Reactor Vessel Weld Metal

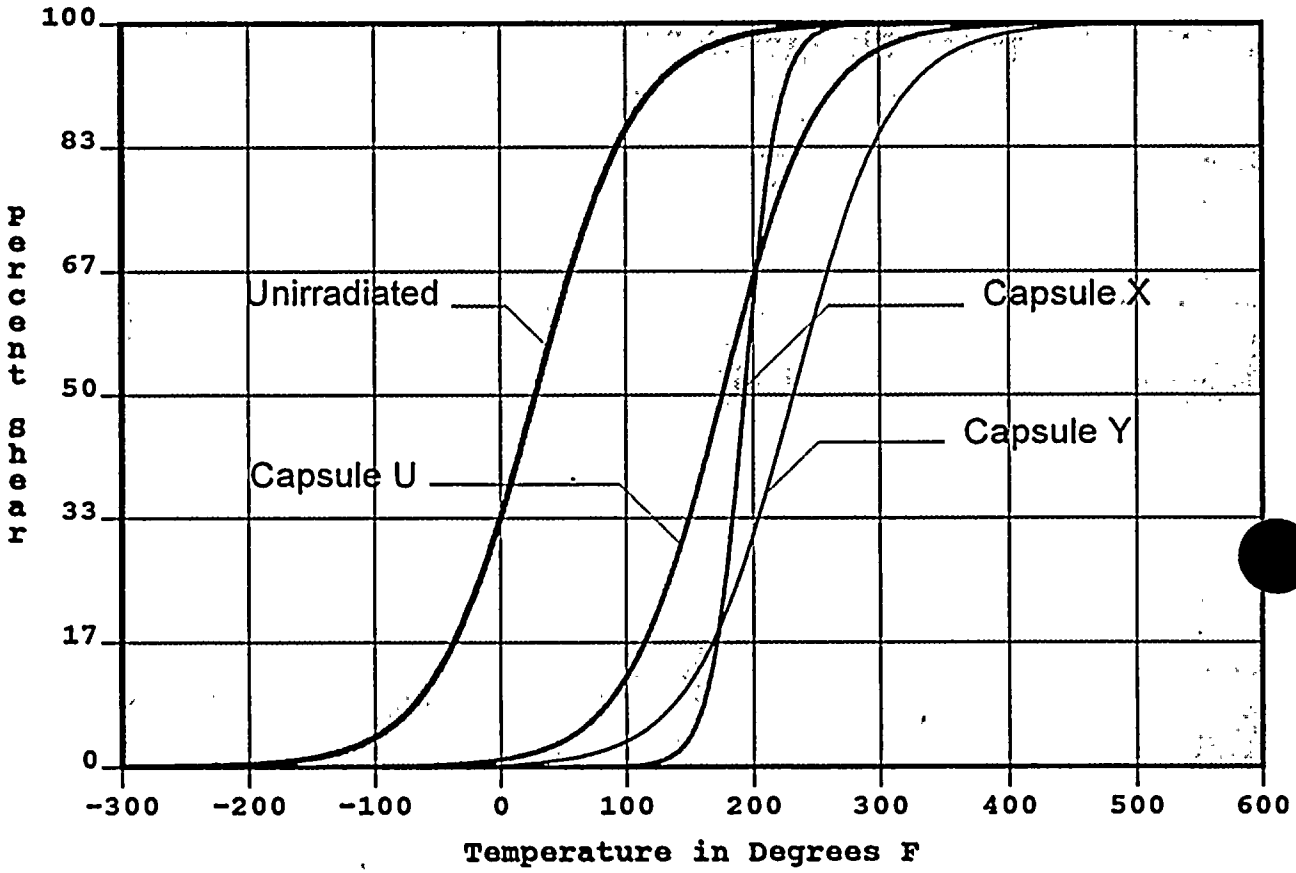


| Curve | Fluence | T @ 50% Shear | d-T @ 50% Shear |
|---|---|---|---|
| 1 | 0.00E+00 | 27.7 | 0.0 |
| 2 | 3.57E+18 | 175.2 | 147.5 |
| 3 | 8.66E+18 | 192.8 | 165.1 |
| 4 | 1.32E+19 | 231.1 | 203.4 |

Figure 5-21 Charpy V-Notch Percent Shear vs. Temperature for Diablo Canyon Unit 2 Reactor Vessel Weld Metal

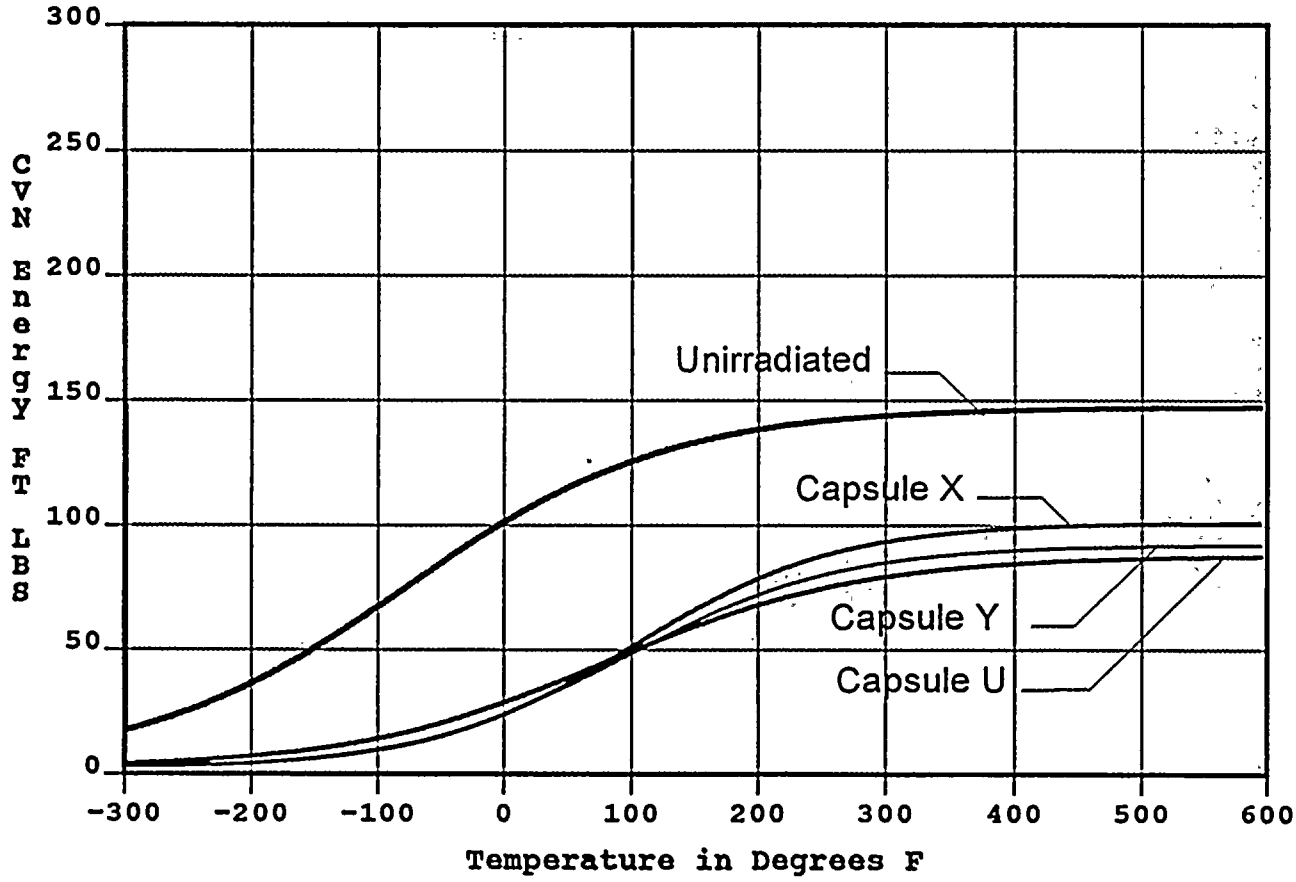


| Curve | Fluence | LSE | d-LSE | USE | d-USE | T @ 30 | d-T @ 30 | T @ 50 | d-T @ 50 |
|---|---|---|---|---|---|---|---|---|---|
| 1 | 0.00E+00 | 2.2 | 0.0 | 147.5 | 0.0 | z-227.4 | 0.0 | z-152.3 | 0.0 |
| 2 | 3.57E+18 | 2.2 | 0.0 | 88.0 | -59.5 | 6.8 | 234.2 | 103.5 | 255.7 |
| 3 | 8.66E+18 | 2.2 | 0.0 | 101.2 | -46.3 | 26.1 | 253.5 | 96.2 | 248.5 |
| 4 | 1.32E+19 | 2.2 | 0.0 | 92.3 | -55.2 | 27.9 | 255.3 | 105.8 | 258.1 |

Figure 5-22 Charpy V-Notch Impact Energy vs. Temperature for Diablo Canyon Unit 2 Reactor Vessel Heat-Affected-Zone (HAZ) Metal

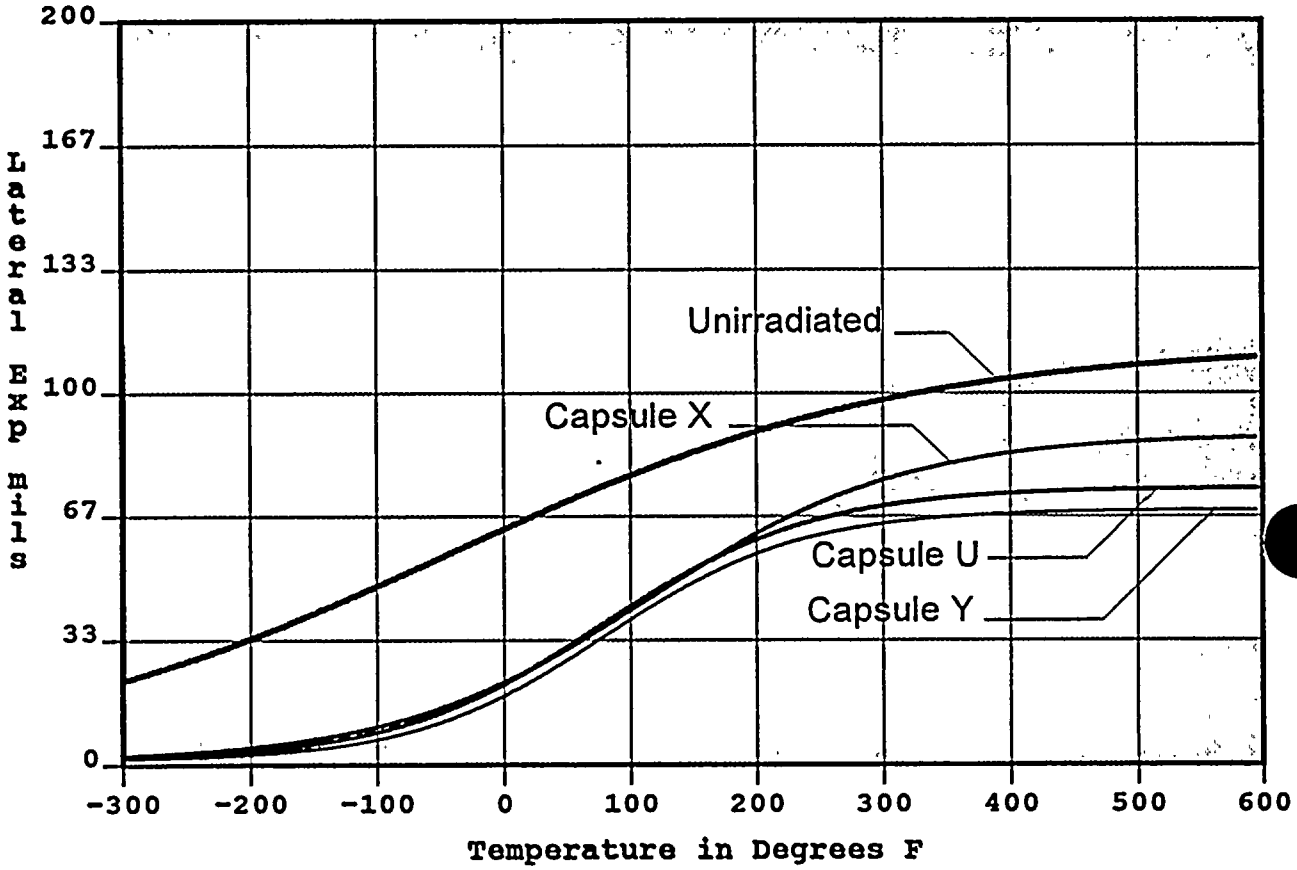


| Curve | Fluence | USLE | d-USLE | T @ LE35 | d-T @ LE35 |
|---|---|---|---|---|---|
| 1 | 0.00E+00 | 112.7 | 0.0 | z-190.1 | 0.0 |
| 2 | 3.57E+18 | 74.3 | -38.5 | 66.2 | 256.4 |
| 3 | 8.66E+18 | 88.7 | -24.1 | 70.1 | 260.2 |
| 4 | 1.32E+19 | 68.3 | -44.4 | 82.2 | 272.3 |

Figure 5-23 Charpy V-Notch Lateral Expansion vs. Temperature for Diablo Canyon Unit 2 Reactor Vessel Heat-Affected-Zone (HAZ) Metal

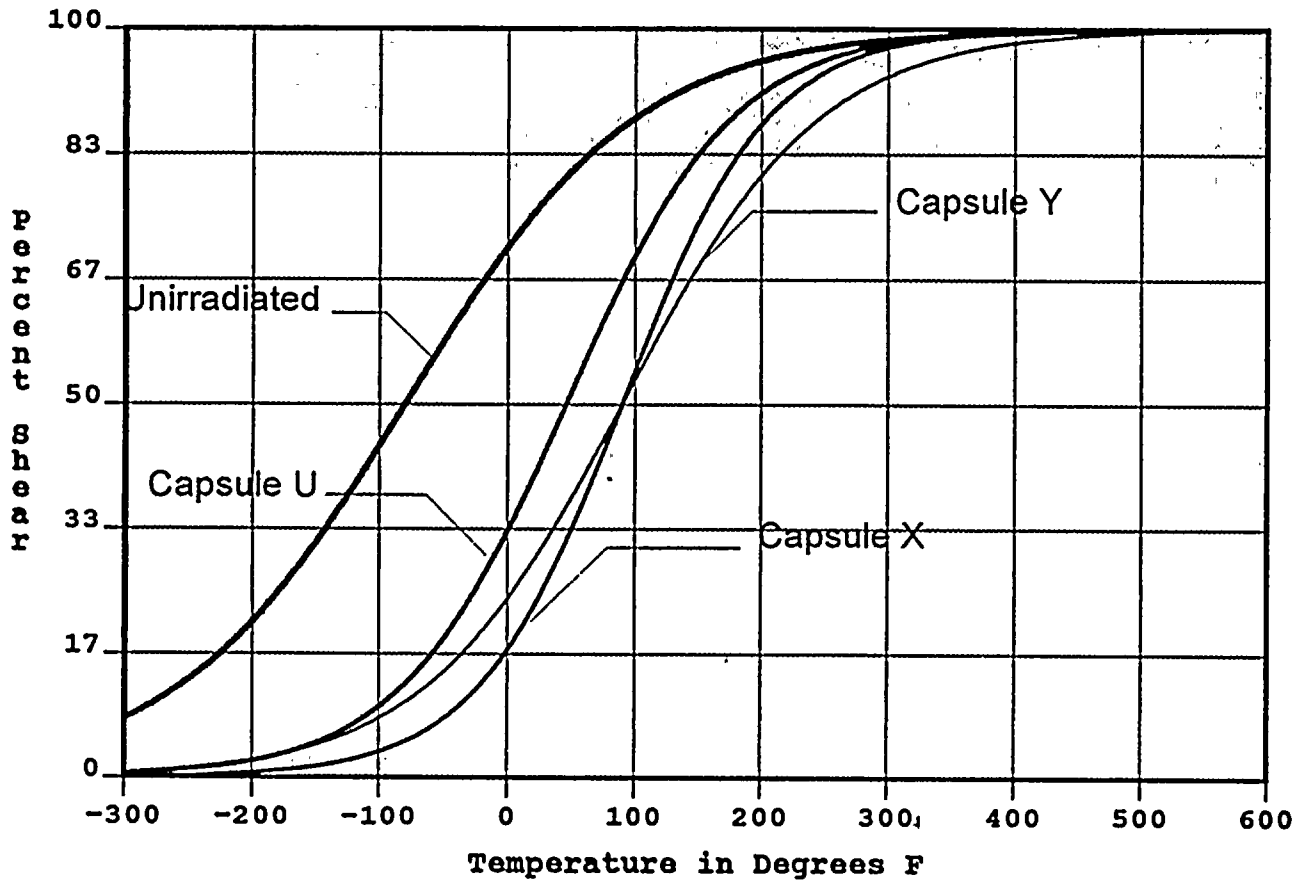


| Curve | Fluence | T @ 50% Shear | d-T @ 50% Shear |
|---|---|---|---|
| 1 | 0.00E+00 | -80.5 | 0.0 |
| 2 | 3.57E+18 | 45.6 | 126.0 |
| 3 | 8.66E+18 | 89.6 | 170.1 |
| 4 | 1.32E+19 | 89.5 | 170.0 |

Figure 5-24 Charpy V-Notch Percent Shear vs. Temperature for Diablo Canyon Unit 2 Reactor Vessel Heat-Affected-Zone (HAZ) Metal

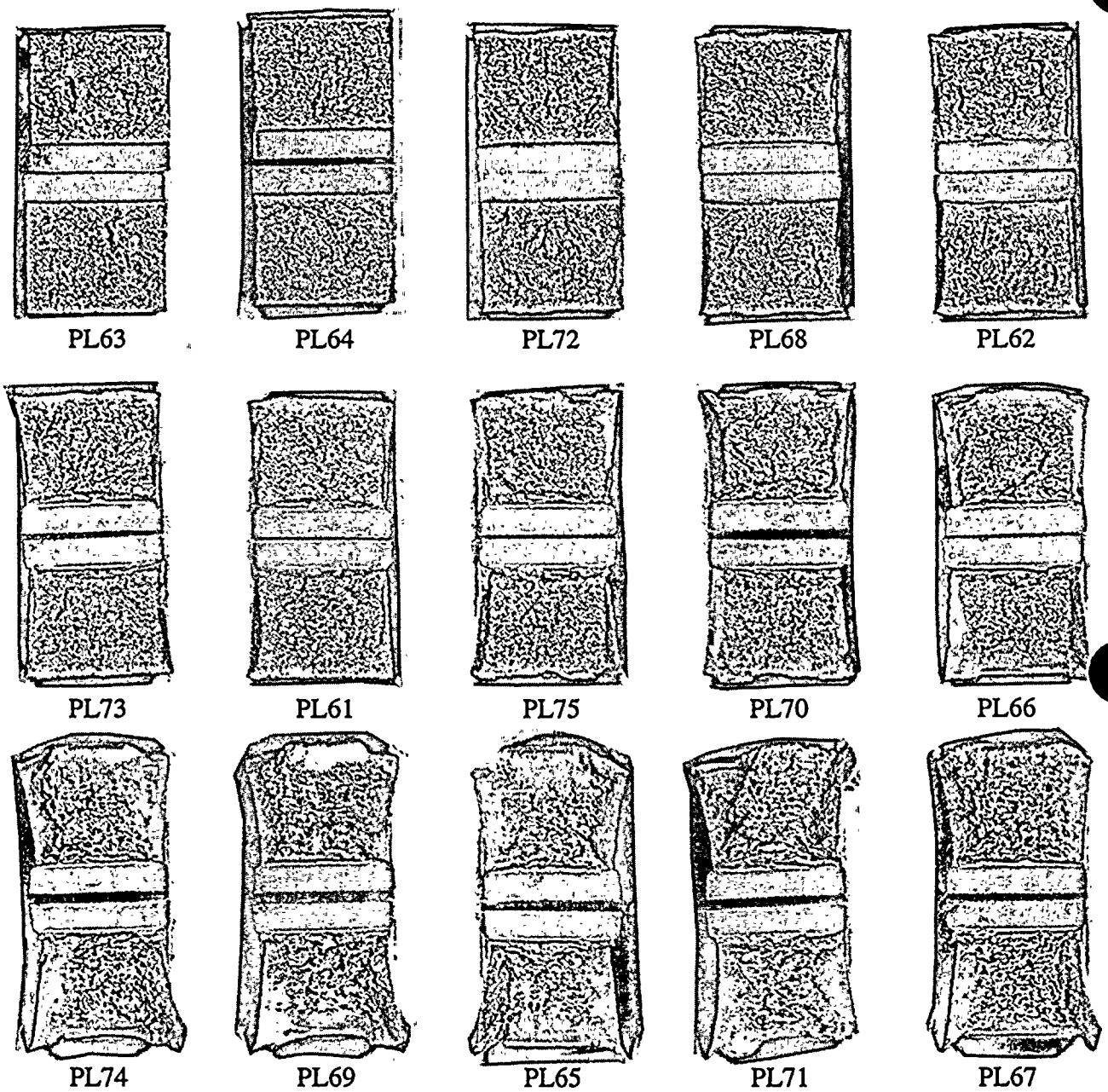


Figure 5-25 Charpy Impact Specimen Fracture Surfaces of the Diablo Canyon Unit 2 Reactor Vessel Intermediate Shell Plate B5454-1 (Longitudinal Orientation)

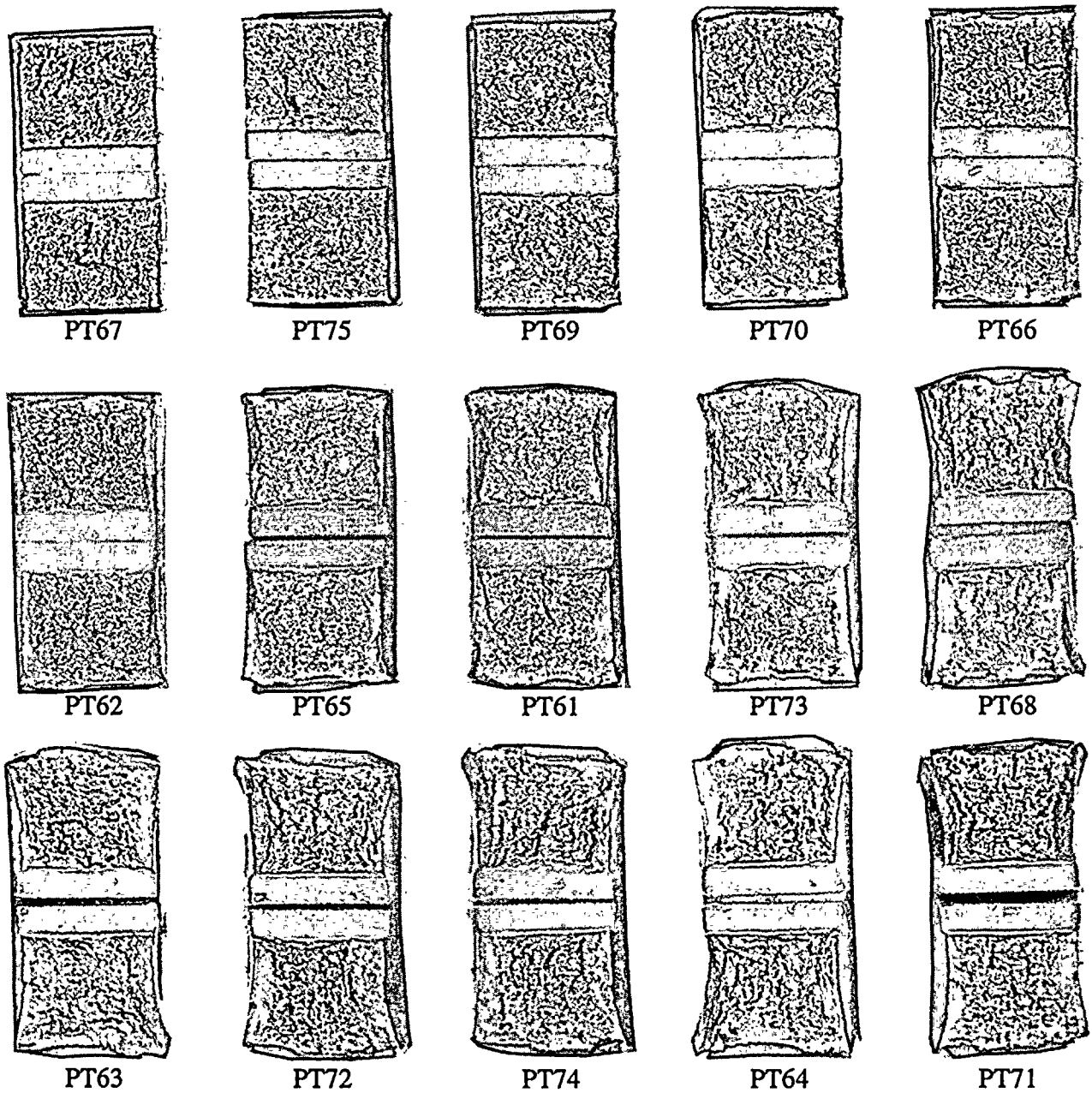


Figure 5-26 Charpy Impact Specimen Fracture Surfaces of the Diablo Canyon Unit 2 Reactor Vessel Intermediate Shell Plate B5454-1 (Transverse Orientation)

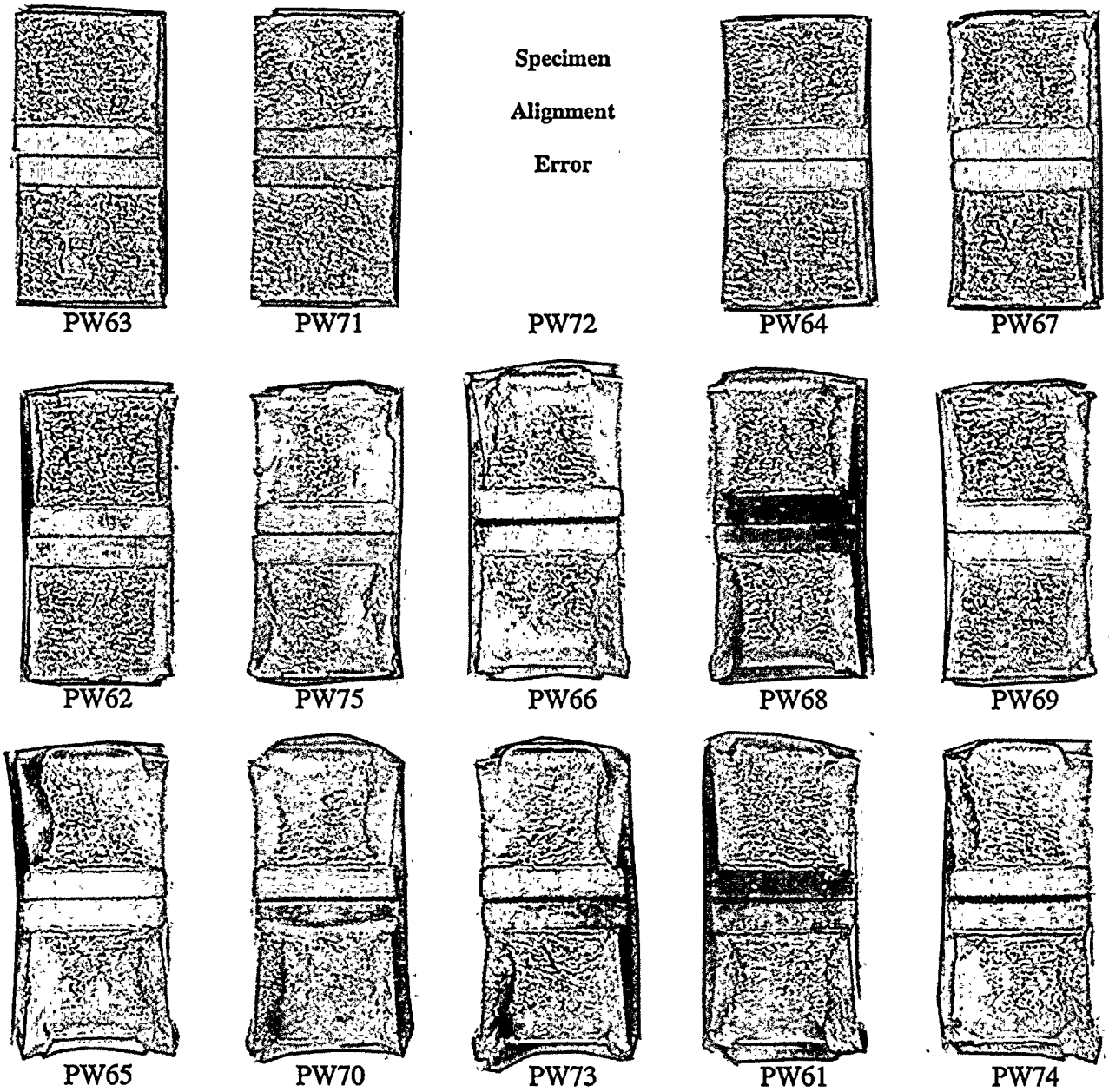


Figure 5-27 Charpy Impact Specimen Fracture Surfaces of the Diablo Canyon Unit 2 Reactor Vessel Weld Metal

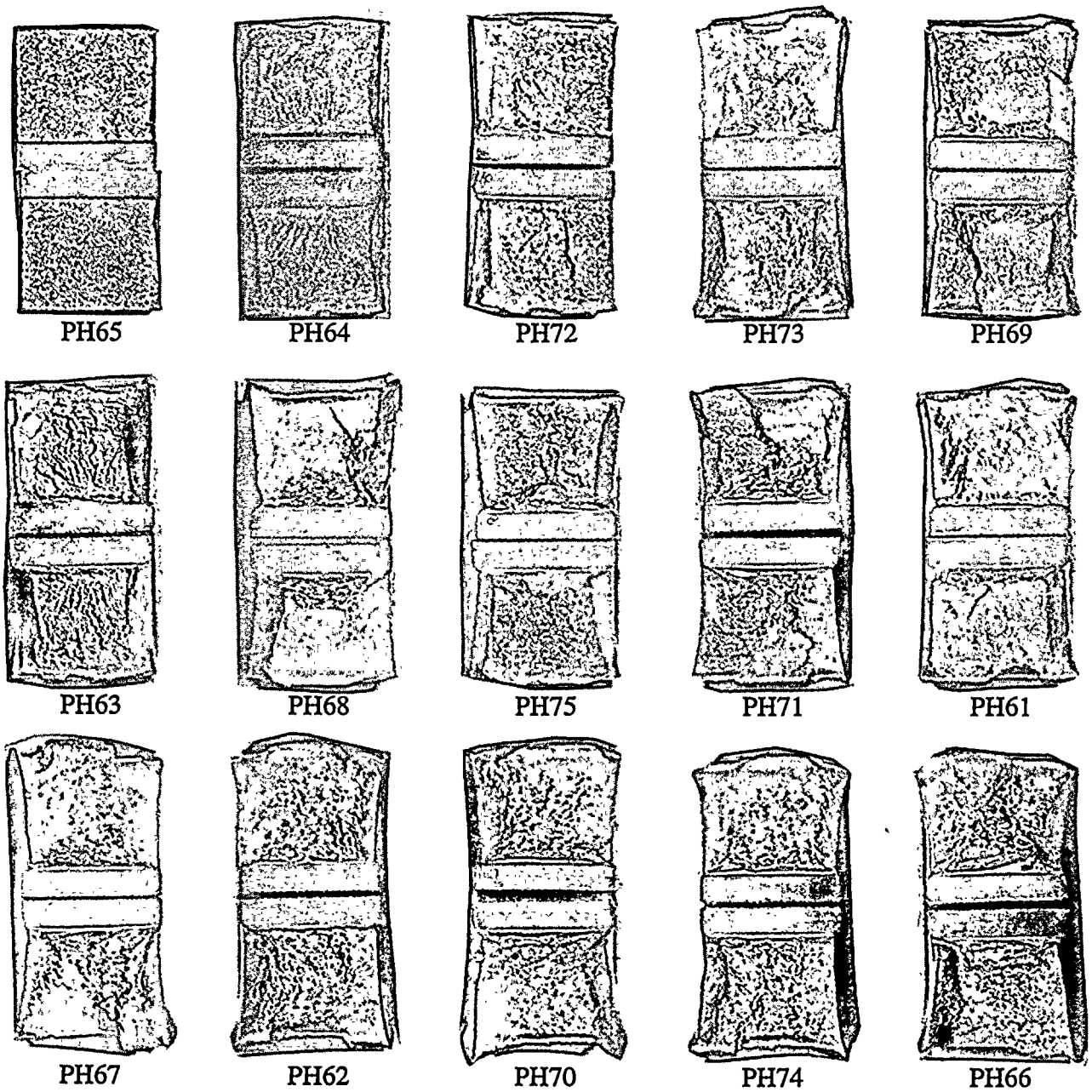


Figure 5-28 Charpy Impact Specimen Fracture Surfaces of the Diablo Canyon Unit 2 Reactor Vessel Weld Heat-Affected-Zone (HAZ) Metal

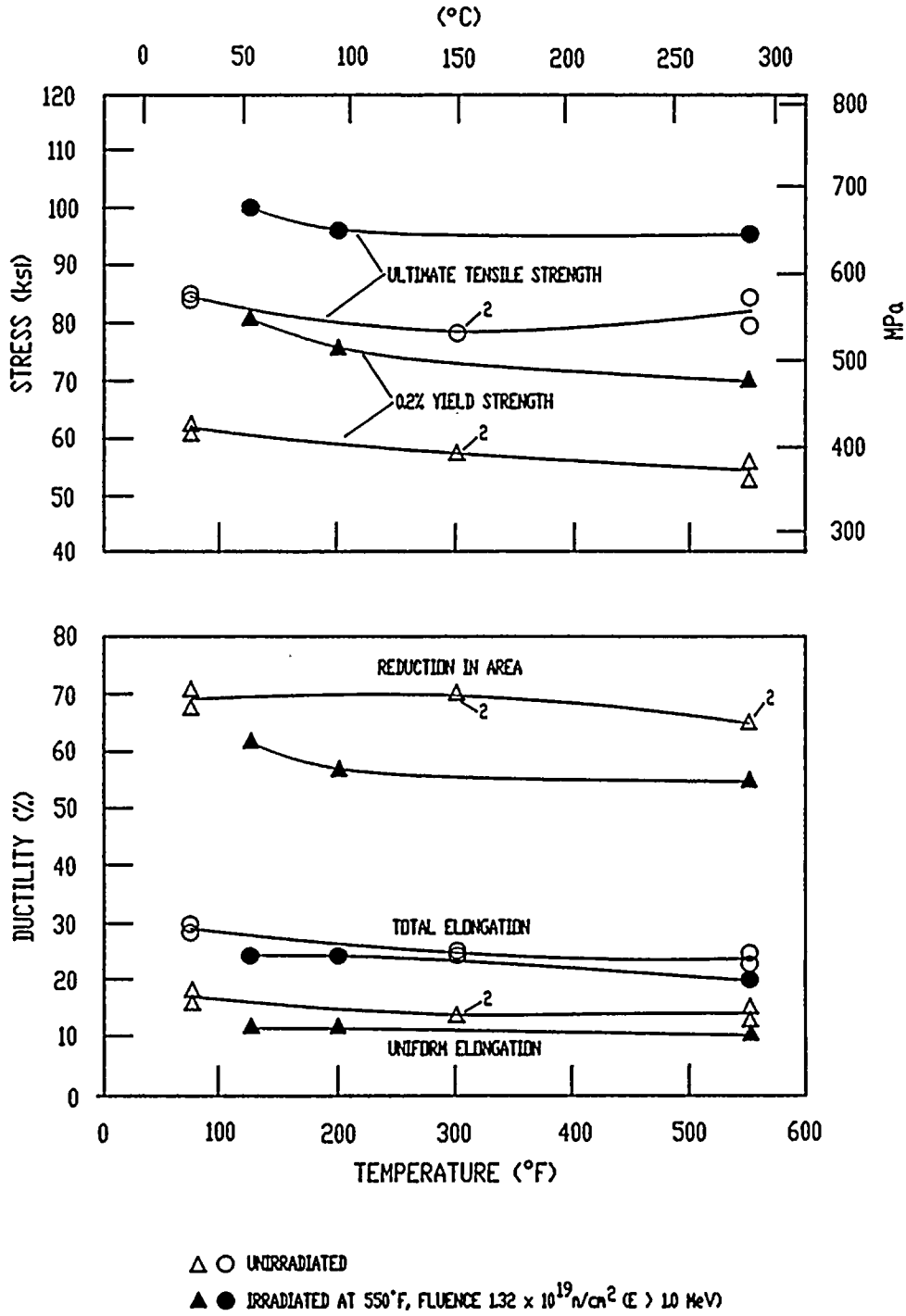


Figure 5-29 Tensile Properties for the Diablo Canyon Unit 2 Reactor Vessel Intermediate Shell Plate B5454-1 (Longitudinal Orientation)

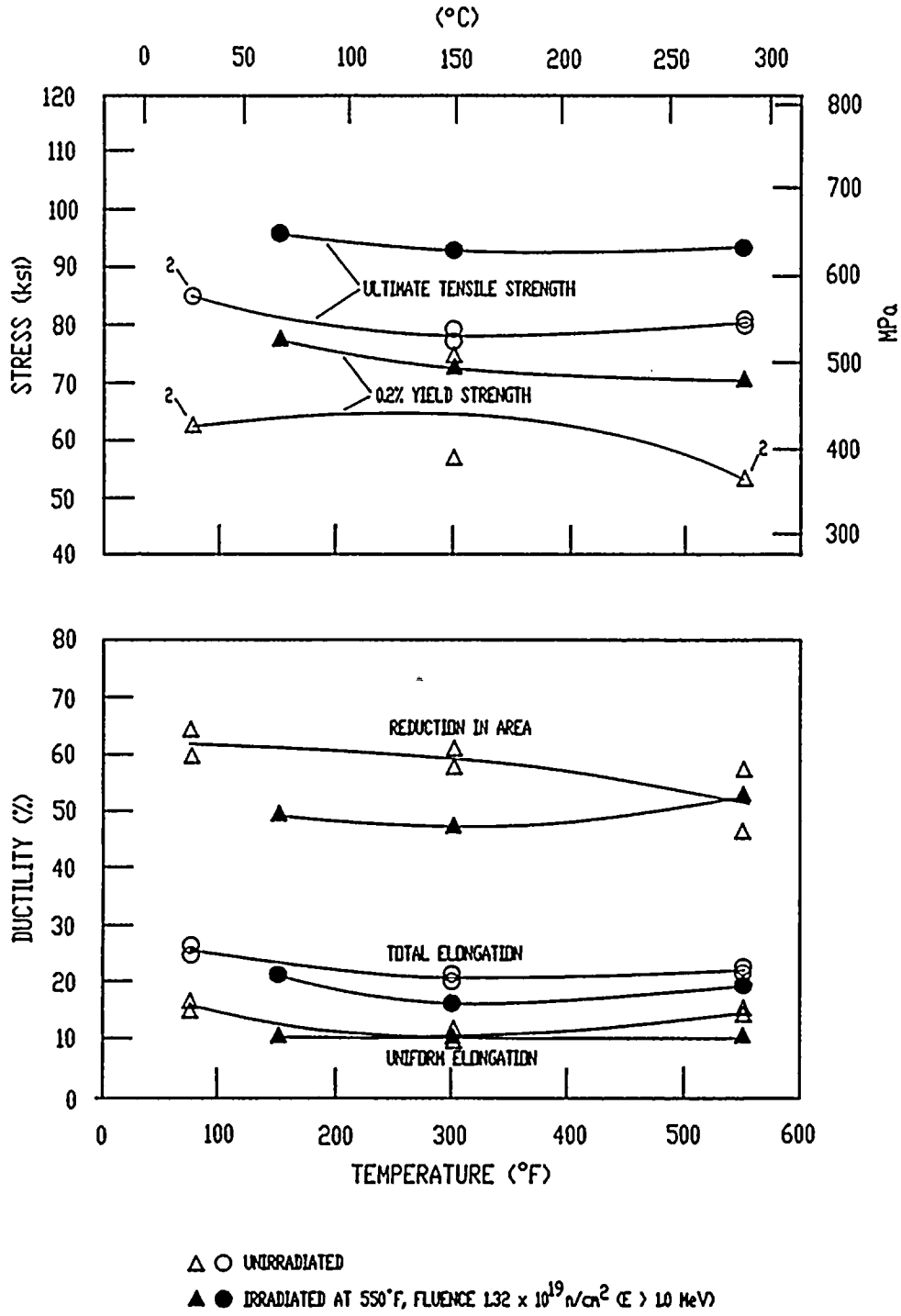


Figure 5-30 Tensile Properties for the Diablo Canyon Unit 2 Reactor Vessel Intermediate Shell Plate B5454-1 (Transverse Orientation)

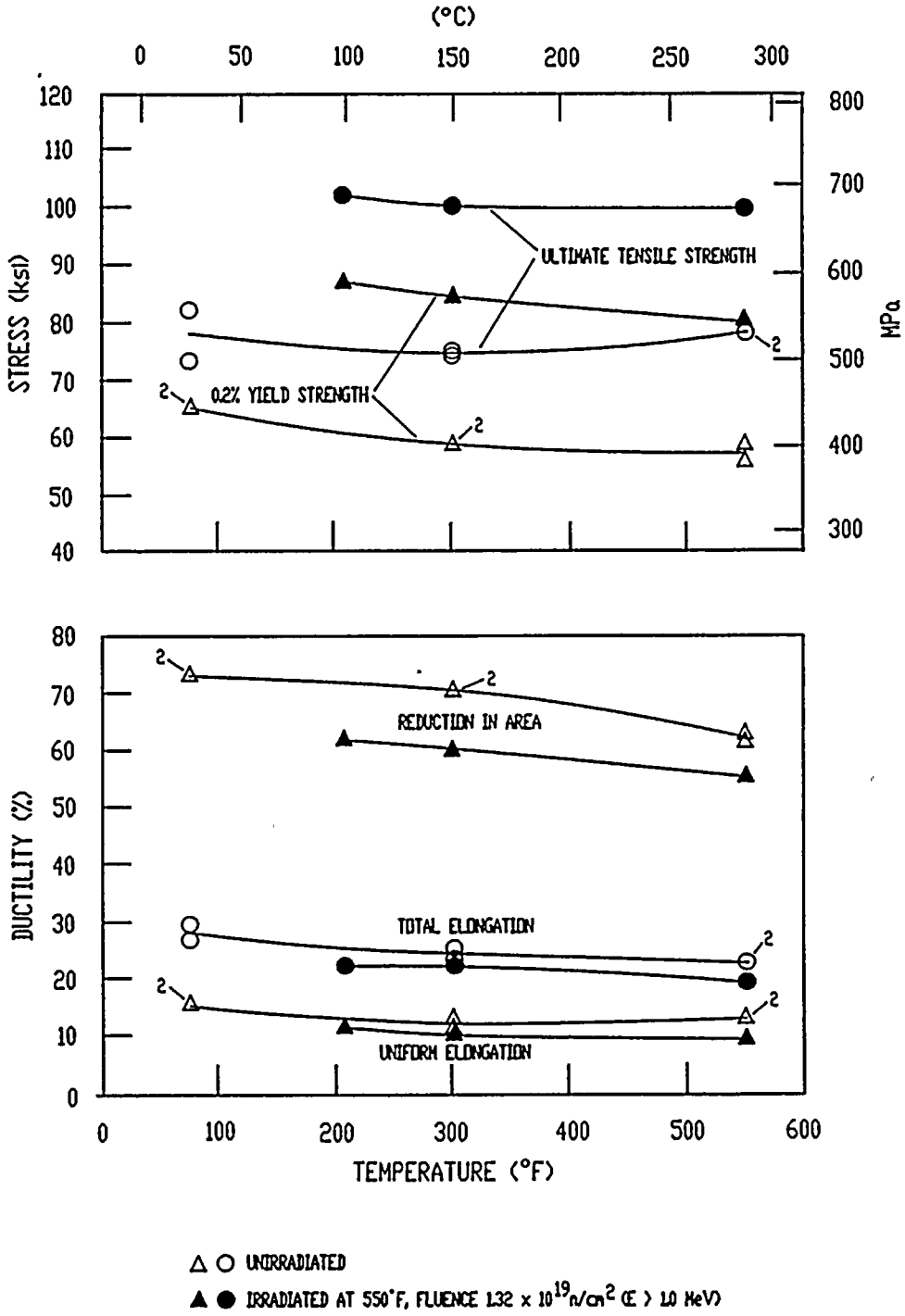


Figure 5-31 Tensile Properties for the Diablo Canyon Unit 2 Reactor Vessel Weld Metal

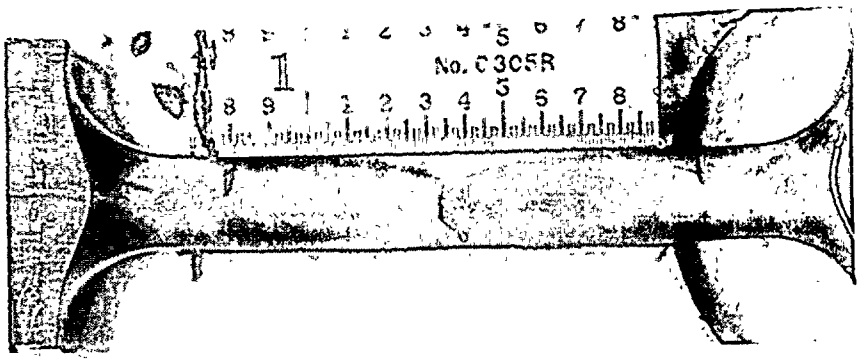

Specimen PL13 tested at 125°F

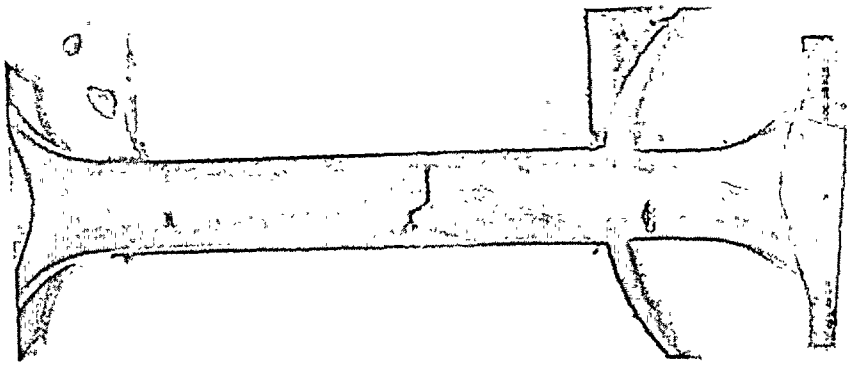

Specimen PL14 tested at 200°F

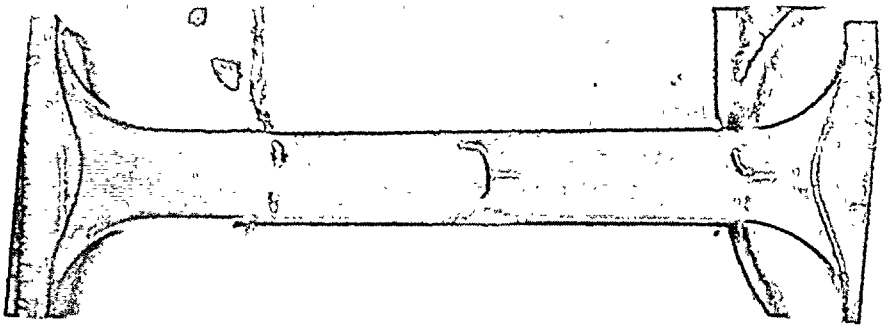

Specimen PL15 tested at 550°F

Figure 5-32 Fractured Tensile Specimens from the Diablo Canyon Unit 2 Reactor Vessel Intermediate Shell Plate B5454-1 (Longitudinal Orientation)

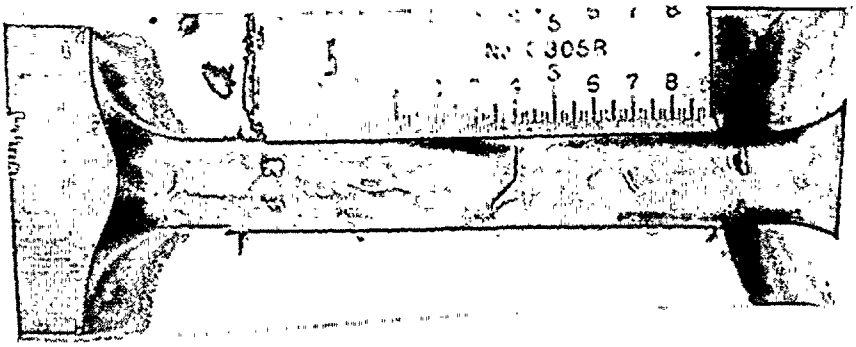

Specimen PT13 tested at 150°F

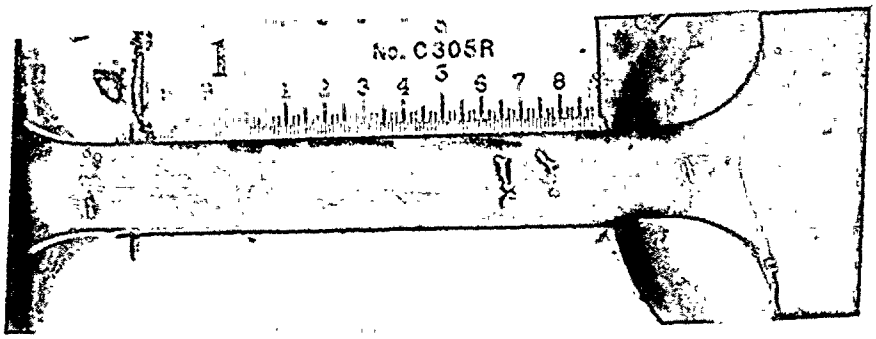


Specimen PT14 tested at 300°F

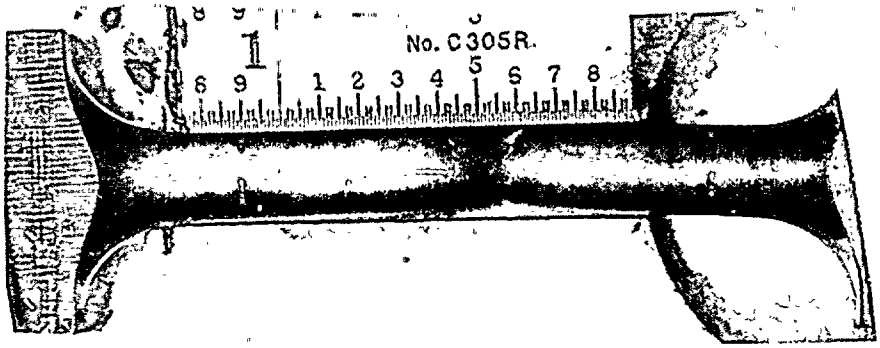


Specimen PT15 tested at 550°F

Figure 5-33 Fractured Tensile Specimens from the Diablo Canyon Unit 2 Reactor Vessel Intermediate Shell Plate B5454-1 (Transverse Orientation)

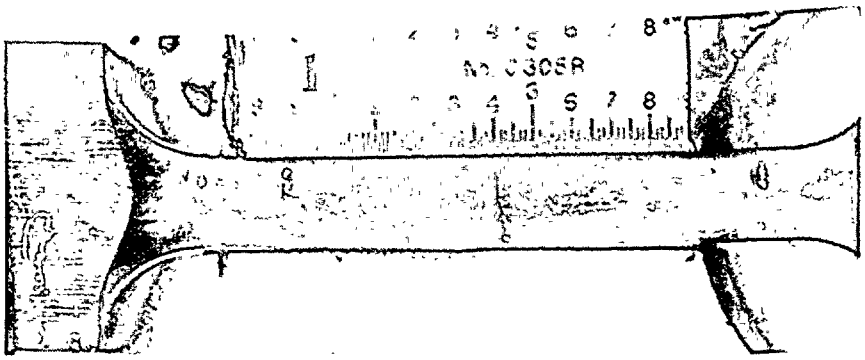

Specimen PW13 tested at 210°F

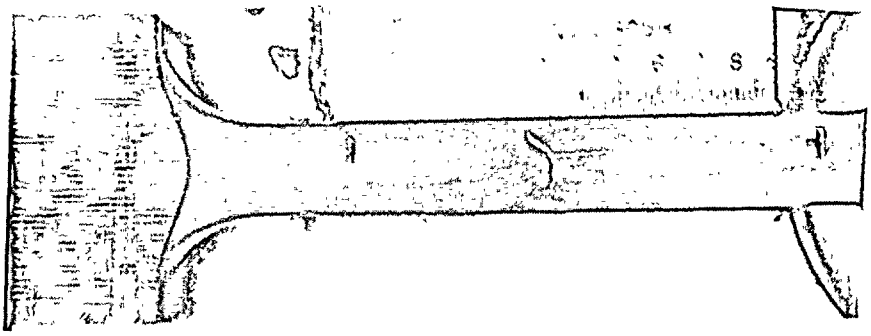

Specimen PW14 tested at 300°F

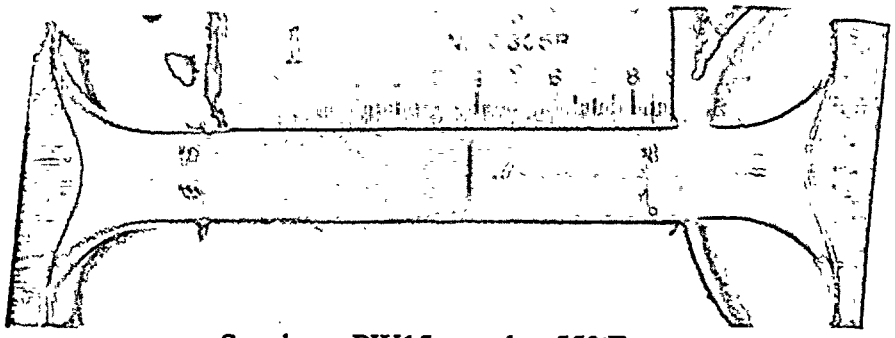

Specimen PW15 tested at 550°F

Figure 5-34 Fractured Tensile Specimens from the Diablo Canyon Unit 2 Reactor Vessel Weld Metal

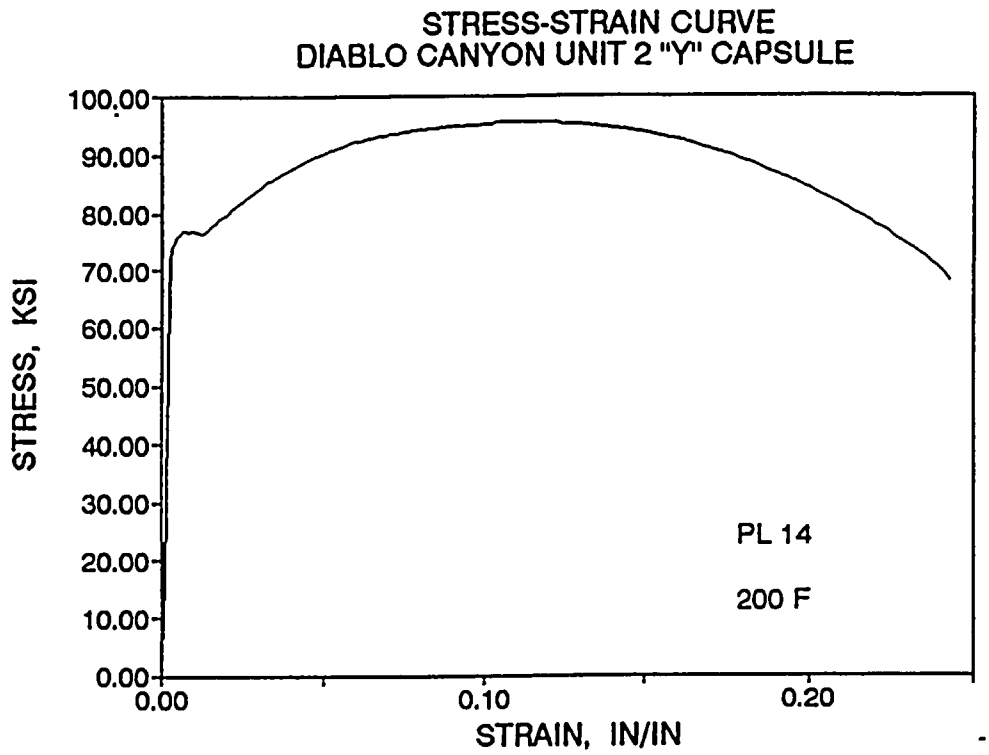


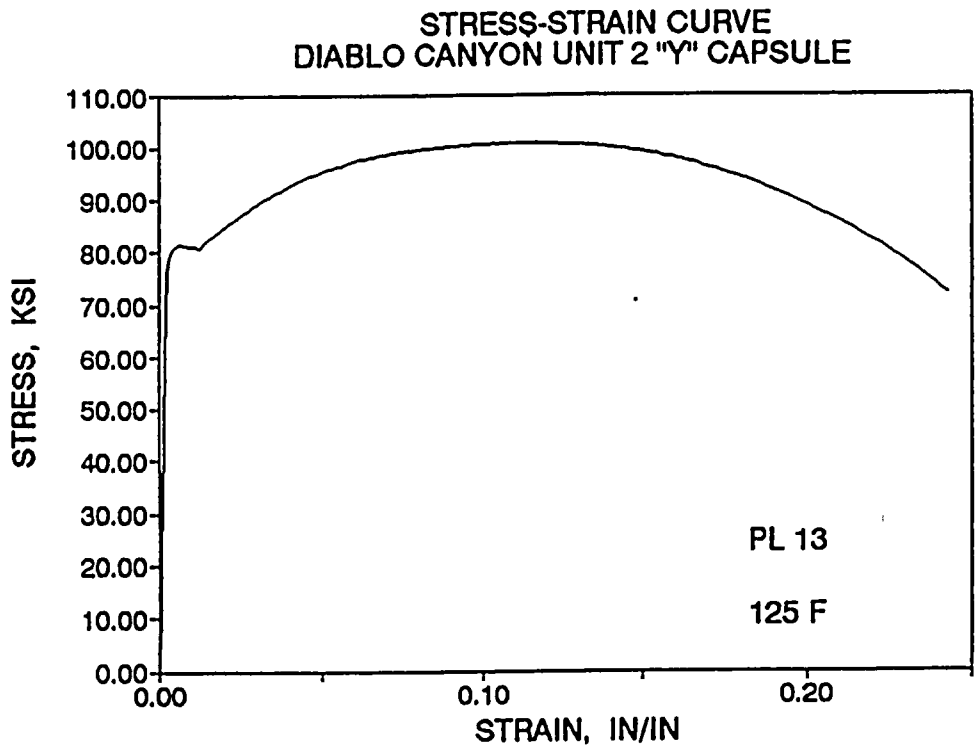


Figure 5-35 Engineering Stress-Strain Curves for Diablo Canyon Unit 2 Reactor Vessel Intermediate Shell Plate B5454-1 Tensile Specimens PL13 and PL14 (Longitudinal Orientation)

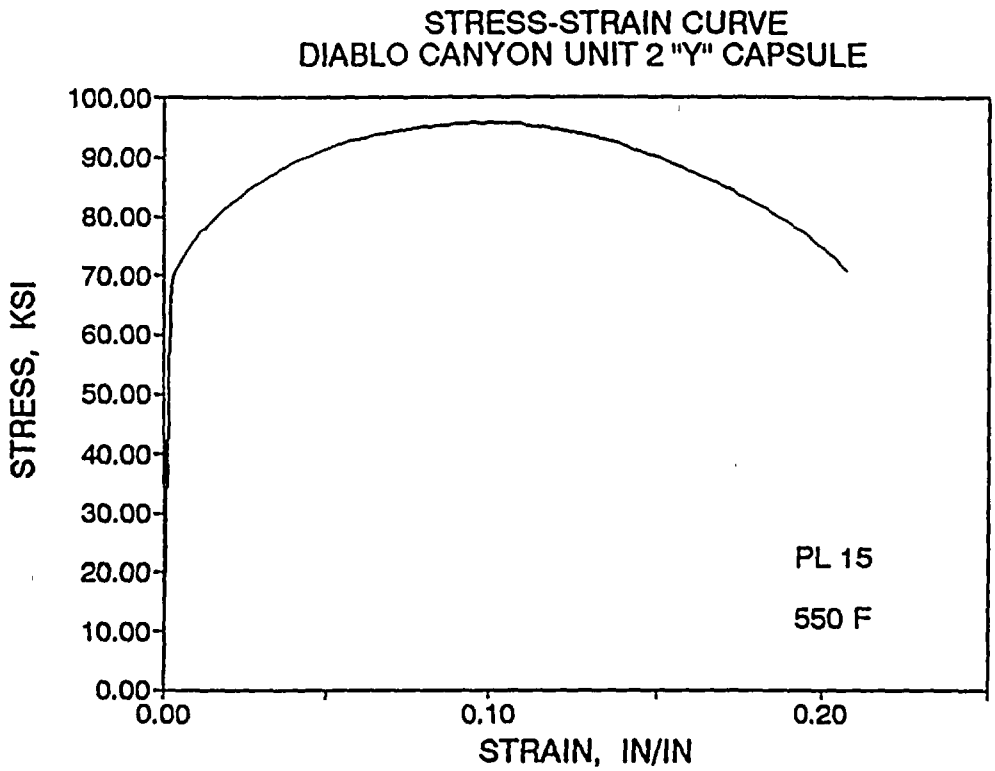


Figure 5-36 Engineering Stress-Strain Curves for Diablo Canyon Unit 2 Reactor Vessel Intermediate Shell Plate B5454-1 Tensile Specimen PL15 (Longitudinal Orientation)

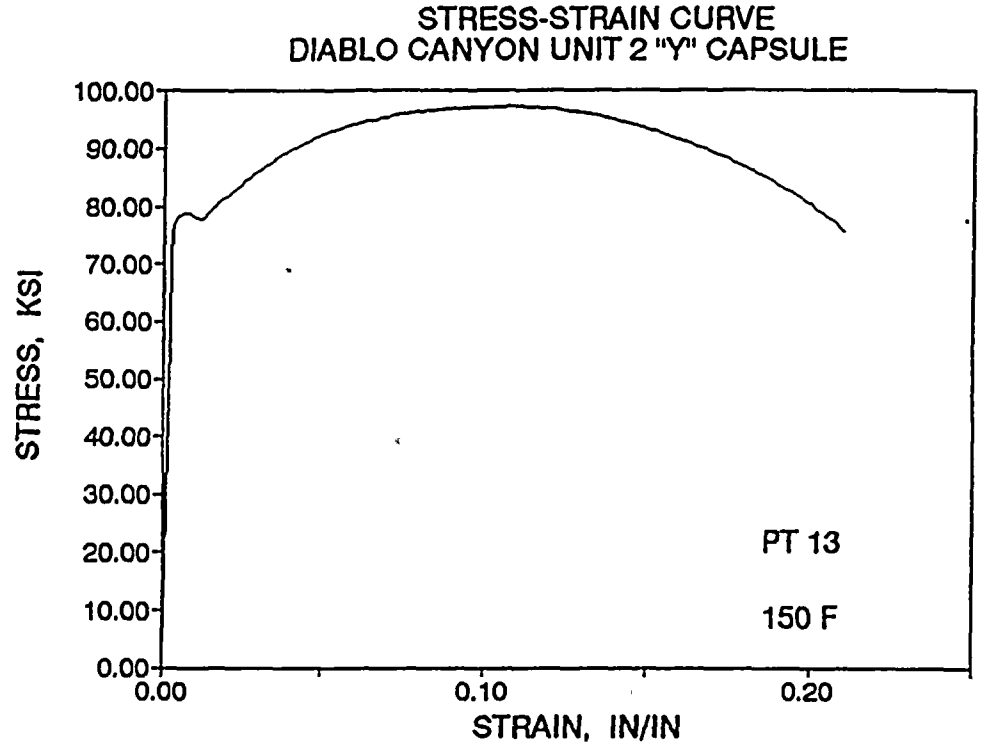


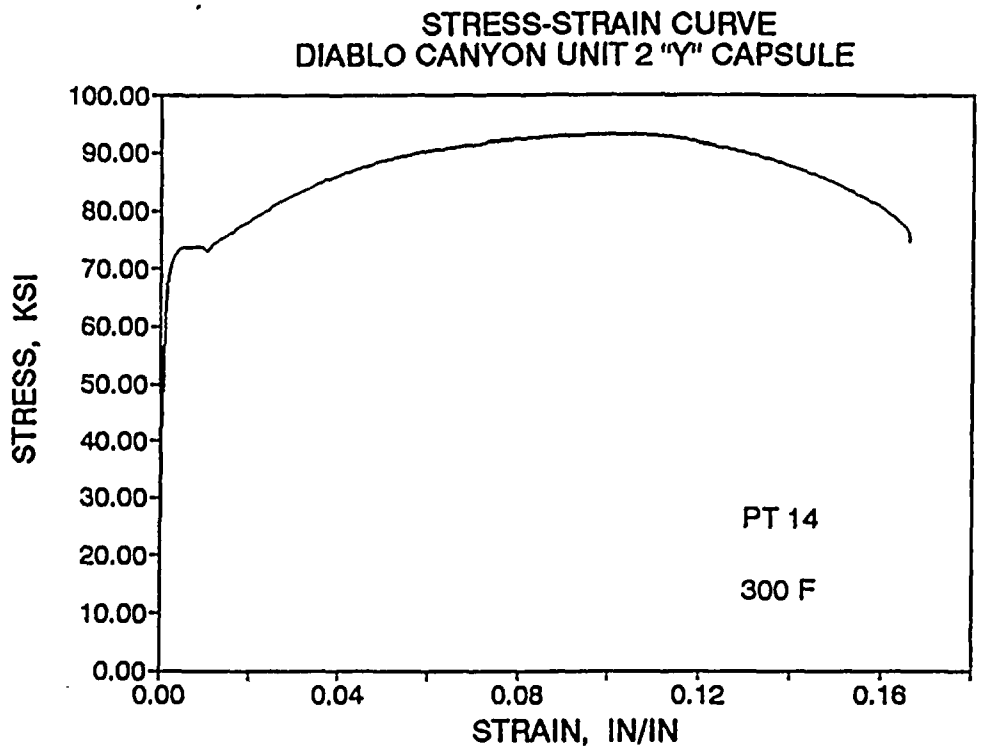


Figure 5-37 Engineering Stress-Strain Curves for Diablo Canyon Unit 2 Reactor Vessel Intermediate Shell Plate B5454-1 Tensile Specimens PT13 and PT14 (Transverse Orientation)

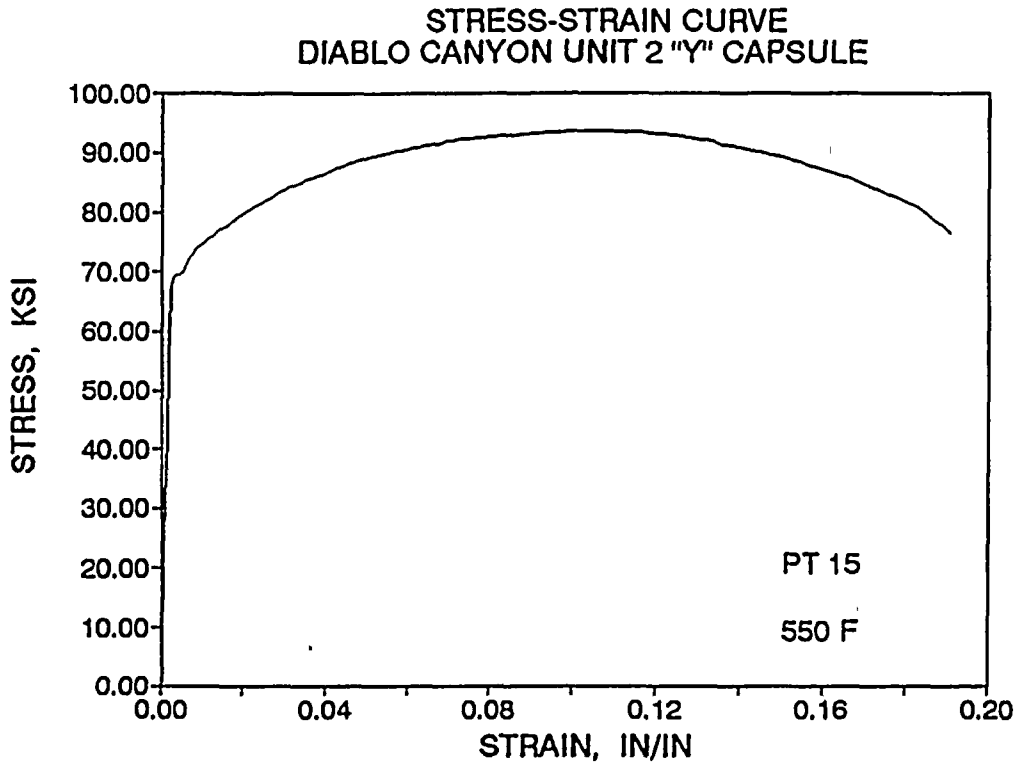


Figure 5-38 Engineering Stress-Strain Curves for Diablo Canyon Unit 2 Reactor Vessel Intermediate Shell Plate B5454-1 Tensile Specimen PT15 (Transverse Orientation)

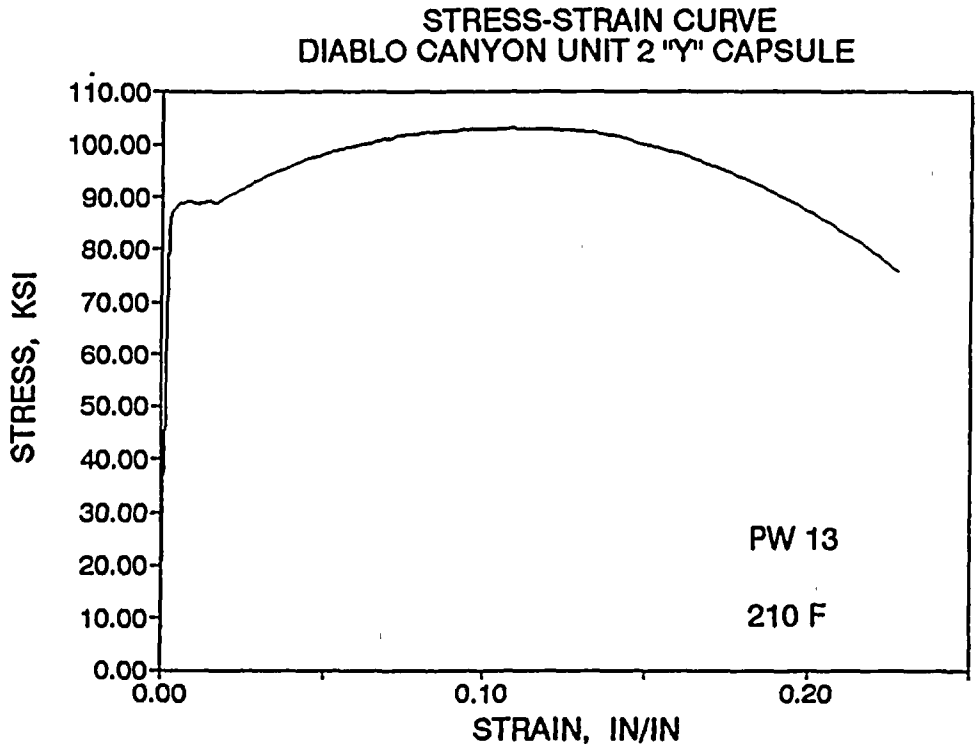


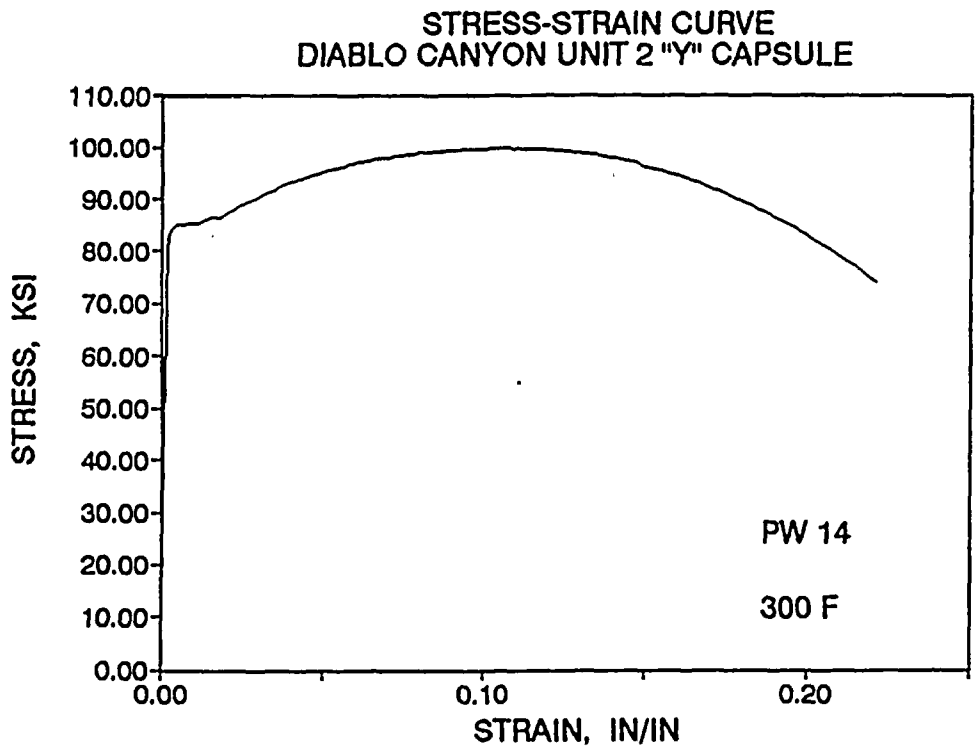


Figure 5-39 Engineering Stress-Strain Curves for Diablo Canyon Unit 2 Reactor Vessel Weld Metal Tensile Specimens PW13 and PW14

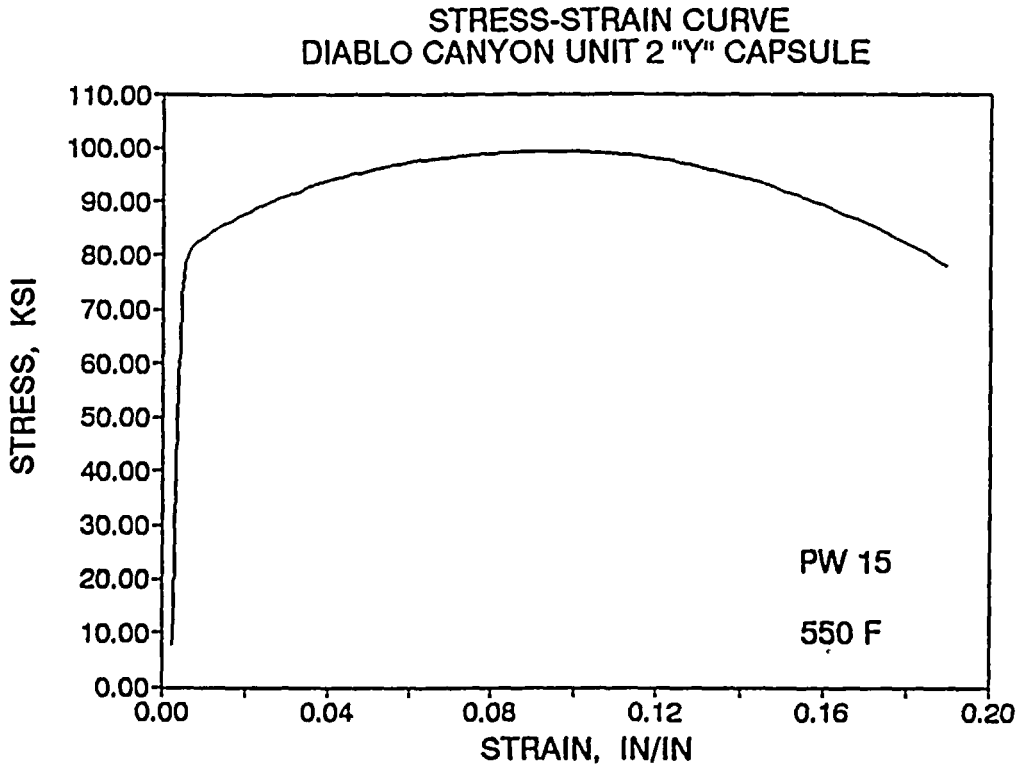


Figure 5-40 Engineering Stress-Strain Curves for Diablo Canyon Unit 2 Reactor Vessel Weld Metal Tensile Specimen PW15

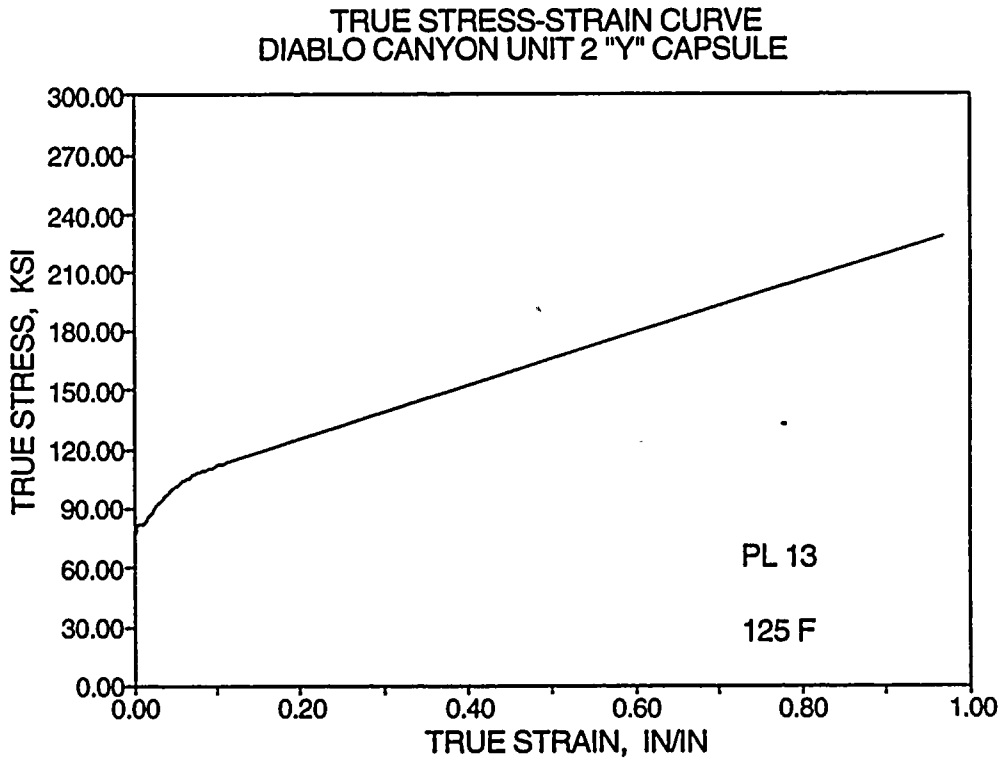


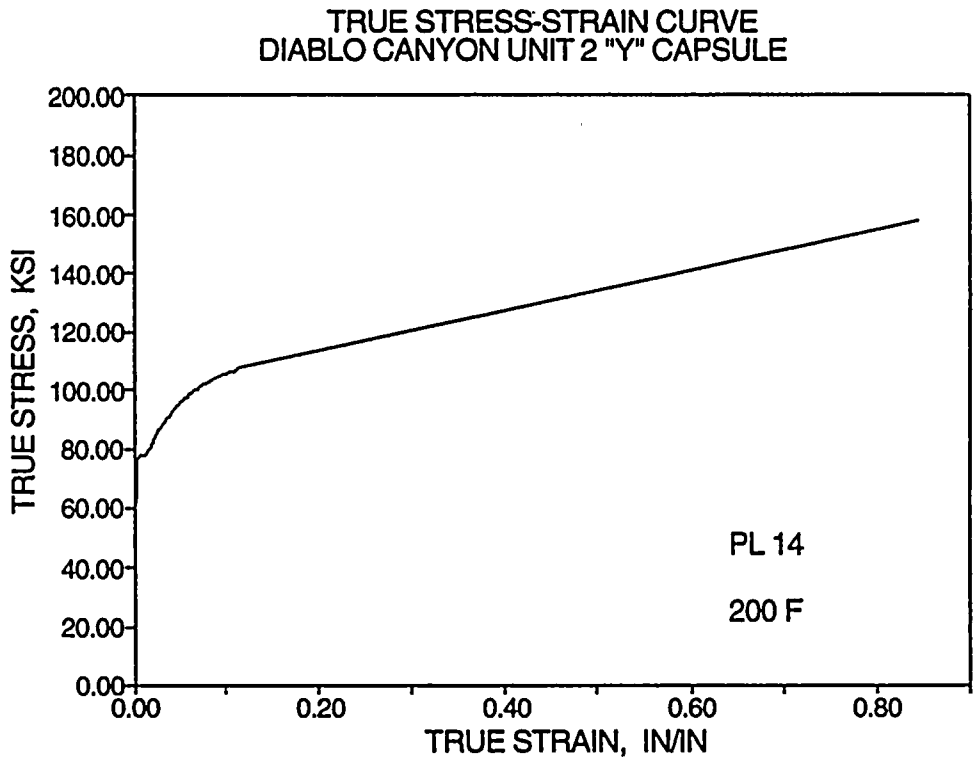


Figure 5-41 True Stress-Strain Curves for Diablo Canyon Unit 2 Reactor Vessel Intermediate Shell Plate B5454-1 Tensile Specimens PL13 and PL14 (Longitudinal Orientation)

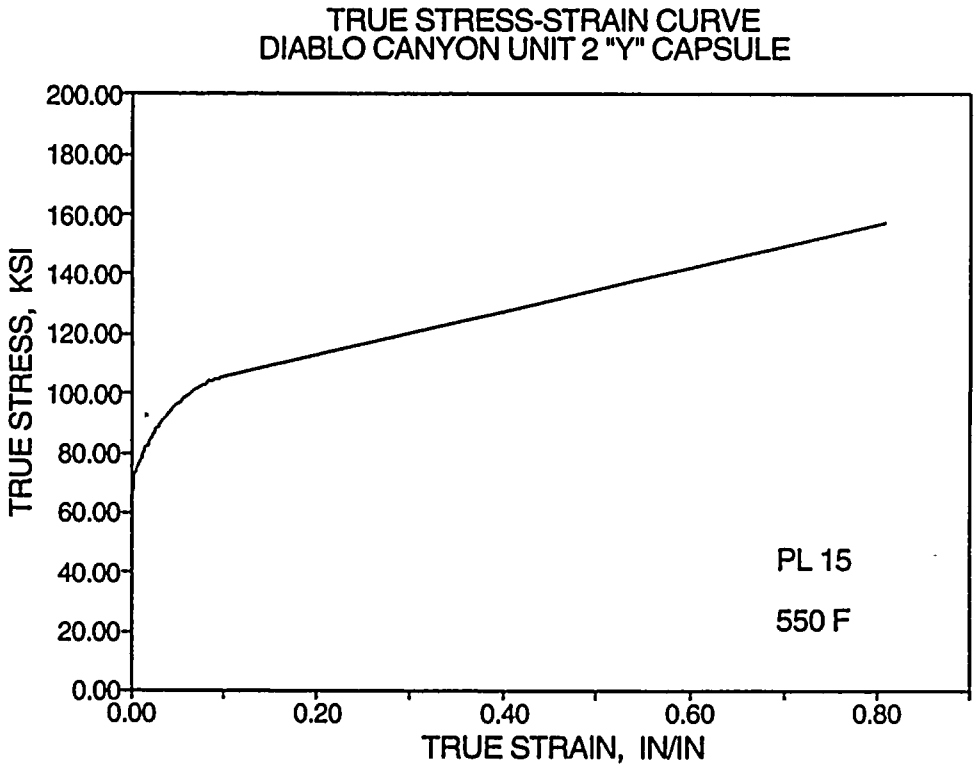


Figure 5-42 True Stress-Strain Curves for Diablo Canyon Unit 2 Reactor Vessel Intermediate Shell Plate B5454-1 Tensile Specimen PL15 (Longitudinal Orientation)

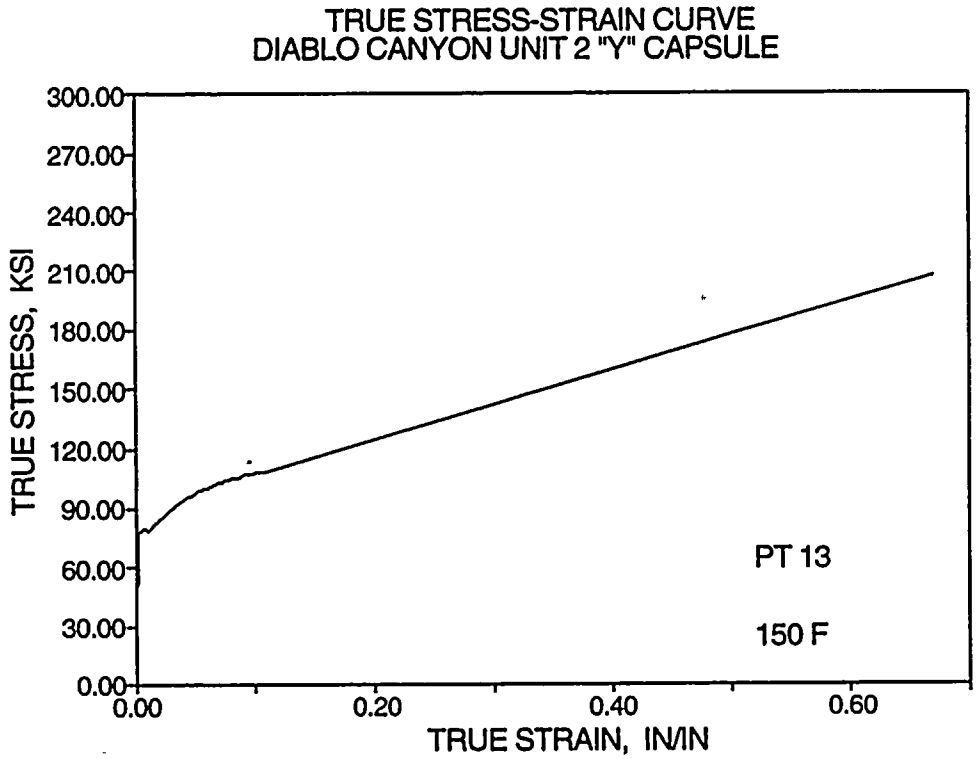


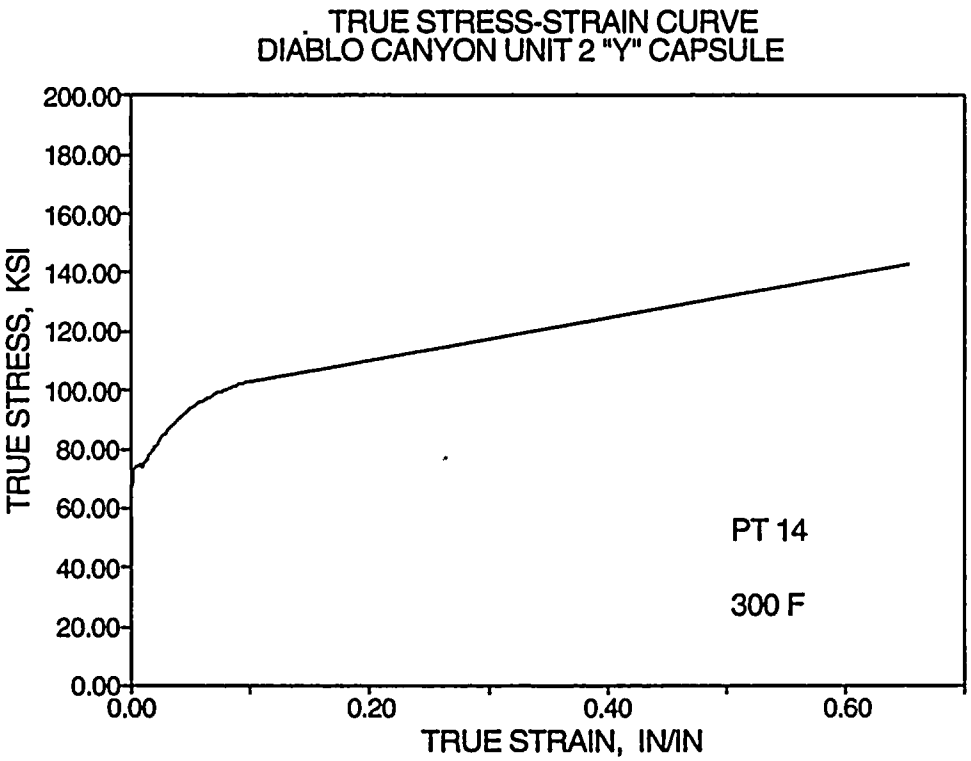


Figure 5-43 True Stress-Strain Curves for Diablo Canyon Unit 2 Reactor Vessel Intermediate Shell Plate B5454-1 Tensile Specimens PT13 and PT14 (Transverse Orientation)

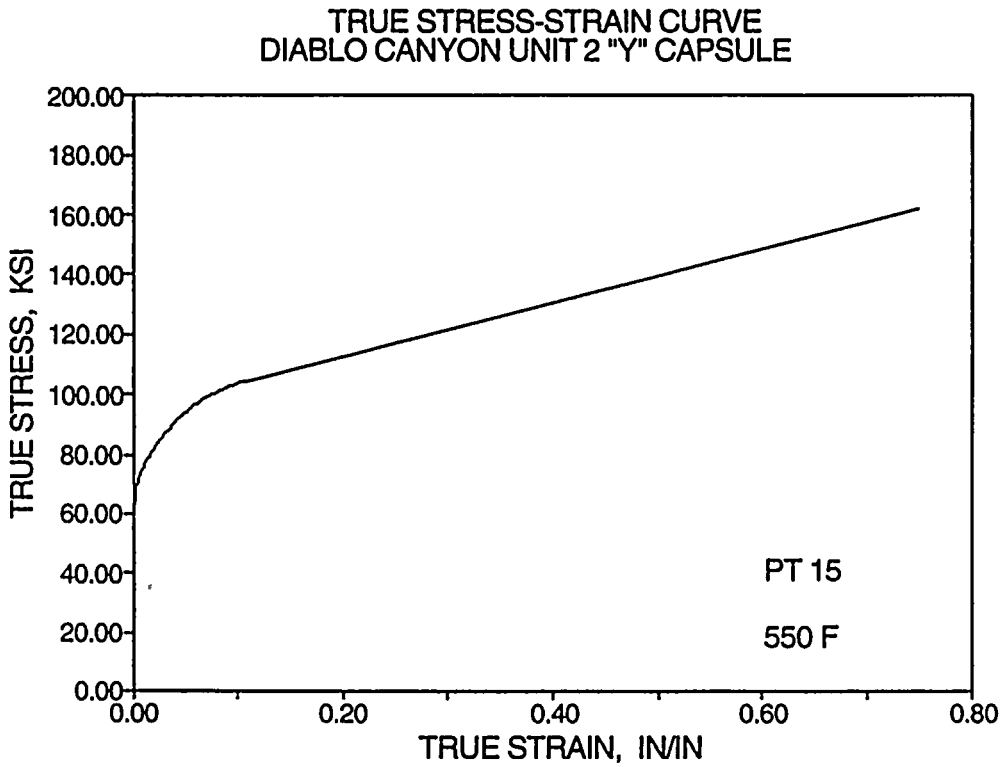


Figure 5-44 True Stress-Strain Curves for Diablo Canyon Unit 2 Reactor Vessel Intermediate Shell Plate B5454-1 Tensile Specimen PT15 (Transverse Orientation)

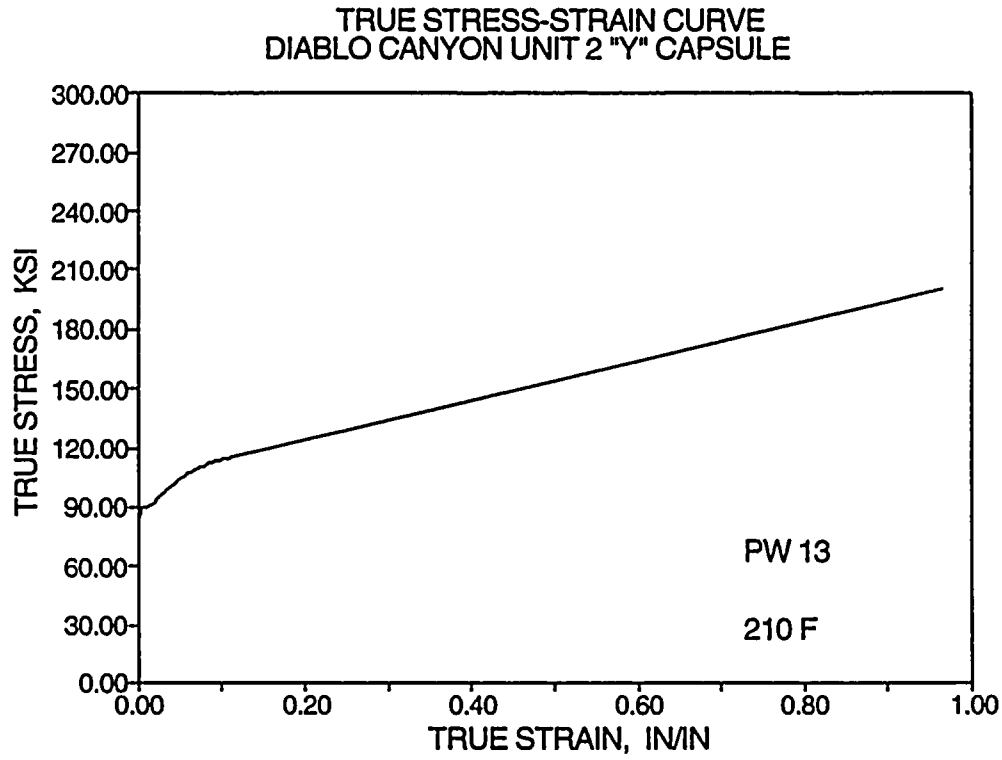


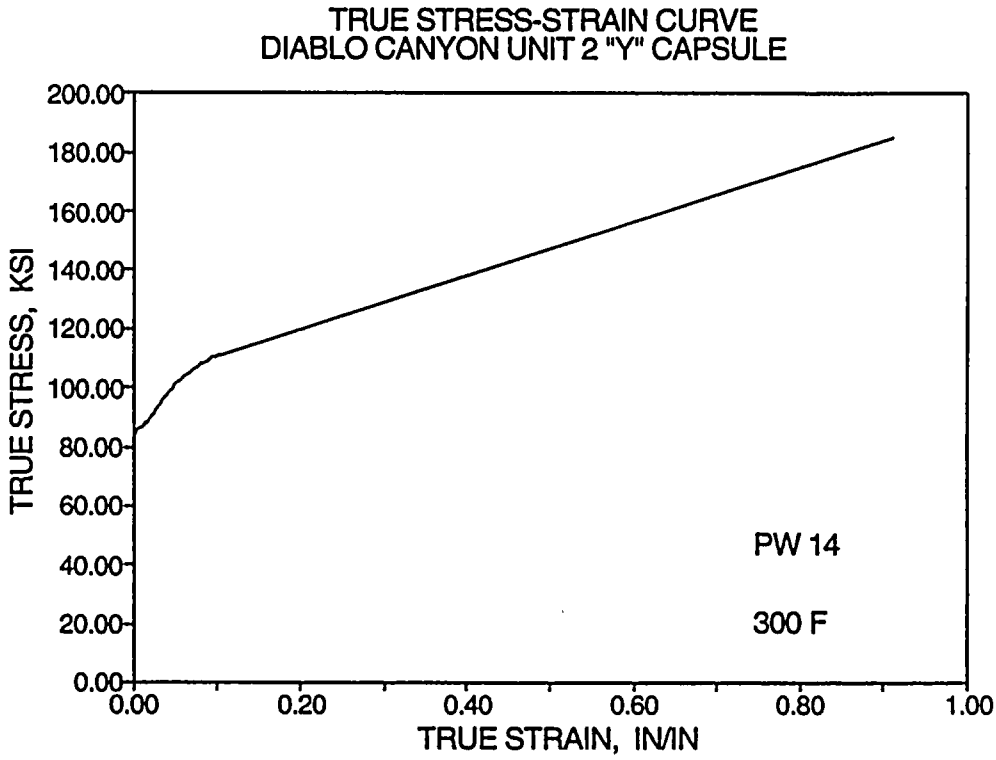


Figure 5-45 True Stress-Strain Curves for Diablo Canyon Unit 2 Reactor Vessel Weld Metal Tensile Specimens PW13 and PW14

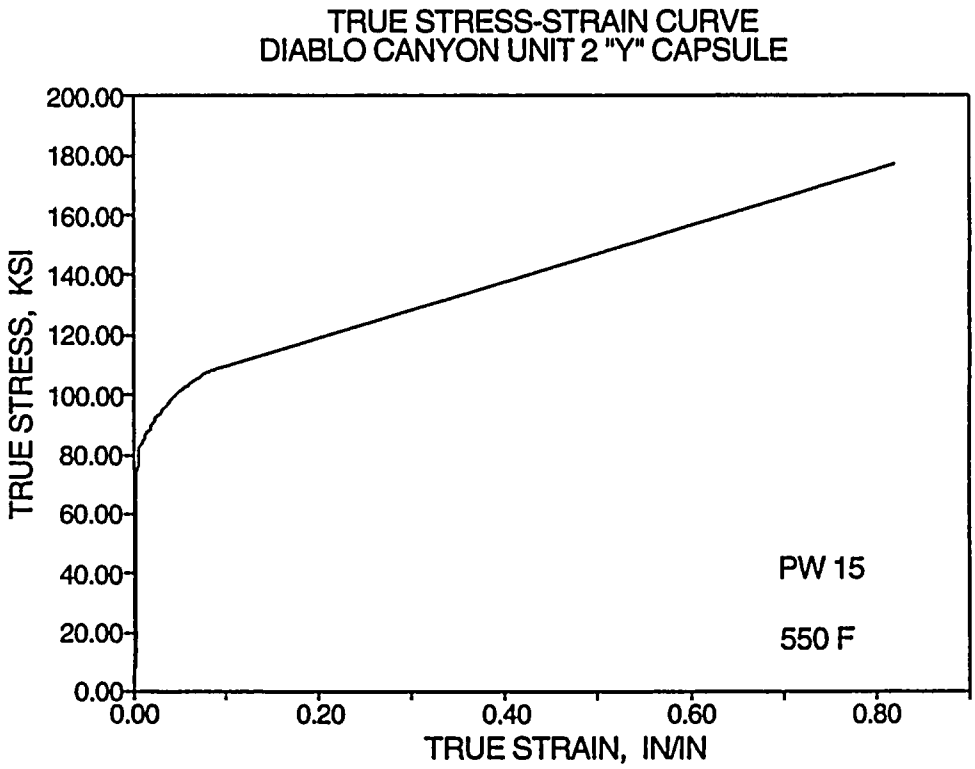


Figure 5-46 True Stress-Strain Curves for Diablo Canyon Unit 2 Reactor Vessel Weld Metal Tensile Specimen PW15

# SECTION 6.0

# RADIATION ANALYSIS AND NEUTRON DOSIMETRY

## 6.1 Introduction

Knowledge of the neutron environment within the reactor pressure vessel and surveillance capsule geometry is required as an integral part of LWR reactor pressure vessel surveillance programs for two reasons. First, in order to interpret the neutron radiation induced material property changes observed in the test specimens, the neutron environment (energy spectrum, flux, fluence) to which the test specimens were exposed must be known. Second, in order to relate the changes observed in the test specimens to the present and future condition of the reactor vessel, a relationship must be established between the neutron environment at various positions within the pressure vessel and that experienced by the test specimens. The former requirement is normally met by employing a combination of rigorous analytical techniques and measurements obtained with passive neutron flux monitors contained in each of the surveillance capsules. The latter information is generally derived solely from analysis.

The use of fast neutron fluence (E > 1.0 MeV) to correlate measured material property changes to the neutron exposure of the material has traditionally been accepted for development of damage trend curves as well as for the implementation of trend curve data to assess vessel condition. In recent years, however, it has been suggested that an exposure model that accounts for differences in neutron energy spectra between surveillance capsule locations and positions within the vessel wall could lead to an improvement in the uncertainties associated with damage trend curves as well as to a more accurate evaluation of damage gradients through the pressure vessel wall.

Because of this potential shift away from a threshold fluence toward an energy dependent damage function for data correlation, ASTM Standard Practice E853[13], "Analysis and Interpretation of Light-Water Reactor Surveillance Results," recommends reporting displacements per iron atom (dpa) along with fluence (E > 1.0 MeV) to provide a database for future reference. The energy dependent dpa function to be used for this evaluation is specified in ASTM Standard Practice E693[14], "Characterizing Neutron Exposures in Ferritic Steels in Terms of Displacements per Atom." The application of the dpa parameter to the assessment of embrittlement gradients through the thickness of the pressure vessel wall has already been promulgated in Revision 2 to Regulatory Guide 1.99, "Radiation Embrittlement of Reactor Vessel Materials."

This section provides the results of the neutron dosimetry evaluations performed in conjunction with the analysis of test specimens contained in surveillance Capsule Y, withdrawn at the end of the 6th fuel cycle. Also included are updates of the dosimetry evaluations for Capsule U, withdrawn at the end of the 1st fuel cycle, and Capsule X, withdrawn at the end of the 3rd fuel cycle. This update is based on current state-of-the-art methodology and nuclear data including recently released neutron transport and dosimetry cross-section libraries derived from the ENDF/B-VI database. This report, in conjunction with the reactor cavity dosimetry evaluations also completed at the end of the 6th fuel cycle[15] provides a consistent up-to-date neutron exposure database for use in evaluating the material properties of the Diablo Canyon Unit 2 reactor vessel.

In each of the capsule dosimetry evaluations, fast neutron exposure parameters in terms of neutron fluence (E > 1.0 MeV), neutron fluence (E > 0.1 MeV), and iron atom displacements (dpa) are established for the capsule irradiation history. The analytical formalism relating the measured capsule exposure to the exposure of the vessel wall is described and used to project the integrated exposure of the vessel wall. Also, uncertainties associated with the derived exposure parameters at the surveillance capsules and with the projected exposure of the pressure vessel are provided.

## 6.2 Discrete Ordinates Analysis

A plan view of the reactor geometry at the core midplane is shown in Figure 4-1. Six irradiation capsules attached to the neutron pads are included in the reactor design to constitute the reactor vessel surveillance program. The capsules are located at azimuthal angles of 56.0°, 58.5°, 124.0°, 236.0°, 238.5°, and 304.0° relative to the core cardinal axis as shown in Figure 4-1. A plan view of a dual surveillance capsule holder attached to the neutron pad is shown in Figure 6-1. The stainless steel specimen containers are 1.182 by 1-inch and approximately 56 inches in height. The containers are positioned axially such that the test specimens are centered on the core midplane, thus spanning the central five feet of the 12-foot high reactor core.

From a neutronic standpoint, the surveillance capsules and associated support structures are significant. The presence of these materials has a marked effect on both the spatial distribution of neutron flux and the neutron energy spectrum in the water annulus between the neutron pad and the reactor vessel. In order to determine the neutron environment at the test specimen location, the capsules themselves must be included in the analytical model.

In performing the fast neutron exposure evaluations for the surveillance capsules and reactor vessel, two distinct sets of transport calculations were carried out. The first, a single computation in the

conventional forward mode, was used primarily to obtain relative neutron energy distributions throughout the reactor geometry as well as to establish relative radial distributions of exposure parameters {$\phi(E > 1.0$ MeV), $\phi(E > 0.1$ MeV), and dpa/sec} through the vessel wall. The neutron spectral information was required for the interpretation of neutron dosimetry withdrawn from the surveillance capsules as well as for the determination of exposure parameter ratios; i.e., [dpa/sec]/ [$\phi(E > 1.0$ MeV)], within the pressure vessel geometry. The relative radial gradient information was required to permit the projection of measured exposure parameters to locations interior to the pressure vessel wall; i.e., the 1/4T, 1/2T, and 3/4T locations.

The second set of calculations consisted of a series of adjoint analyses relating the fast neutron flux, $\phi(E > 1.0$ MeV), at surveillance capsule positions and at several azimuthal locations on the pressure vessel inner radius to neutron source distributions within the reactor core. The source importance functions generated from these adjoint analyses provided the basis for all absolute exposure calculations and comparison with measurement. These importance functions, when combined with fuel cycle-specific neutron source distributions, yielded absolute predictions of neutron exposure at the locations of interest for each cycle of irradiation. They also established the means to perform similar predictions and dosimetry evaluations for all subsequent fuel cycles. It is important to note that the cycle-specific neutron source distributions utilized in these analyses included not only spatial variations of fission rates within the reactor core but also accounted for the effects of varying neutron yield per fission and fission spectrum introduced by the build-up of plutonium as the burnup of individual fuel assemblies increased.

The absolute cycle-specific data from the adjoint evaluations together with the relative neutron energy spectra and radial distribution information from the reference forward calculation provided the means to:

1 - Evaluate neutron dosimetry obtained from surveillance capsules.
2 - Relate dosimetry results to key locations at the inner radius and through the thickness of the pressure vessel wall.
3 - Enable a direct comparison of analytical prediction with measurement.
4 - Establish a mechanism for projection of pressure vessel exposure as the design of each new fuel cycle evolves.

The forward transport calculation for the reactor model summarized in Figures 4-1 and 6-1 was carried out in R,$\theta$ geometry using the DORT two-dimensional discrete ordinates code Version 2.7.3[16] and the BUGLE-93 cross-section library[17]. The BUGLE-93 library is a 47 energy group ENDF/B-VI based

data set produced specifically for light water reactor applications. In these analyses anisotropic scattering was treated with a $P_3$ expansion of the scattering cross-sections and the angular discretization was modeled with an $S_8$ order of angular quadrature.

The core power distribution utilized in the reference forward transport calculation was derived from statistical studies of long-term operation of Westinghouse 4-loop plants. Inherent in the development of this reference core power distribution is the use of an out-in fuel management strategy; i.e., fresh fuel on the core periphery. Furthermore, for the peripheral fuel assemblies, the neutron source was increased by a $2\sigma$ margin derived from the statistical evaluation of plant-to-plant and cycle-to-cycle variations in peripheral power. Since it is unlikely that any single reactor would exhibit power levels on the core periphery at the nominal + $2\sigma$ value for a large number of fuel cycles, the use of this reference distribution is expected to yield somewhat conservative results.

All adjoint calculations were also carried out using an $S_8$ order of angular quadrature and the $P_3$ cross-section approximation from the BUGLE-93 library. Adjoint source locations were chosen at several azimuthal locations along the pressure vessel inner radius as well as at the geometric center of each surveillance capsule. Again, these calculations were run in R,$\theta$ geometry to provide neutron source distribution importance functions for the exposure parameter of interest, in this case $\phi(E > 1.0 \text{ MeV})$.

Having the importance functions and appropriate core source distributions, the response of interest could be calculated as:

$$R(r,\theta) = \int_r \int_\theta \int_E I(r,\theta,E)\ S(r,\theta,E)\ r\ dr\ d\theta\ dE$$

where: $R(r,\theta)$ = $\phi(E > 1.0 \text{ MeV})$ at radius r and azimuthal angle $\theta$.

$I(r,\theta,E)$= Adjoint source importance function at radius r, azimuthal angle $\theta$, and neutron source energy E.

$S(r,\theta,E)$= Neutron source strength at core location r,$\theta$ and energy E.

Although the adjoint importance functions used in this analysis were based on a response function defined by the threshold neutron flux $\phi(E > 1.0 \text{ MeV})$, prior calculations[18] have shown that, while the implementation of low leakage loading patterns significantly impacts both the magnitude and spatial distribution of the neutron field, changes in the relative neutron energy spectrum are of second order. Thus, for a given location, the ratio of [dpa/sec]/[$\phi(E > 1.0 \text{ MeV})$] is insensitive to changing core source distributions. In the application of these adjoint importance functions to the Diablo Canyon

Unit 2 reactor, therefore, the iron atom displacement rates (dpa/sec) and the neutron flux $\phi(E > 0.1$ MeV) were computed on a cycle-specific basis by using [dpa/sec]/[$\phi(E > 1.0$ MeV)] and [$\phi(E > 0.1$ MeV)]/[$\phi(E > 1.0$ MeV)] ratios from the forward analysis in conjunction with the cycle-specific $\phi(E > 1.0$ MeV) solutions from the individual adjoint evaluations.

The reactor core power distributions used in the plant-specific adjoint calculations were taken from the fuel cycle design reports for the first six operating cycles of Diablo Canyon Unit 2 [19 through 24].

Selected results from the neutron transport analyses are provided in Tables 6-1 through 6-5. The data listed in these tables establishes the means for absolute comparisons of analysis and measurement for the capsule irradiation periods and provides the means to correlate dosimetry results with the corresponding exposure of the pressure vessel wall.

In Table 6-1, the calculated exposure parameters [$\phi(E > 1.0$ MeV), $\phi(E > 0.1$ MeV), and dpa/sec] are given at the geometric center of the two azimuthally symmetric surveillance capsule positions (56° and 58.5°) for both the reference and the plant-specific core power distributions. The plant-specific data, based on the adjoint transport analysis, is meant to establish the absolute comparison of measurement with analysis. The reference data derived from the forward calculation is provided as a conservative exposure evaluation against which plant-specific fluence calculations can be compared. Similar data is given in Table 6-2 for the pressure vessel inner radius. Again, the three pertinent exposure parameters are listed for the reference and cycles 1 through 6 plant-specific power distributions.

It is important to note that the data for the vessel inner radius was taken at the clad/base metal interface, and thus, represents the maximum predicted exposure levels of the vessel plates and welds. Also, in regard to the pressure vessel, three sets of values are included for the 30° azimuthal location. This is necessary due to the non-symmetry of the neutron pads in the vicinity of surveillance capsule attachments. With no capsule holder present, the pad span ranges from 30° to 45° in the respective octant. Likewise, pad spans of 27.5° to 45° and 25° to 45° exist in octants containing single and double surveillance capsule holders, respectively.

Radial gradient information applicable to $\phi(E > 1.0$ MeV), $\phi(E > 0.1$ MeV), and dpa/sec is given in Tables 6-3, 6-4, and 6-5, respectively. The data, obtained from the reference forward neutron transport calculation, are presented on a relative basis for each exposure parameter at several azimuthal locations. Exposure distributions through the vessel wall may be obtained by normalizing the

calculated or projected exposure at the vessel inner radius to the gradient data listed in Tables 6-3 through 6-5.

For example, the neutron flux $\phi(E > 1.0\ MeV)$ at the 1/4T depth in the pressure vessel wall along the 45° azimuth is given by:

$$\phi_{1/4T}(45^o) = \phi(220.35,\ 45^o)\ F(225.87,\ 45^o)$$

where: $\phi_{1/4T}(45°)$ = Projected neutron flux at the 1/4T position on the 45° azimuth.

$\phi(220.35,45°)$ = Projected or calculated neutron flux at the vessel inner radius on the 45° azimuth.

$F(225.87,45°)$ = Ratio of the neutron flux at the 1/4T position to the flux at the vessel inner radius for the 45° azimuth. This data is obtained from Table 6-3

Similar expressions apply for exposure parameters expressed in terms of $\phi(E > 0.1\ MeV)$ and dpa/sec where the attenuation function F is obtained from Tables 6-4 and 6-5, respectively.

## 6.3 Neutron Dosimetry

The passive neutron sensors included in the Diablo Canyon Unit 2 surveillance program are listed in Table 6-6. Also given in Table 6-6 are the primary nuclear reactions and associated nuclear constants that were used in the evaluation of the neutron energy spectrum within the surveillance capsules and in the subsequent determination of the various exposure parameters of interest [$\phi(E > 1.0\ MeV)$, $\phi(E > 0.1\ MeV)$, dpa/sec]. The relative locations of the neutron sensors within the capsules are shown in Figure 4-2. The iron, nickel, copper, and cobalt-aluminum monitors, in wire form, were placed in holes drilled in spacers at several axial levels within the capsules. The cadmium-shielded uranium and neptunium fission monitors were accommodated within the dosimeter block located near the center of the capsule.

The use of passive monitors such as those listed in Table 6-6 does not yield a direct measure of the energy dependent neutron flux at the point of interest. Rather, the activation or fission process is a measure of the integrated effect that the time and energy dependent neutron flux has on the target material over the course of the irradiation period. An accurate assessment of the average neutron flux level incident on the various monitors may be derived from the activation measurements only if the irradiation parameters are well known. In particular, the following variables are of interest:

- The measured specific activity of each monitor.
- The physical characteristics of each monitor.

- The operating history of the reactor.
- The energy response of each monitor.
- The neutron energy spectrum at the monitor location.

The specific activity of each of the neutron monitors was determined using established ASTM procedures[13,14,25-36]. Following sample preparation and weighing, the activity of each monitor was determined by means of a lithium-drifted germanium, Ge(Li), gamma spectrometer. The irradiation history of the Diablo Canyon Unit 2 reactor was obtained from NUREG-0020, "Licensed Operating Reactors Status Summary Report," for the cycles 1 through 6 operating period. The irradiation history applicable to the exposure of Capsules Y, X, and U is given in Table 6-7.

Having the measured specific activities, the physical characteristics of the sensors, and the operating history of the reactor, reaction rates referenced to full power operation were determined from the following equation:

$$R = \frac{A}{N_0 \, F \, Y \sum \frac{P_j}{P_{ref}} C_j \, [1-e^{-\lambda t_j}] \, [e^{-\lambda t_d}]}$$

where:

| | | |
|---|---|---|
| R | = | Reaction rate averaged over the irradiation period and referenced to operation at a core power level of $P_{ref}$ (rps/nucleus). |
| A | = | Measured specific activity (dps/gm). |
| $N_0$ | = | Number of target element atoms per gram of sensor. |
| F | = | Weight fraction of the target isotope in the sensor material. |
| Y | = | Number of product atoms produced per reaction. |
| $P_j$ | = | Average core power level during irradiation period j (MW). |
| $P_{ref}$ | = | Maximum or reference power level of the reactor (MW). |
| $C_j$ | = | Calculated ratio of $\phi(E > 1.0 \text{ MeV})$ during irradiation period j to the time weighted average $\phi(E > 1.0 \text{ MeV})$ over the entire irradiation period. |
| $\lambda$ | = | Decay constant of the product isotope (1/sec). |
| $t_j$ | = | Length of irradiation period j (sec). |
| $t_d$ | = | Decay time following irradiation period j (sec). |

and the summation is carried out over the total number of monthly intervals comprising the irradiation period.

In the equation describing the reaction rate calculation, the ratio $[P_j]/[P_{ref}]$ accounts for month-by-month variation of reactor core power level within any given fuel cycle as well as over multiple fuel cycles. The ratio $C_j$, which can be calculated for each fuel cycle using the adjoint transport technology discussed in Section 6.2, accounts for the change in sensor reaction rates caused by variations in flux level induced by changes in core spatial power distributions from fuel cycle to fuel cycle. For a single cycle irradiation, $C_j$ is normally taken to be 1.0. However, for multiple cycle irradiations, particularly those employing low leakage fuel management, the additional $C_j$ term should be employed. The impact of changing flux levels for constant power operation can be quite significant for sensor sets that have been irradiated for many cycles in a reactor that has transitioned from non-low leakage to low leakage fuel management or for sensor sets contained in surveillance capsules that have been moved from one capsule location to another.

For the irradiation history of Capsules Y, X, and U, the flux level term in the reaction rate calculations was developed from the plant-specific analysis provided in Table 6-1. Measured and saturated reaction product specific activities as well as the derived full power reaction rates are listed in Tables 6-8 through 6-10. The specific activities and reaction rates of the U-238 sensors provided in Tables 6-8 through 6-10 include corrections for U-235 impurities, plutonium build-in, and gamma ray induced fissions. Corrections for gamma ray induced fissions were also included in the specific activities and reaction rates for the Np-237 sensors as well.

Values of key fast neutron exposure parameters were derived from the measured reaction rates using the FERRET least squares adjustment code[37]. The FERRET approach used the measured reaction rate data, sensor reaction cross-sections, and a calculated trial spectrum as input and proceeded to adjust the group fluxes from the trial spectrum to produce a best fit (in a least squares sense) to the measured reaction rate data. The "measured" exposure parameters along with the associated uncertainties were then obtained from the adjusted spectrum.

In the FERRET evaluations, a log-normal least squares algorithm weights both the a priori values and the measured data in accordance with the assigned uncertainties and correlations. In general, the measured values f are linearly related to the flux $\phi$ by some response matrix A:

$$f_i^{(s,\alpha)} = \sum_g A_{ig}^{(s)} \phi_g^{(\alpha)}$$

where i indexes the measured values belonging to a single data set s, g designates the energy group,

and $\alpha$ delineates spectra that may be simultaneously adjusted. For example,

$$R_i = \sum_g \sigma_{ig} \phi_g$$

relates a set of measured reaction rates $R_i$ to a single spectrum $\phi_g$ by the multi-group reaction cross-section $\sigma_{ig}$. The log-normal approach automatically accounts for the physical constraint of positive fluxes, even with large assigned uncertainties.

In the least squares adjustment, the continuous quantities (i.e., neutron spectra and cross-sections) were approximated in a multi-group format consisting of 53 energy groups. The trial input spectrum was converted to the FERRET 53 group structure using the SAND-II code[38]. This procedure was carried out by first expanding the 47 group calculated spectrum into the SAND-II 620 group structure using a SPLINE interpolation procedure in regions where group boundaries do not coincide. The 620 point spectrum was then re-collapsed into the group structure used in FERRET.

The sensor set reaction cross-sections, obtained from the ENDF/B-VI dosimetry file[39], were also collapsed into the 53 energy group structure using the SAND-II code. In this instance, the trial spectrum, as expanded to 620 groups, was employed as a weighting function in the cross-section collapsing procedure. Reaction cross-section uncertainties in the form of a 53 x 53 covariance matrix for each sensor reaction were also constructed from the information contained on the ENDF/B-VI data files. These matrices included energy group to energy group uncertainty correlations for each of the individual reactions. However, correlations between cross-sections for different sensor reactions were not included. The omission of this additional uncertainty information does not significantly impact the results of the adjustment.

Due to the importance of providing a trial spectrum that exhibits a relative energy distribution close to the actual spectrum at the sensor set locations, the neutron spectrum input to the FERRET evaluation was taken from the center of the surveillance capsule modeled in the reference forward transport calculation. While the 53 x 53 group covariance matrices applicable to the sensor reaction cross-sections were developed from the ENDF/B-VI data files, the covariance matrix for the input trial spectrum was constructed from the following relation:

$$M_{gg'} = R_n^2 + R_g R_{g'} P_{gg'}$$

where $R_n$ specifies an overall fractional normalization uncertainty (i.e., complete correlation) for the set of values. The fractional uncertainties $R_g$ specify additional random uncertainties for group g that are correlated with a correlation matrix given by:

$$P_{gg'} = [1-\theta]\ \delta_{gg'} + \theta\ e^{-H}$$

where:

$$H = \frac{(g-g')^2}{2\ \gamma^2}$$

The first term in the correlation matrix equation specifies purely random uncertainties, while the second term describes short range correlations over a group range $\gamma$ ($\theta$ specifies the strength of the latter term). The value of $\delta$ is 1 when g = g' and 0 otherwise. For the trial spectrum used in the current evaluations, a short range correlation of $\gamma = 6$ groups was used. This choice implies that neighboring groups are strongly correlated when $\theta$ is close to 1. Strong long range correlations (or anti-correlations) were justified based on information presented by R. E. Maerker[40]. Maerker's results are closely duplicated when $\gamma = 6$.

The uncertainties associated with the measured reaction rates included both statistical (counting) and systematic components. The systematic component of the overall uncertainty accounts for counter efficiency, counter calibrations, irradiation history corrections, and corrections for competing reactions in the individual sensors.

Results of the FERRET evaluations of the Capsules Y, X, and U dosimetry are given in Table 6-11. The data summarized in this table includes fast neutron exposure evaluations in terms of $\Phi(E > 1.0\ \text{MeV})$, $\Phi(E > 0.1\ \text{MeV})$, and dpa. In general, excellent results were achieved in the fits of the adjusted spectra to the individual measured reaction rates. The measured and FERRET adjusted reaction rates for each reaction are given in Tables 6-12 through 6-14. An examination of Tables 6-12 through 6-14 shows that, in all cases, reaction rates calculated with the adjusted spectra match the measured reaction rates to better than 6%. The adjusted spectra from the least squares evaluation is given in Tables 6-15 through 6-17 in the FERRET 53 energy group structure.

In Table 6-18, absolute comparisons of the measured and calculated fluence at the center of each capsule are presented. The results for the Capsules Y and X dosimetry evaluations, M/C ratios of 0.86 and 1.03 respectively, are consistent with results obtained from similar evaluations of dosimetry

using methodologies based on ENDF/B-VI cross-sections. The Capsule U comparison showing the measurement to exceed calculation 20% is somewhat inconsistent both with prior experience as well as with cavity dosimetry irradiated also during cycle 1[15]. This discrepancy, however, is not large enough to exclude the Capsule U measurements from the overall Diablo Canyon Unit 2 database.

### 6.4 Projections of Pressure Vessel Exposure

The best estimate exposure of the Diablo Canyon Unit 2 reactor pressure vessel was developed using a combination of absolute plant-specific transport calculations and all available plant-specific measurement data. In the case of the Diablo Canyon Unit 2, the measurement database is considerable, including the three internal surveillance capsule measurements described in this report as well as 16 midplane cavity measurements discussed in reference 15. That is, a 19-point measurement database exists for this reactor.

Combining this overall measurement database with the plant-specific calculations, the best estimate vessel exposure is obtained from the following relationship:

$$\Phi_{Best\ Est.} = K\ \Phi_{Calc.}$$

where: $\Phi_{Best\ Est.}$ = The best estimate fast neutron exposure at the location of interest.

K = The plant-specific measurement/calculation (M/C) bias factor derived from all available surveillance capsule and reactor cavity dosimetry data.

$\Phi_{Calc.}$ = The absolute calculated fast neutron exposure at the location of interest.

The approach defined in the above equation is based on the premise that the measurement data represents the most accurate plant-specific information available at the locations of the dosimetry; and, further, the use of the measurement data on a plant-specific basis essentially removes biases present in the analytical approach and mitigates the uncertainties that would result from the use of analysis alone.

That is, at the measurement points, the uncertainty in the best estimate exposure is dominated by the uncertainties in the measurement process. At locations within the pressure vessel wall, additional uncertainty is incurred due to the analytically determined relative ratios among the various measurement points and locations within the pressure vessel wall.

For Diablo Canyon Unit 2, the derived plant-specific bias factors for the neutron flux (E > 1.0 MeV) was 0.901 ± 0.080. The standard deviation of 0.080 represents an uncertainty in the bias factor of ± 8.9% at the 1σ level. Bias factors of this magnitude are fully consistent with experience using the BUGLE-93 cross-section library.

The use of the bias factor of 0.901 derived from the measurement database acts to remove plant-specific biases associated with the definition of the core source, actual versus assumed reactor dimensions, and operational variations in water density within the reactor. As a result, the overall uncertainty in the best estimate exposure projections within the vessel wall depends on the individual uncertainties in the measurement process, the uncertainty in the dosimetry location, and, in the uncertainty in the calculated ratio of the neutron exposure at the point of interest to that at the measurement location.

The uncertainty in the derived neutron flux for an individual measurement is obtained directly from the results of a least squares evaluation of dosimetry data. The least squares approach combines individual uncertainty in the calculated neutron energy spectrum, the uncertainties in dosimetry cross-sections, and the uncertainties in measured foil specific activities to produce a net uncertainty in the derived neutron flux at the measurement point. The associated uncertainty in the plant-specific bias factor, K, derived from the M/C database, in turn, depends on the total number of available measurements as well as on the uncertainty of each measurement. Because of the dependence on the size of the overall database, plants that have incorporated supplemental reactor cavity dosimetry will, in general, have a lower uncertainty than plants with measurements from internal surveillance capsules alone.

The positioning uncertainties for dosimetry are taken from parametric studies of sensor position performed as part a series of analytical sensitivity studies included in the qualification of the methodology. The uncertainties in the exposure ratios relating dosimetry results to positions within the vessel wall are again based on the analytical sensitivity studies of the vessel thickness tolerance for the cavity data and on downcomer water density variations and vessel inner radius tolerance for the surveillance capsule measurements. Thus, this portion of the overall uncertainty is controlled entirely by dimensional tolerances associated with the reactor design and by the operational characteristics of the reactor.

The net uncertainty in the bias factor, K, is combined with the uncertainty from the analytical sensitivity study to define the overall fluence uncertainty at the pressure vessel wall. In the case of

Diablo Canyon Unit 2, the derived uncertainties in the bias factor, K, and the additional uncertainty from the analytical sensitivity studies combine to yield a net uncertainty of ±10%.

Based on this best estimate approach, neutron exposure projections at key locations on the pressure vessel inner radius are given in Table 6-19. Along with the current (7.0 EFPY) exposure, projections are also provided for exposure periods of 12, 16, and 32 EFPY. Projections for future operation were based on the assumption that the average exposure rates characteristic of the low leakage loading patterns incorporated during fuel cycles 5 and 6 would continue to be applicable throughout plant life.

In the calculation of exposure gradients within the pressure vessel wall for Diablo Canyon Unit 2 reactor vessel, exposure projections to 12, 16, and 32 EFPY were also employed. Data based on both a $\Phi(E > 1.0\ \text{MeV})$ slope and a plant-specific dpa slope through the vessel wall is provided in Table 6-20.

In order to access $RT_{NDT}$ versus fluence curves, dpa equivalent fast neutron fluence levels for the 1/4T and 3/4T positions were defined by the relations:

$$\phi(1/4T) = \phi(0T)\ \frac{dpa(1/4T)}{dpa(0T)}$$

and

$$\phi(3/4T) = \phi(0T)\ \frac{dpa(3/4T)}{dpa(0T)}$$

Using this approach results in the dpa equivalent fluence values listed in Table 6-20. In Table 6-21, updated lead factors are listed for each of the Diablo Canyon Unit 2 surveillance capsules. Lead factor data based on the accumulated fluence through cycle 6 is provided for each remaining capsule.

FIGURE 6-1

PLAN VIEW OF A DUAL REACTOR VESSEL SURVEILLANCE CAPSULE

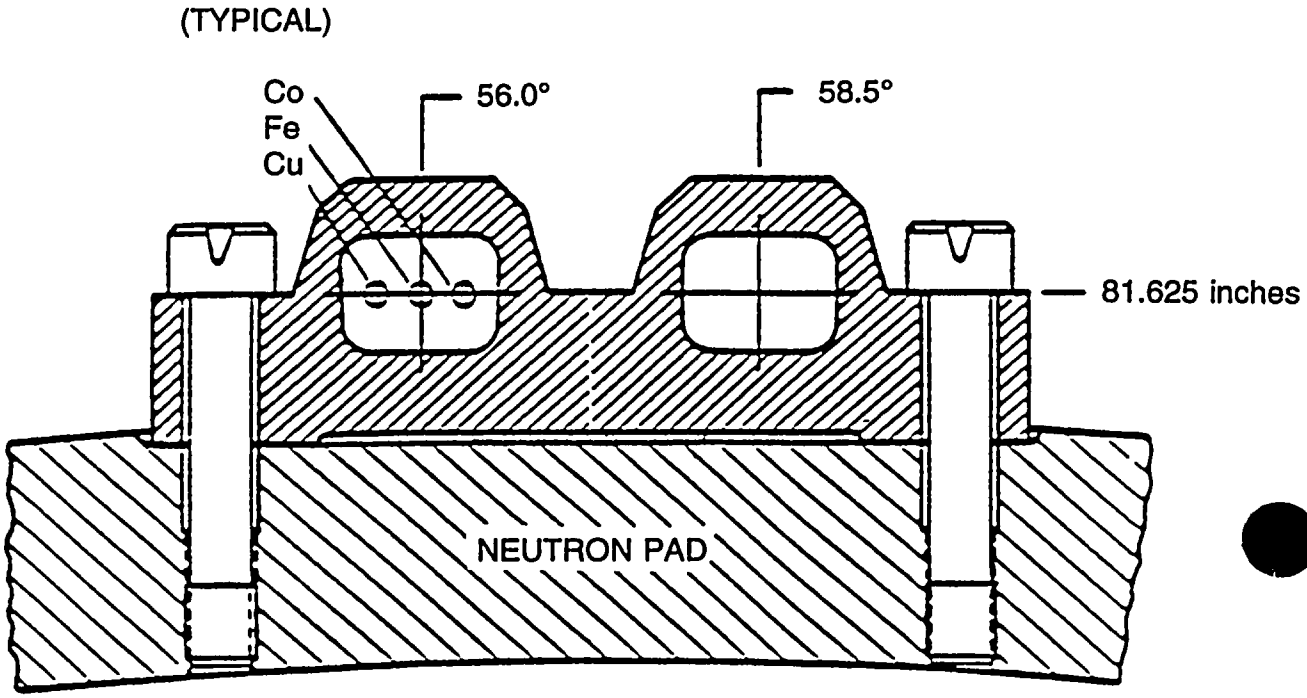

TABLE 6-1

CALCULATED FAST NEUTRON EXPOSURE RATES AT THE SURVEILLANCE CAPSULE CENTER

$\phi$ (E >1.0 MeV) [n/cm$^2$-sec]

| LOCATION | 58.5° | 56.0° |
|---|---|---|
| Reference | 1.19E+11 | 1.32E+11 |
| CYCLE 1 | 8.59E+10 | 9.49E+10 |
| CYCLE 2 | 7.50E+10 | 8.41E+10 |
| CYCLE 3 | 7.10E+10 | 7.84E+10 |
| CYCLE 4 | 6.51E+10 | 7.01E+10 |
| CYCLE 5 | 6.25E+10 | 6.92E+10 |
| CYCLE 6 | 6.23E+10 | 6.89E+10 |

$\phi$ (E > 0.1 MeV) [n/cm$^2$-sec]

| LOCATION | 58.5° | 56.0° |
|---|---|---|
| Reference | 5.23E+11 | 5.91E+11 |
| CYCLE 1 | 3.78E+11 | 4.24E+11 |
| CYCLE 2 | 3.30E+11 | 3.76E+11 |
| CYCLE 3 | 3.12E+11 | 3.51E+11 |
| CYCLE 4 | 2.86E+11 | 3.14E+11 |
| CYCLE 5 | 2.75E+11 | 3.10E+11 |
| CYCLE 6 | 2.74E+11 | 3.08E+11 |

Iron Displacement Rate [dpa/sec]

| LOCATION | 58.5° | 56.0° |
|---|---|---|
| Reference | 2.28E-10 | 2.55E-10 |
| CYCLE 1 | 1.65E-10 | 1.83E-10 |
| CYCLE 2 | 1.44E-10 | 1.63E-10 |
| CYCLE 3 | 1.36E-10 | 1.52E-10 |
| CYCLE4 | 1.25E-10 | 1.36E-10 |
| CYCLE 5 | 1.20E-10 | 1.34E-10 |
| CYCLE 6 | 1.19E-10 | 1.33E-10 |

TABLE 6-2

CALCULATED AZIMUTHAL VARIATION OF FAST NEUTRON EXPOSURE RATES AT THE PRESSURE VESSEL CLAD/BASE METAL INTERFACE

$\phi(E > 1.0MeV)$ [n/cm$^2$-sec]

| | 0.0° | 15.0° | 30.0°(a) | 30.0°(b) | 30.0°(c) | 45.0° |
|---|---|---|---|---|---|---|
| Reference | 1.51E+10 | 2.40E+10 | 2.87E+10 | 2.13E+10 | 1.48E+10 | 2.88E+10 |
| CYCLE 1 | 1.05E+10 | 1.63E+10 | 2.04E+10 | 1.27E+10 | 1.06E+10 | 2.03E+10 |
| CYCLE 2 | 8.12E+09 | 1.28E+10 | 1.79E+10 | 1.12E+10 | 9.26E+09 | 1.78E+10 |
| CYCLE 3 | 8.29E+09 | 1.23E+10 | 1.70E+10 | 1.06E+10 | 8.78E+09 | 1.55E+10 |
| CYCLE 4 | 8.78E+09 | 1.51E+10 | 1.59E+10 | 9.89E+09 | 8.21E+09 | 1.48E+10 |
| CYCLE 5 | 7.46E+09 | 1.18E+10 | 1.52E+10 | 9.44E+09 | 7.84E+09 | 1.47E+10 |
| CYCLE 6 | 7.75E+09 | 1.20E+10 | 1.51E+10 | 9.39E+09 | 7.80E+09 | 1.48E+10 |

$\phi(E > 0.1MeV)$ [n/cm$^2$-sec]

| | 0.0° | 15.0° | 30.0°(a) | 30.0°(b) | 30.0°(c) | 45.0° |
|---|---|---|---|---|---|---|
| Reference | 3.09E+10 | 4.97E+10 | 6.03E+10 | 4.47E+10 | 3.11E+10 | 7.05E+10 |
| CYCLE 1 | 2.15E+10 | 3.39E+10 | 4.29E+10 | 2.67E+10 | 2.22E+10 | 4.96E+10 |
| CYCLE 2 | 1.66E+10 | 2.64E+10 | 3.76E+10 | 2.34E+10 | 1.95E+10 | 4.35E+10 |
| CYCLE 3 | 1.70E+10 | 2.55E+10 | 3.57E+10 | 2.22E+10 | 1.84E+10 | 3.79E+10 |
| CYCLE 4 | 1.80E+10 | 3.13E+10 | 3.34E+10 | 2.08E+10 | 1.72E+10 | 3.63E+10 |
| CYCLE 5 | 1.53E+10 | 2.45E+10 | 3.18E+10 | 1.98E+10 | 1.65E+10 | 3.61E+10 |
| CYCLE 6 | 1.59E+10 | 2.48E+10 | 3.17E+10 | 1.97E+10 | 1.64E+10 | 3.62E+10 |

Iron Atom Displacement Rate [dpa/sec]

| | 0.0° | 15.0° | 30.0°(a) | 30.0°(b) | 30.0°(c) | 45.0° |
|---|---|---|---|---|---|---|
| Reference | 2.34E-11 | 3.68E-11 | 4.40E-11 | 2.74E-11 | 2.28E-11 | 4.53E-11 |
| CYCLE 1 | 1.62E-11 | 2.50E-11 | 3.13E-11 | 1.95E-11 | 1.62E-11 | 3.19E-11 |
| CYCLE 2 | 1.26E-11 | 1.95E-11 | 2.74E-11 | 1.71E-11 | 1.42E-11 | 2.80E-11 |
| CYCLE 3 | 1.28E-11 | 1.89E-11 | 2.60E-11 | 1.62E-11 | 1.34E-11 | 2.44E-11 |
| CYCLE 4 | 1.36E-11 | 2.31E-11 | 2.43E-11 | 1.52E-11 | 1.26E-11 | 2.34E-11 |
| CYCLE 5 | 1.15E-11 | 1.81E-11 | 2.32E-11 | 1.45E-11 | 1.20E-11 | 2.32E-11 |
| CYCLE 6 | 1.20E-11 | 1.84E-11 | 2.31E-11 | 1.44E-11 | 1.19E-11 | 2.33E-11 |

(a) Indicates 30° location in octants with a 15° neutron pad span.
(b) Indicates 30° location in octants with a 17.5° neutron pad span; applicable to 120° and 300° welds.
(c) Indicates 30° location in octants with a 20° neutron pad span; applicable to 60° and 240° welds.

TABLE 6-3

RELATIVE RADIAL DISTRIBUTION OF $\phi(E > 1.0\ MeV)$

WITHIN THE PRESSURE VESSEL WALL

| Radius (cm) | 0. 0° | 15.0° | 30.0° | 45.0° |
|---|---|---|---|---|
| 220.35[1] | 1.00 | 1.00 | 1.00 | 1.00 |
| 221.00 | 0.959 | 0.958 | 0.958 | 0.957 |
| 222.30 | 0.852 | 0.850 | 0.847 | 0.846 |
| 223.60 | 0.739 | 0.736 | 0.733 | 0.730 |
| 224.89 | 0.634 | 0.630 | 0.627 | 0.623 |
| 225.87[2] | 0.562 | 0.557 | 0.554 | 0.548 |
| 227.01 | 0.487 | 0.482 | 0.479 | 0.473 |
| 228.63 | 0.395 | 0.390 | 0.387 | 0.381 |
| 230.09 | 0.326 | 0.321 | 0.319 | 0.312 |
| 231.39 | 0.274 | 0.269 | 0.267 | 0.260 |
| 232.68 | 0.229 | 0.225 | 0.224 | 0.217 |
| 234.14 | 0.188 | 0.184 | 0.182 | 0.176 |
| 235.76 | 0.150 | 0.146 | 0.145 | 0.140 |
| 236.90[3] | 0.127 | 0.124 | 0.123 | 0.118 |
| 237.88 | 0.110 | 0.107 | 0.107 | 0.102 |
| 239.18 | 0.091 | 0.089 | 0.088 | 0.083 |
| 240.47 | 0.075 | 0.073 | 0.072 | 0.068 |
| 241.77 | 0.061 | 0.058 | 0.057 | 0.054 |
| 242.42[4] | 0.058 | 0.055 | 0.055 | 0.051 |

NOTES: 1) Base Metal Inner Radius
2) Base Metal 1/4T
3) Base Metal 3/4T
4) Base Metal Outer Radius

TABLE 6-4

RELATIVE RADIAL DISTRIBUTION OF $\phi(E > 0.1$ MeV)

WITHIN THE PRESSURE VESSEL WALL

| Radius (cm) | 0. 0° | 15.0° | 30.0° | 45.0° |
|---|---|---|---|---|
| 220.35[1] | 1.00 | 1.00 | 1.00 | 1.00 |
| 221.00 | 1.01 | 1.01 | 1.01 | 1.01 |
| 222.30 | 1.00 | 0.997 | 0.996 | 0.989 |
| 223.60 | 0.967 | 0.958 | 0.956 | 0.945 |
| 224.89 | 0.922 | 0.909 | 0.908 | 0.893 |
| 225.87[2] | 0.884 | 0.869 | 0.869 | 0.850 |
| 227.01 | 0.837 | 0.821 | 0.821 | 0.800 |
| 228.63 | 0.770 | 0.753 | 0.754 | 0.729 |
| 230.09 | 0.710 | 0.692 | 0.693 | 0.667 |
| 231.39 | 0.657 | 0.639 | 0.640 | 0.612 |
| 232.68 | 0.604 | 0.587 | 0.588 | 0.558 |
| 234.14 | 0.546 | 0.529 | 0.531 | 0.500 |
| 235.76 | 0.484 | 0.469 | 0.470 | 0.438 |
| 236.90[3] | 0.441 | 0.427 | 0.428 | 0.396 |
| 237.88 | 0.403 | 0.391 | 0.392 | 0.360 |
| 239.18 | 0.356 | 0.345 | 0.346 | 0.313 |
| 240.47 | 0.310 | 0.300 | 0.300 | 0.267 |
| 241.77 | 0.265 | 0.252 | 0.253 | 0.220 |
| 242.42[4] | 0.256 | 0.242 | 0.242 | 0.210 |

NOTES: 1) Base Metal Inner Radius
2) Base Metal 1/4T
3) Base Metal 3/4T
4) Base Metal Outer Radius

TABLE 6-5

RELATIVE RADIAL DISTRIBUTION OF dpa/sec

WITHIN THE PRESSURE VESSEL WALL

| Radius (cm) | 0. 0° | 15.0° | 30.0° | 45.0° |
|---|---|---|---|---|
| 220.35[1] | 1.00 | 1.00 | 1.00 | 1.00 |
| 221.00 | 0.965 | 0.964 | 0.965 | 0.965 |
| 222.30 | 0.877 | 0.876 | 0.874 | 0.878 |
| 223.60 | 0.785 | 0.782 | 0.781 | 0.788 |
| 224.89 | 0.699 | 0.695 | 0.695 | 0.703 |
| 225.87[2] | 0.638 | 0.634 | 0.635 | 0.642 |
| 227.01 | 0.575 | 0.571 | 0.571 | 0.579 |
| 228.63 | 0.495 | 0.491 | 0.492 | 0.500 |
| 230.09 | 0.432 | 0.427 | 0.429 | 0.437 |
| 231.39 | 0.383 | 0.378 | 0.380 | 0.387 |
| 232.68 | 0.339 | 0.334 | 0.337 | 0.342 |
| 234.14 | 0.295 | 0.291 | 0.293 | 0.297 |
| 235.76 | 0.252 | 0.248 | 0.250 | 0.253 |
| 236.90[3] | 0.224 | 0.221 | 0.223 | 0.224 |
| 237.88 | 0.202 | 0.199 | 0.201 | 0.201 |
| 239.18 | 0.175 | 0.173 | 0.174 | 0.172 |
| 240.47 | 0.150 | 0.148 | 0.149 | 0.145 |
| 241.77 | 0.128 | 0.124 | 0.125 | 0.120 |
| 242.42[4] | 0.124 | 0.119 | 0.120 | 0.115 |

NOTES: 1) Base Metal Inner Radius
2) Base Metal 1/4T
3) Base Metal 3/4T
4) Base Metal Outer Radius

TABLE 6-6

NUCLEAR PARAMETERS USED IN THE EVALUATION OF NEUTRON SENSORS

| Monitor Material | Reaction of Interest | Target Weight Fraction | Response Range | Product Half-Life | Fission Yield (%) |
|---|---|---|---|---|---|
| Copper | $Cu^{63}(n,\alpha)Co^{60}$ | 0.6917 | E > 4.7 MeV | 5.271 yrs | |
| Iron | $Fe^{54}(n,p)Mn^{54}$ | 0.0580 | E > 1.0 MeV | 312.5 days | |
| Nickel | $Ni^{58}(n,p)Co^{58}$ | 0.6827 | E > 1.0 MeV | 70.78 days | |
| Uranium-238* | $U^{238}(n,f)Cs^{137}$ | 1.0 | E > 0.4 MeV | 30.17 yrs | 6.00 |
| Neptunium-237* | $Np^{237}(n,f)Cs^{137}$ | 1.0 | E > 0.08 MeV | 30.17 yrs | 6.27 |
| Cobalt-Aluminum* | $Co^{59}(n,\gamma)Co^{60}$ | 0.0015 | .4ev>E>0.015 MeV | 5.271 yrs | |
| Cobalt-Aluminum | $Co^{59}(n,\gamma)Co^{60}$ | 0.0015 | E > 0.015 MeV | 5.271 yrs | |

*Denotes that monitor is cadmium shielded.

TABLE 6-7

MONTHLY THERMAL GENERATION DURING THE FUEL CYCLES

OF THE DIABLO CANYON UNIT 2 REACTOR

| MONTH | THERMAL GENERATION (MWt-hr) | MONTH | THERMAL GENERATION (MWt-Hr | MONTH | THERMAL GENERATION (MWt-hr) |
|---|---|---|---|---|---|
| 10/85 | 0229128 | 7/87 | 0729408 | 12/88 | 1453954 |
| 11/85 | 0916009 | 8/87 | 2318389 | 1/89 | 2529925 |
| 12/85 | 0971006 | 9/87 | 2451827 | 2/89 | 2270596 |
| 1/86 | 0557756 | 10/87 | 2467954 | 3/89 | 2531522 |
| 2/86 | 0229168 | 11/87 | 1862406 | 4/89 | 1451915 |
| 3/86 | 1372940 | 12/87 | 2373238 | 5/89 | 2461503 |
| 4/86 | 2058587 | 1/88 | 2477205 | 6/89 | 2448471 |
| 5/86 | 2297349 | 2/88 | 1626091 | 7/89 | 1980765 |
| 6/86 | 2008247 | 3/88 | 2257456 | 8/89 | 2271022 |
| 7/86 | 1782564 | 4/88 | 2401972 | 9/89 | 2402618 |
| 8/86 | 2414317 | 5/88 | 2530899 | 10/89 | 2069980 |
| 9/86 | 2000642 | 6/88 | 2357323 | 11/89 | 1992152 |
| 10/86 | 2385417 | 7/88 | 1204457 | 12/89 | 2454799 |
| 11/86 | 2360827 | 8/88 | 1696999 | 1/90 | 2533568 |
| 12/86 | 2327040 | 9/88 | 1109402 | 2/90 | 2261182 |
| 1/87 | 2308286 | | | 3/90 | 0238760 |
| 2/87 | 1778567 | | | | |
| 3/87 | 1509455 | | | | |
| 4/87 | 0182858 | | | | |

| MONTH | THERMAL GENERATION (MWt-hr) | MONTH | THERMAL GENERATION (MWt-Hr | MONTH | THERMAL GENERATION (MWt-hr) |
|---|---|---|---|---|---|
| 4/90 | 0011813 | 10/91 | 0278902 | 5/93 | 2210729 |
| 5/90 | 1886810 | 11/91 | 2419834 | 6/93 | 2453399 |
| 6/90 | 2455880 | 12/91 | 2537334 | 7/93 | 2537228 |
| 7/90 | 2367147 | 1/92 | 2515214 | 8/93 | 2535680 |
| 8/90 | 2506381 | 2/92 | 2331904 | 9/93 | 2453620 |
| 9/90 | 2437271 | 3/92 | 2007919 | 10/93 | 2536310 |
| 10/90 | 2383626 | 4/92 | 2454447 | 11/93 | 2420604 |
| 11/90 | 2242075 | 5/92 | 2535697 | 12/93 | 2378469 |
| 12/90 | 2535655 | 6/92 | 2416838 | 1/94 | 2515705 |
| 1/91 | 2354000 | 7/92 | 2535598 | 2/94 | 2275091 |
| 2/91 | 2190222 | 8/92 | 2330087 | 3/94 | 2107924 |
| 3/91 | 2477147 | 9/92 | 2454095 | 4/94 | 1711048 |
| 4/91 | 2368703 | 10/92 | 2535173 | 5/94 | 2536908 |
| 5/91 | 2458916 | 11/92 | 2419114 | 6/94 | 2453677 |
| 6/91 | 2453996 | 12/92 | 2534755 | 7/94 | 2534657 |
| 7/91 | 2534420 | 1/93 | 2420178 | 8/94 | 2536515 |
| 8/91 | 2379451 | 2/93 | 2096545 | 9/94 | 1869962 |
| | | 3/93 | 0372137 | | |

TABLE 6-8

MEASURED AND SATURATED ACTIVITIES AND REACTION RATES

SURVEILLANCE CAPSULE Y

| Reaction | Measured Activity (dps/gm) | Saturated Activity (dps/gm) | Reaction Rate (rps/atom) |
|---|---|---|---|
| Cu-63 (n,α) Co-60 | | | |
| 95-218 Top | 1.28E+05 | 2.45E+05 | 3.73E-17 |
| 95-223 Mid | 1.38E+05 | 2.64E+05 | 4.03E-17 |
| 95-228 Bottom | 1.34E+05 | 2.56E+05 | 3.91E-17 |
| ** AVERAGES ** | 1.33E+05 | 2.55E+05 | 3.89E-17 |
| Fe-54 (n,p) Mn-54 | | | |
| 95-220 Top | 1.32E+06 | 2.16E+06 | 3.45E-15 |
| 95-225 Mid | 1.44E+06 | 2.35E+06 | 3.76E-15 |
| 95-230 Bottom | 1.41E+06 | 2.31E+06 | 3.69E-15 |
| ** AVERAGES ** | 1.39E+06 | 2.27E+06 | 3.63E-15 |
| Ni-58 (n,p) Co-58 | | | |
| 95-219 Top | 8.21E+06 | 3.41E+07 | 4.87E-15 |
| 95-224 Middle | 8.79E+06 | 3.65E+07 | 5.21E-15 |
| 95-229 Bottom | 8.96E+06 | 3.72E+07 | 5.31E-15 |
| ** AVERAGES ** | 8.65E+06 | 3.59E+07 | 5.13E-15 |
| Co-59 (n,γ) Co-60 | | | |
| 95-216 Top | 2.60E+07 | 4.96E+07 | 3.24E-12 |
| 95-221 Middle | 2.32E+07 | 4.43E+07 | 2.89E-12 |
| 95-226 Bottom | 2.43E+07 | 4.65E+07 | 3.53E-12 |
| ** AVERAGES ** | 2.45E+07 | 4.68E+07 | 3.22E-12 |
| Co-59 (n,γ) Co-60 (Cd) | | | |
| 95-217 Top | 1.48E+07 | 2.83E+07 | 1.85E-12 |
| 95-222 Middle | 1.37E+07 | 2.62E+07 | 1.71E-12 |
| 95-227 Bottom | 1.44E+07 | 2.75E+07 | 1.80E-12 |
| ** AVERAGES ** | 1.43E+07 | 2.73E+07 | 1.79E-12 |
| U-238 (n,f) Cs-137 (Cd) | | | |
| 95-214 Middle | 4.25E+05 | 2.93E+06 | 1.93E-14 |
| Np-237 (n,f) Cs-137 (Cd) | | | |
| 95-215 Middle | 4.02E+06 | 2.78E+07 | 1.74E-13 |

TABLE 6-9

MEASURED AND SATURATED ACTIVITIES AND REACTION RATES

SURVEILLANCE CAPSULE X

| Reaction | Measured Activity (dps/gm) | Saturated Activity (dps/gm) | Reaction Rate (rps/atom) |
|---|---|---|---|
| Cu-63 (n,α) Co-60 | | | |
| 95-218 Top | 8.85E+04 | 2.99E+05 | 4.56E-17 |
| 95-228 Bottom | 9.23E+04 | 3.12E+05 | 4.76E-17 |
| ** AVERAGES ** | 9.04E+04 | 3.06E+05 | 4.66E-17 |
| Fe-54 (n,p) Mn-54 | | | |
| 95-220 Top | 1.41E+06 | 2.77E+06 | 4.43E-15 |
| 95-225 Mid | 1.49E+06 | 2.93E+06 | 4.68E-15 |
| 95-230 Bottom | 1.48E+06 | 2.91E+06 | 4.65E-15 |
| ** AVERAGES ** | 1.46E+06 | 2.87E+06 | 4.59E-15 |
| Ni-58 (n,p) Co-58 | | | |
| 95-219 Top | 7.23E+06 | 4.31E+07 | 6.15E-15 |
| 95-224 Middle | 7.64E+06 | 4.55E+07 | 6.49E-15 |
| 95-229 Bottom | 7.57E+06 | 4.51E+07 | 6.44E-15 |
| ** AVERAGES ** | 7.48E+06 | 4.46E+07 | 6.36E-15 |
| Co-59 (n,γ) Co-60 | | | |
| 95-216 Top | 2.17E+07 | 7.34E+07 | 4.79E-12 |
| 95-221 Middle | 1.95E+07 | 6.58E+07 | 4.29E-12 |
| 95-226 Bottom | 2.12E+07 | 7.15E+07 | 4.67E-12 |
| ** AVERAGES ** | 2.08E+07 | 7.02E+07 | 4.58E-12 |
| Co-59 (n,γ) Co-60 (Cd) | | | |
| 95-217 Top | 1.21E+07 | 4.09E+07 | 2.67E-12 |
| 95-222 Middle | 1.12E+07 | 3.79E+07 | 2.47E-12 |
| 95-227 Bottom | 1.20E+07 | 4.06E+07 | 2.65E-12 |
| ** AVERAGES ** | 1.18E+07 | 3.98E+07 | 2.60E-12 |
| U-238 (n,f) Cs-137 (Cd) | | | |
| 95-214 Middle | 2.89E+05 | 4.29E+06 | 2.83E-14 |
| Np-237 (n,f) Cs-137 (Cd) | | | |
| 95-215 Middle | 3.10E+06 | 4.60E+07 | 2.89E-13 |

TABLE 6-10

MEASURED AND SATURATED ACTIVITIES AND REACTION RATES

SURVEILLANCE CAPSULE U

| Reaction | Measured Activity (dps/gm) | Saturated Activity (dps/gm) | Reaction Rate (rps/atom) |
|---|---|---|---|
| Cu-63 (n,α) Co-60 | | | |
| 95-218 Top | 3.91E+04 | 3.50E+05 | 5.34E-17 |
| 95-223 Mid | 4.13E+04 | 3.70E+05 | 5.64E-17 |
| 95-228 Bottom | 4.04E+04 | 3.62E+05 | 5.52E-17 |
| ** AVERAGES ** | 4.03E+04 | 3.61E+05 | 5.50E-17 |
| Fe-54 (n,p) Mn-54 | | | |
| 95-220 Top | 1.13E+06 | 3.55E+06 | 5.67E-15 |
| 95-225 Mid | 1.21E+06 | 3.80E+06 | 6.07E-15 |
| 95-230 Bottom | 1.18E+06 | 3.70E+06 | 5.92E-15 |
| ** AVERAGES ** | 1.17E+06 | 3.68E+06 | 5.89E-15 |
| Ni-58 (n,p) Co-58 | | | |
| 95-219 Top | 5.43E+06 | 5.54E+07 | 7.92E-15 |
| 95-224 Middle | 5.62E+06 | 5.74E+07 | 8.19E-15 |
| 95-229 Bottom | 5.79E+06 | 5.91E+07 | 8.44E-15 |
| ** AVERAGES ** | 5.61E+06 | 5.73E+07 | 8.18E-15 |
| Co-59 (n,γ) Co-60 | | | |
| 95-216 Top | 1.04E+07 | 9.31E+07 | 6.08E-12 |
| 95-221 Middle | 9.59E+06 | 8.59E+07 | 5.60E-12 |
| 95-226 Bottom | 9.93E+06 | 8.89E+07 | 5.80E-12 |
| ** AVERAGES ** | 8.97E+06 | 8.93E+07 | 5.83E-12 |
| Co-59 (n,γ) Co-60 (Cd) | | | |
| 95-217 Top | 5.71E+06 | 5.11E+07 | 3.34E-12 |
| 95-222 Middle | 5.38E+06 | 4.82E+07 | 3.14E-12 |
| 95-227 Bottom | 5.72E+06 | 5.12E+07 | 3.34E-12 |
| ** AVERAGES ** | 5.60E+06 | 5.02E+07 | 3.27E-12 |
| U-238 (n,f) Cs-137 (Cd) | | | |
| 95-214 Middle | 1.16E+05 | 5.21E+06 | 3.44E-14 |
| Np-237 (n,f) Cs-137 (Cd) | | | |
| 95-215 Middle | 1.36E+06 | 6.11E+07 | 3.84E-13 |

TABLE 6-11

SUMMARY OF NEUTRON DOSIMETRY RESULTS

SURVEILLANCE CAPSULES Y, X, AND U

Measured Flux and Fluence for Capsule Y

| Quantity | Flux (n/cm$^2$-sec) | Fluence (n/cm$^2$) | Uncertainty |
|---|---|---|---|
| $\phi$ (E > 1.0 MeV) | 5.93E+10 | 1.32E+19 | ± 8. % |
| $\phi$ (E > 0.1 MeV) | 2.66E+11 | 5.90E+19 | ±16. % |
| dpa/sec | 1.16E-10 | 2.57E-02 | ±11. % |
| $\phi$ (E < 0.414 eV) | 5.54E+10 | 1.23E+19 | ±24. % |

Measured Flux and Fluence for Capsule X

| Quantity | Flux (n/cm$^2$-sec) | Fluence (n/cm$^2$) | Uncertainty |
|---|---|---|---|
| $\phi$ (E > 1.0 MeV) | 8.83E+10 | 8.66E+18 | ± 8. % |
| $\phi$ (E > 0.1 MeV) | 4.32E+11 | 4.24E+19 | ±16. % |
| dpa/sec | 1.80E-10 | 1.77E-02 | ±11. % |
| $\phi$ (E < 0.414 eV) | 8.35E+10 | 8.19E+18 | ±23. % |

Measured Flux and Fluence for Capsule U

| Quantity | Flux (n/cm$^2$-sec) | Fluence (n/cm$^2$) | Uncertainty |
|---|---|---|---|
| $\phi$ (E > 1.0 MeV) | 1.14E+11 | 3.57E+18 | ± 8. % |
| $\phi$ (E > 0.1 MeV) | 5.51E+11 | 1.73E+19 | ±16. % |
| dpa/sec | 2.30E-10 | 7.21E-03 | ±11. % |
| $\phi$ (E < 0.414 eV) | 1.07E+11 | 3.35E+18 | ±23. % |

TABLE 6-12

COMPARISON OF MEASURED AND FERRET CALCULATED

REACTION RATES AT THE SURVEILLANCE CAPSULE CENTER

SURVEILLANCE CAPSULE Y

| | REACTION RATE (RPS/NUCLEUS) | | RATIO MEAS/CALC |
|---|---|---|---|
| Reaction | Meas | Adj Calc | Adj Calc |
| Cu63(n,α)Co60 | 3.89E-17 | 3.82E-17 | 1.02 |
| Fe-54(n,f)Mn-54 | 3.63E-17 | 3.71E-17 | 0.98 |
| Ni-58(n,p)Co-58 | 5.13E-15 | 5.19E-15 | 0.99 |
| U-238(n,f)Cs-137 (Cd) | 1.93E-14 | 1.88E-14 | 1.03 |
| Np-237(n,f)Cs-137(Cd) | 1.74E-13 | 1.76E-13 | 0.99 |
| Co59(n,γ)Co60 | 3.05E-12 | 3.04E-12 | 1.00 |
| Co59(n,γ)Co60 (Cd) | 1.78E-12 | 1.79E-12 | 1.00 |

TABLE 6-13

COMPARISON OF MEASURED AND FERRET CALCULATED

REACTION RATES AT THE SURVEILLANCE CAPSULE CENTER

SURVEILLANCE CAPSULE X

| | REACTION RATE (RPS/NUCLEUS) | | RATIO MEAS/CALC |
|---|---|---|---|
| Reaction | Meas | Adj Calc | Adj Calc |
| Cu63(n,α)Co60 | 4.66E-17 | 4.56E-17 | 1.02 |
| Fe-54(n,f)Mn-54 | 4.58E-15 | 4.72E-15 | 0.97 |
| Ni-58(n,p)Co-58 | 6.36E-15 | 6.67E-15 | 0.95 |
| U-238(n,f)Cs-137 (Cd) | 2.83E-14 | 2.66E-14 | 1.06 |
| Np-237(n,f)Cs-137(Cd) | 2.89E-13 | 2.83E-13 | 1.02 |
| Co59(n,γ)Co60 | 4.58E-12 | 4.55E-12 | 1.01 |
| Co59(n,γ)Co60 (Cd) | 2.59E-12 | 2.61E-12 | 1.00 |

TABLE 6-14

COMPARISON OF MEASURED AND FERRET CALCULATED

REACTION RATES AT THE SURVEILLANCE CAPSULE CENTER

SURVEILLANCE CAPSULE U

| | REACTION RATE (RPS/NUCLEUS) | | RATIO MEAS/CALC |
|---|---|---|---|
| Reaction | Meas | Adj Calc | Adj Calc |
| Cu63(n,α)Co60 | 5.50E-17 | 5.43E-17 | 1.01 |
| Fe-54(n,f)Mn-54 | 5.89E-15 | 5.98E-15 | 0.98 |
| Ni-58(n,p)Co-58 | 8.18E-15 | 8.46E-15 | 0.97 |
| U-238(n,f)Cs-137 (Cd) | 3.44E-14 | 3.37E-14 | 1.02 |
| Np-237(n,f)Cs-137(Cd) | 3.84E-13 | 3.69E-13 | 1.04 |
| Co59(n,γ)Co60 | 5.82E-12 | 5.79E-12 | 1.01 |
| Co59(n,γ)Co60 (Cd) | 3.27E-12 | 3.29E-12 | 1.00 |

TABLE 6-15

ADJUSTED NEUTRON ENERGY SPECTRUM AT THE

CENTER OF SURVEILLANCE CAPSULE Y

| Group # | Energy (MeV) | Flux (n/cm$^2$-sec) | Group # | Energy (MeV) | Flux (n/cm$^2$-sec) |
|---|---|---|---|---|---|
| 1 | 1.73E+01 | 5.05E+06 | 28 | 9.12E-03 | 1.41E+10 |
| 2 | 1.49E+01 | 1.09E+07 | 29 | 5.53E-03 | 1.78E+10 |
| 3 | 1.35E+01 | 4.01E+07 | 30 | 3.36E-03 | 5.60E+09 |
| 4 | 1.16E+01 | 1.10E+08 | 31 | 2.84E-03 | 5.37E+09 |
| 5 | 1.00E+01 | 2.46E+08 | 32 | 2.40E-03 | 5.21E+09 |
| 6 | 8.61E+00 | 4.21E+08 | 33 | 2.04E-03 | 1.52E+10 |
| 7 | 7.41E+00 | 9.96E+08 | 34 | 1.23E-03 | 1.46E+10 |
| 8 | 6.07E+00 | 1.47E+09 | 35 | 7.49E-04 | 1.34E+10 |
| 9 | 4.97E+00 | 2.97E+09 | 36 | 4.54E-04 | 1.21E+10 |
| 10 | 3.68E+00 | 3.39E+09 | 37 | 2.75E-04 | 1.29E+10 |
| 11 | 2.87E+00 | 6.56E+09 | 38 | 1.67E-04 | 1.28E+10 |
| 12 | 2.23E+00 | 8.88E+09 | 39 | 1.01E-04 | 1.34E+10 |
| 13 | 1.74E+00 | 1.21E+10 | 40 | 6.14E-05 | 1.33E+10 |
| 14 | 1.35E+00 | 1.39E+10 | 41 | 3.73E-05 | 1.32E+10 |
| 15 | 1.11E+00 | 2.40E+10 | 42 | 2.26E-05 | 1.29E+10 |
| 16 | 8.21E-01 | 2.82E+10 | 43 | 1.37E-05 | 1.25E+10 |
| 17 | 6.39E-01 | 3.11E+10 | 44 | 8.32E-06 | 1.21E+10 |
| 18 | 4.98E-01 | 2.16E+10 | 45 | 5.04E-06 | 1.16E+10 |
| 19 | 3.88E-01 | 3.29E+10 | 46 | 3.06E-06 | 1.15E+10 |
| 20 | 3.02E-01 | 3.56E+10 | 47 | 1.86E-06 | 1.14E+10 |
| 21 | 1.83E-01 | 3.58E+10 | 48 | 1.13E-06 | 8.06E+09 |
| 22 | 1.11E-01 | 2.70E+10 | 49 | 6.83E-07 | 8.98E+09 |
| 23 | 6.74E-02 | 2.15E+10 | 50 | 4.14E-07 | 1.20E+10 |
| 24 | 4.09E-02 | 1.22E+10 | 51 | 2.51E-07 | 1.09E+10 |
| 25 | 2.55E-02 | 1.37E+10 | 52 | 1.52E-07 | 9.74E+09 |
| 26 | 1.99E-02 | 7.02E+09 | 53 | 9.24E-08 | 2.28E+10 |
| 27 | 1.50E-02 | 1.24E+10 | | | |

Note: Tabulated energy levels represent the upper energy in each group.

TABLE 6-16

ADJUSTED NEUTRON ENERGY SPECTRUM AT THE

CENTER OF SURVEILLANCE CAPSULE X

| Group # | Energy (MeV) | Flux (n/cm$^2$-sec) | Group # | Energy (MeV) | Flux (n/cm$^2$-sec) |
|---|---|---|---|---|---|
| 1 | 1.73E+01 | 6.06E+06 | 28 | 9.12E-03 | 1.97E+10 |
| 2 | 1.49E+01 | 1.29E+07 | 29 | 5.53E-03 | 2.56E+10 |
| 3 | 1.35E+01 | 4.72E+07 | 30 | 3.36E-03 | 8.00E+09 |
| 4 | 1.16E+01 | 1.28E+08 | 31 | 2.84E-03 | 7.67E+09 |
| 5 | 1.00E+01 | 2.88E+08 | 32 | 2.40E-03 | 7.45E+09 |
| 6 | 8.61E+00 | 4.98E+08 | 33 | 2.04E-03 | 2.17E+10 |
| 7 | 7.41E+00 | 1.19E+09 | 34 | 1.23E-03 | 2.08E+10 |
| 8 | 6.07E+00 | 1.81E+09 | 35 | 7.49E-04 | 1.89E+10 |
| 9 | 4.97E+00 | 3.76E+09 | 36 | 4.54E-04 | 1.70E+10 |
| 10 | 3.68E+00 | 4.49E+09 | 37 | 2.75E-04 | 1.86E+10 |
| 11 | 2.87E+00 | 9.08E+09 | 38 | 1.67E-04 | 1.90E+10 |
| 12 | 2.23E+00 | 1.30E+10 | 39 | 1.01E-04 | 1.95E+10 |
| 13 | 1.74E+00 | 1.85E+10 | 40 | 6.14E-05 | 1.93E+10 |
| 14 | 1.35E+00 | 2.21E+10 | 41 | 3.73E-05 | 1.90E+10 |
| 15 | 1.11E+00 | 3.93E+10 | 42 | 2.26E-05 | 1.84E+10 |
| 16 | 8.21E-01 | 4.73E+10 | 43 | 1.37E-05 | 1.77E+10 |
| 17 | 6.39E-01 | 5.26E+10 | 44 | 8.32E-06 | 1.69E+10 |
| 18 | 4.98E-01 | 3.67E+10 | 45 | 5.04E-06 | 1.61E+10 |
| 19 | 3.88E-01 | 5.56E+10 | 46 | 3.06E-06 | 1.57E+10 |
| 20 | 3.02E-01 | 5.82E+10 | 47 | 1.86E-06 | 1.54E+10 |
| 21 | 1.83E-01 | 5.85E+10 | 48 | 1.13E-06 | 1.09E+10 |
| 22 | 1.11E-01 | 4.29E+10 | 49 | 6.83E-07 | 1.21E+10 |
| 23 | 6.74E-02 | 3.31E+10 | 50 | 4.14E-07 | 1.61E+10 |
| 24 | 4.09E-02 | 1.77E+10 | 51 | 2.51E-07 | 1.54E+10 |
| 25 | 2.55E-02 | 2.08E+10 | 52 | 1.52E-07 | 1.42E+10 |
| 26 | 1.99E-02 | 9.68E+09 | 53 | 9.24E-08 | 3.79E+10 |
| 27 | 1.50E-02 | 1.70E+10 | | | |

Note: Tabulated energy levels represent the upper energy in each group.

TABLE 6-17

ADJUSTED NEUTRON ENERGY SPECTRUM AT THE

CENTER OF SURVEILLANCE CAPSULE U

| Group # | Energy (MeV) | Flux (n/cm$^2$-sec) | Group # | Energy (MeV) | Flux (n/cm$^2$-sec) |
|---|---|---|---|---|---|
| 1 | 1.73E+01 | 7.00E+06 | 28 | 9.12E-03 | 2.40E+10 |
| 2 | 1.49E+01 | 1.50E+07 | 29 | 5.53E-03 | 3.11E+10 |
| 3 | 1.35E+01 | 5.51E+07 | 30 | 3.36E-03 | 9.72E+09 |
| 4 | 1.16E+01 | 1.51E+08 | 31 | 2.84E-03 | 9.32E+09 |
| 5 | 1.00E+01 | 3.42E+08 | 32 | 2.40E-03 | 9.06E+09 |
| 6 | 8.61E+00 | 6.00E+08 | 33 | 2.04E-03 | 2.65E+10 |
| 7 | 7.41E+00 | 1.45E+09 | 34 | 1.23E-03 | 2.55E+10 |
| 8 | 6.07E+00 | 2.26E+09 | 35 | 7.49E-04 | 2.33E+10 |
| 9 | 4.97E+00 | 4.78E+09 | 36 | 4.54E-04 | 2.10E+10 |
| 10 | 3.68E+00 | 5.75E+09 | 37 | 2.75E-04 | 2.31E+10 |
| 11 | 2.87E+00 | 1.17E+10 | 38 | 1.67E-04 | 2.40E+10 |
| 12 | 2.23E+00 | 1.67E+10 | 39 | 1.01E-04 | 2.42E+10 |
| 13 | 1.74E+00 | 2.37E+10 | 40 | 6.14E-05 | 2.40E+10 |
| 14 | 1.35E+00 | 2.86E+10 | 41 | 3.73E-05 | 2.35E+10 |
| 15 | 1.11E+00 | 5.09E+10 | 42 | 2.26E-05 | 2.27E+10 |
| 16 | 8.21E-01 | 6.11E+10 | 43 | 1.37E-05 | 2.18E+10 |
| 17 | 6.39E-01 | 6.76E+10 | 44 | 8.32E-06 | 2.07E+10 |
| 18 | 4.98E-01 | 4.68E+10 | 45 | 5.04E-06 | 1.96E+10 |
| 19 | 3.88E-01 | 7.06E+10 | 46 | 3.06E-06 | 1.92E+10 |
| 20 | 3.02E-01 | 7.35E+10 | 47 | 1.86E-06 | 1.88E+10 |
| 21 | 1.83E-01 | 7.33E+10 | 48 | 1.13E-06 | 1.33E+10 |
| 22 | 1.11E-01 | 5.35E+10 | 49 | 6.83E-07 | 1.49E+10 |
| 23 | 6.74E-02 | 4.10E+10 | 50 | 4.14E-07 | 2.00E+10 |
| 24 | 4.09E-02 | 2.18E+10 | 51 | 2.51E-07 | 1.93E+10 |
| 25 | 2.55E-02 | 2.55E+10 | 52 | 1.52E-07 | 1.81E+10 |
| 26 | 1.99E-02 | 1.18E+10 | 53 | 9.24E-08 | 4.94E+10 |
| 27 | 1.50E-02 | 2.08E+10 | | | |

Note: Tabulated energy levels represent the upper energy in each group.

TABLE 6-18

COMPARISON OF CALCULATED AND MEASURED NEUTRON EXPOSURE LEVELS FOR DIABLO CANYON UNIT 2 SURVEILLANCE CAPSULES Y, X, AND U

CAPSULE Y

| | Calculated | Measured | M/C |
|---|---|---|---|
| Fluence (E > 1.0 MeV) [n/cm$^2$-sec] | 1.54E+19 | 1.32E+19 | 0.86 |
| Fluence (E > 0.1 MeV) [n/cm$^2$-sec] | 6.77E+19 | 5.90E+19 | 0.87 |
| dpa | 2.95E-02 | 2.57E-02 | 0.87 |

CAPSULE X

| | Calculated | Measured | M/C |
|---|---|---|---|
| Fluence (E > 1.0 MeV) [n/cm$^2$-sec] | 8.38E+18 | 8.66E+18 | 1.03 |
| Fluence (E > 0.1 MeV) [n/cm$^2$-sec] | 3.75E+19 | 4.24E+19 | 1.13 |
| dpa | 1.62E-02 | 1.77E-02 | 1.09 |

CAPSULE U

| | Calculated | Measured | M/C |
|---|---|---|---|
| Fluence (E > 1.0 MeV) [n/cm$^2$-sec] | 2.97E+18 | 3.57E+18 | 1.20 |
| Fluence (E > 0.1 MeV) [n/cm$^2$-sec] | 1.33E+19 | 1.73E+19 | 1.30 |
| dpa | 5.76E-03 | 7.21E-03 | 1.25 |

TABLE 6-19

NEUTRON EXPOSURE PROJECTIONS AT KEY LOCATIONS

ON THE PRESSURE VESSEL CLAD/BASE METAL INTERFACE

BEST ESTIMATE EXPOSURE (7.0 EFPY) AT THE PRESSURE VESSEL INNER RADIUS

| | 0.0° | 15.0° | 30.0°(a) | 30.0°(b) | 30.0°(c) | 45.0° |
|---|---|---|---|---|---|---|
| E > 1.0 | 1.68E+18 | 2.66E+18 | 3.34E+18 | 2.08E+18 | 1.73E+18 | 3.22E+18 |
| E > 0.1 | 3.44E+18 | 5.51E+18 | 7.01E+18 | 4.37E+18 | 3.62E+18 | 7.88E+18 |
| dpa | 2.60E-03 | 4.07E-03 | 5.11E-03 | 3.19E-03 | 2.64E-03 | 5.07E-03 |

BEST ESTIMATE EXPOSURE (12 EFPY) AT THE PRESSURE VESSEL INNER RADIUS

| | 0.0° | 15.0° | 30.0°(a) | 30.0°(b | 30.0°(c) | 45.0° |
|---|---|---|---|---|---|---|
| E > 1.0 | 2.75E+18 | 4.34E+18 | 5.47E+18 | 3.41E+18 | 2.83E+18 | 5.31E+18 |
| E > 0.1 | 5.64E+18 | 8.99E+18 | 1.15E+19 | 7.16E+18 | 5.94E+18 | 1.30E+19 |
| dpa | 4.26E-03 | 6.65E-03 | 8.39E-03 | 5.22E-03 | 4.34E-03 | 8.35E-03 |

BEST ESTIMATE EXPOSURE (16 EFPY) AT THE PRESSURE VESSEL INNER RADIUS

| | 0.0° | 15.0° | 30.0°(a) | 30.0°(b) | 30.0°(c) | 45.0° |
|---|---|---|---|---|---|---|
| E > 1.0 | 3.62E+18 | 5.69E+18 | 7.19E+18 | 4.48E+18 | 3.72E+18 | 6.99E+18 |
| E > 0.1 | 7.41E+18 | 1.18E+19 | 1.51E+19 | 9.41E+18 | 7.81E+18 | 1.71E+19 |
| dpa | 5.60E-03 | 8.72E-03 | 1.10E-02 | 6.87E-03 | 5.70E-03 | 1.10E-02 |

BEST ESTIMATE EXPOSURE (32 EFPY) AT THE PRESSURE VESSEL INNER RADIUS

| | 0.0° | 15.0° | 30.0°(a) | 30.0°(b) | 30°(c) | 45° |
|---|---|---|---|---|---|---|
| E > 1.0 | 7.08E+18 | 1.11E+19 | 1.41E+19 | 8.77E+18 | 7.27E+18 | 1.37E+19 |
| E > 0.1 | 1.45E+19 | 2.30E+19 | 2.95E+19 | 1.84E+19 | 1.53E+19 | 3.35E+19 |
| dpa | 1.10E-02 | 1.70E-02 | 2.16E-02 | 1.34E-02 | 1.11E-02 | 2.16E-02 |

(a) Indicates 30° location in octants with a 15° neutron pad span.
(b) Indicates 30° location in octants with a 17.5° neutron pad span; applicable to 120° and 300° welds.
(c) Indicates 30° location in octants with a 20° neutron pad span; applicable to 60° and 240° welds.

TABLE 6-20

NEUTRON EXPOSURE VALUES WITHIN THE

DIABLO CANYON UNIT 2 REACTOR VESSEL

FLUENCE BASED ON E > 1.0 MeV SLOPE

| | 0.0° | 15.0° | 30.0° (a) | 30.0° (b) | 30.0° (c) | 45.0° |
|---|---|---|---|---|---|---|
| | | | 12 EFPY FLUENCE | | | |
| SURFACE | 2.75E+18 | 4.34E+18 | 5.47E+18 | 3.41E+18 | 2.83E+18 | 5.31E+18 |
| 1/4T | 1.55E+18 | 2.42E+18 | 3.03E+18 | 1.89E+18 | 1.57E+18 | 2.91E+18 |
| 3/4T | 3.51E+17 | 5.38E+17 | 6.74E+17 | 4.20E+17 | 3.49E+17 | 6.26E+17 |
| | | | 16 EFPY FLUENCE | | | |
| SURFACE | 3.62E+18 | 5.69E+18 | 7.19E+18 | 4.48E+18 | 3.72E+18 | 6.99E+18 |
| 1/4T | 2.03E+18 | 3.17E+18 | 3.99E+18 | 2.48E+18 | 2.06E+18 | 3.83E+18 |
| 3/4T | 4.61E+17 | 7.06E+17 | 8.86E+17 | 5.52E+17 | 4.58E+17 | 8.24E+17 |
| | | | 32 EFPY FLUENCE | | | |
| SURFACE | 7.08E+18 | 1.11E+19 | 1.41E+19 | 8.77E+18 | 7.27E+18 | 1.37E+19 |
| 1/4T | 3.98E+18 | 6.19E+18 | 7.80E+18 | 4.86E+18 | 4.03E+18 | 7.52E+18 |
| 3/4T | 9.01E+17 | 1.38E+18 | 1.73E+18 | 1.08E+18 | 8.96E+17 | 1.62E+18 |

FLUENCE BASED ON dpa SLOPE

| | 0.0° | 15° | 30.0° (a) | 30° (b) | 30..0° (c) | 45.0° |
|---|---|---|---|---|---|---|
| | | | 12 EFPY FLUENCE | | | |
| SURFACE | 2.75E+18 | 4.34E+18 | 5.47E+18 | 3.41E+18 | 2.83E+18 | 5.31E+18 |
| 1/4T | 1.76E+18 | 2.75E+18 | 3.47E+18 | 2.16E+18 | 1.80E+18 | 3.41E+18 |
| 3/4T | 6.18E+17 | 9.58E+17 | 1.22E+18 | 7.60E+17 | 6.31E+17 | 1.19E+18 |
| | | | 16 EFPY FLUENCE | | | |
| SURFACE | 3.62E+18 | 5.69E+18 | 7.19E+18 | 4.48E+18 | 3.72E+18 | 6.99E+18 |
| 1/4T | 2.31E+18 | 3.61E+18 | 4.57E+18 | 2.84E+18 | 2.36E+18 | 4.49E+18 |
| 3/4T | 8.12E+17 | 1.26E+18 | 1.60E+18 | 9.99E+17 | 8.29E+17 | 1.57E+18 |
| | | | 32 EFPY FLUENCE | | | |
| SURFACE | 7.08E+18 | 1.11E+19 | 1.41E+19 | 8.77E+18 | 7.27E+18 | 1.37E+19 |
| 1/4T | 4.52E+18 | 7.04E+18 | 8.93E+18 | 5.56E+18 | 4.62E+18 | 8.81E+18 |
| 3/4T | 1.59E+18 | 2.45E+18 | 3.14E+18 | 1.95E+18 | 1.62E+18 | 3.07E+18 |

(a) Indicates 30° location in octants with a 15° neutron pad span.
(b) Indicates 30° location in octants with a 17.5° neutron pad span; applicable to 120° and 300° welds.
(c) Indicates 30° location in octants with a 20° neutron pad span; applicable to 60° and 240° welds.

TABLE 6-21

UPDATED LEAD FACTORS FOR DIABLO CANYON UNIT 2

SURVEILLANCE CAPSULES

| CAPSULE | LEAD FACTOR |
|---|---|
| V[d] | 4.15 |
| U[a] | 4.64 |
| X[b] | 4.65 |
| W[d] | 4.58 |
| Y[c] | 4.15 |
| Z[d] | 4.58 |

[a] - Withdrawn at the end of Cycle 1.
[b] - Withdrawn at the end of Cycle 3.
[c] - Withdrawn at the end of Cycle 6.
[d] - Capsules remaining in the reactor.

## SECTION 7.0

## RECOMMENDED SURVEILLANCE CAPSULE REMOVAL SCHEDULE

The following surveillance capsule removal schedule meets the requirements of ASTM E185-82 and is recommended for future capsules to be removed from the Diablo Canyon Unit 2 reactor vessel:

TABLE 7-1

Recommended Surveillance Capsule Removal Schedule for the Diablo Canyon Unit 2 Reactor Vessel

| Capsule | Capsule Location (degree) | Lead Factor | Withdrawal EFPY[a] | Fluence ($n/cm^2$, E > 1.0 MeV) |
|---|---|---|---|---|
| U[b] | 56.0 | 4.64 | 0.99 | $3.57 \times 10^{18}$ |
| X[b] | 236.0 | 4.65 | 3.11 | $8.66 \times 10^{18}$ |
| Y[b] | 238.5 | 4.15 | 7.0 | $1.32 \times 10^{19}$ |
| W | 124.0 | 4.58 | 10.6 | $2.097 \times 10^{19}$ [c] |
| V | 58.5 | 4.15 | Standby | ----- |
| Z | 304.0 | 4.58 | Standby | ------ |

NOTES:
(a) Effective Full Power Years (EFPY) from plant startup.
(b) Plant-specific evaluation.
(c) Approximately equal to the projected peak vessel fluence at 48 EFPY.

## SECTION 8.0
## REFERENCES


1. Regulatory Guide 1.99, Revision 2, "Radiation Embrittlement of Reactor Vessel Materials", U.S. Nuclear Regulatory Commission, May, 1988.

2. Code of Federal Regulations, 10 CFR Part 50, Appendix G, "Fracture Toughness Requirements", U.S. Nuclear Regulatory Commission, Washington, D.C.

3. WCAP-8783, "Pacific Gas and Electric Company Diablo Canyon Unit No. 2 Reactor Vessel Radiation Surveillance Program", J. A. Davidson and S. E. Yanichko, December 1976.

4. Section III of the ASME Boiler and Pressure Vessel Code, Appendix G, "Protection Against Nonductile Failure".

5. ASTM E208, "Standard Test Method for Conducting Drop-Weight Test to Determine Nil-Ductility Transition Temperature of Ferritic Steels", in ASTM Standards, Section 3, American Society for Testing and Materials, Philadelphia, PA.

6. Code of Federal Regulations, 10 CFR Part 50, Appendix H, "Reactor Vessel Material Surveillance Program Requirements", U.S. Nuclear Regulatory Commission, Washington, D.C.

7. ASTM E185-82, "Standard Practice for Conducting Surveillance Tests for Light-Water Cooled Nuclear Power Reactor Vessels", E706 (IF), in ASTM Standards, Section 3, American Society for Testing and Materials, Philadelphia, PA, 1993.

8. ASTM E23-93a, "Standard Test Methods for Notched Bar Impact Testing of Metallic Materials", in ASTM Standards, Section 3, American Society for Testing and Materials, Philadelphia, PA, 1993.

9. ASTM A370-92, "Standard Test Methods and Definitions for Mechanical Testing of Steel Products", in ASTM Standards, Section 3, American Society for Testing and Materials, Philadelphia, PA, 1993.

10. ASTM E8-93, "Standard Test Methods for Tension Testing of Metallic Materials", in ASTM Standards, Section 3, American Society for Testing and Materials, Philadelphia, PA, 1993.

11. ASTM E21-92, "Standard Test Methods for Elevated Temperature Tension Tests of Metallic Materials", in ASTM Standards, Section 3, American Society for Testing and Materials, Philadelphia, PA, 1993.

12. ASTM E83-93, "Standard Practice for Verification and Classification of Extensometers", in ASTM Standards, Section 3, American Society for Testing and Materials, Philadelphia, PA, 1993.

13. ASTM E853-87, "Standard Practice for Analysis and Interpretation of Light-Water Reactor Surveillance Results", in ASTM Standards, Section 12, American Society for Testing and Materials, Philadelphia, PA, 1993.

14. ASTM E693-79, "Standard Practice for Characterizing Neutron Exposures in Ferritic Steels in Terms of Displacements per Atom (dpa)", in ASTM Standards, Section 12, American Society for Testing and Materials, Philadelphia, PA, 1993.

15. WCAP-14350-R0, "Pacific Gas and Electric Company Reactor Cavity Neutron Measurement Program for Diablo Canyon Unit 2 - Cycles 1 through 6", S. L. Anderson, May 1995.

16. RSIC Computer Code Collection CCC-543, "TORT-DORT Two- and Three-Dimensional Discrete Ordinates Transport, Version 2.7.3", May 1993.

17. RSIC Data Library Collection DLC-175, "BUGLE-93, Production and Testing of the VITAMIN-B6 Fine Group and the BUGLE-93 Broad Group Neutron/Photon Cross-Section Libraries Derived from ENDF/B-VI Nuclear Data", April 1994.

18. R. E. Maerker, et al, "Accounting for Changing Source Distributions in Light Water Reactor Surveillance Dosimetry Analysis", Nuclear Science and Engineering, Volume 94, Pages 291-308, 1986.

19. WCAP-10593, "The Nuclear Design and Core Physics Characteristics of the Diablo Canyon Power Plant Unit 2 - Cycle 1", J. A. Vestovich, et. al., July 1984. [Westinghouse Proprietary Class 2]

20. WCAP-11450-R0, "The Nuclear Design and Core Physics Characteristics of the Diablo Canyon Power Plant Unit 2 - Cycle 2", M. W. Fecteau, et. al., May 1987. [Westinghouse Proprietary Class 2]

21. WCAP-11962-R0, "The Nuclear Design and Core Physics Characteristics of the Diablo Canyon Power Plant Unit 2 - Cycle 3", M. W. Fecteau, et. al., October 1988. [Westinghouse Proprietary Class 2]

22. WCAP-12492-R0, "The Nuclear Design and Core Physics Characteristics of the Diablo Canyon Power Plant Unit 2 - Cycle 4", M. W. Fecteau, et. al., February 1990. [Westinghouse Proprietary Class 2]

23. WCAP-13050- R0, "The Nuclear Design and Core Physics Characteristics of the Diablo Canyon Power Plant Unit 2 - Cycle 5", M. W. Fecteau, et. al., August 1991. [Westinghouse Proprietary Class 2]

24. WCAP-13623-R0, "The Nuclear Design and Core Physics Characteristics of the Diablo Canyon Power Plant Unit 2 - Cycle 6", M. W. Fecteau, et. al., February 1992. [Westinghouse Proprietary Class 2]

25. ASTM Designation E482-89, "Standard Guide for Application of Neutron Transport Methods for Reactor Vessel Surveillance", in ASTM Standards, Section 12, American Society for Testing and Materials, Philadelphia, PA, 1993.

26. ASTM Designation E560-84, "Standard Recommended Practice for Extrapolating Reactor Vessel Surveillance Dosimetry Results", in ASTM Standards, Section 12, American Society for Testing and Materials, Philadelphia, PA, 1993.

27. ASTM Designation E706-87, "Standard Master Matrix for Light-Water Reactor Pressure Vessel Surveillance Standard", in ASTM Standards, Section 12, American Society for Testing and Materials, Philadelphia, PA, 1993.

28. ASTM Designation E261-90, "Standard Practice for Determining Neutron Fluence Rate, Fluence, and Spectra by Radioactivation Techniques", in ASTM Standards, Section 12, American Society for Testing and Materials, Philadelphia, PA, 1993.

29. ASTM Designation E262-86, "Standard Method for Determining Thermal Neutron Reaction and Fluence Rates by Radioactivation Techniques", in ASTM Standards, Section 12, American Society for Testing and Materials, Philadelphia, PA, 1993.

30. ASTM Designation E263-88, "Standard Method for Measuring Fast-Neutron Reaction Rates by Radioactivation of Iron", in ASTM Standards, Section 12, American Society for Testing and Materials, Philadelphia, PA, 1993.

31. ASTM Designation E264-92, "Standard Method for Measuring Fast-Neutron Reaction Rates by Radioactivation of Nickel", in ASTM Standards, Section 12, American Society for Testing and Materials, Philadelphia, PA, 1993.

32. ASTM Designation E481-92, "Standard Method for Measuring Neutron-Fluence Rate by Radioactivation of Cobalt and Silver", in ASTM Standards, Section 12, American Society for Testing and Materials, Philadelphia, PA, 1993.

33. ASTM Designation E523-87, "Standard Test Method for Measuring Fast-Neutron Reaction Rates by Radioactivation of Copper", in ASTM Standards, Section 12, American Society for Testing and Materials, Philadelphia, PA, 1993.

34. ASTM Designation E704-90, "Standard Test Method for Measuring Reaction Rates by Radioactivation of Uranium-238", in ASTM Standards, Section 12, American Society for Testing and Materials, Philadelphia, PA, 1993.

35. ASTM Designation E705-90, "Standard Test Method for Measuring Reaction Rates by Radioactivation of Neptunium-237", in ASTM Standards, Section 12, American Society for Testing and Materials, Philadelphia, PA, 1993.

36. ASTM Designation E1005-84, "Standard Test Method for Application and Analysis of Radiometric Monitors for Reactor Vessel Surveillance", in ASTM Standards, Section 12, American Society for Testing and Materials, Philadelphia, PA, 1993.

37. HEDL-TME 79-40, "FERRET Data Analysis Core", F. A. Schmittroth, Hanford Engineering Development Laboratory, Richland, WA, September 1979.

38. AFWL-TR-7-41, Vol. I-IV, "A Computer-Automated Iterative Method of Neutron Flux Spectra Determined by Foil Activation", W. N. McElroy, S. Berg and T. Crocket, Air Force Weapons Laboratory, Kirkland AFB, NM, July 1967.

39. RSIC Data Library Collection DLC-178, "SNLRML Recommended Dosimetry Cross-Section Compendium", July 1994.

40. EPRI-NP-2188, "Development and Demonstration of an Advanced Methodology for LWR Dosimetry Applications", R. E. Maerker, et al., 1981.

# APPENDIX A

# LOAD-TIME RECORDS FOR CHARPY IMPACT TESTS

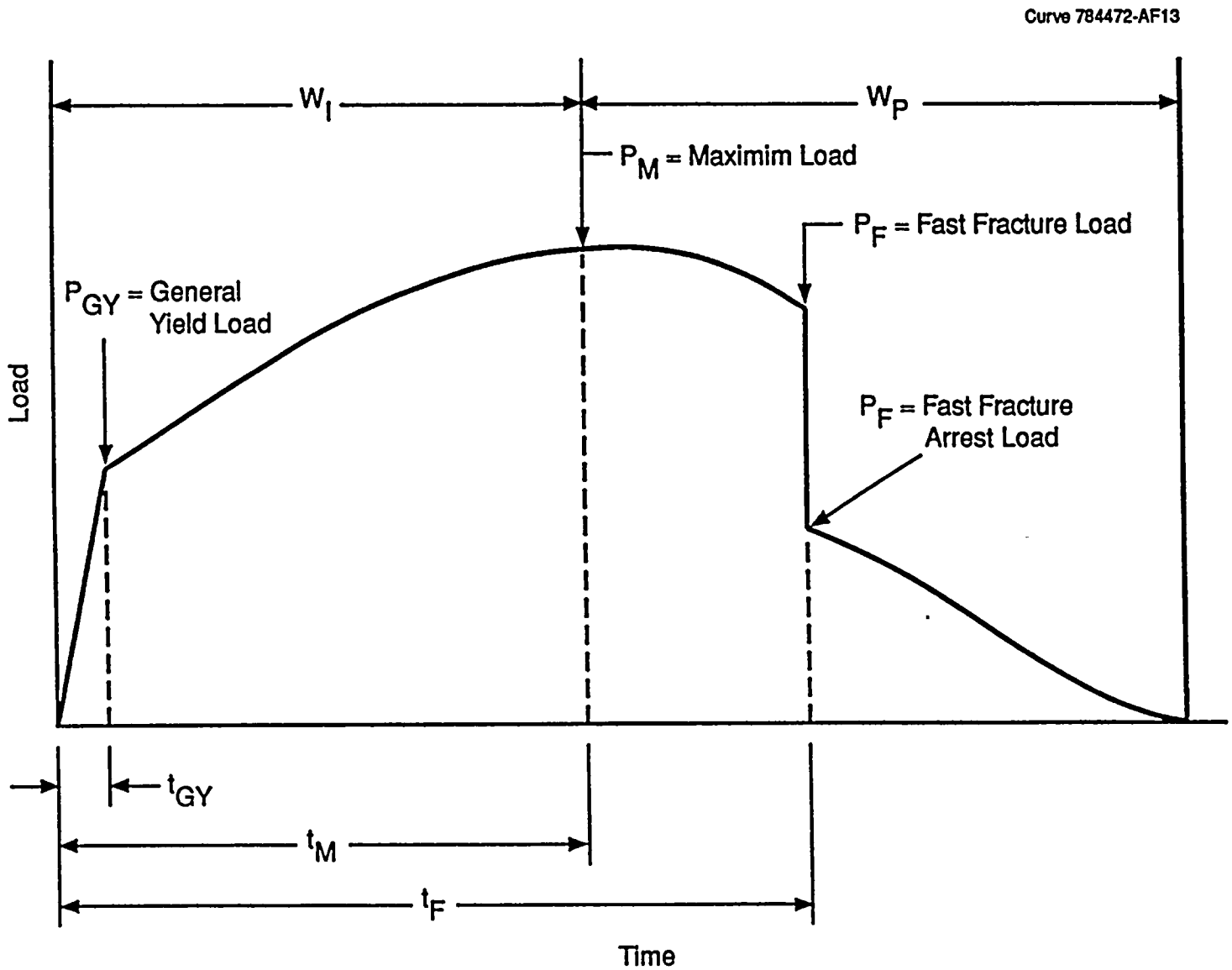


$W_I$ = Fracture Initiation Region
$W_P$ = Fracture Propagation Region

$t_{GY}$ = Time to General Yielding
$t_M$ = Time to Maximum Load
$t_F$ = Time to Fast (Brittle) Fracture Start

Fig. A-1-Idealized load-time record

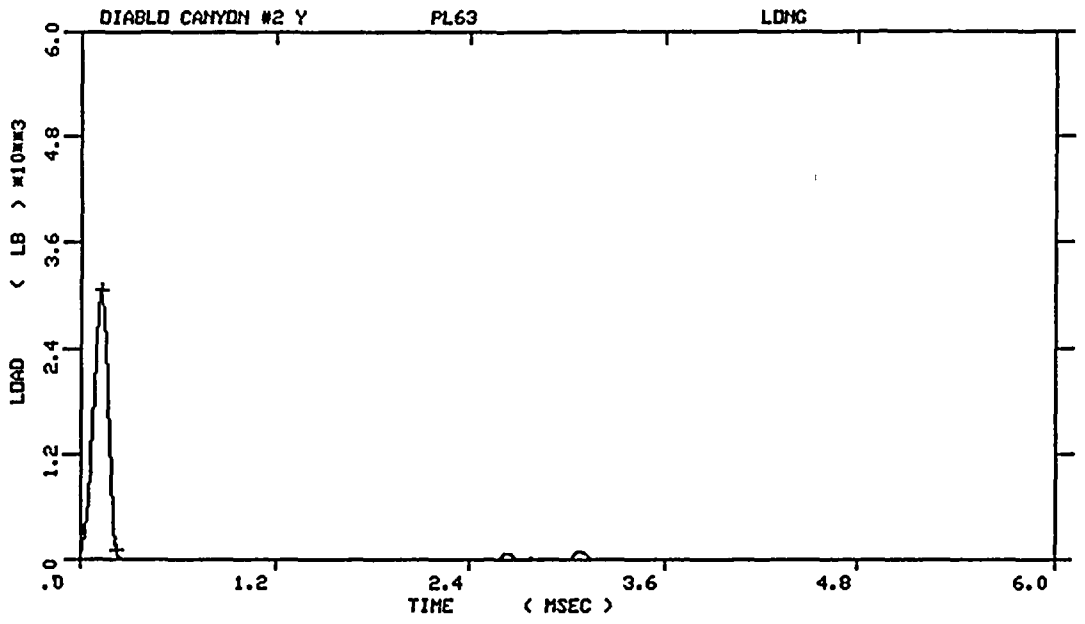


DIABLO CANYON #2 Y
SPECIMEN NUMBER :PL63
MATERIAL :LONG
CAPSULE :DIABLO CANYON
:#2 Y

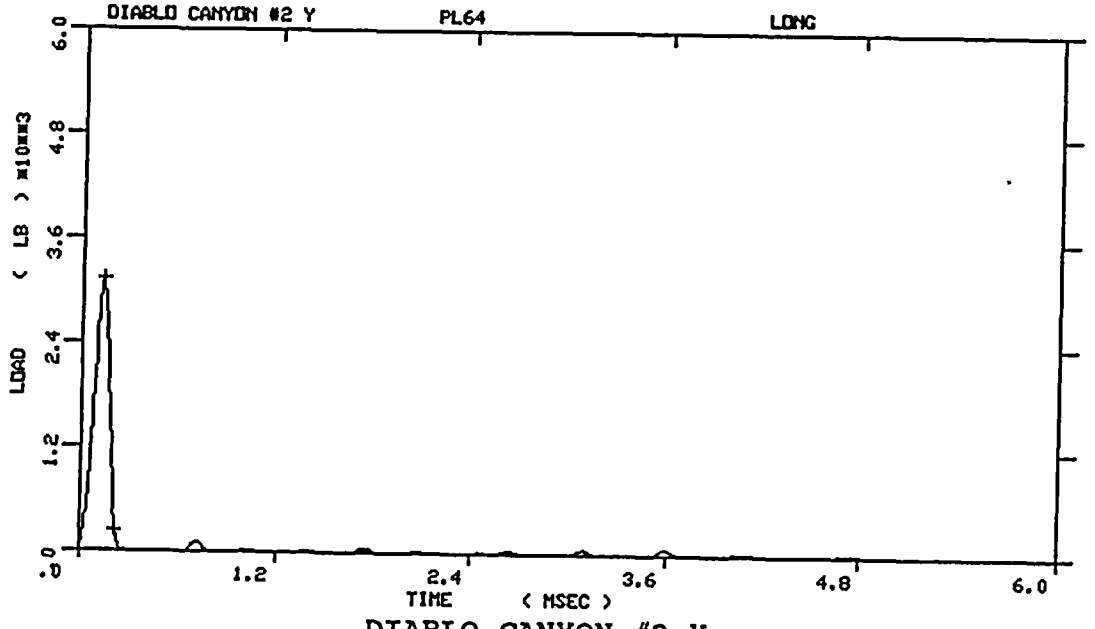


DIABLO CANYON #2 Y
SPECIMEN NUMBER :PL64
MATERIAL :LONG
CAPSULE :DIABLO CANYON
:#2 Y

Figure A-2. Load-time records for Specimens PL63 and PL64.

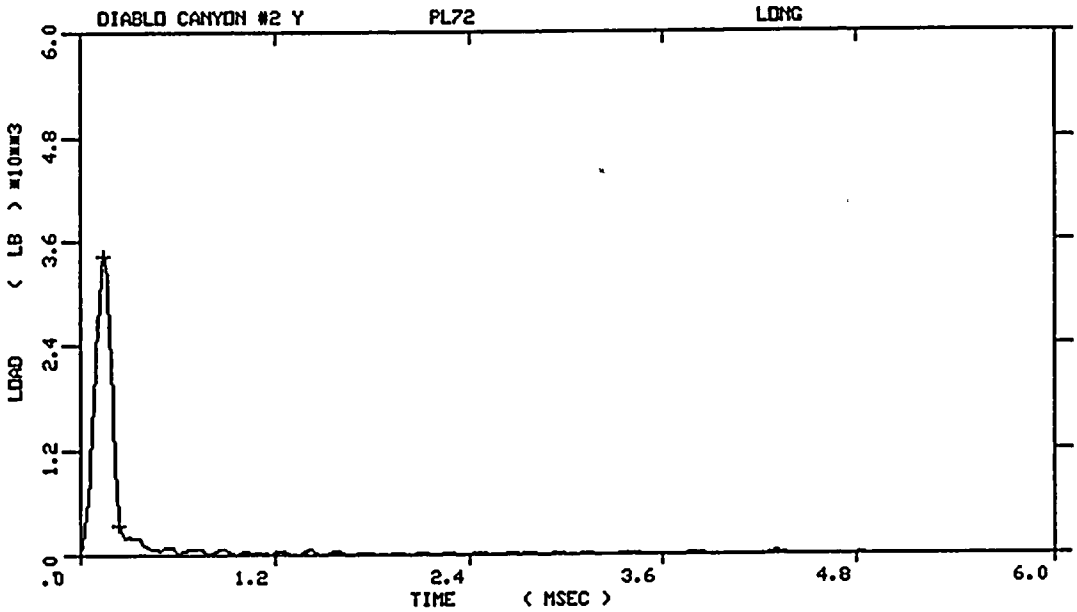


DIABLO CANYON #2 Y
SPECIMEN NUMBER :PL72
MATERIAL :LONG
CAPSULE :DIABLO CANYON
:#2 Y

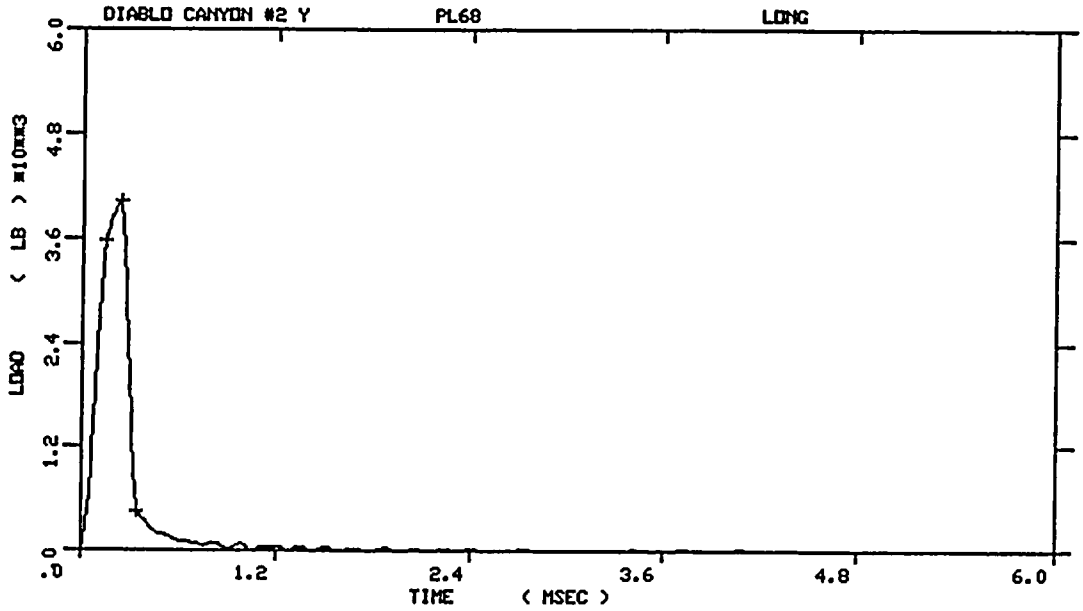


DIABLO CANYON #2 Y
SPECIMEN NUMBER :PL68
MATERIAL :LONG
CAPSULE :DIABLO CANYON
:#2 Y

Figure A-3. Load-time records for Specimens PL72 and PL68.

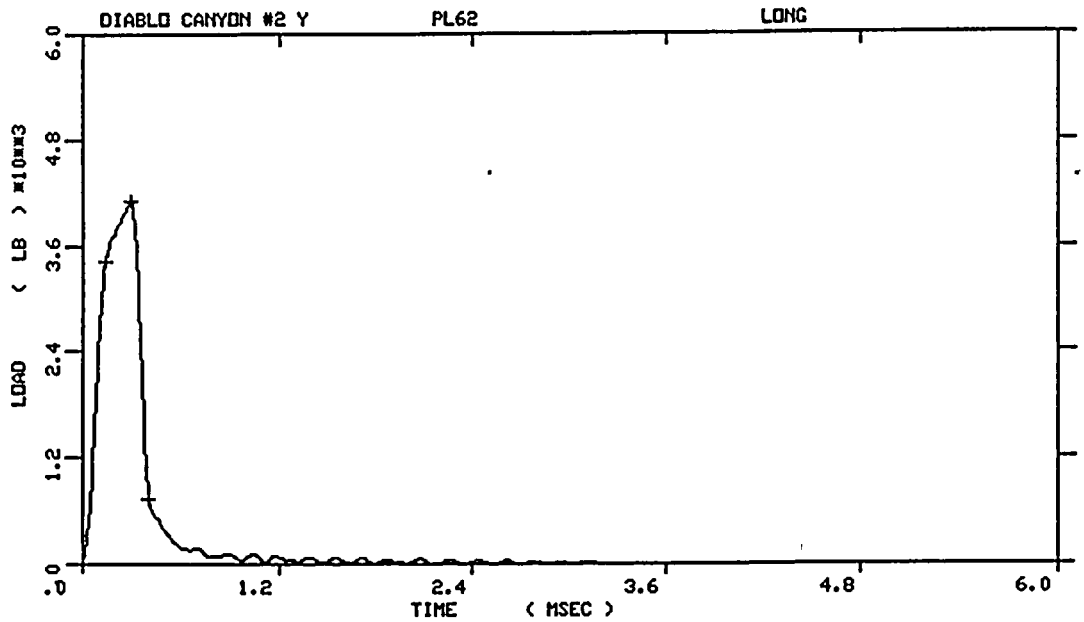


DIABLO CANYON #2 Y
SPECIMEN NUMBER :PL62
MATERIAL :LONG
CAPSULE :DIABLO CANYON
:#2 Y

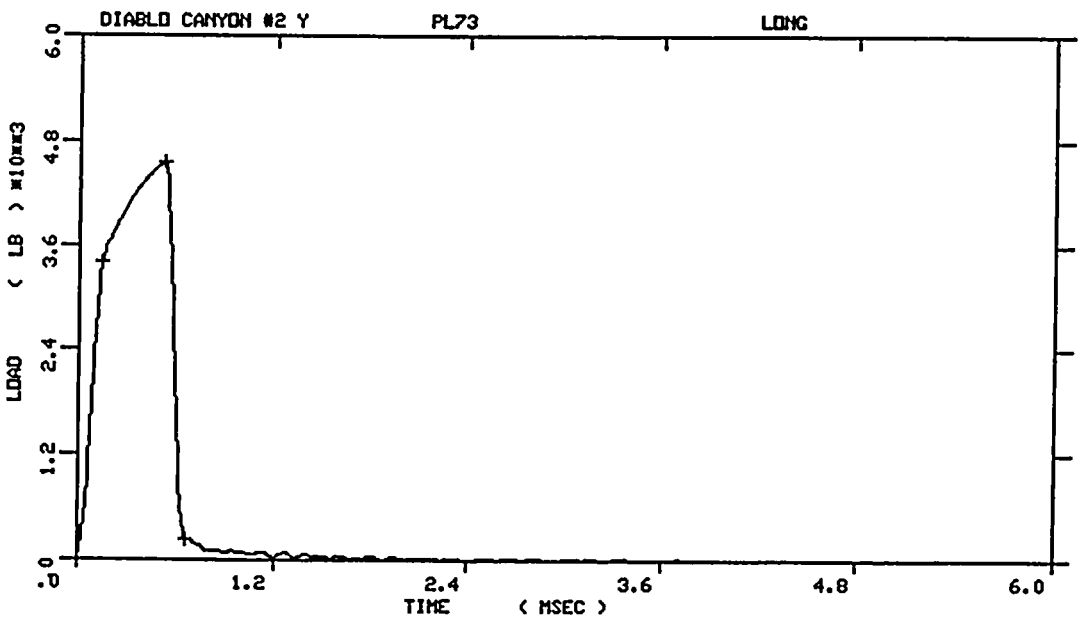


DIABLO CANYON #2 Y
SPECIMEN NUMBER :PL73
MATERIAL :LONG
CAPSULE :DIABLO CANYON
:#2 Y

Figure A-4. Load-time records for Specimens PL62 and PL73.

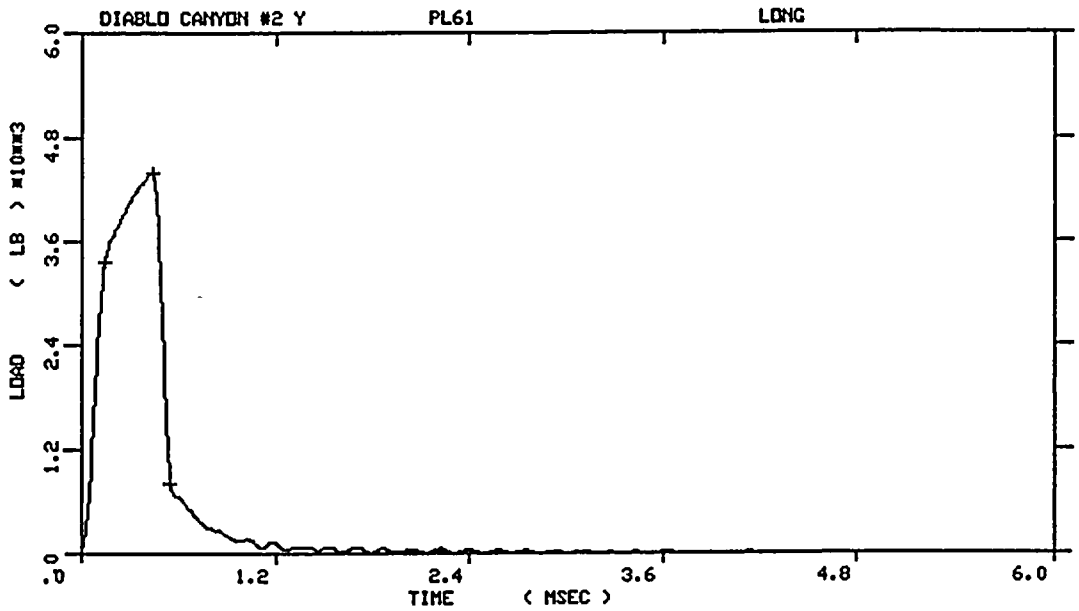


DIABLO CANYON #2 Y
SPECIMEN NUMBER :PL61
MATERIAL :LONG
CAPSULE :DIABLO CANYON
:#2 Y

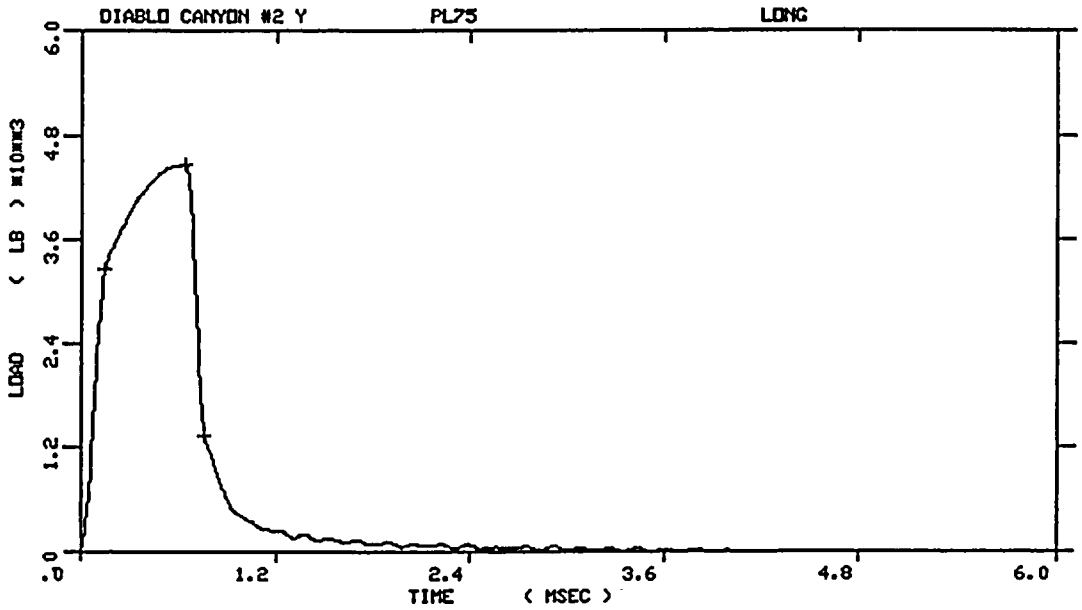


DIABLO CANYON #2 Y
SPECIMEN NUMBER :PL75
MATERIAL :LONG
CAPSULE :DIABLO CANYON
:#2 Y

Figure A-5. Load-time records for Specimens PL61 and PL75.

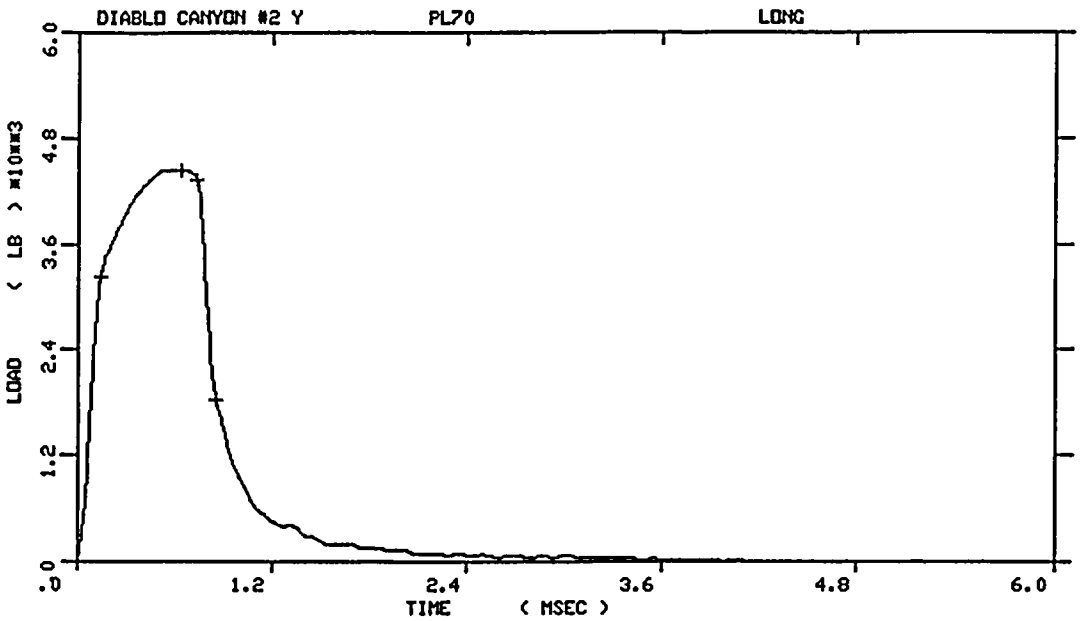


DIABLO CANYON #2 Y
SPECIMEN NUMBER :PL70
MATERIAL :LONG
CAPSULE :DIABLO CANYON
:#2 Y

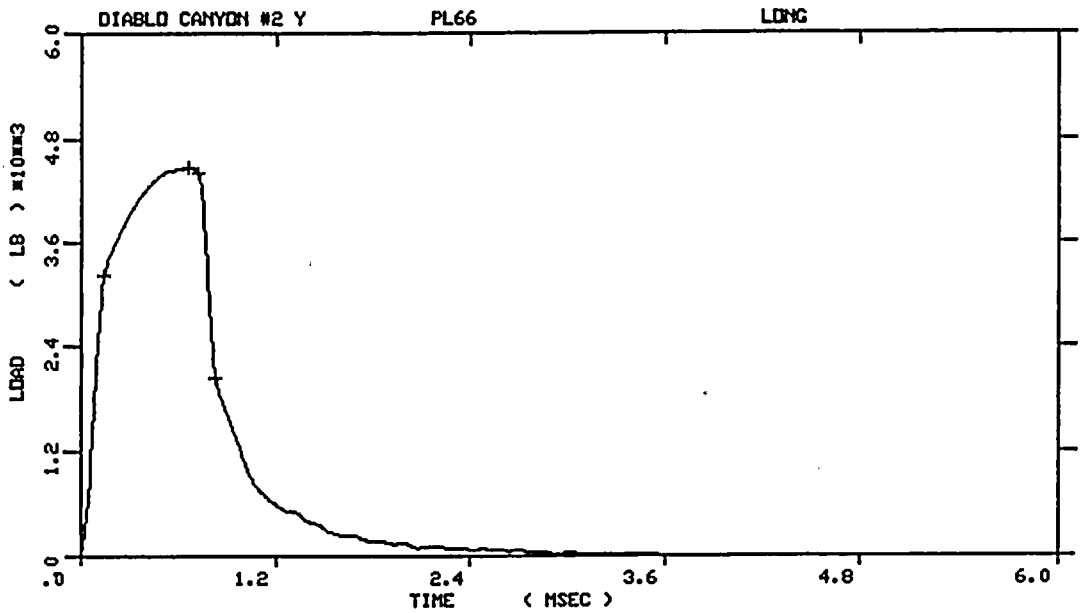


DIABLO CANYON #2 Y
SPECIMEN NUMBER :PL66
MATERIAL :LONG
CAPSULE :DIABLO CANYON
:#2 Y

Figure A-6. Load-time records for Specimens PL70 and PL66.

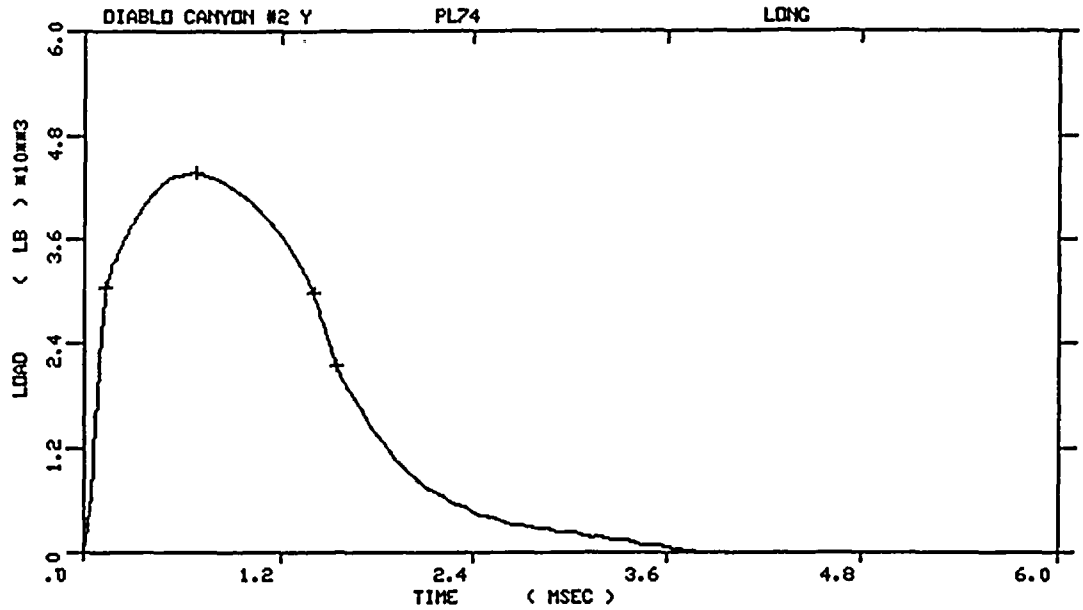


DIABLO CANYON #2 Y
SPECIMEN NUMBER :PL74
MATERIAL :LONG
CAPSULE :DIABLO CANYON
:#2 Y

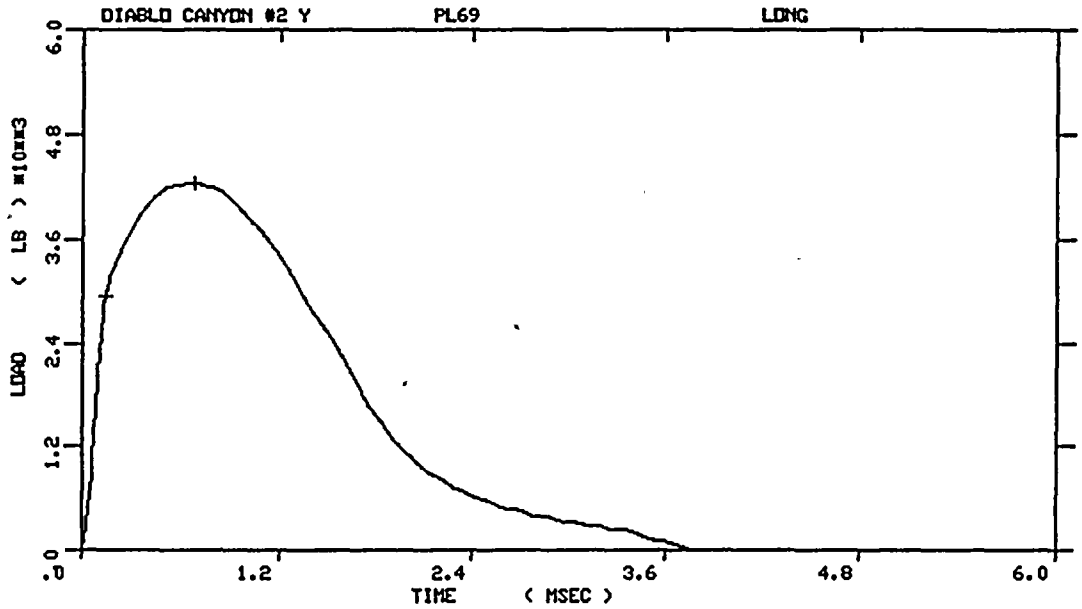


DIABLO CANYON #2 Y
SPECIMEN NUMBER :PL69
MATERIAL :LONG
CAPSULE :DIABLO CANYON
:#2 Y

Figure A-7. Load-time records for Specimens PL74 and PL69.

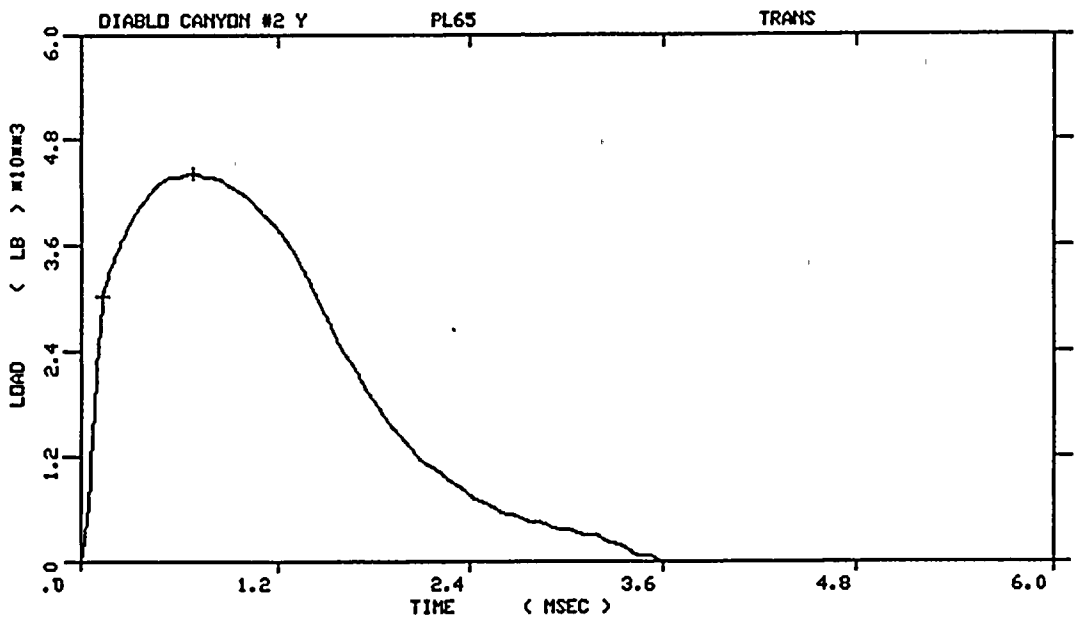


DIABLO CANYON #2 Y
SPECIMEN NUMBER :PL65
MATERIAL :LONG
CAPSULE :DIABLO CANYON
:#2 Y

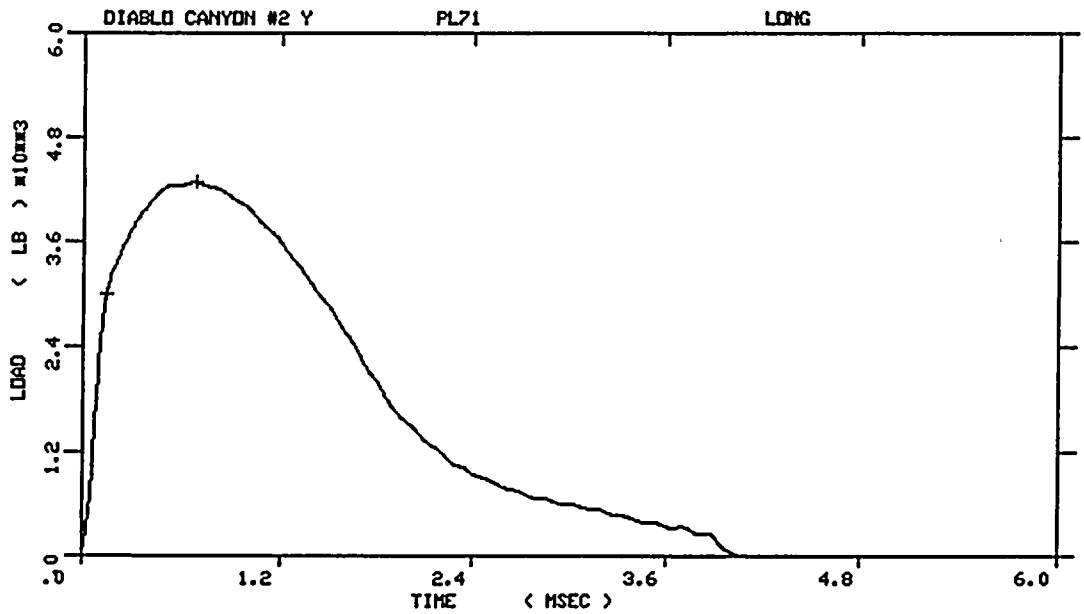


DIABLO CANYON #2 Y
SPECIMEN NUMBER :PL71
MATERIAL :LONG
CAPSULE :DIABLO CANYON
:#2 Y

Figure A-8. Load-time records for Specimens PL65 and PL71.

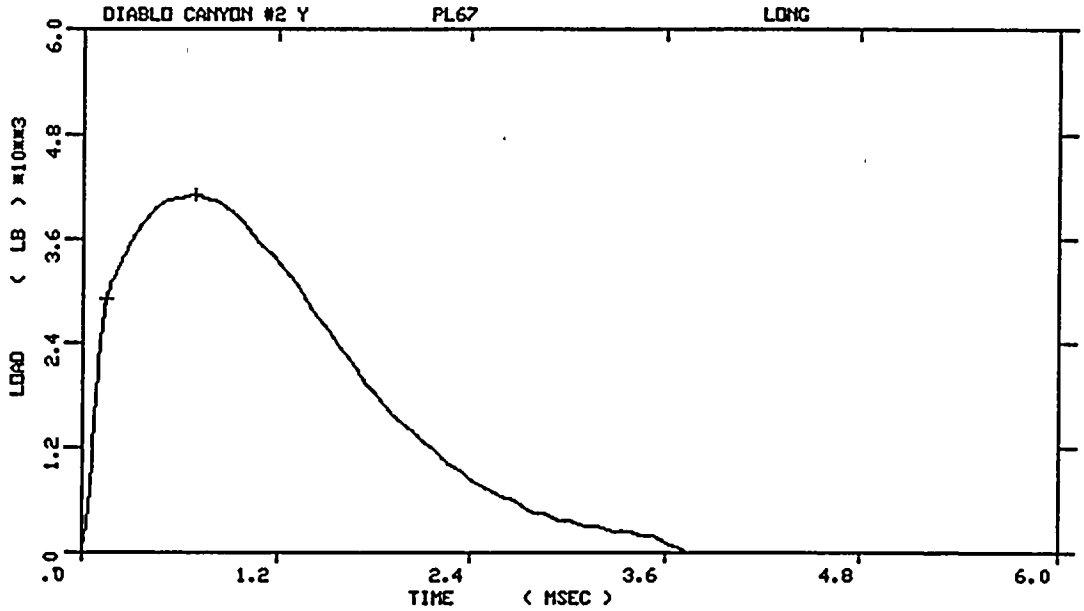


DIABLO CANYON #2 Y
SPECIMEN NUMBER :PL67
MATERIAL :LONG
CAPSULE :DIABLO CANYON
:#2 Y

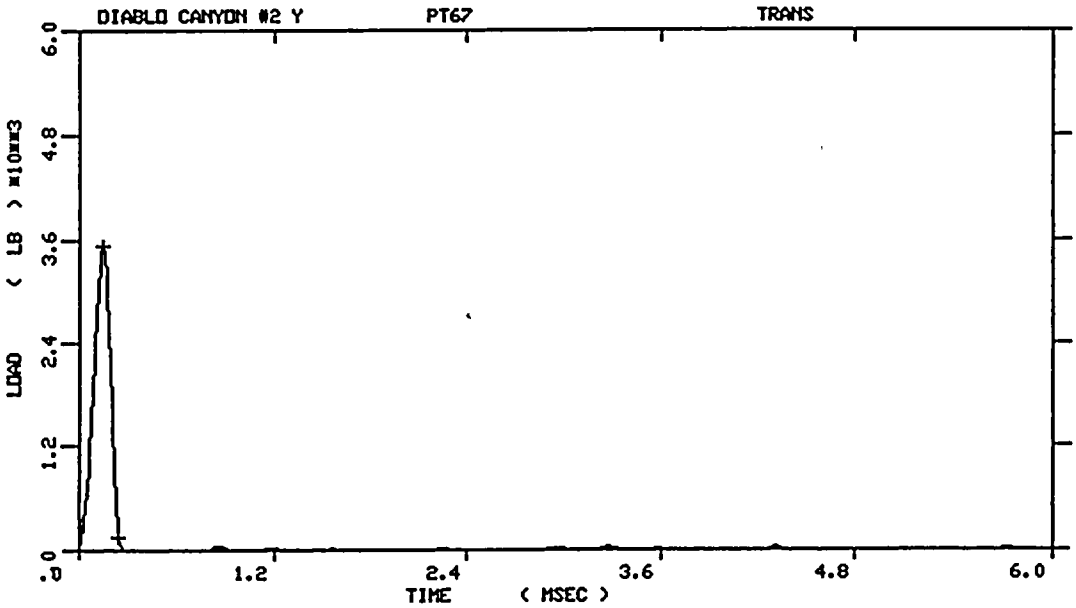


DIABLO CANYON #2 Y
SPECIMEN NUMBER :PT67
MATERIAL :TRANS
CAPSULE :DIABLO CANYON
:#2 Y

Figure A-9. Load-time records for Specimens PL67 and PT67.

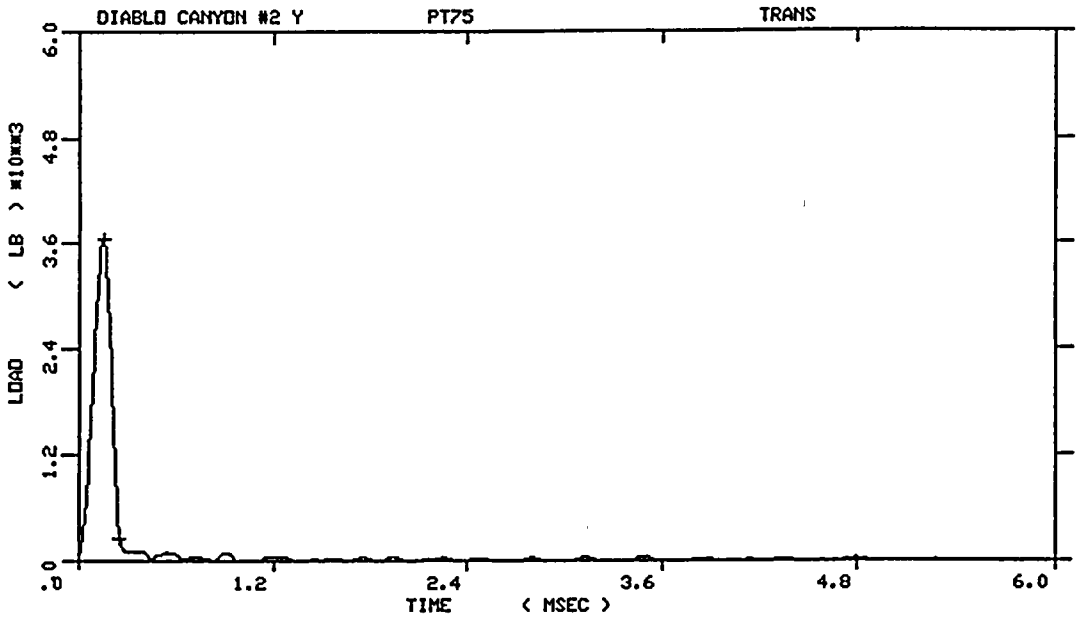


DIABLO CANYON #2 Y
SPECIMEN NUMBER :PT75
MATERIAL :TRANS
CAPSULE :DIABLO CANYON
:#2 Y

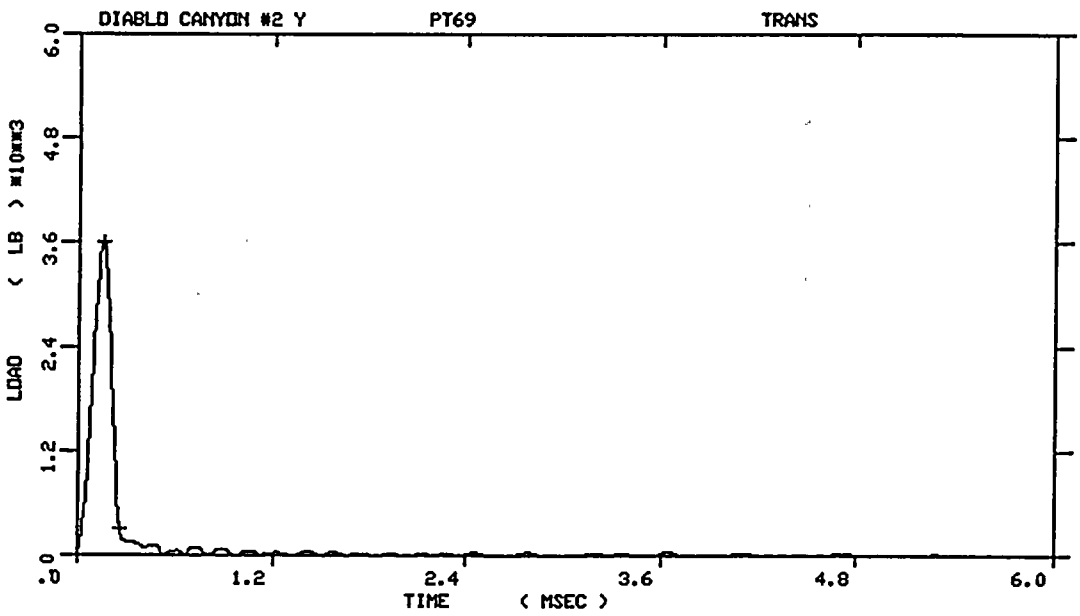


DIABLO CANYON #2 Y
SPECIMEN NUMBER :PT69
MATERIAL :TRANS
CAPSULE :DIABLO CANYON
:#2 Y

Figure A-10. Load-time records for Specimens PT75 and PT69.

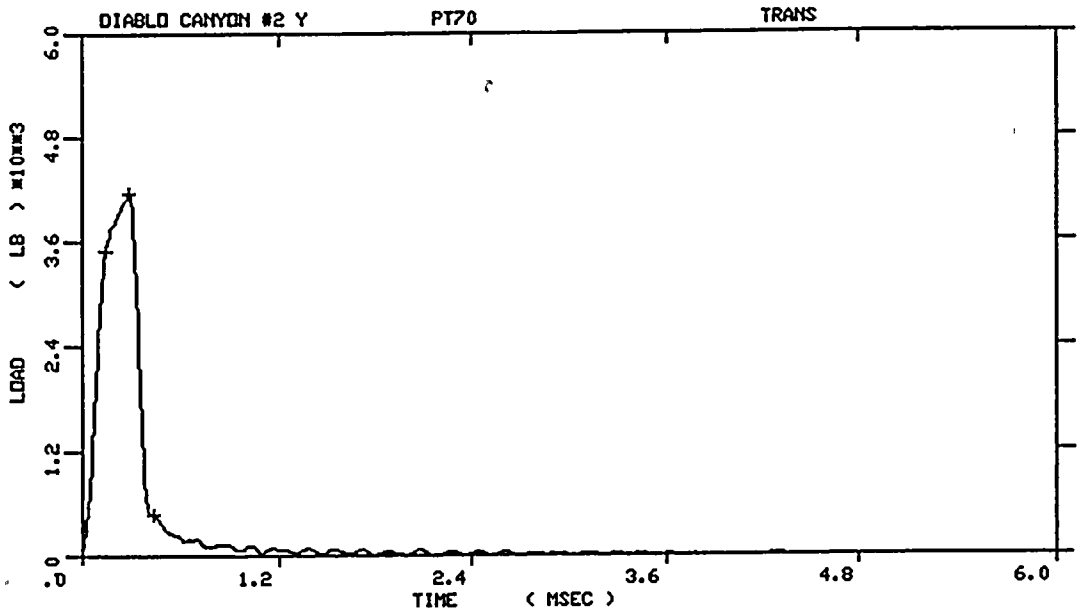


DIABLO CANYON #2 Y
SPECIMEN NUMBER :PT70
MATERIAL :TRANS
CAPSULE :DIABLO CANYON
:#2 Y

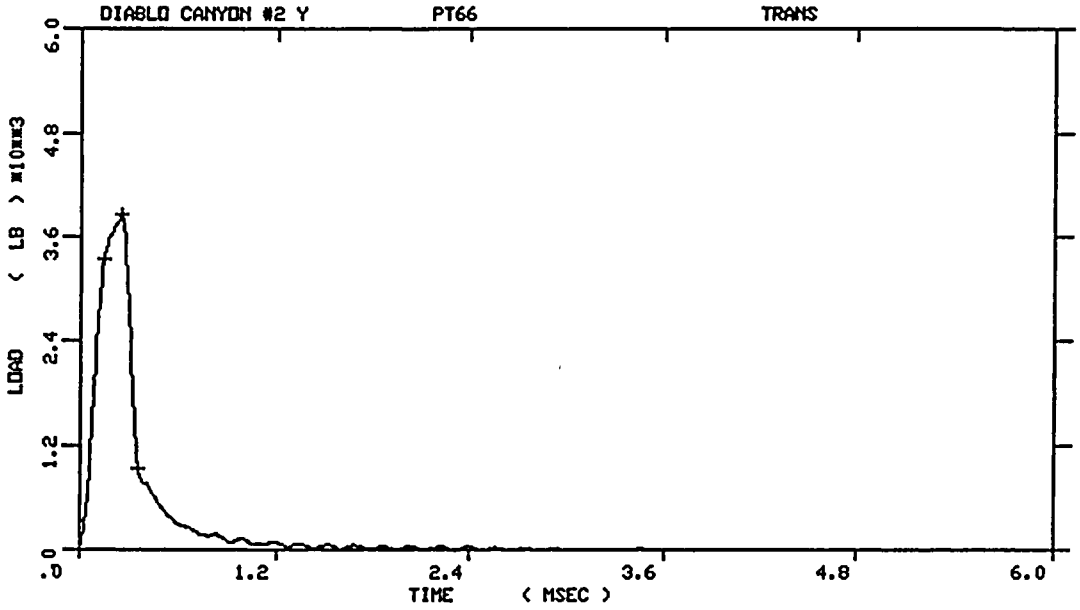


DIABLO CANYON #2 Y
SPECIMEN NUMBER :PT66
MATERIAL :TRANS
CAPSULE :DIABLO CANYON
:#2 Y

Figure A-11. Load-time records for Specimens PT70 and PT66.

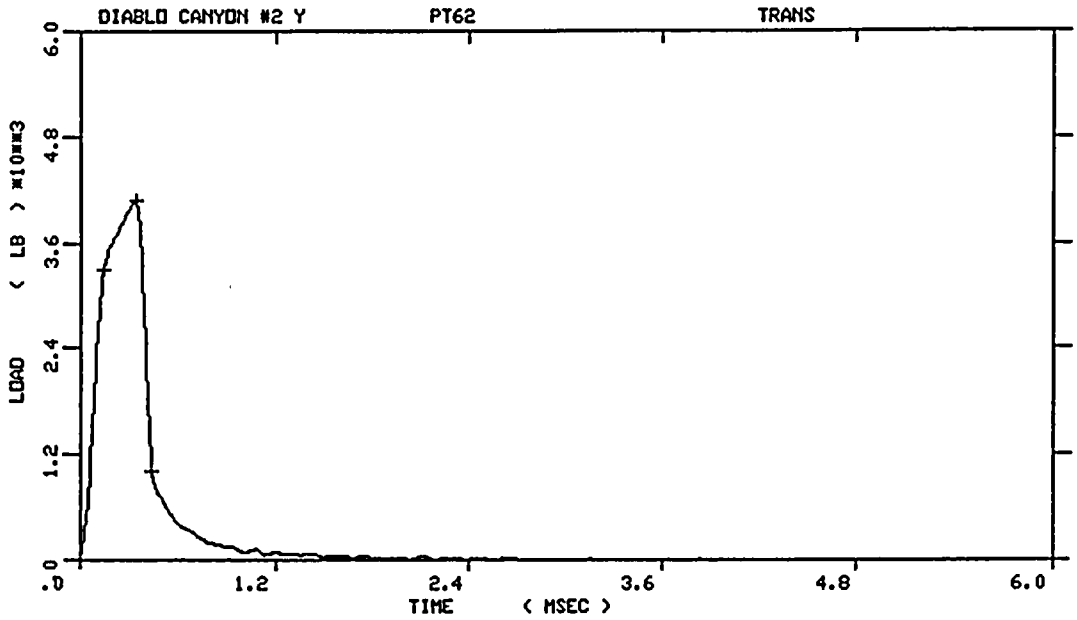


DIABLO CANYON #2 Y
SPECIMEN NUMBER :PT62
MATERIAL :TRANS
CAPSULE :DIABLO CANYON
:#2 Y

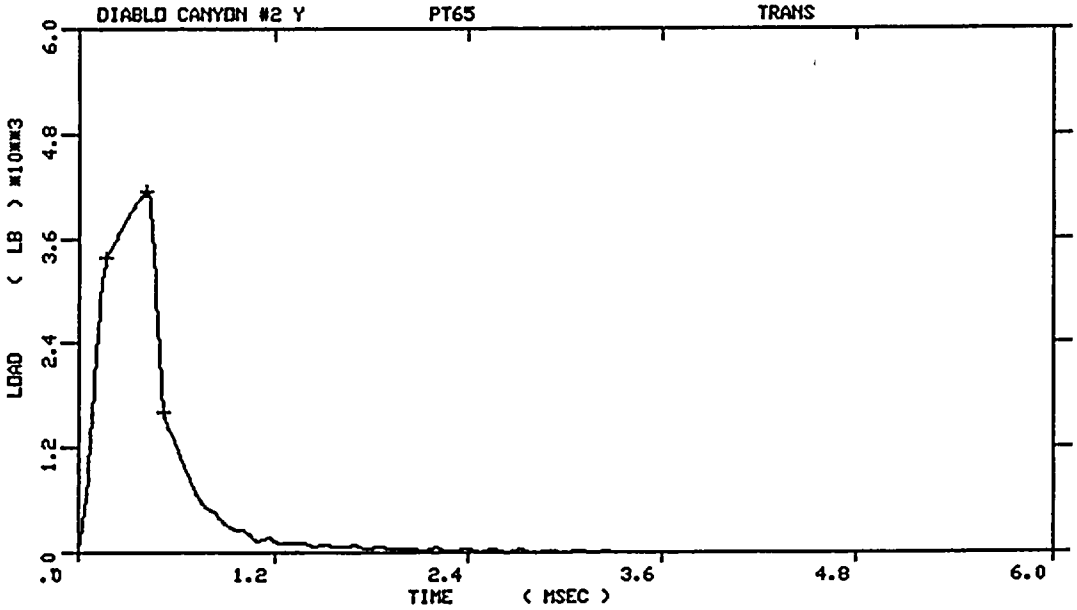


DIABLO CANYON #2 Y
SPECIMEN NUMBER :PT65
MATERIAL :TRANS
CAPSULE :DIABLO CANYON
:#2 Y

Figure A-12. Load-time records for Specimens PT62 and PT65.

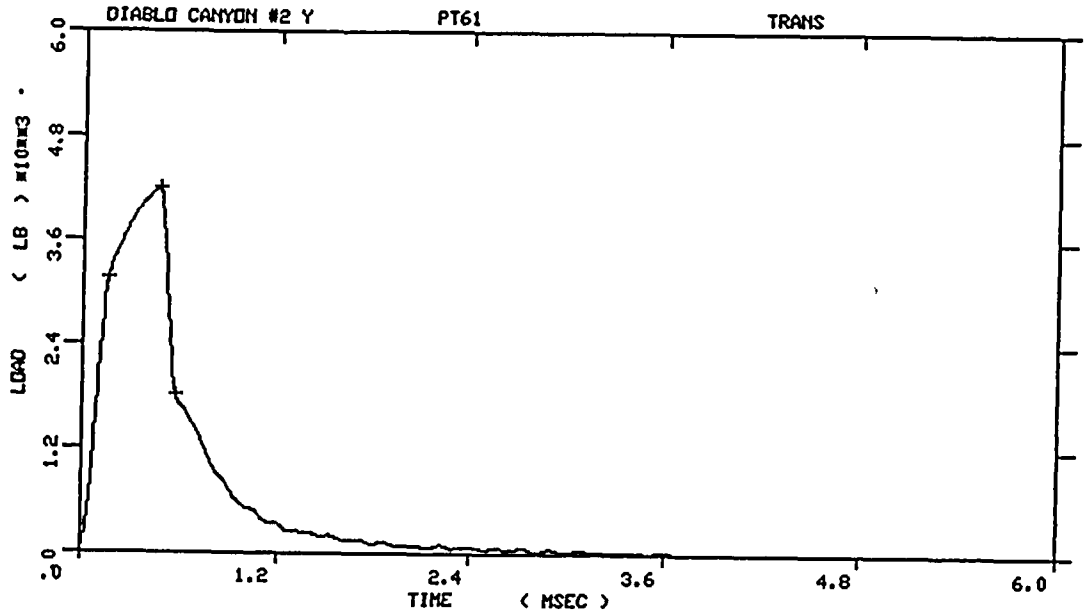


DIABLO CANYON #2 Y
SPECIMEN NUMBER :PT61
MATERIAL :TRANS
CAPSULE :DIABLO CANYON
:#2 Y

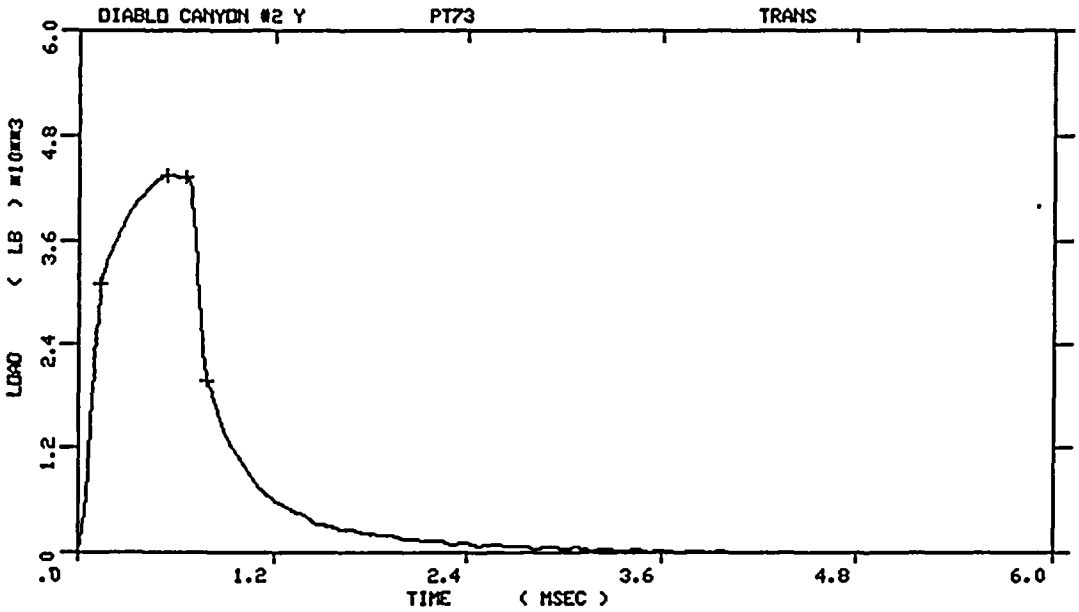


DIABLO CANYON #2 Y
SPECIMEN NUMBER :PT73
MATERIAL :TRANS
CAPSULE :DIABLO CANYON
:#2 Y

Figure A-13. Load-time records for Specimens PT61 and PT73.

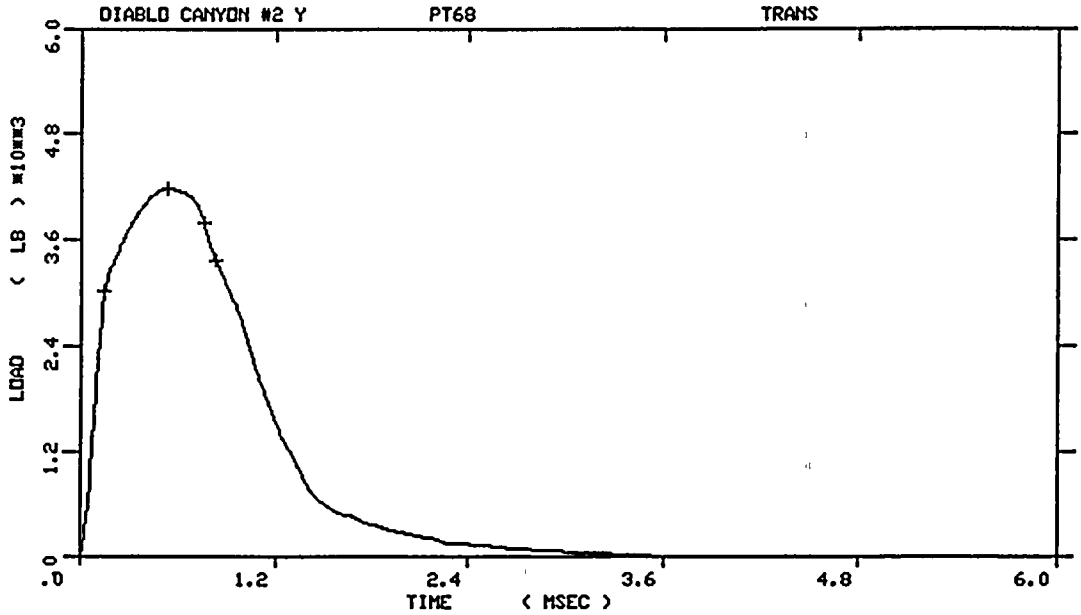


DIABLO CANYON #2 Y
SPECIMEN NUMBER :PT68
MATERIAL :TRANS
CAPSULE :DIABLO CANYON
:#2 Y

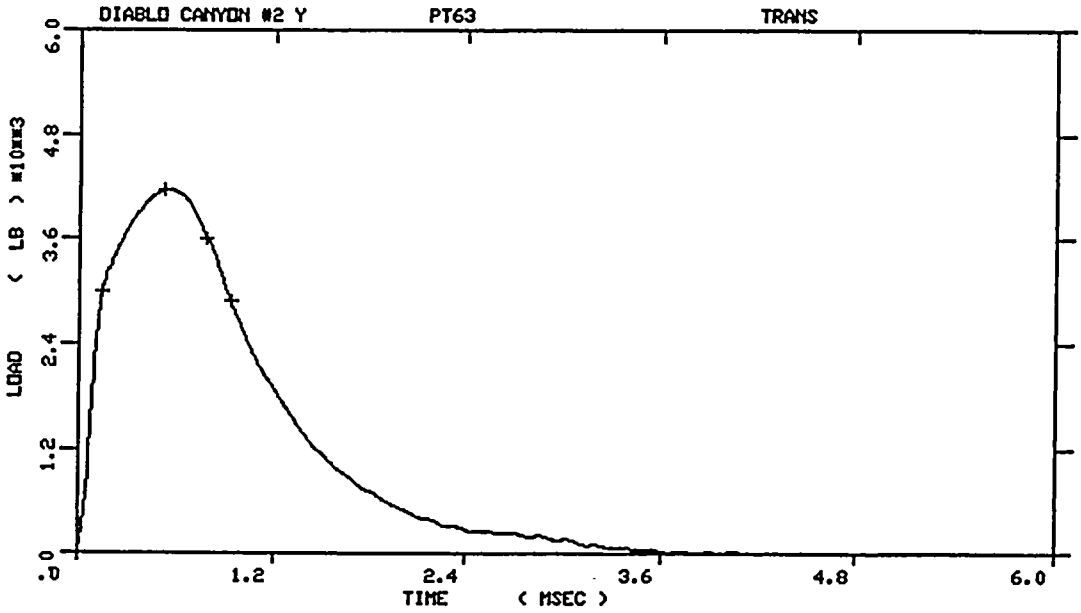


DIABLO CANYON #2 Y
SPECIMEN NUMBER :PT63
MATERIAL :TRANS
CAPSULE :DIABLO CANYON
:#2 Y

Figure A-14. Load-time records for Specimens PT68 and PT63.

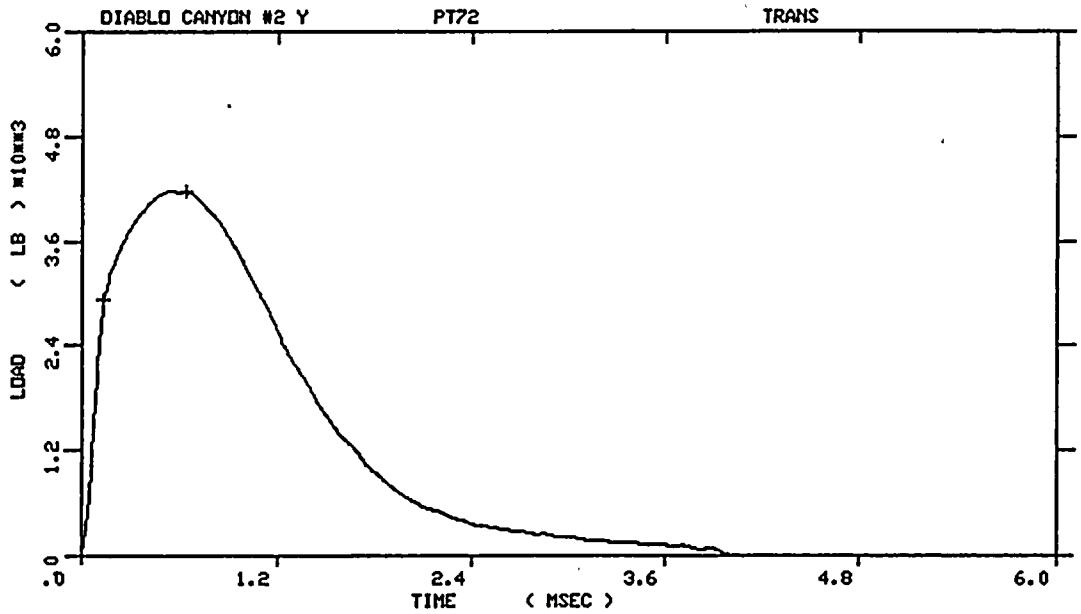


DIABLO CANYON #2 Y
SPECIMEN NUMBER :PT72
MATERIAL :TRANS
CAPSULE :DIABLO CANYON
:#2 Y

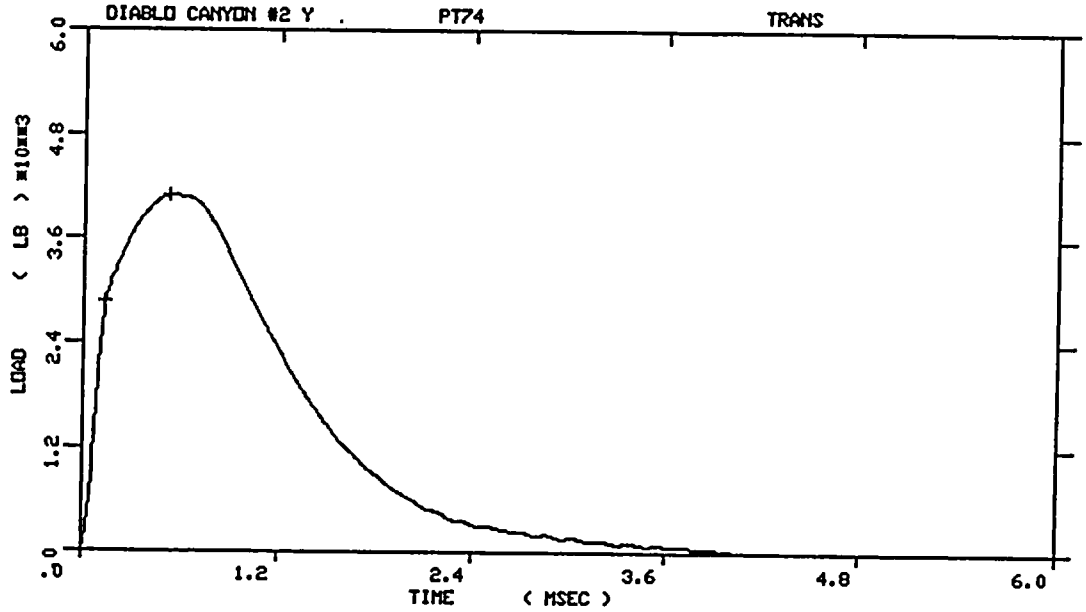


DIABLO CANYON #2 Y
SPECIMEN NUMBER :PT74
MATERIAL :TRANS
CAPSULE :DIABLO CANYON
:#2 Y

Figure A-15. Load-time records for Specimens PT72 and PT74.

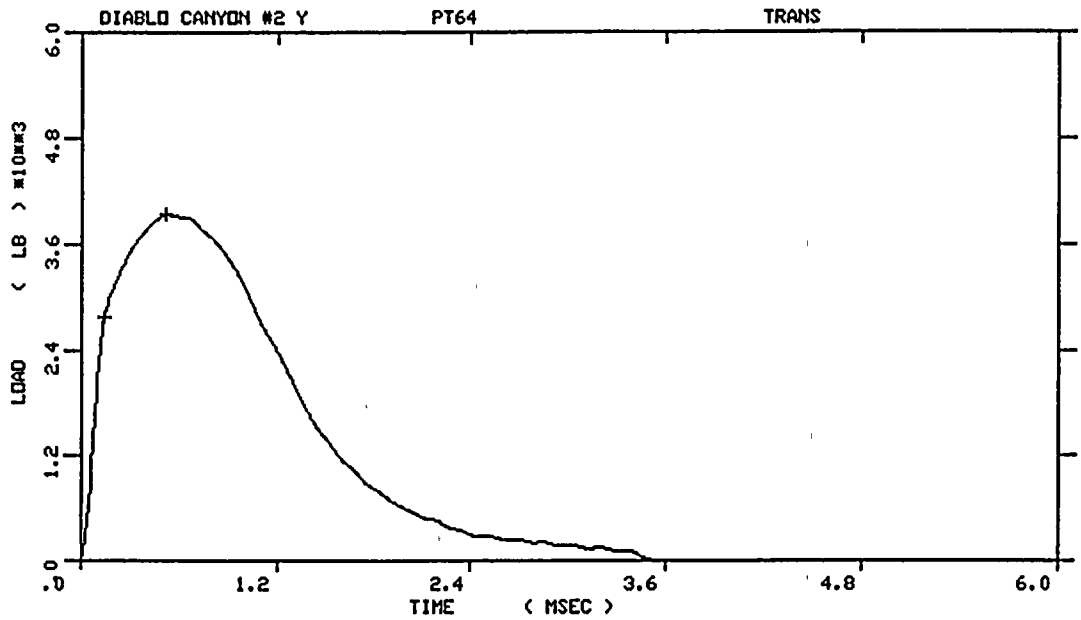


DIABLO CANYON #2 Y
SPECIMEN NUMBER :PT64
MATERIAL :TRANS
CAPSULE :DIABLO CANYON
:#2 Y

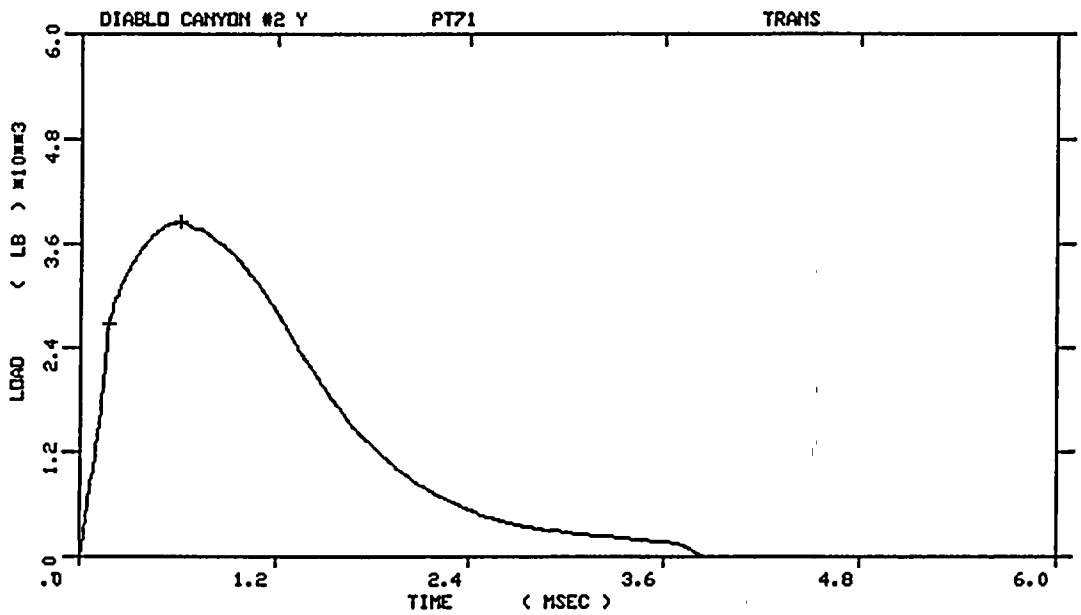


DIABLO CANYON #2 Y
SPECIMEN NUMBER :PT71
MATERIAL :TRANS
CAPSULE :DIABLO CANYON
:#2 Y

Figure A-16. Load-time records for Specimens PT64 and PT71.

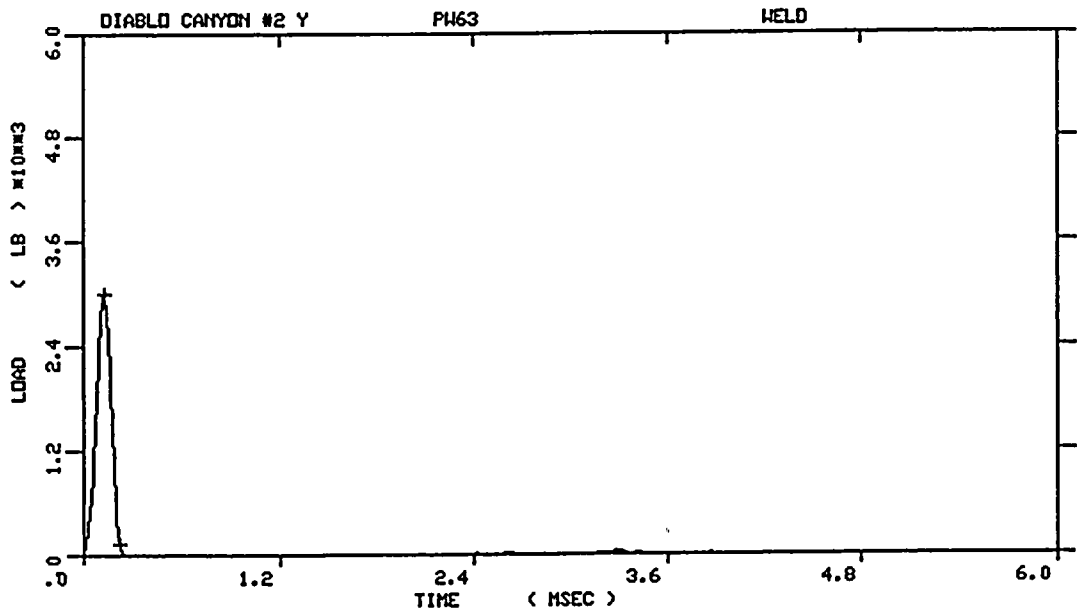


DIABLO CANYON #2 Y
SPECIMEN NUMBER :PW63
MATERIAL :WELD
CAPSULE :DIABLO CANYON
:#2 Y

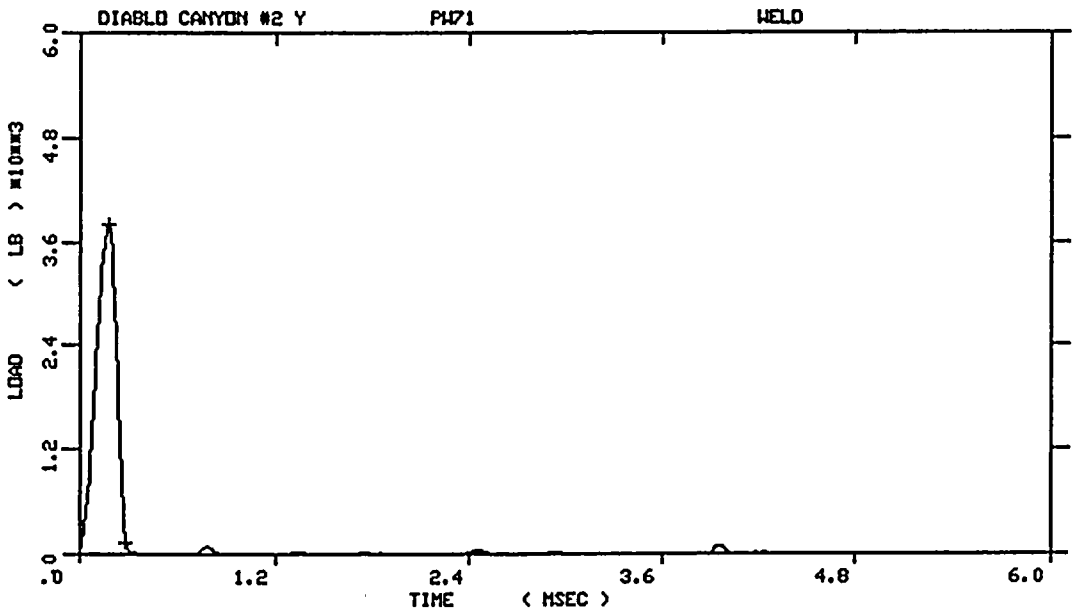


DIABLO CANYON #2 Y
SPECIMEN NUMBER :PW71
MATERIAL :WELD
CAPSULE :DIABLO CANYON
:#2 Y

Figure A-17. Load-time records for Specimens PW63 and PW71.

Specimen Alignment Error - Test Data Invalid.

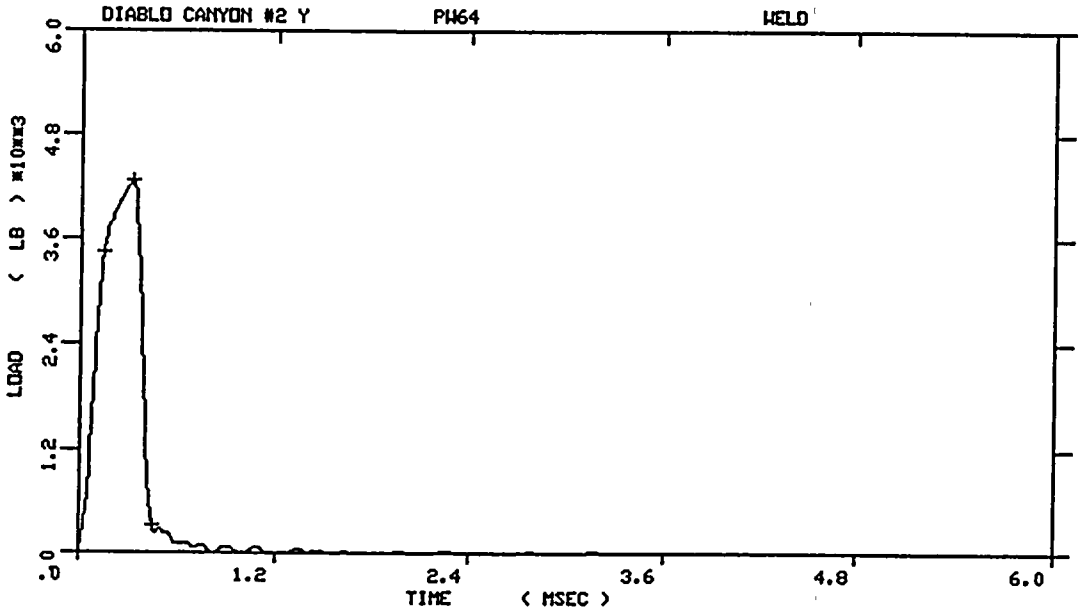


DIABLO CANYON #2 Y
SPECIMEN NUMBER :PW64
MATERIAL :WELD
CAPSULE :DIABLO CANYON
:#2 Y

Figure A-18. Load-time records for Specimens PW72 and PW64.

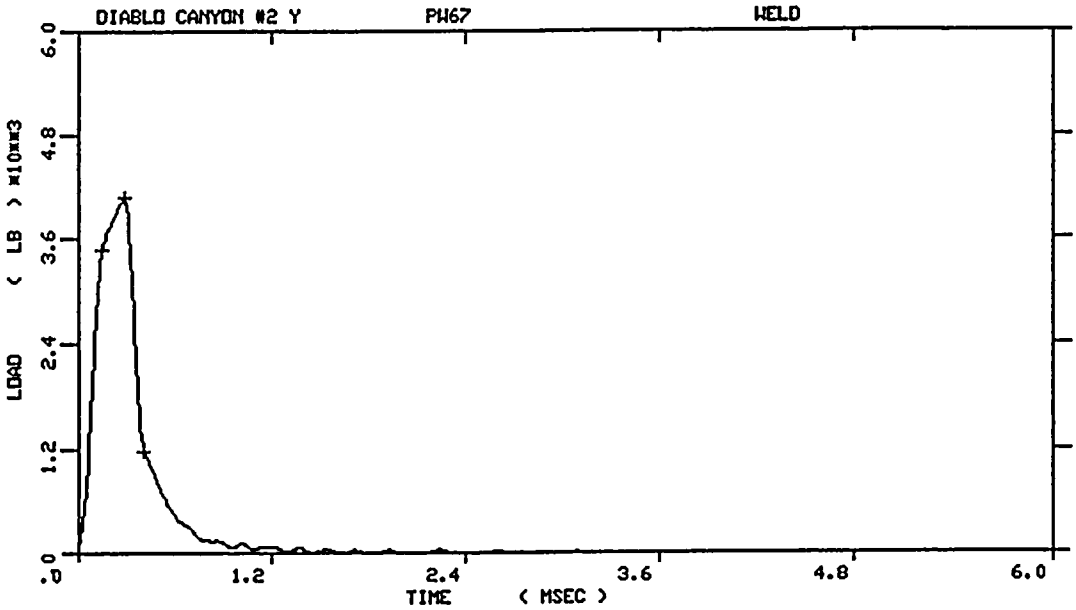


DIABLO CANYON #2 Y
SPECIMEN NUMBER :PW67
MATERIAL :WELD
CAPSULE :DIABLO CANYON
:#2 Y

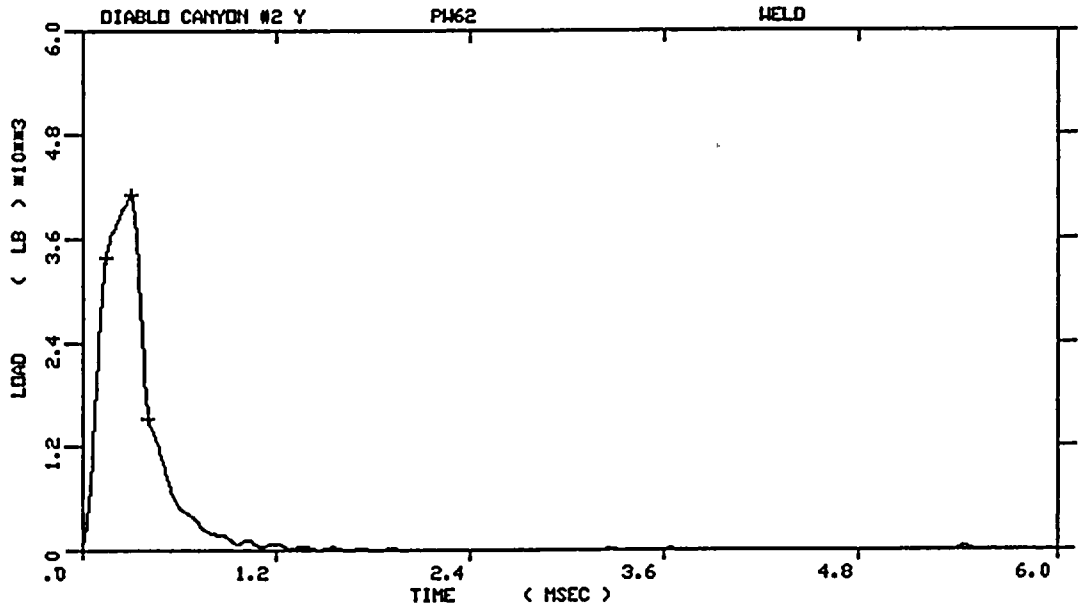


DIABLO CANYON #2 Y
SPECIMEN NUMBER :PW62
MATERIAL :WELD
CAPSULE :DIABLO CANYON
:#2 Y

Figure A-19. Load-time records for Specimens PW67 and PW62.

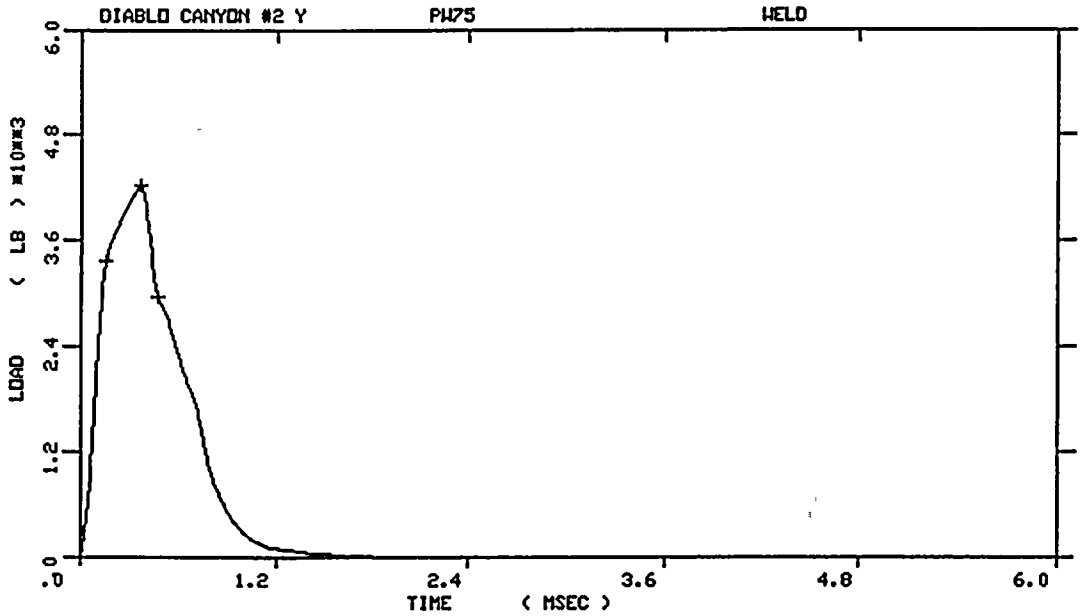


DIABLO CANYON #2 Y
SPECIMEN NUMBER :PW75
MATERIAL :WELD
CAPSULE :DIABLO CANYON
:#2 Y

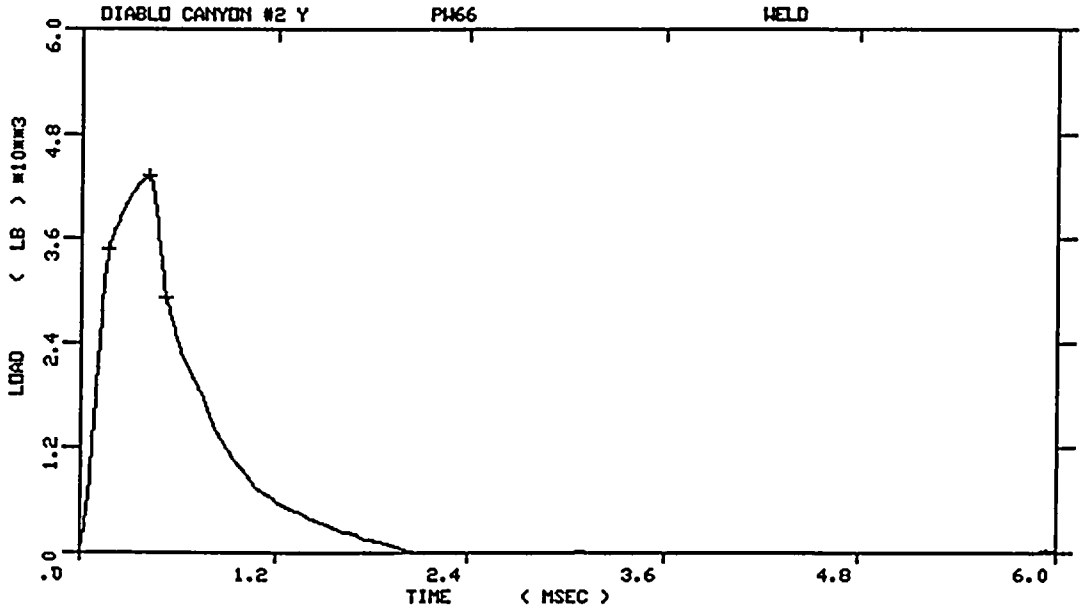


DIABLO CANYON #2 Y
SPECIMEN NUMBER :PW66
MATERIAL :WELD
CAPSULE :DIABLO CANYON
:#2 Y

Figure A-20. Load-time records for Specimens PW75 and PW66.

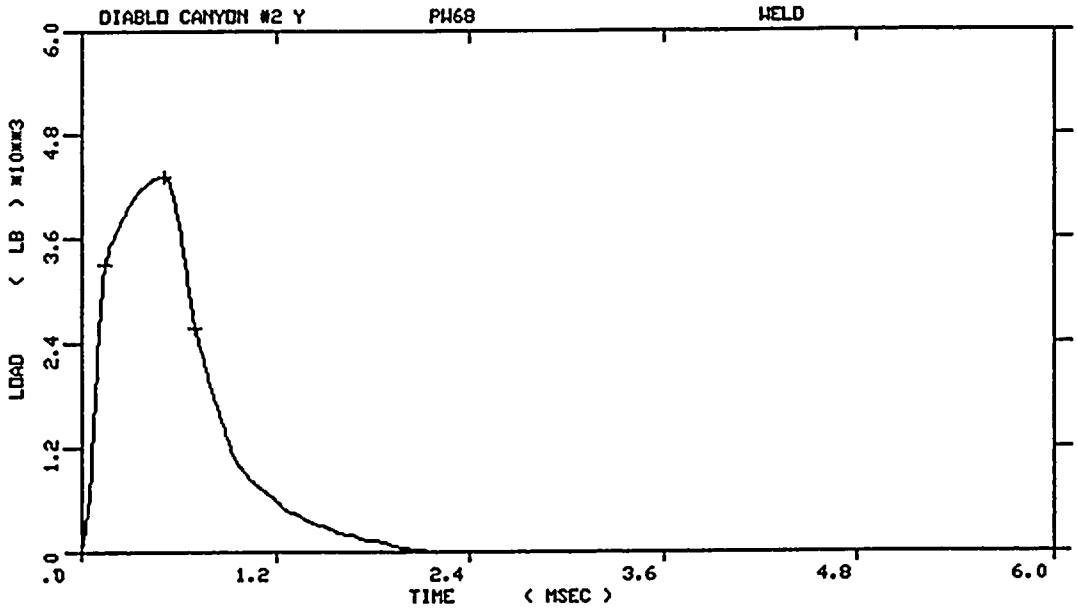


DIABLO CANYON #2 Y
SPECIMEN NUMBER :PW68
MATERIAL :WELD
CAPSULE :DIABLO CANYON
:#2 Y

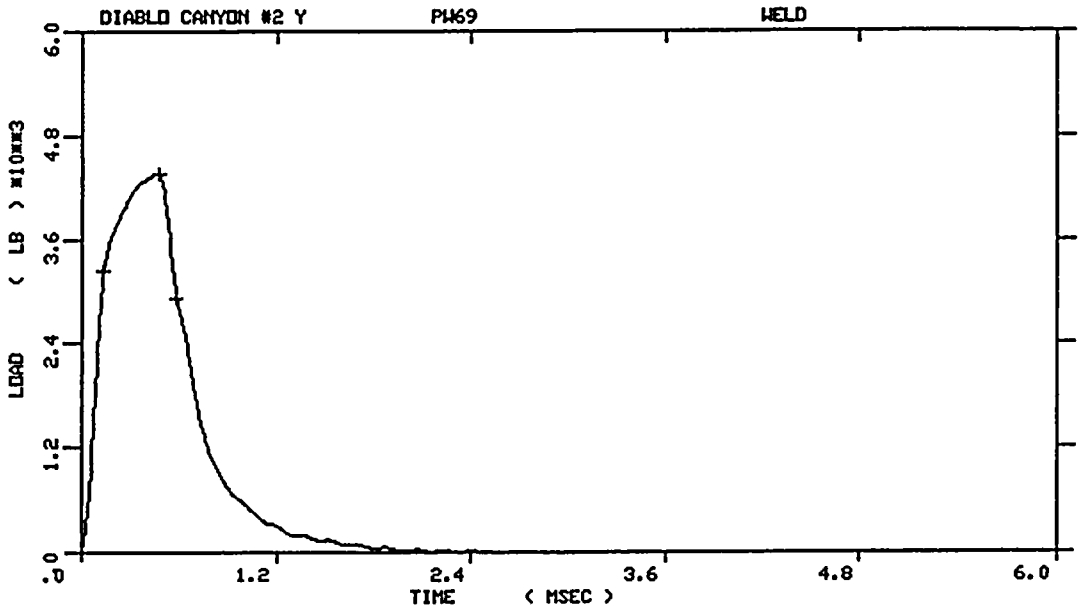


DIABLO CANYON #2 Y
SPECIMEN NUMBER :PW69
MATERIAL :WELD
CAPSULE :DIABLO CANYON
:#2 Y

Figure A-21. Load-time records for Specimens PW68 and PW69.

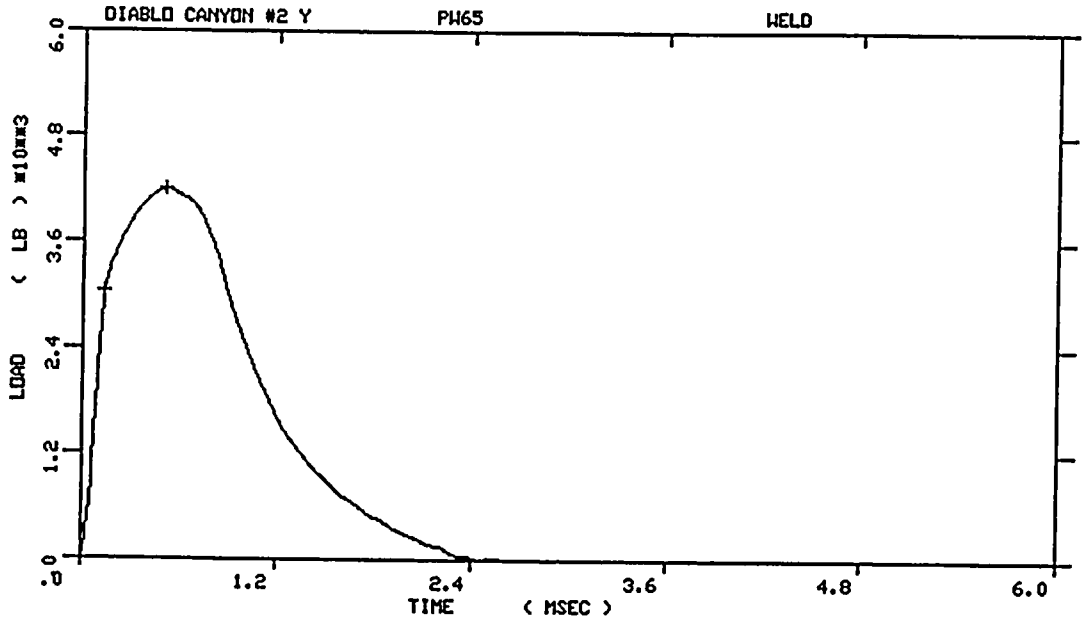


DIABLO CANYON #2 Y
SPECIMEN NUMBER :PW65
MATERIAL :WELD
CAPSULE :DIABLO CANYON
:#2 Y

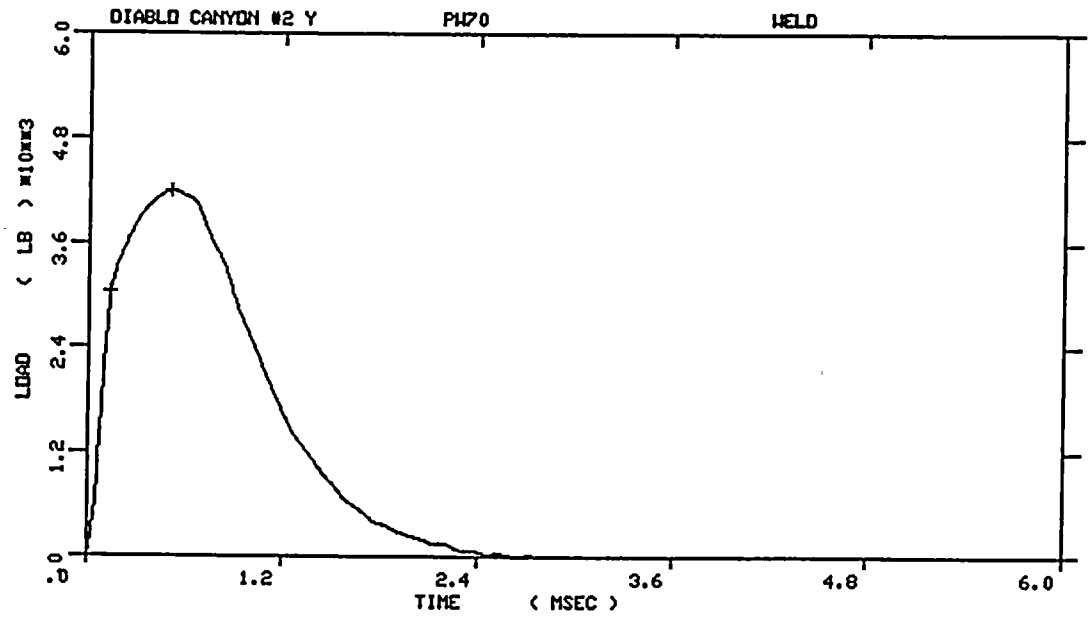


DIABLO CANYON #2 Y
SPECIMEN NUMBER :PW70
MATERIAL :WELD
CAPSULE :DIABLO CANYON
:#2 Y

Figure A-22. Load-time records for Specimens PW65 and PW70.

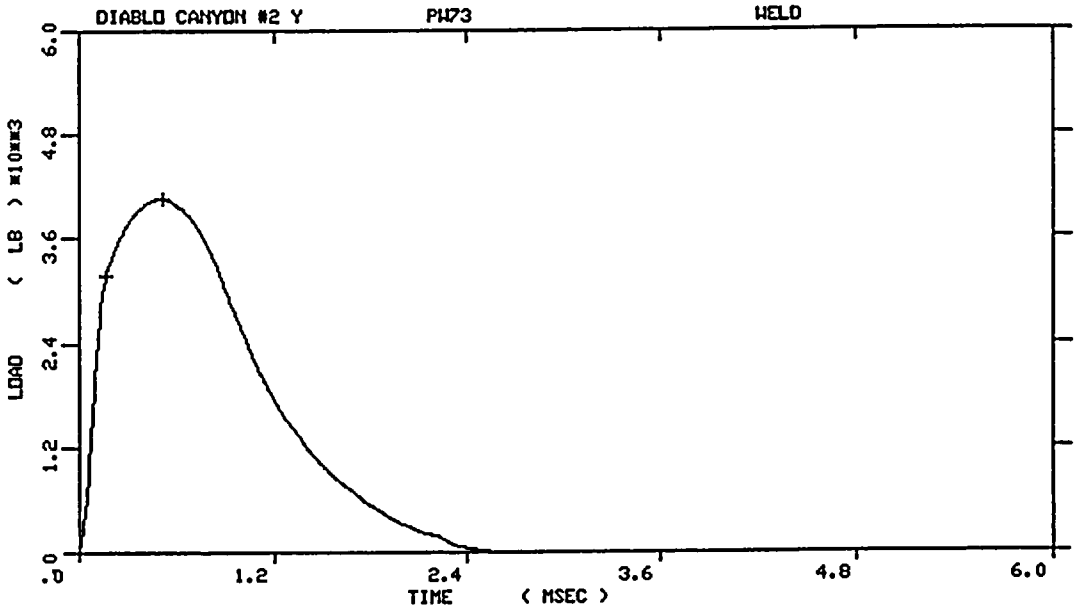


DIABLO CANYON #2 Y

SPECIMEN NUMBER :PW73
MATERIAL :WELD
CAPSULE :DIABLO CANYON
:#2 Y

Computer Error - No Instrumented Data Available

Figure A-23. Load-time records for Specimens PW73 and PW61.

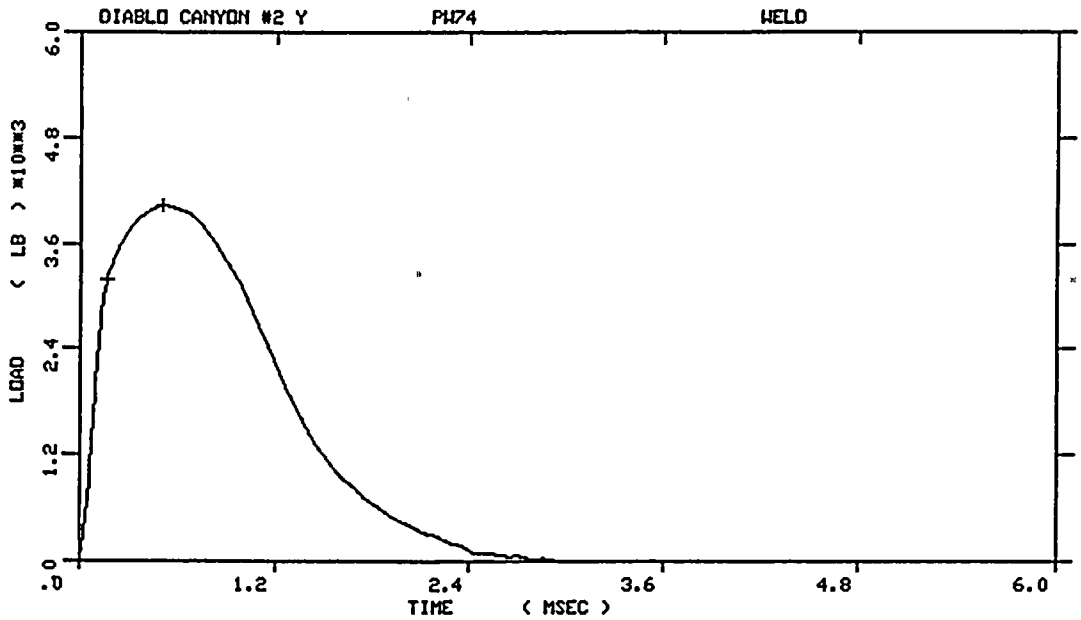


DIABLO CANYON #2 Y
SPECIMEN NUMBER :PW74
MATERIAL :WELD
CAPSULE :DIABLO CANYON
:#2 Y

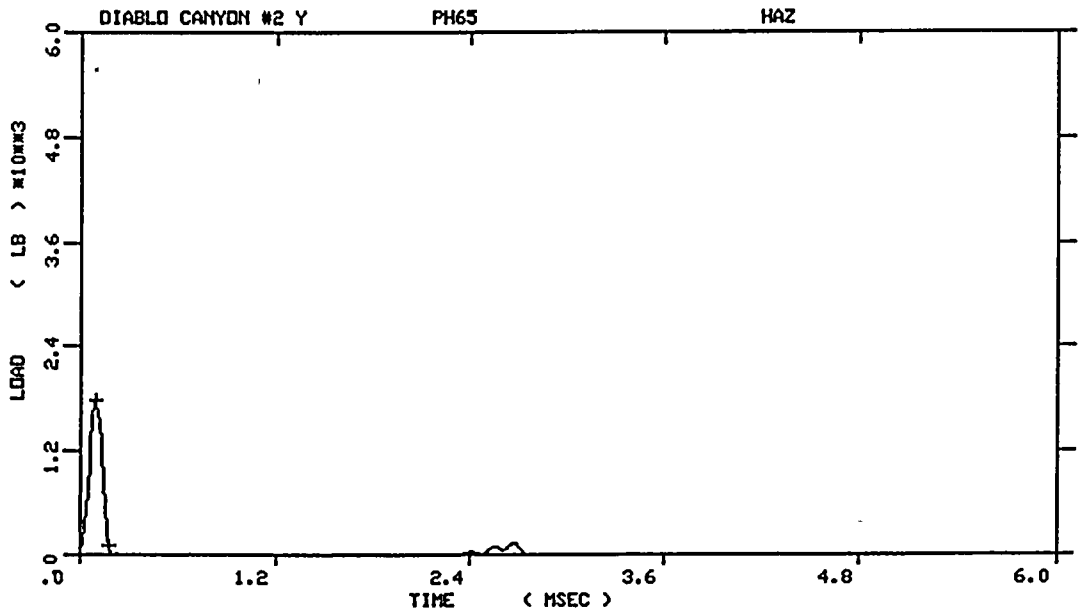


DIABLO CANYON #2 Y
SPECIMEN NUMBER :PH65
MATERIAL :HAZ
CAPSULE :DIABLO CANYON
:#2 Y

Figure A-24. Load-time records for Specimens PW74 and PH65.

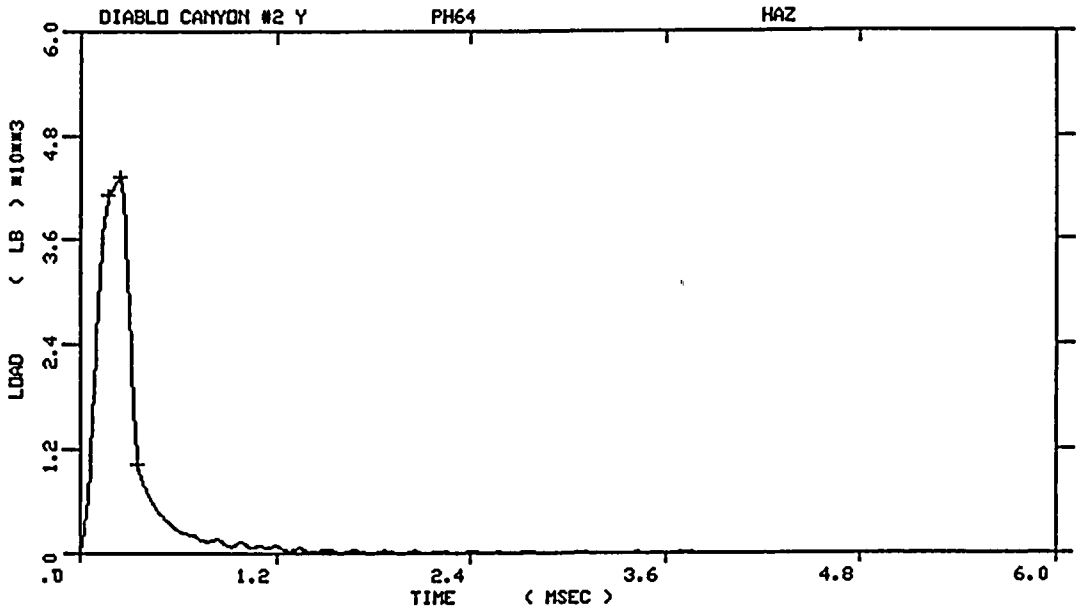


DIABLO CANYON #2 Y
SPECIMEN NUMBER :PH64
MATERIAL :HAZ
CAPSULE :DIABLO CANYON
:#2 Y

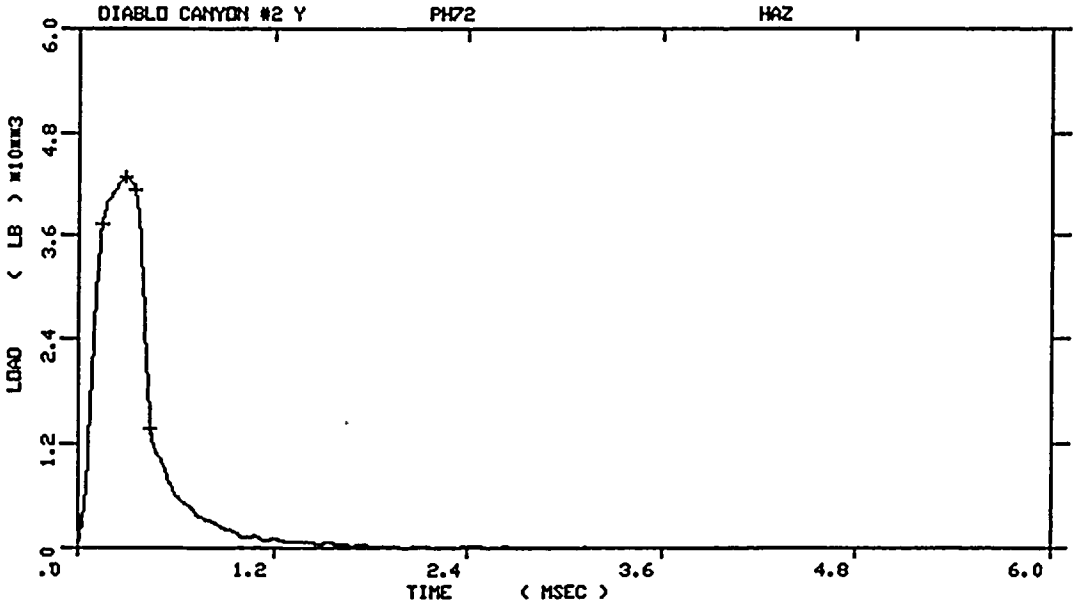


DIABLO CANYON #2 Y
SPECIMEN NUMBER :PH72
MATERIAL :HAZ
CAPSULE :DIABLO CANYON
:#2 Y

Figure A-25. Load-time records for Specimens PH64 and PH72.

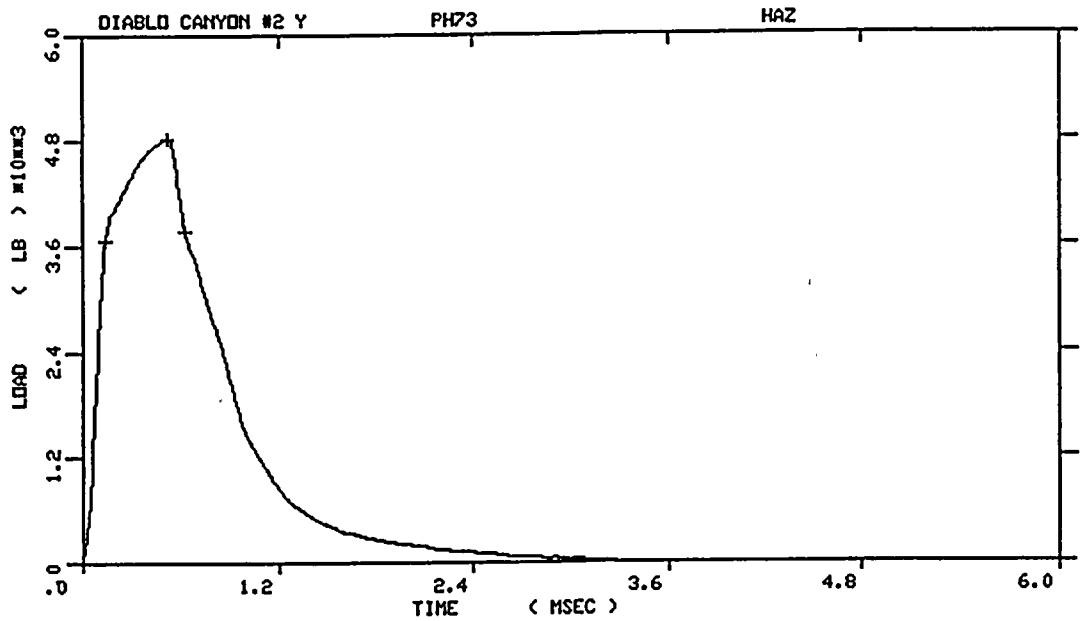


DIABLO CANYON #2 Y
SPECIMEN NUMBER :PH73
MATERIAL :HAZ
CAPSULE :DIABLO CANYON
:#2 Y

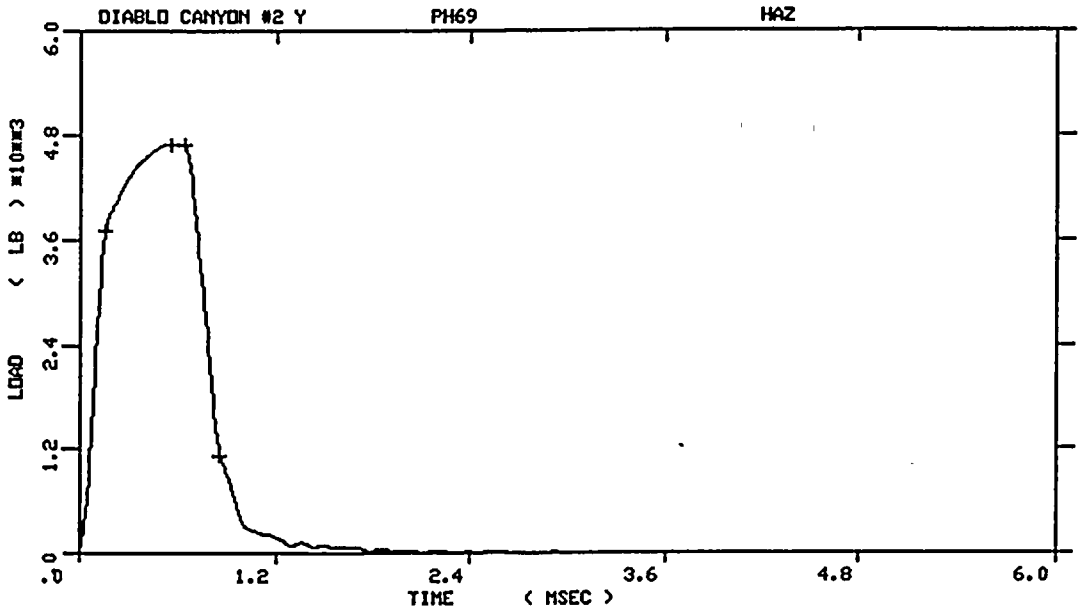


DIABLO CANYON #2 Y
SPECIMEN NUMBER :PH69
MATERIAL :HAZ
CAPSULE :DIABLO CANYON
:#2 Y

Figure A-26. Load-time records for Specimens PH73 and PH69.

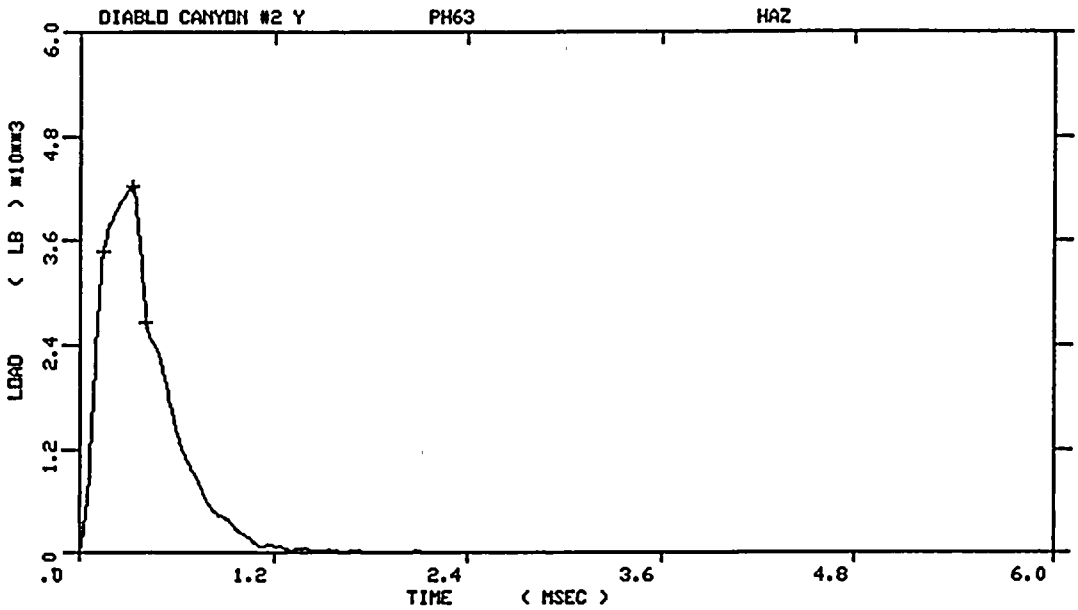


DIABLO CANYON #2 Y
SPECIMEN NUMBER :PH63
MATERIAL :HAZ
CAPSULE :DIABLO CANYON
:#2 Y

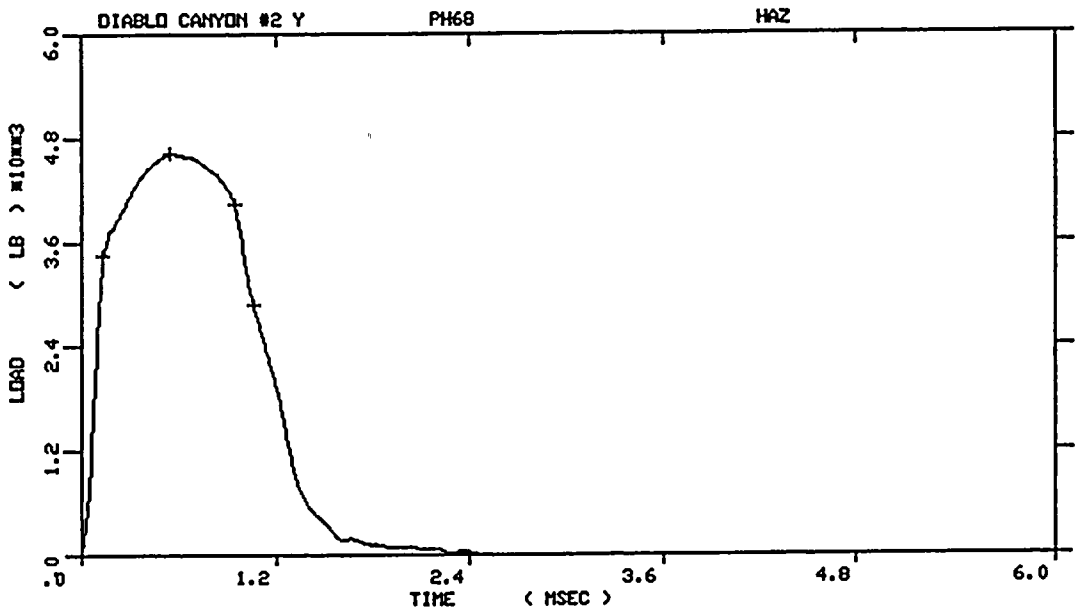


DIABLO CANYON #2 Y
SPECIMEN NUMBER :PH68
MATERIAL :HAZ
CAPSULE :DIABLO CANYON
:#2 Y

Figure A-27. Load-time records for Specimens PH63 and PH68.

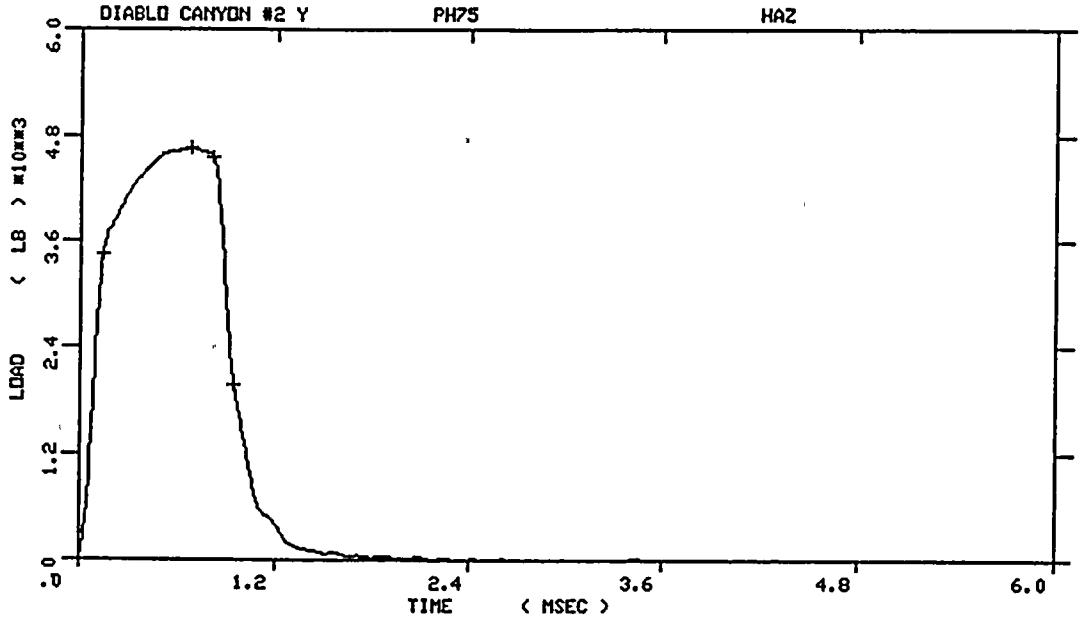


DIABLO CANYON #2 Y
SPECIMEN NUMBER :PH75
MATERIAL :HAZ
CAPSULE :DIABLO CANYON
:#2 Y

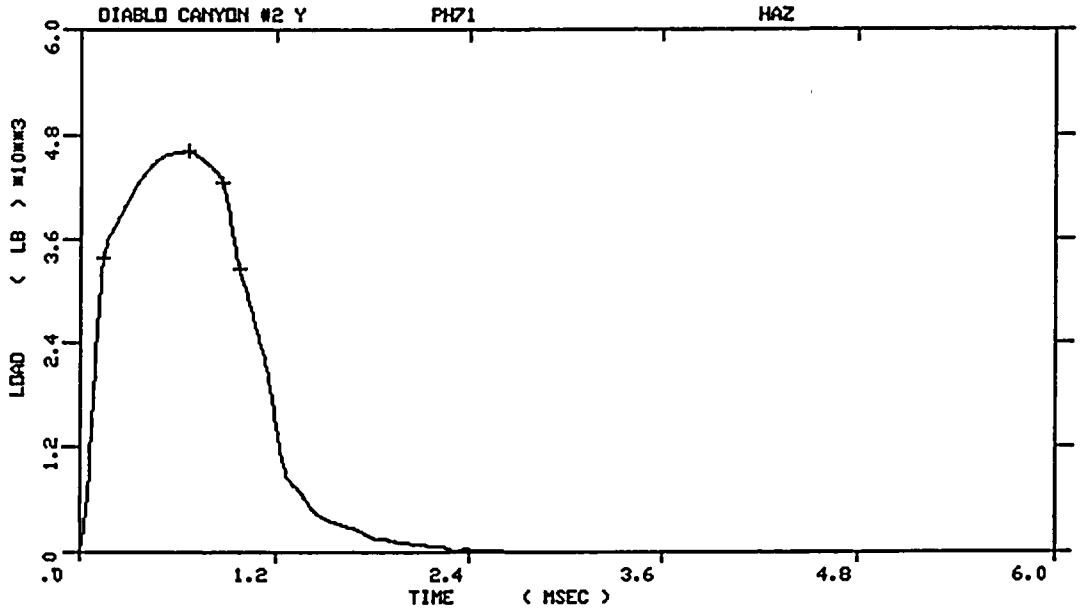


DIABLO CANYON #2 Y
SPECIMEN NUMBER :PH71
MATERIAL :HAZ
CAPSULE :DIABLO CANYON
:#2 Y

Figure A-28. Load-time records for Specimens PH75 and PH71.

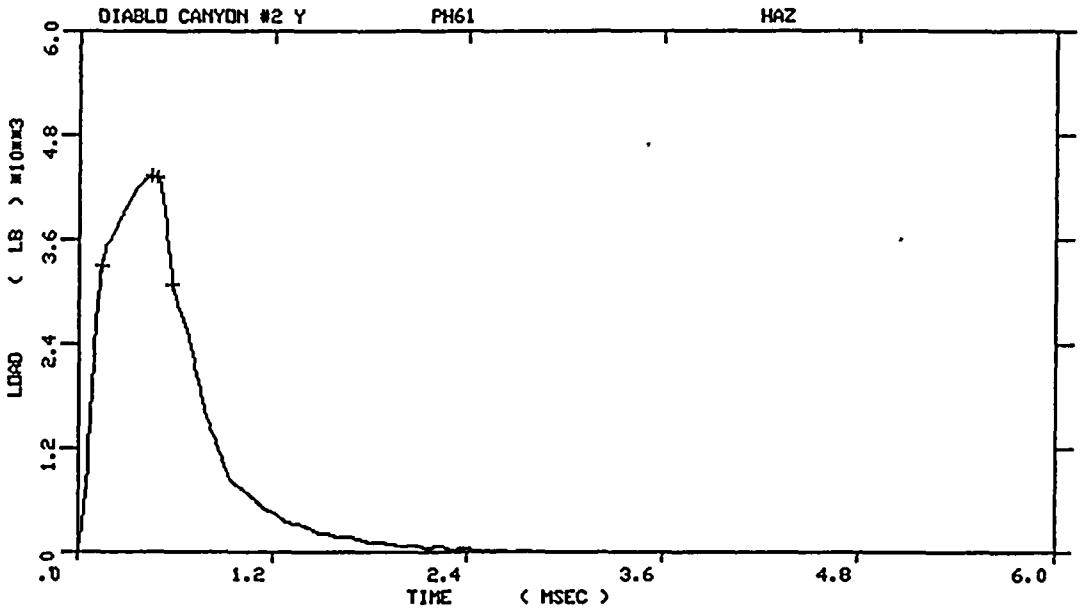


DIABLO CANYON #2 Y
SPECIMEN NUMBER :PH61
MATERIAL :HAZ
CAPSULE :DIABLO CANYON
:#2 Y

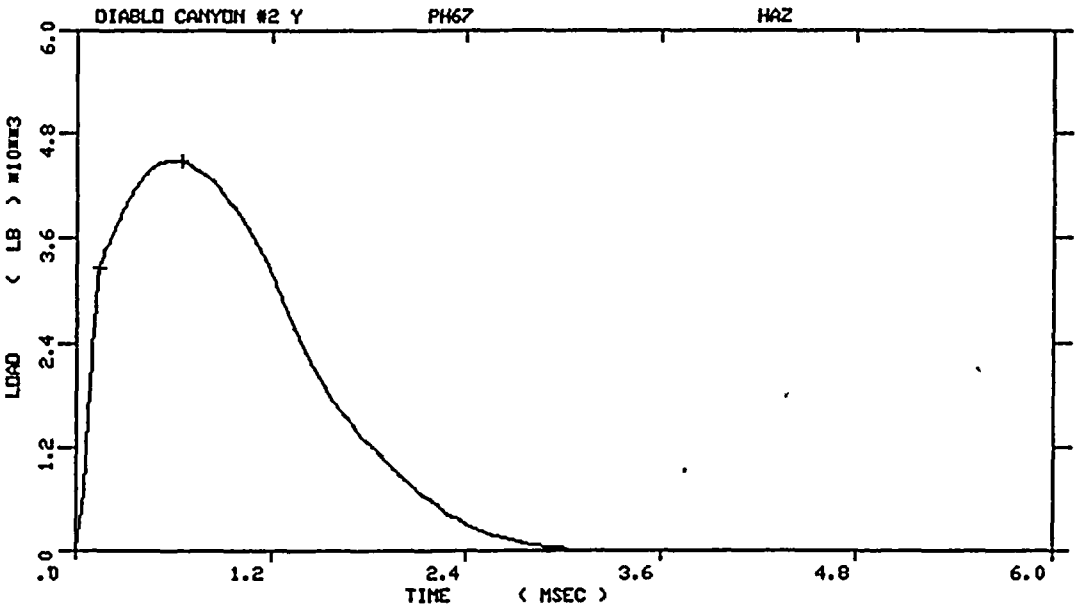


DIABLO CANYON #2 Y
SPECIMEN NUMBER :PH67
MATERIAL :HAZ
CAPSULE :DIABLO CANYON
:#2 Y

Figure A-29. Load-time records for Specimens PH61 and PH67.

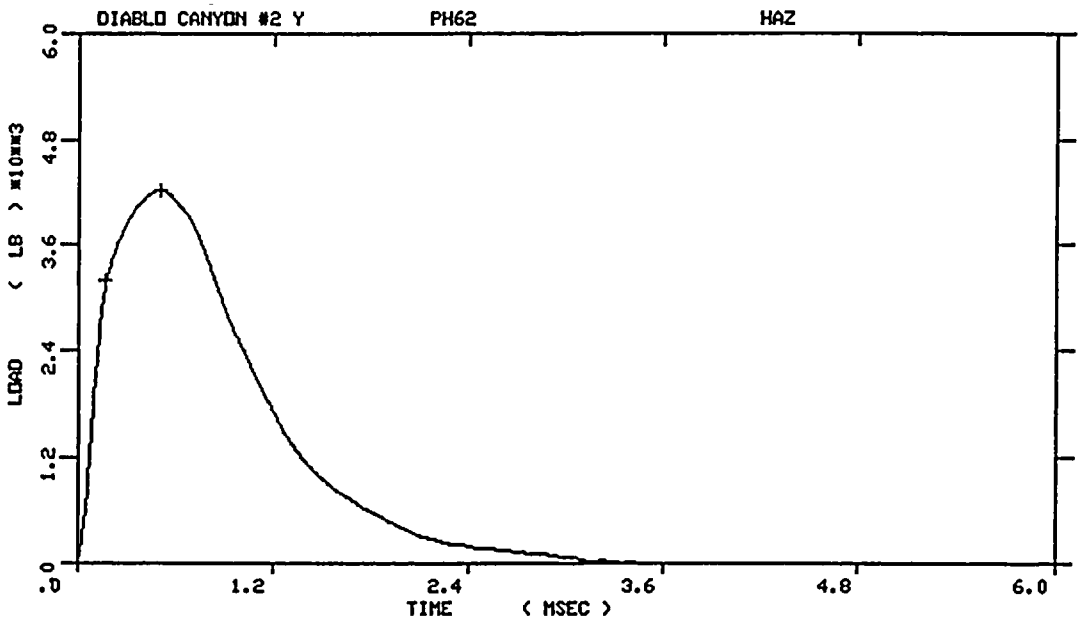


DIABLO CANYON #2 Y
SPECIMEN NUMBER :PH62
MATERIAL :HAZ
CAPSULE :DIABLO CANYON
:#2 Y

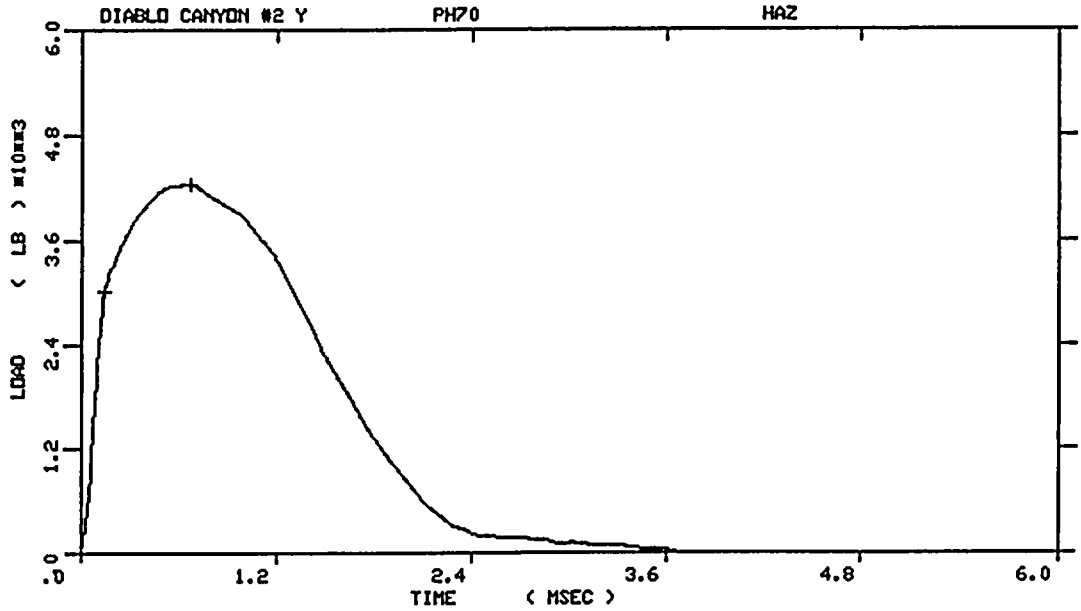


DIABLO CANYON #2 Y
SPECIMEN NUMBER :PH70
MATERIAL :HAZ
CAPSULE :DIABLO CANYON
:#2 Y

Figure A-30. Load-time records for Specimens PH62 and PH70.

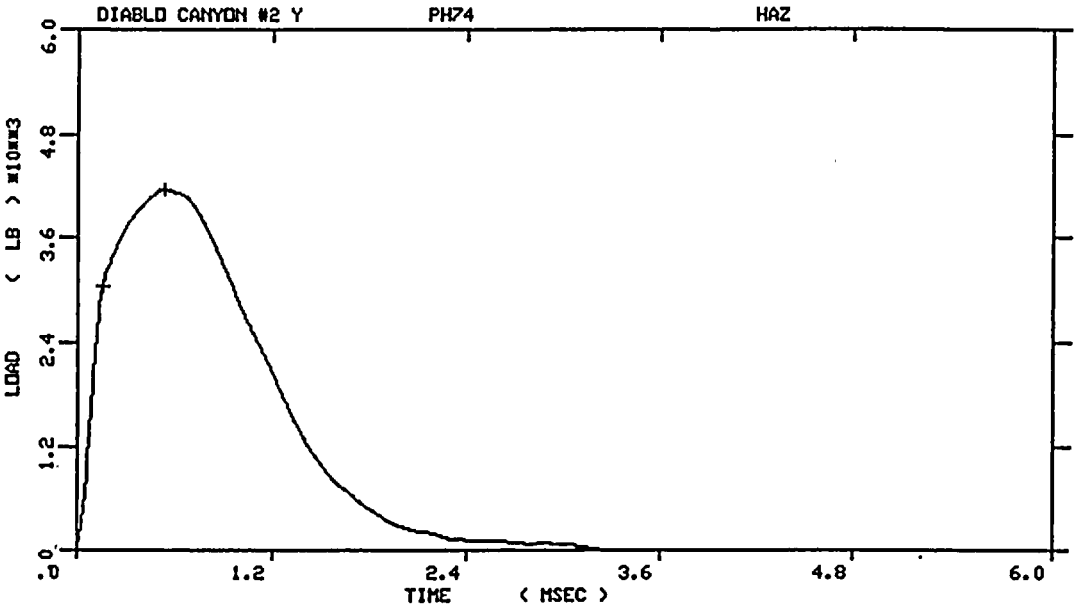


DIABLO CANYON #2 Y
SPECIMEN NUMBER :PH74
MATERIAL :HAZ
CAPSULE :DIABLO CANYON
:#2 Y

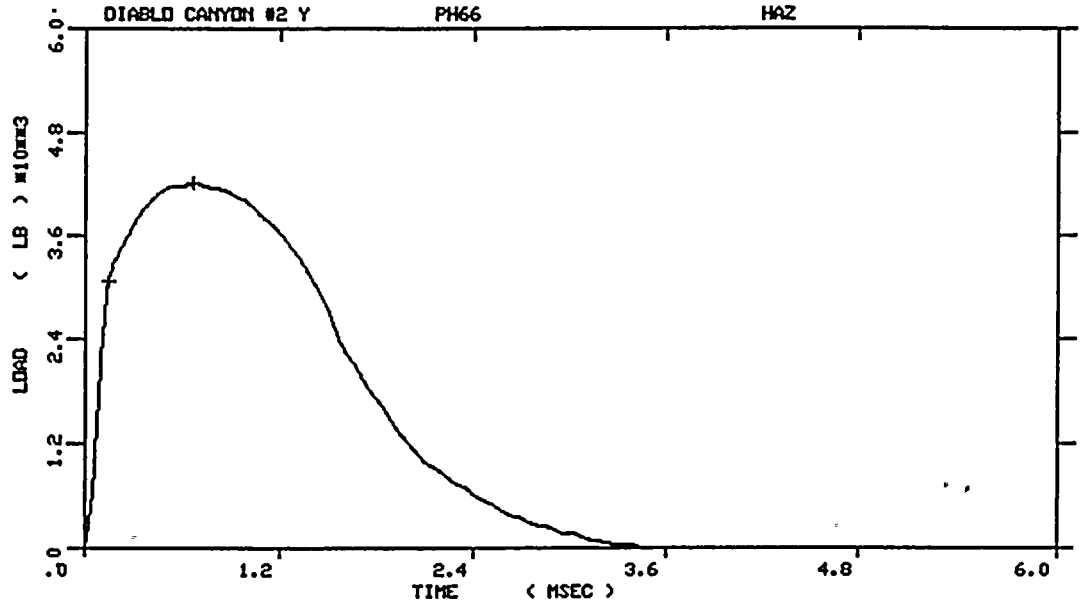


DIABLO CANYON #2 Y
SPECIMEN NUMBER :PH66
MATERIAL :HAZ
CAPSULE :DIABLO CANYON
:#2 Y

Figure A-31. Load-time records for Specimens PH74 and PH66.